

**The Study of Phosphoinositide 3-Kinase
Signalling in *Giardia intestinalis***

Priyavudh Herabutya

A thesis submitted for the degree of
Doctor of Philosophy

School of Biological Sciences
Royal Holloway University of London

30 January 2015

DECLARATION

I, Priyavudh Herabutya, hereby declare that the work carried out and presented in this thesis is my own.

Signature:

Date:

ABSTRACT

Phosphoinositide 3-kinase signalling pathways are critical in the regulation of several cellular mechanisms studied in mammalian and yeast cells. Recent studies have identified and characterised two putative phosphoinositide 3-kinase (PI3K) genes in *Giardia intestinalis* called *GiPI3K1* and *GiPI3K2*, which have homology to Class I and Class III PI3K isoforms, respectively. *G. intestinalis* is a parasitic protozoan causing diarrhoea and malabsorption throughout the world. It has been hypothesised that *Giardia* processes such as cell growth, differentiation and vesicle trafficking, all of which are important for parasite proliferation and disease transmission, may be mediated by the PI3K signalling mechanism. This research aims to test this hypothesis using bioinformatics and a range of experimental approaches.

We used BLAST and Clustal W analysis to further characterise *PI3K* genes and identify and characterise additional putative ancillary components of lipid signalling cascades. A limited number of such components was identified in the *Giardia* genome by homology searching, but two genes with high homology to *Saccharomyces cerevisiae* glycogen synthases kinase-3 (GSK-3) were found with 40% identity to *Giardia* GSK sequence alignment. To investigate the putative functionality of these lipid signalling kinases in *Giardia*, we exposed parasite trophozoites to a range of well characterised specific inhibitors of GSK and PI3K and measured their effect on parasite growth. Also, we initiated encystation of trophozoites to cysts cells and exposed to inhibitors to observe their effect. As an alternative to cell counting, we developed a quantitative spectrophotometric method that correlates cell number to methylene blue staining. The PI3K inhibitor LY294002 showed the strong inhibition of trophozoite growth. However PI-103, a recently described specific inhibitor of PI3K, showed no evidence of reducing trophozoites' proliferation. Neither did wortmanin, a potent and irreversible inhibitor of PI3K. The structural features of *Giardia* PI3K that may explain these observations will be discussed. Exposure to inhibitory concentrations of CT99021, a specific inhibitor of GSK-3, had no detectable effect on *Giardia* growth. This was not unexpected as, in mammalian cells and other eukaryotes, protein kinase B-mediated phosphorylation of GSK-3 prevents cell cycle arrest as a result of GSK3-mediated phosphorylation of specific cyclins. This result, however, rules out the possibility that the growth inhibition of *Giardia* trophozoites observed with LY294002 could be the result of non-specific GSK-3 inhibition.

ACKNOWLEDGMENTS

I would like to dedicate this thesis to my Grandmother, my loving Mum and Dad for their continuous encouragement, tremendous patience, relentless support and for given me this great opportunity in my life.

I am forever grateful for the advice, guidance and constant encouragement from my supervisor, Dr. Jorge Tovar-Torres over the length of this Ph.D. I would like to thank all members of the Jorge Tovar laboratories for their support, in particular Neil Sommerville, Lynn Grignard and Helen Bennett. I would also like to thank other members of the lab, especially Arnold Junior Tatsinkam, Paul De Saram and Anila Iqbal for their help and support. Special thanks to Kamonchanok Tharanurak and Chanida Kaewkor for their kind help. Finally, thank you to my family and friends for their cheerfulness and encouragement throughout my Ph.D.

TABLE OF CONTENTS

ABSTRACT	3
ACKNOWLEDGEMENTS	4
TABLE OF CONTENTS	5
LIST OF FIGURES	9
LIST OF TABLES	12
ABBREVIATIONS	13
CHAPTER 1: INTRODUCTION	16
1.1 The biology of <i>Giardia</i>	16
1.2 Parasite encystation	17
1.3 Lipids and lipid signalling	19
1.4 Phosphoinositide 3-kinase (PI3K)	21
1.5 Phosphatases	25
1.6 PI3K inhibitors	25
1.7 Specificity and targets of PI3K inhibitors	28
1.8 Putative PI3Ks in <i>Giardia</i>	33
1.9 Aims and Objectives	39
CHAPTER 2: MATERIALS AND METHODS	40
2.1 Bioinformatics	40
2.1.1 <i>Giardia lamblia</i> genome database search with translation BLAST and pairwise alignment	40
2.1.2 Protein analysis and identification of domains	41
2.1.3 Protein structure analysis	41
2.1.4 Multiple alignments	42
2.1.5 Protein subcellular localisation sites	42

2.2	Cell culture	42
2.2.1	Trophozoite culture	42
2.2.2	Induction of <i>Giardia</i> encystation	43
2.2.3	Cell counts	43
2.2.4	Purification and counting of cysts	43
2.2.5	Colorimetric quantitation of cell growth	44
2.2.5.1	Standard curve for colorimetric assay	44
2.2.5.2	Standard growth curve	45
2.2.5.3	Fixation of trophozoites to tissue culture plate	46
2.2.6	Statistic representation	47
2.3	Chemical inhibition studies	47
2.3.1	Inhibitor preparation	47
2.3.2	Inhibitor treatment on trophozoites	47
2.3.3	Inhibitor treatment of encysting cultures	48
2.3.4	Inhibitor treatment of trophozoites	48
2.4	Lipids	49
2.4.1	Extraction of PI(3,4,5)P ₃ from <i>Giardia intestinalis</i> , <i>Dictyostelium discoideum</i> and mouse fibroblast cell lines	49
2.4.2	Detection and quantification of PI(3,4,5)P ₃	50
2.5	Imaging	51
2.5.1	Electron microscopy	51
2.5.1.1	Scanning electron microscopy	51
2.5.1.2	Transmission electron microscopy	52
2.5.2	Light immunomicroscopy	53
2.5.2.1	Immunofluorescence analysis	53
2.5.2.2	Confocal microscopy	54

CHAPTER 3: BIOINFORMATICS SEQUENCE ANALYSIS OF <i>G. INTESTINALIS</i> SIGNALLING PROTEINS PHOSPHOINOSITIDE 3-KINASES AND GLYCOGEN SYNTHASE KINASES		55
3.1	Introduction	55
3.2	Experimental results	59
3.2.1	Identification of putative PI3K and GSK in <i>G. intestinalis</i>	59
3.2.2	Analysis of the domains in PI3Ks and GSKs in <i>G. intestinalis</i>	65
3.2.3	Functional analysis of GiPI3Ks and GiGSKs	72
3.2.4	Prediction of GiPI3Ks and GiGSKs protein localisation sites in cell through bioinformatics learning algorithms	76
3.3	Discussion	80
CHAPTER 4: INVESTIGATING THE EFFECT OF PI3K AND GSK INHIBITION ON <i>G. INTESTINALIS</i>		82
4.1	Introduction	82
4.2	Experimental results	85
4.2.1	Effect of PI3K inhibitor LY294002 on <i>G. intestinalis</i>	85
4.2.2	Effect of known PI3Ks inhibitors LY294002, wortmannin and PI-103 on trophozoite proliferation over time	90
4.2.3	Effect of Puromycin on <i>Giardia</i> trophozoites	96
4.2.4	Inhibition of Glycogen synthase kinase-3	99
4.2.5	Effect of co-exposure to PI3K and GSK-3 inhibitor on <i>Giardia</i> trophozoites	105
4.2.6	The importance of PI3K activity during encystation process	108
4.2.7	Detection and quantitation of phosphatidylinositol (3,4,5)-trisphosphate in cell cultures	119
4.3	Discussion	122
CHAPTER 5: USING SCANNING AND TRANSMISSION ELECTRON MICROSCOPY TO INVESTIGATE THE EFFECT OF LY294002 ON <i>G. INTESTINALIS</i>		130
5.1	Introduction	130

5.2	Experimental results	131
5.2.1	Scanning electron microscopy images of <i>G. intestinalis</i> trophozoites	131
5.2.2	SEM images of <i>G. intestinalis</i> encysting cells	139
5.2.3	Transmission electron microscopy images of <i>G. intestinalis</i> trophozoites	150
5.2.4	TEM images of <i>G. intestinalis</i> encysting cells	151
5.2.5	Ultrastructural investigation on <i>G. intestinalis</i> trophozoites under the effect of LY294002	157
5.2.6	CWP2 immunofluorescence study in <i>G. intestinalis</i>	163
5.3	Discussion	166
CHAPTER 6: DISCUSSION		171
6.1	Research hypothesis	171
6.2	Summary of findings	171
6.3	Limitations of approaches used and ideas for improvement	176
6.4	Implications of research and future work	177
6.5	Conclusion	179
BIBLIOGRAPHY		180

LIST OF FIGURES

Figure 1.1: <i>Giardia intestinalis</i> interaction with the human intestine.	17
Figure 1.2: Phosphatidylinositol and examples of phosphorylated phosphatidylinositol.	20
Figure 1.3: Overview of intracellular signalling transduction pathways to regulate chemotaxis involving PI3K, PKB and other components.	24
Figure 1.4: The mechanism of two common inhibitors binding into PI3K active site.	28
Figure 1.5: Signalling pathways illustrating GSK3 putative protein kinase regulation in mammalian cells.	31
Figure 1.6: The mammalian schematic of GSK-3 α and GSK-3 β .	32
Figure 1.7: Detailed sequence analysis of the kinase domains of GiPI3K1 and GiPI3K2.	34
Figure 1.8: Domain structure of GiPI3K1 and GiPI3K2 compared to other PI3Ks.	36
Figure 1.9: The analysis of GiPI3K1 and GiPI3K2 using RT-PCR.	37
Figure 2.1: Standard curve for colorimetric assay.	44
Figure 2.2: Standard growth curve.	46
Figure 2.3: PIP ₃ Mass ELISA standard curve.	51
Figure 3.1: GSK domain pairwise alignments for GiGSKa and GiGSKb sequences.	69
Figure 3.2: Secondary structure prediction of Serine/Threonine protein kinase, catalytic domains in <i>Giardia</i> GSKa and GSKb.	71
Figure 3.3: GiGSKa and GiGSKb Serine/Threonine kinase catalytic domain alignment on crystal structure of <i>Homo sapiens</i> glycogen synthase kinase-3 beta (HsGSK3 β).	72
Figure 3.4: Detailed sequence investigation of Serine/Threonine kinase catalytic domain of GiGSKa and GiGSKb.	74
Figure 3.5: Multiple alignment of Serine/Threonine kinase catalytic domain (S_TKc).	75
Figure 4.1: <i>Giardia intestinalis</i> growth curve over a 168-hour period.	86
Figure 4.2: Inhibition of trophozoites proliferation by PI3K inhibitor LY294002.	87
Figure 4.3: Effect of wortmannin on trophozoite proliferation.	89
Figure 4.4: Effect of PI-103 treatment on trophozoites proliferation.	90
Figure 4.5: Effect of LY294002 inhibition on trophozoites population over	

a 48-hour period.	91
Figure 4.6: The effect of LY294002 inhibitor can be reversed by subculturing in inhibitor-free medium.	92
Figure 4.7: The effect of LY294002 and DRB exposure over a 48-hour period.	94
Figure 4.8: Exposure of trophozoites to different concentrations of PI-103.	95
Figure 4.9: The effect of puromycin on <i>Giardia</i> trophozoites proliferation over 144 hours.	97
Figure 4.10: The effect of puromycin and LY294002 inhibition over 48 hours.	97
Figure 4.11: Pre-treated with puromycin trophozoites cell proliferation observed after subculturing.	98
Figure 4.12: Effect of CT99021 over 48-hour period.	101
Figure 4.13: Effect of Lithium chloride over 48-hour period.	102
Figure 4.14: Overall result of inhibitors treatment on <i>Giardia</i> trophozoites.	104
Figure 4.15: Effect of double inhibitor treatment on trophozoite proliferation.	107
Figure 4.16: Effect of double inhibitor treatment to monitor trophozoite proliferation.	108
Figure 4.17: Total cell number under encystation.	113
Figure 4.18: Effect of PI3K inhibition in encysting cultures.	114-115
Figure 4.19: Effect of PI3K inhibition in encysting cultures.	117-118
Figure 4.20: Investigation on phosphatidylinositol (3,4,5)-triphosphate (PIP ₃) level in <i>G. intestinalis</i> .	121
Figure 4.21: Mammalian class IA PI3K signalling pathway impacts on cell growth, survival and metabolism.	126
Figure 4.22: Encystation process images at 4 hours and 8 hours.	129
Figure 5.1: <i>Giardia intestinalis</i> trophozoites morphology.	132
Figure 5.2: Trophozoites cells treated with LY294002 cell morphology.	133
Figure 5.3: Comparison of <i>Giardia trophozoite</i> cells treated with LY294002 over 24 hours and 48 hours.	135
Figure 5.4: Proportion of morphologically-altered trophozoite cells in groups of PI3K-inhibited cells treated with LY294002 and control-treated trophozoites.	136
Figure 5.5: <i>Giardia intestinalis</i> trophozoites under LY294002 treatment.	138
Figure 5.6: <i>Giardia intestinalis</i> under encysting medium over 48 hours.	140

Figure 5.7: Encystation experiment with <i>G. intestinalis</i> over a period of 48 hours.	141
Figure 5.8: General view of <i>Giardia</i> under encysting medium and LY294002 treatment.	144
Figure 5.9: Encystation experiment with LY294002 and DMSO treatment.	145
Figure 5.10: <i>Giardia intestinalis</i> cells in encysting medium under LY294002 treatment at different concentration.	148
Figure 5.11: Encystation experiment to harvest cyst after 48 hours of trophozoites incubation in encysting medium.	149
Figure 5.12: <i>Giardia intestinalis</i> trophozoite cells	151
Figure 5.13: <i>Giardia intestinalis</i> under encystations medium for a period of 72 hours.	153
Figure 5.14: <i>Giardia</i> cells incubated in encystations medium for 24 and 48 hours.	155
Figure 5.15: Ultrastructure studies of <i>G. intestinalis</i> under encystation process.	156
Figure 5.16: <i>Giardia</i> trophozoites incubated for 24 and 48 hours in the presence of LY294002.	158
Figure 5.17: Ultrastructural studies of <i>G. intestinalis</i> treated with LY294002.	159
Figure 5.18: <i>Giardia intestinalis</i> treated with LY294002 over a period of 72 hours.	161
Figure 5.19: Comparison of <i>Giardia</i> trophozoites treated with LY294002 against <i>Giardia</i> trophozoites incubated in encystations medium.	162
Figure 5.20: Immunofluorescence microscopy of <i>G. intestinalis</i> encysting cells stained with anti-CWP2.	164
Figure 5.21: CWP2 staining in LY294002-treated cells.	165

LIST OF TABLES

Table 1.1: Analysis of the giardial PI3K domains.	35
Table 3.1: <i>G. lamblia</i> genome contents in comparison to other eukaryotic species.	58
Table 3.2: Percentage identity and probability values of putative <i>G. intestinalis</i> PI3K sequences.	60
Table 3.3: Percentage identity and probability values of putative <i>G. intestinalis</i> GSK-3 sequences.	61
Table 3.4: Probability and percentage identity values of matches from the non-redundant database of nucleotide sequences at NCBI to all three <i>G. intestinalis</i> ORF following tBLASTn.	62
Table 3.5: Analysis of the putative <i>G. intestinalis</i> GSK sequences following tBLASTn.	64
Table 3.6: Investigation of giardial PI3K proteins.	66
Table 3.7: Investigation of giardial GSK proteins.	66
Table 3.8: The subcellular localisation of GiPI3K1 and GiPI3K2 prediction using the internet program PSORTII.	78
Table 3.9: The subcellular localisation of GiGSKa and GiGSKb prediction using the internet program PSORTII.	79
Table 4.1: Quantification table showing amount of PIP ₃ detected in different species.	120
Table 4.2: A brief summary showing specificities of PI3Ks inhibitors.	123

ABBREVIATIONS

ATP	Adenosine TriPhosphate
BLAST	Basic Local Alignment Search Tool
BLASTn	Nucleotide BLAST
bp	base pair
cAMP	cyclic Adenine MonoPhosphate
CCVs	Clathrin Coated Vesicles
Cdc	Cell division cycle
CDK	Cyclin Dependent Kinase
CKII	Casein Kinase II
CMGC	Cyclin-dependent kinase, Mitogen activated protein kinases, Glycogen synthase kinases and Cyclin-like kinases
CT99021	6-[2-[[4-(2,4-dichlorophenyl)-5-(5-methyl-1H-imidazol-2-yl)pyrimidin-2-yl]amino]ethylamino]-pyridine-3-carbonitrile
CWP	Cyst Wall Protein
DAPI	4',6-Diamidino-2-phenylindole
DB	Data Base
DMSO	Dimethyl Sulfoxide
DNA	DeoxyriboNucleic Acid
DNA-PK	DNA-dependent protein kinase
DRB	5,6-Dichloro-1- β -D-RibofuranosylBenzimidazole
EGF	Epidermal Growth Factor
eIF	eukaryotic Initiation Factor
ELISA	Enzyme-Linked Immunosorbent Assay
ELV	Electron Lucent Vesicle
ER	Endoplasmic Reticulum
ESV	Encystation-specific Secretory Vesicle
FITC	Fluorescein Isothiocyanate
fMLP	formyl-Methionyl-Leucyl-Phenylalanine
GalNAc	N-acetylgalactosamine
GiGSKa	<i>G. intestinalis</i> GSKa
GiGSKb	<i>G. intestinalis</i> GSKb
GiPI3K1	<i>G. intestinalis</i> PI3K1
GiPI3K2	<i>G. intestinalis</i> PI3K2
GPCR	G Protein Coupled Receptor

GSK-3	Glycogen Synthase Kinase-3
HIPK	Homeo-domain Interacting Protein Kinase
IRS1	Insulin-Regulator Substrate 1
IscS	Iron-sulphur cluster S
kV	kilovolts
LiCl	Lithium Chloride
LY294002	2-(4-Morpholinyl)-8-phenyl-4H-1-benzopyran-4-one
mA	Milliampere
MAPK	Mitogen Activated Protein Kinase
MAPKAP-K1	MAPK-activated protein kinase 1
MB	Median Body
MTM	Myotubularin
MTMR	Myotubularin Related Protein
mTOR	mammalian Target Of Rapamycin
NCBI	National Center for Biotechnology Information
NLS	Nuclear Localisation Signal
ORF	Open Reading Frame
PBS	Phosphate Buffered Saline
PDK1	3' -Phosphoinositide dependent protein kinase
PH	Pleckstrin Homology
PI	Phosphatidylinositol
PI(3)P	Phosphatidylinositol 3-phosphate
PI(3,4)P ₂	Phosphatidylinositol 3,4-bisphosphate
PI(3,4,5)P ₃	Phosphatidylinositol (3,4,5)-trisphosphate
PI(4)P	Phosphatidylinositol 4-phosphate
PI(4,5)P ₂	Phosphatidylinositol 4,5-bisphosphate
PI(5)P	Phosphatidylinositol 5-phosphate
PI-103	(3-[4-(4-morpholinyl)pyrido[3',2':4,5]furo[3,2-d]pyrimidin-2-yl]-phenol)
PI3K	Phosphoinositide 3-Kinase
PI4K	Phosphoinositide 4-Kinase
PIK	Phosphoinositide Kinase
PIP ₃	Phosphatidylinositol (3,4,5)-trisphosphate
PKB	Protein Kinase B
PLK1	Polo-like Kinase 1
PPI _n	Polyphosphoinositides
PTEN	Phosphatase and tensin homologue deleted on chromosome 10

PTK	Protein Tyrosine Kinase
PV	Peripheral Vesicle
PX	PhoX (phagocyte oxidase)-homology
RTK	Receptor Tyrosine Kinase
S_Tkc	Serine/Threonine protein Kinase Catalytic domain
S6K	S6 kinase
SH2	Src Homology 2
SMART	Simple Modular Architecture Research Tool
smMLCK	smooth muscle Myosin Light Chain Kinase
tBLASTn	Translational BLAST
TORC	Target Of Rapamycin Complex
TRITC	TetramethylRhodamine IsothioCyanate
VD	Ventral Disk
Vps	Vacuole protein sorting
VSP	Variant Specific Protein

CHAPTER 1: Introduction

1.1 The biology of *Giardia*

Giardia intestinalis (also known as *Giardia lamblia* and *Giardia duodenalis*) is a flagellated unicellular eukaryotic microorganism that inhabits the upper small intestine of its vertebrate hosts and causes the most common waterborne diarrhoea in the United States and worldwide (Barwick *et al.*, 2000). In developing countries, there is a very high prevalence and incidence of infection, with data suggesting that long-term growth retardation can result from chronic giardiasis (Fraser *et al.*, 2000). Giardiasis is believed to have an estimated worldwide prevalence of hundreds of millions cases annually. Moreover, giardial infections affect the 2.5 million annual deaths that results from diarrheal disease (Adam, 2001). *Giardia* infect the host through contaminated food and water or via faecal-oral route (Lauwaet *et al.*, 2007). This often occur in places with inadequate sanitation such as in less-developed countries. The clinical manifestations of giardiasis in humans vary from an acute or chronic disease to asymptomatic infection with the latter being more common in humans (Farthing, 1994). The symptoms in humans caused by *G. intestinalis* include abdominal pain, diarrhoea, malabsorption, weight loss, nausea and vomiting. Parasite colonisation occurs in the small intestine, where *G. intestinalis* is able to cause illness in humans. Attempt to control intestinal protozoa such as *Giardia* demands further research into the biology of the parasite as well as effective drug treatments. Current available treatments for *Giardia* infection include the use of anti-protozoal drugs, particularly metronidazole and tinidazole, other susceptible drugs include albendazole, furazolidone, nitazoxanide and paromycin are used to lesser extent with the cure rate of similar to or less than metronidazole and tinidazole (Upcroft, 2001). However, reports of drug failures and drug resistance have been known, raising concern that the present drugs use for treatment will become increasingly ineffective (Upcroft, 2001). Therefore, this highlight the importance of developing new drug treatment to combat *Giardia* infection.

When *G. intestinalis* multiplies, it causes damage to the intestinal mucosal wall by shortening of the crypts and villi (Buret, 1990). This might be one of the many ways in which *G. intestinalis* is able to cause diarrhoea, through the disruption of epithelial walls in the small intestine, resulting in malabsorption. The life cycle of *Giardia* consists of two

specific stages; the cyst and the trophozoite. The infection stage is initiated through ingestion of the cyst form, which later excysts into trophozoites in the upper small intestine of the host (Figure 1.1). The trophozoites divide by binary fission and increase the population on the intestinal surface; they move with the help of flagella and attach themselves to the epithelium by a unique cytoskeletal organelle called the ventral disk, thus causing diarrhoea and malabsorption. However, some trophozoites differentiate again, through the process of encystation into the cyst form that allows them to survive in an unfavourable environment in the jejunum. The infective cysts are then passed in the faeces, therefore completing the life cycle by infecting new hosts (Adam, 2001, Lujan *et al.*, 1997).

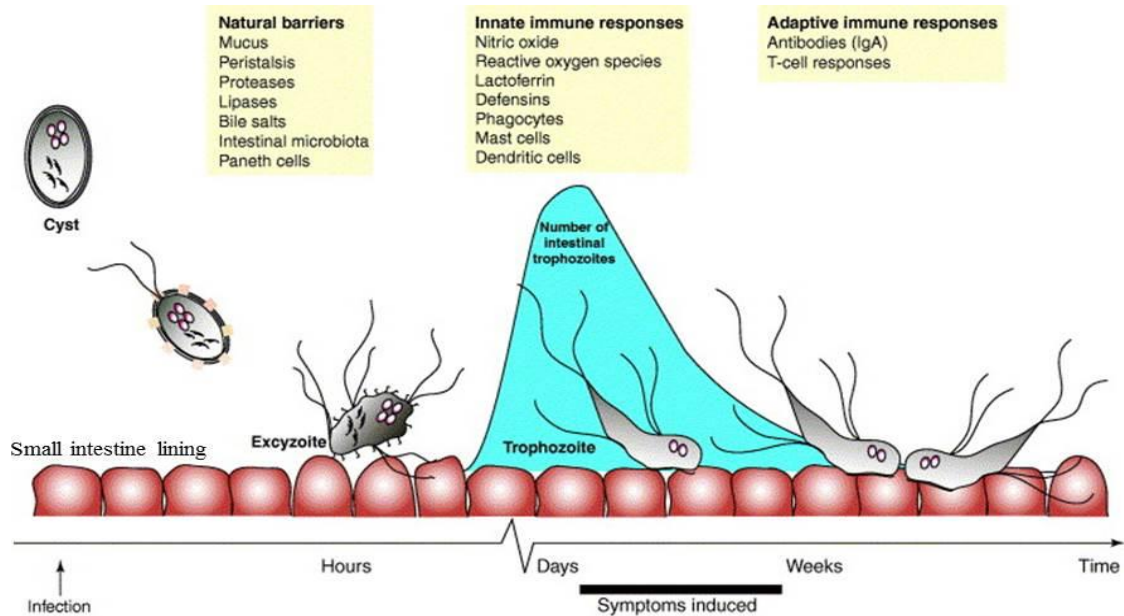


Figure 1.1: *Giardia intestinalis* interaction with the human intestine.

The initiation of *Giardia* infection in the small intestine begins with ingestion of cysts. These cysts then excyst on the upper surface of the small intestine releasing excyzoites. The excyzoite differentiates into trophozoites and multiplies in number in a matter of days in the intestinal lumen. Once a certain number of trophozoites is reached, the symptoms of Giardiasis follows; this usually takes about six to fifteen days following the initial infection. An overview of the complex immune system in the intestine with natural barriers, innate and adaptive immune responses are shown here in the order in which they interact with *Giardia* during infection. Image adapted from Roxström-Lindquist *et al.* (2006).

1.2 Parasite encystation

Encystation is an adaptive process of *G. intestinalis* that is triggered when trophozoites detect a depletion of nutrients in the lower small intestine. This process can be explained in four basic stages: i) Detection of the stimulus for initiation of encystation and the regulation of encystation gene expression; ii) Formation of encystation-specific secretory vesicles (ESVs) and the synthesis, intracellular signalling and transport of

the cyst wall components via ESVs; iii) Assembly of the extracellular cyst wall; and iv) Nuclear division and DNA replication (Adam, 2001 and Lujan *et al.*, 1997). Once encystation has been initiated, the trophozoites will no longer be able to replicate and attach to enterocytes. At the later stage, the trophozoites are more rounded and their oxygen and glucose uptake decreases. Cyst wall construction takes place as encystation ESVs transport soluble cyst wall proteins (CWPs) and release them at the cell surface. Due to the higher level of calcium concentration surrounding the cell's outer membrane, once CWPs are deposited, they aggregate to form the network of fibres of the protein/carbohydrate-rich cyst wall (Stefanic *et al.*, 2006). The cyst wall mostly consists of a novel N-acetylgalactosamine (GalNAc) polysaccharide. It is only synthesised during encystation through a five-enzyme pathway which is stimulated at the transcription level (Lopez *et al.*, 2003). During encystation, DNA replication occurs twice with no interference from cytokinesis; thus, each cyst formed is quadrinucleate (Lujan *et al.*, 1997).

Giardia, like most eukaryotic cells, requires cholesterol for membrane biogenesis, but it is unable to synthesise cholesterol and phospholipids. The initial work of Gillin *et al.* (1987) demonstrated the process of *Giardia* encystation *in vitro* for the first time. The studies on *Giardia* encystation have revealed essentially how *Giardia* initiates the process of differentiating into infective cysts which is vital for the transmission of *Giardia*. *Giardia* encystation in the laboratory can be demonstrated through two methods: i) Cholesterol starvation, and ii) Uptake of bile salt. The studies on encystation by several research groups have made important observations that cholesterol and bile salt availability is important in the differentiation of this parasite (Lujan *et al.*, 1996). Cholesterol is crucial for the parasite because it is utilised to make a new membrane during growth; evidence from *in vitro* studies suggests that cholesterol deprivation induces encystation (Lujan *et al.*, 1996). Because cholesterol starvation triggers encystation, this suggests the involvement of lipid and lipid signalling in parasite differentiation. Bile salts are steroids that aid in the degradation, solubilisation and absorption of lipids from the intestinal lumen. These bile salts are synthesised by the liver from cholesterol and released into the proximal duodenum which is later reabsorbed by an active transport system in the distal ileum (Thomson *et al.*, 1993). The research of Lujan *et al.* (1997) on *in vitro* encystation reported three observations: i) *Giardia* can grow in the absence of bile salts, indicating that these compounds are not essential for trophozoites; ii) Small amounts of bile salts in *Giardia* increase growth because they solubilise lipids and increase their availability to the cells;

and iii) High concentrations of bile salts prevent the uptake of cholesterol and therefore favour encystation. Moreover, recent studies have suggested that components of lipid signalling pathways are present in the *Giardia* genome and may be functional (Cox *et al.*, 2006; Tovar *et al.*, unpublished data).

1.3 Lipids and lipid signalling

The metabolic pathway of *Giardia* involves lipids and how they utilise exogenous lipids for metabolic purposes is important for the survival of the parasite. *Giardia* trophozoites are found in the infected host's small intestine and are therefore continuously exposed to bile acids and dietary fats, therefore it was suggested that lipids and cholesterol may play important roles in the parasite life cycle. *Giardia* are able to take up the lipids and cholesterol that they need from lipoprotein particles present in the host intestine and tissue *in vivo* and from growth medium *in vitro*. It has been reported that *in vitro* cultured trophozoites are capable of internalising the surrounding lipids in the culture medium and transporting these lipids to different locations of the cell. The locations where these lipids are transported include: plasma membrane, cytoplasm, ER and nuclear membranes (Yichoy *et al.*, 2011). Once acquired, these exogenous phospholipids have been shown to undergo fatty acid remodelling (by deacylation/reacylation reactions), which allow these protozoa to alter lipids, bypassing the need to synthesise entirely new phospholipid molecules (Das *et al.*, 2002).

Phosphatidylinositol belongs to a class of the phosphatidylglycerides, which contain a glycerol backbone, acyl chains, phosphodiester linkage and an inositol ring. Phosphorylated forms of phosphatidylinositol are called phosphoinositides, and play important roles in lipid signalling, intracellular signalling and membrane trafficking. The inositol ring can be phosphorylated onto phosphatidylinositol (PI) to form polyphosphoinositides (PPI_n) (Michell *et al.*, 2006). Both PI and PPI_n can be phosphorylated by Phosphoinositide 3-kinase (PI3K) to form many different PPI_n species. Their structures and nomenclature are described below (Figure 1.2):

Phosphatidylinositol monophosphates:

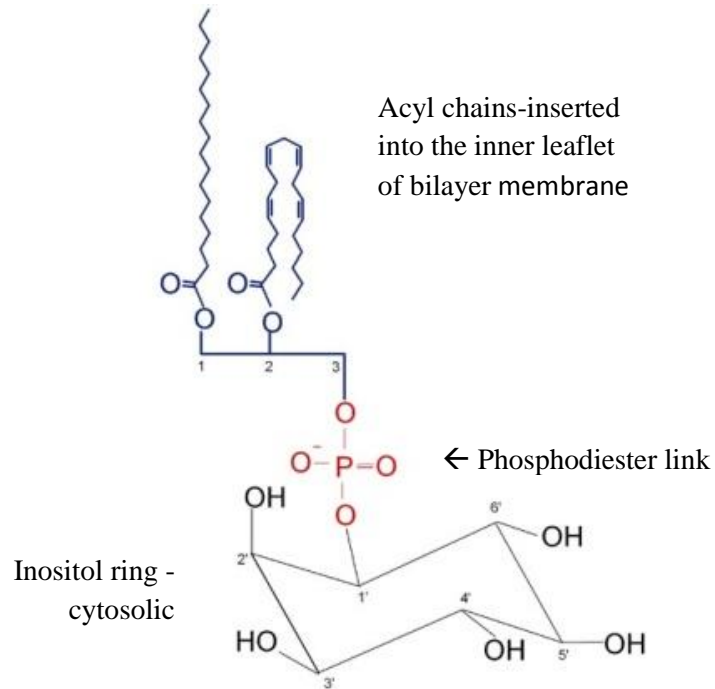
- Phosphatidylinositol 3-phosphate (PtdIns(3)P or PI(3)P)
- Phosphatidylinositol 4-phosphate (PtdIns(4)P or PI(4)P)
- Phosphatidylinositol 5-phosphate (PtdIns(5)P or PI(5)P)

Phosphatidylinositol bisphosphates:

- Phosphatidylinositol 3,4-bisphosphate (PtdIns(3,4)P or PI(3,4)P₂)
- Phosphatidylinositol 3,5-bisphosphate (PtdIns(3,5)P or PI(3,5)P₂)
- Phosphatidylinositol 4,5-bisphosphate (PtdIns(4,5)P or PI(4,5)P₂)

Phosphatidylinositol triphosphate:

- Phosphatidylinositol 3,4,5-trisphosphate (PtdIns(3,4,5)P or PI(3,4,5)P₃)



Phosphatidylinositol (PI)

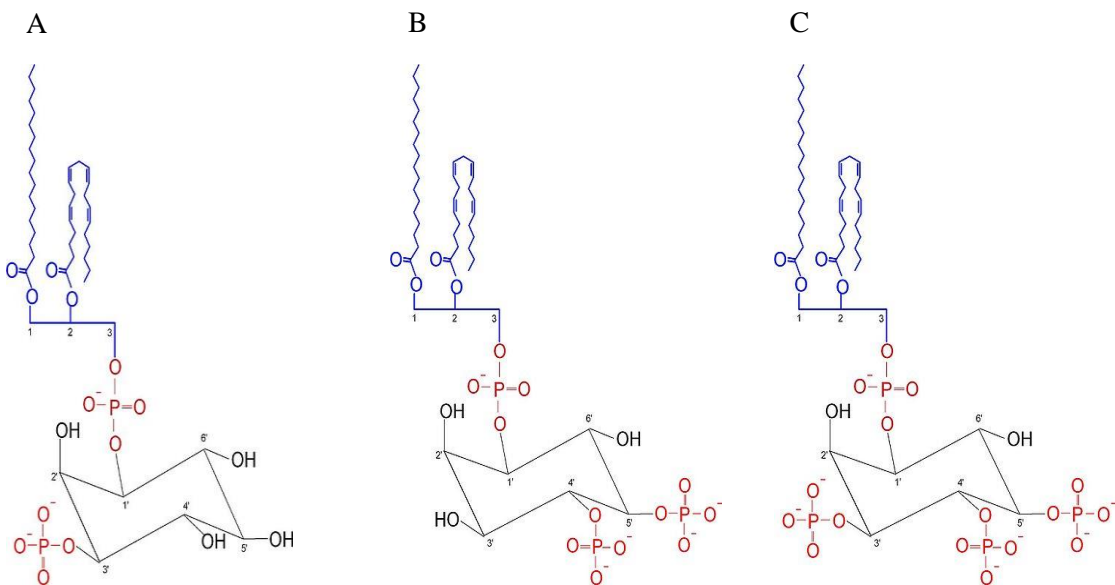


Figure 1.2: Phosphatidylinositol and examples of phosphorylated phosphatidylinositol.

The skeletal structures of phosphatidylinositol (PI) and polyphosphoinositides (PPI_n). The structures of phosphorylated phosphatidylinositol are shown here as a result of PI3K activity: A phosphatidylinositol (3)-phosphate (PI(3)P), B phosphatidylinositol (4,5)-bisphosphate (PI(4,5)P₂) and C phosphatidylinositol (3,4,5)-triphosphate (PI(3,4,5)P₃).

The structures of the illustrated phosphatidylinositol and polyphosphoinositides were taken from Backer (2000).

These PPI_n types make up a minor fraction of the complete cellular lipids in eukaryotic cells. However, the cell continuously monitors its regulation because of its vital roles. The function of PI3Ks in a living cell is crucial in many cellular signal transduction pathways. When it is triggered in response to a variety of agonists, PI3K activity results in the 3-phosphorylated PPI_n. The resulting 3-phosphorylated PPI_n initiates an array of intracellular pathways. An example would be where the PPI_n attaches itself to signalling molecules that may bind to the cellular membrane. This would then trigger the interaction between the membrane signalling components, allowing downstream signalling pathways to be controlled. However, PI3K signalling can be inhibited by the action of these two PPI_n phosphatases: i) myotubularin-related protein (MTMR) and PTEN (a phosphatase and tensin homologue deleted on chromosome 10) (Zhou *et al.*, 2003). Thus, one can see that PPI_n phosphatases such as MTMR and PTEN act as antagonists of PI3K signalling by dephosphorylating PPI_n species.

1.4 Phosphoinositide 3-kinase (PI3K)

PI3Ks were discovered in the 1980s and are a family of related intracellular signal transducer enzymes. They are capable of phosphorylating the D3 position hydroxyl group of the inositol ring of PI, therefore generating intracellular lipid second messengers. Moreover, PI3Ks are also able to place the phosphate moiety on positions 4 and 5 of the inositol rings (Figure 1.2).

The PI3K family is divided into three different classes. The classifications of PI3Ks are based on primary structure, regulation and *in vitro* lipid substrate specificity.

Class I – Class I PI3Ks are responsible for the production of phosphatidylinositol 3-phosphate. PI3Ks can be activated by different types of cell surface receptors, including G-protein-coupled receptors and protein tyrosine kinase receptor. Class I PI3K are divided into class IA and IB (Fruman *et al.*, 1998; Gharbi *et al.*, 2007). Class IA PI3K are heterodimeric molecules composed of a 55-85 kilo Dalton (kDa) regulatory subunit and a 110 kDa catalytic subunit. Class IA PI3K each contain one of five regulatory subunits:

p85 α , p55 α , p50 α , p85 β or p55 γ . These regulatory subunits are attached to catalytic subunits such as p110 α , p110 β and p110 δ , which are present in the human genome. All of the regulatory subunits contain two Src homology 2 domains flanking a p110-binding site. The Src homology 2 (SH2 domain) is a structurally conserved domain contained within the Src oncoprotein and is present in many other intracellular signal-transducing proteins. The most highly expressed regulatory subunit is p85 α ; p85 isoforms also possess an N-terminal Src homology 2 and Src homology 3 domain. The Src homology 2 and Src homology 3 domains, also known as SH2 and SH3 domains, are approximately 100 and 60 amino acids in length, respectively. The SH2 domain plays a vital role in cellular communication, whereas the SH3 domain recognises specific cellular proteins by interactions with short contiguous peptide sequences that are rich in proline residues (Ren *et al.*, 1993). Both of these domains mediate the recruitment and regulation of class IA PI3Ks by activated protein tyrosine kinases (PTKs), with PI3K typically being recruited directly to the receptor via binding to the auto-phosphorylation site or via substrate proteins such as insulin-regulator substrate 1 (IRS1) (Fry *et al.*, 1994). Class IB PI3K is named PI3 γ and consists of the 110 kDa catalytic subunit. PI3K in class IB only interacts with the regulatory subunit p101 (Vanhaesebroeck *et al.*, 1999). The regulatory subunit p101 contains no obvious signalling modules or motifs; class IB PI3Ks indirectly interact with G-protein-coupled receptors such as the formyl-methionyl-leucyl-phenylalanine (fMLP) receptor (Foster *et al.*, 2003). Therefore, the class IB PI3K can be activated by the G-protein-coupled receptor through the unique regulatory subunit p101 (Stephens *et al.*, 1997).

Class II – The first isoform of class II PI3Ks was identified in *Drosophila melanogaster* (MacDougall *et al.*, 1995). Class II PI3Ks are structurally different from class I PI3Ks, in that they do not have p85 or p101 regulatory subunits; however, they do have additional regulatory domains, including the Phox homology (PX) and C-terminal C2 domain. PX domains function in localising the protein to PPI α -containing membranes, through binding with PtdIns3P (Djordjevic and Driscoll, 2002). C-terminal C2 domains present in other proteins are understood to act as a calcium-dependent phospholipid binding motif to mediate the translocation of proteins to membranes (Foster *et al.*, 2003). The function of class II PI3Ks, like class I PI3Ks, is linked to diverse receptor-mediated signalling processes that include integrin signalling in platelets, chemokine signalling, insulin, and epidermal growth factor (EGF) and platelet-derived growth factor signalling

(Arcaro *et al.*, 2000, MacDougall *et al.*, 2004). There are three mammalian isoforms of class II PI3Ks: PI3K-C2 α , PI3K-C2 β and PI3K-C2 γ (Foster *et al.*, 2003). In mammalian studies, most PI3K-C2 α and PI3K-C2 β forms are ubiquitously expressed, whereas PI3K-C2 γ can be found only in hepatocytes. *In vitro* experiments by Foster *et al.* (2003) showed that Class II PI3Ks are able to phosphorylate PI and PI(4)P but not PI(4,5)P₂. Although little is known about the functions of class II PI3Ks *in vivo*, upon lysophosphatidic acid (LPA) stimulation, PI(3)P formation can be inhibited at the plasma membrane in PI3K-C2 β knockdown cells (Maffucci *et al.*, 2005). Moreover, a study by Maffucci *et al.* (2005) highlighted that once PI3K-C2 β is activated, they are recruited towards the plasma membrane which is similar to the behaviour of class I PI3Ks. PI3K-C2 α is reported to be a target for a growing number of receptors in the plasma membrane and is associated with clathrin-coated vesicles (CCVs) (Domin *et al.*, 2000). It is important to note that of all the mammalian enzymes, PI3K-C2 α is the most resistant to wortmannin, a common inhibitor of PI3K (Arcaro *et al.*, 2000). It is known that class II PI3Ks are the least common of all three classes of PI3K.

Class III – The first class III PI3K was identified in *Saccharomyces cerevisiae* as a structure known as Vacuole protein sorting mutant 34 (Vps 34). Vps 34 is reported to be associated with a protein kinase, Vps 15, which is described to be the regulatory subunit of Vps 34. Class III PI3Ks are different from class I and II in that they are PI-specific enzymes producing only PI(3)P, which is an important phospholipid for the processes of membrane trafficking. *S. cerevisiae* class III PI3K, Vps 34 and Vps 15, are required for the secretion and sorting of proteins from the trans-Golgi to the vacuole (Stack *et al.*, 1993). The Class III PI3K Vps 34 is regulated by Vps 15 regulatory subunit through phosphorylation, allowing Vps 34 to be targeted to the Golgi membrane in *S. cerevisiae* (Stack *et al.*, 1995). Vps 34 enzymes are the sole PI3K that will only utilise phosphatidylinositol as a substrate; this is due to the make-up of the substrate recognition loop. However, class I and II PI3K have multiple basic residues that bind to PIP and PIP₂. In comparison to class I and II enzymes, the substrate region of Vps 34 is relatively uncharged; therefore, only limiting it to phosphatidylinositol (Backer, 2008).

Class III PI3Ks enzymes are localised at the cytoplasm of the intracellular membrane and are involved in the regulation of autophagy, phagosome formation and maturation and endosome to Golgi retrograde transport (Kihara *et al.*, 2001, Vieira *et al.*, 2001, Burda *et al.*, 2002). *Schizosaccharomyces pombe* and *S. cerevisiae* do not have class

I PI3Ks to generate PI(3,4,5)P₃ as they only possess class III PI3K. However, research suggests that the synthesis of PI(3,4,5)P₃ requires Vps 34 and PI(4,5)kinase (Mitra *et al.*, 2004). In the study of autophagy, one group found that in mammalian cells autophagosomes function is largely impaired in Vps 34-null cells. This statement was supported by the lack of electron-dense material in intracellular vacuoles identified through EM studies (Jaber *et al.*, 2012). The studies of Vps 34-null cells (deletion of 755 of the 887 amino acids of Vps 34) show that Vps 34 is important in functional autophagy and crucial for normal liver and heart function in mice (Jaber *et al.*, 2012). Apart from yeast and human cells, the homologues of Vps 34 have been identified in *Dictyostelium discoideum*, *Drosophila melanogaster* and *Caenorhabditis elegans* (Yan and Backer, 2007).

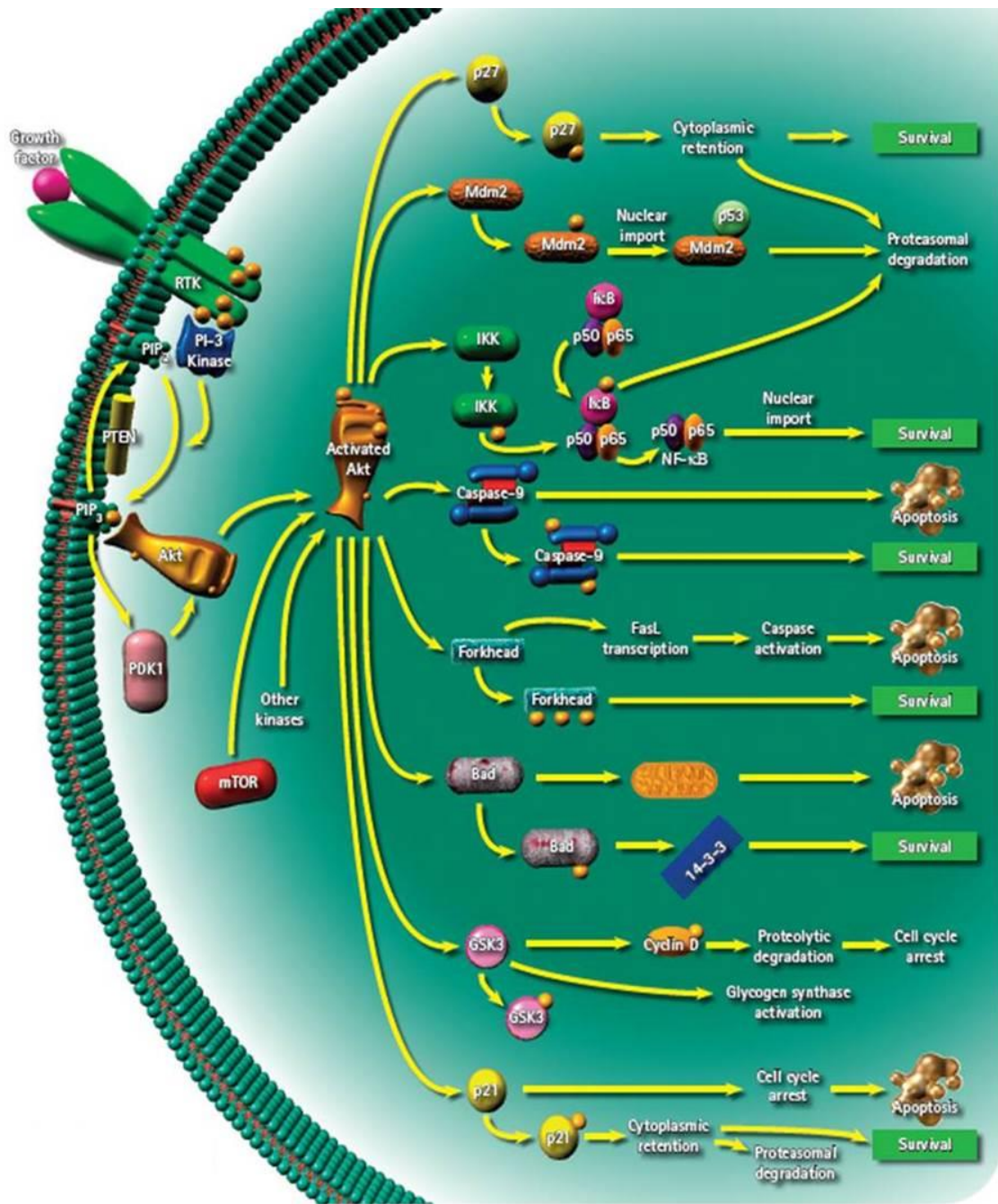


Figure 1.3: Overview of intracellular signalling transduction pathways to regulate chemotaxis involving PI3K, Akt/PKB and other components.

PI(3,4,5)P₃ is essential to the recruitment and activation of several molecules such as PKB, PDK1 and other kinases. Growth factor binding to the receptor tyrosine kinase (RTK) initiates PI3K activation. Activated PI3K produces PIP₃ at the leading edge, thus initiating several molecules such as AKt/PKB, PDK1, and mTOR, which then continue to further activate other components within the signalling pathway. This Figure illustrates the importance of PI3K and the critical role it has in the formation of PI(3,4,5)P₃, an essential component in this intracellular signalling cascade. Furthermore, PTEN acting as a phosphatase to dephosphorylate phosphatidylinositol can negatively regulate intracellular levels of PI(3,4,5)P₃. Image adapted from Merck Biosciences.

1.5 Phosphatases

Polyphosphoinositide phosphatase PTEN protein has been identified in the human body and linked to human diseases. PTEN is a phosphatase protein and its role in dephosphorylation leads to its involvement in regulation of the cell cycle, preventing cells from growing and dividing too rapidly (Chu *et al.*, 2004). PTEN is a phosphatidylinositol 3,4,5-triphosphate phosphatase that negatively regulates intracellular levels of PI(3,4,5)P₃ in cells and functions as a tumour suppressor by negatively regulating the PKB signalling pathway. It is described as a tumour suppressor because the mutated PTEN gene increases the risk of tumorigenesis. If PTEN is mutated, the level of PI(3,4,5)P₃ in the cell will increase, which results in uncontrolled downstream signalling through the PKB signalling pathway. The consequences include increased cell cycling, cell division and the prevention of programmed cell death, all of which can lead to tumour formation (Pendaries *et al.*, 2003).

The dual-specific lipid phosphatases, Myotubularin (MTM) and MTMR, are dual-specific phosphatases that dephosphorylate PI(3)P and PI(3,5)P₂, suggesting an involvement in intracellular trafficking and membrane signalling (Majerus *et al.*, 2003). There are 14 members of the ubiquitously expressed MTMR phosphatases, eight of which are catalyst active phosphatases, while six are inactive due to their lack of catalytically essential residues (Bolis *et al.*, 2006). In recent studies, a truncating mutation has been found in the hMTMR2 gene, which has 65% sequence homology to hMTM1. Patients with these mutations were found to develop an autosomal recessive form of Charcot-Marie-Tooth disease (type 4B), which is a demyelinating motor and sensory neuropathy linked to chromosome 11q23 (Laporte *et al.*, 2001, Nicot and Laporte, 2008). Mutation in the MTM1 gene causes an X-linked myotubular myopathy, a severe congenital myopathy disorder that affects new-born males with an estimated 1 out of every 50,000 worldwide (McEntagart *et al.*, 2002).

1.6 PI3K inhibitors

The study of PI3Ks has determined the important functional roles they play in various cell types with the help of PI3Ks inhibitors. Several approaches can be applied to measure the effects of PI3K inhibition with the treatment of wortmannin and LY294002, two common PI3K inhibitors. Exposure of PI3K inhibitors on mammalian cells at high concentrations causes the inhibition of cell growth and apoptosis (Stein and Waterfield,

2000). The *in vivo* approach aims to investigate the function of PI3K and has been carried out by labelling cells directly with a radioactive phosphate and the subsequent harvesting of lipids for analysis following inhibitor treatment. The inhibition is measured by determining the level of radioactive phosphate in phosphorylated products compared with untreated controls by separation, using either thin layer chromatography or high pressure liquid chromatography (Vlahos *et al.*, 1994, Woscholski *et al.*, 1994a, Arcaro and Wymann, 1993).

The PI3K inhibitor wortmannin, derived from the fungal metabolite *Penicillium funiculosum*, was originally known as a potent inhibitor of the phagocytes, neutrophils respiratory burst and was subsequently shown to inhibit smooth muscle myosin light chain kinase (smMLCK) (Baggiolini *et al.*, 1987; Nakanishi *et al.*, 1992). However, it later became apparent that wortmannin is a far more potent inhibitor of PI3Ks family in yeasts and mammals. Although Wortmannin was the first inhibitor of PI3K to be described, it has a broad inhibitory profile across different classes of PI3Ks (Gharbi *et al.*, 2007). It is important to note that when using wortmannin, its mode of action is through the irreversible inhibition of PI3Ks by covalent modification of a key ATP binding site (Walker *et al.*, 1999). Wortmannin causes a large conformational change to the ATP-binding site when it covalently modifies Lys 833 (Class IB PI3K), preventing the binding of substrates from taking place (Figure 1.4) (Walker *et al.*, 2000). In mammalian cells, wortmannin is effective in nanomolar concentrations; at higher concentrations, wortmannin can inhibit several protein kinases such as polo-like kinase 1 (PLK1), phosphoinositide 4-kinase (PI4K) and the mammalian target of rapamycin (mTOR) (Bain *et al.*, 2007).

LY294002 is another commonly used inhibitor of PI3K. Although a less potent inhibitor of PI3Ks, LY294002 has been the inhibitor of choice when cells are incubated for prolonged periods because of its greater stability in aqueous solution (Walker *et al.*, 2000). LY294002 was synthetically generated based on the chemical structure of the bioflavonoid quercetin, which was shown to inhibit mammalian PI3Ks (Matter *et al.*, 1992). LY294002 inhibits PI3Ks and other protein kinases by acting as a competitive inhibitor for the ATP binding site within the kinase domain (Walker *et al.*, 2000). A study by Bains *et al.* (2007) showed that using a cell-based assay, LY294002 inhibits class I PI3Ks at a concentration of 10-50 μ M. It has also been reported to inhibit other kinases, such as Target of rapamycin complex 1 (TORC1), Casein kinase II (CKII) and Polo-like kinase (PLK1) at concentrations similar to those that inhibit PI3Ks (Bains *et al.*, 2007). The inhibition of

these enzymes by LY294002 is reversible upon the removal of the inhibitor. The molecular structure of LY294002 is presented in Figure 1.4.

PI-103 is a small synthetic molecule of the pyridofuopyrimidine class. In cell-based assays PI-103 blocks class I PI3Ks completely at a concentration of 0.5 μM (Bain *et al.*, 2007). Although PI-103 is more potent than inhibitors that are selective only for PI3K (Wortmannin, LY294002), PI-103 was shown to inhibit TORC1 with similar potency to Class I PI3K (Fan *et al.* 2006). The study of PI-103 showed high anti-tumour activity in glioma xenografts, where PI-103 induced G(0) – G(1) phase causing cell cycle arrest and apoptosis, as characterised by activation of caspase-3 and caspase-9 (Chiarini *et al.*, 2009). Furthermore, PI-103 caused PKB dephosphorylation leading to the activation of a downstream protein kinase, glycogen synthase kinase-3 β .

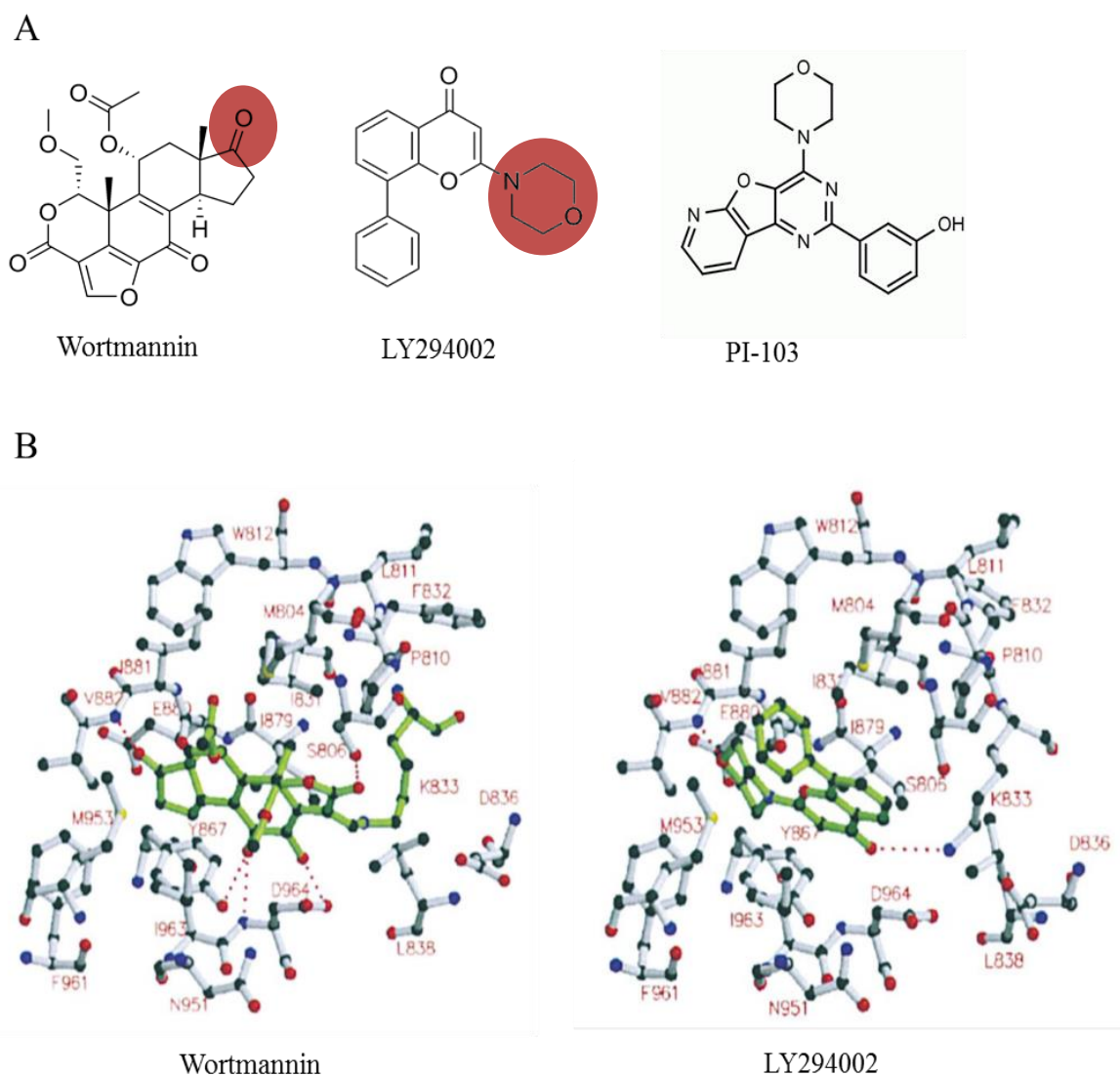


Figure 1.4: The mechanism of two common inhibitors binding into PI3K active site.

A, illustration of the molecular structure of wortmannin, LY294002 and PI-103. Both wortmannin and LY294002 bind within the ATP-binding site of *Sus scrofa* PI3K γ and interact with Val 882 (circled in red). B, illustration of wortmannin and LY294002 binding to the PI3K active site. Unlike LY294002, wortmannin causes a large conformational change to the ATP-binding site when it covalently modifies Lys 833 so that the residues 832-838 and 871-876 move away from the pocket. This illustration was adapted from Walker *et al.* (2000).

1.7 Specificity and targets of PI3K inhibitors

To understand the effect of PI3K in cellular proliferation, a PI3K inhibitor was used to determine this through cell counts over a given time course *in vitro*. LY294002, inhibitor of PI3K, was used at different concentrations to see whether the inhibition of cell proliferation occurred in the trophozoite of *G. intestinalis* (Cox *et al.*, 2006). One of the

main reasons behind the development of PI3K inhibitors is the fact that mutations in PI3K or PTEN can cause cancers (Bain *et al.*, 2007).

Giardia has 276 putative protein kinases, none of which are tyrosine-specific or histidine kinases. However, it is important to note that 180 of these putative protein kinases belong to the NIMA (Never in mitosis Gene A)-Related Kinase (NEK) family and that 137 of them are predicted to be catalytically inactive. Most organisms on the other hand have fewer than 10 NEK kinases (Morrison *et al.*, 2007). Below are some of the important protein kinases and their descriptions:

Casein Kinase II (CKII) – This is a serine/threonine-selective protein kinase that phosphorylates acidic proteins such as Casein. It consists of a tetramer of 2 α subunits and 2 β subunits. Casein kinase II plays a key role in cell cycle control, cellular differentiation and proliferation (Allende *et al.*, 1995; McElhinny *et al.*, 1996). Furthermore, it has been reported that CKII activity is increased in response to Wnt3a stimulation and is essential for the Wnt signalling pathway (Gao and Wang, 2006). The mammalian study of CKII suggests that inhibitors of CKII could increase the host's innate and adaptive immunity against cancer by enhancing the cytotoxicity of NK cells and cytotoxic T cells (Kim *et al.*, 2008). The precise mechanism of CKII function is not clearly explained; however, high levels of CKII are associated with rapid proliferating cells even though CKII is expressed in all stages of the cell cycle (Bosc *et al.*, 1999, Bain *et al.*, 2007). Bain *et al.* (2007) illustrated that upon exposure of LY294002 at a concentration of 50 μ M to CKII, the percentage activity of CKII was reduced by >75% relative to untreated enzyme.

Polo-like kinase 1 (PLK1) – This enzyme is involved in cell cycle regulation. It mediates G2/M transition, the activation of cdc 5 and mitotic processes, including centrosome maturation, bipolar spindle formation, activation of the anaphase-promoting complex, chromosome segregation and actin ring formation (cytokinesis). They are all important in the regulation of key steps during cell division, like DNA damage repair pathways, apoptosis and progression of the cell cycle (van de Weerd and Medema, 2006). Studies have shown that the loss of PLK1 expression can induce pro-apoptotic pathways and inhibit growth (Spankuch-schmitt *et al.*, 2002). Polo-like kinase therefore is important for the study of cell cycle regulation in a variety of organisms as well as *Giardia*. To determine the roles of PLK in *Giardia* cell cycle regulation, exposure of trophozoites to LY294002 (50 μ M) could lead to cell cycle arrest. Bain *et al.* (2007) demonstrated that

exposure of purified PLK1 protein to LY294002 will reduce the percentage activity of the purified protein by 73%.

Homeo-domain interacting protein kinase 2 (HIPK2) – This protein kinase belongs to the HIPK serine-threonine kinase family, which also includes two other members, HIPK1 and HIPK3. HIPK2 is a polypeptide composed of 1189 amino acids and was reported to act as a co-repressor for homeodomain transcription factors and is highly conserved in various organisms (Pierantoni *et al.*, 2002; Giraud *et al.*, 2004). HIPK2 localises to nuclear speckles, since it contains multiple nuclear localisation signals and a speckle retention signal (SRS) (Kim *et al.*, 1999). Nuclear speckles are also known as splicing speckles. Speckles are subnuclear structures that are enriched in pre-mRNA splicing factors that are located in the interchromatin regions of the nucleoplasm of mammalian cells. The proteins encoded by HIPK family genes all have functional domains, such as a kinase domain, a homeodomain-interacting domain, a PEST sequence and a tyrosine and histidine residue-rich domain (Kim *et al.*, 1999). Recent studies have shown that HIPK2 interacts with p53, a tumour suppressor protein, and carboxyl-terminal-binding protein, a co-repressor protein for various transcription factors. These interactions were reported to induce apoptosis, involving the kinase activity of HIPK2 (D’Orazi *et al.*, 2002). The tumour suppressor p53 is believed to play a central role in detecting DNA damage and directs the nature of the subsequent cell responses. These reports suggest that HIPK2 interacts with some proteins that regulate cell growth and cell differentiation. Therefore, studying the inhibition of HIPK2 in *Giardia* may influence the cell growth and differentiation of trophozoites. Bain *et al.* (2007) showed that HIPK2 can be inhibited when exposed to LY294002 at 10 μ M with 38% of activity remaining.

Glycogen synthase kinase-3 (GSK-3) is another essential putative protein kinase in *Giardia* that is involved in signal transduction, cell survival and protein synthesis. GSK-3 is a ubiquitously expressed, highly conserved serine/threonine protein kinase found in all eukaryotes. Originally, it was identified as a regulator of glycogen metabolism, GSK-3 acts as a downstream regulatory switch for many signalling pathways, for example, cellular responses to Growth factors (Figure 1.5), Insulin, WNT, RTKs (receptor tyrosine kinases) and GPCR (Sayas *et al.*, 2006; Ciaraldi *et al.*, 2010; Wu and Pan, 2010). The activity of GSK-3 is inhibited by PKB phosphorylation in response to growth factor stimulation (Cantley, 2002). In addition to glycogen synthase, GSK-3 phosphorylates a broad range of substrates including several transcription factors and translation initiation factor (eIF2B)

(Welsh *et al.*, 1996). GSK-3 has been implicated in the signalling pathways in *Dictyostelium* (Harwood *et al.*, 1995), *Drosophila* (Siegfried *et al.*, 1992) and *Xenopus* (Dominguez *et al.*, 1995).

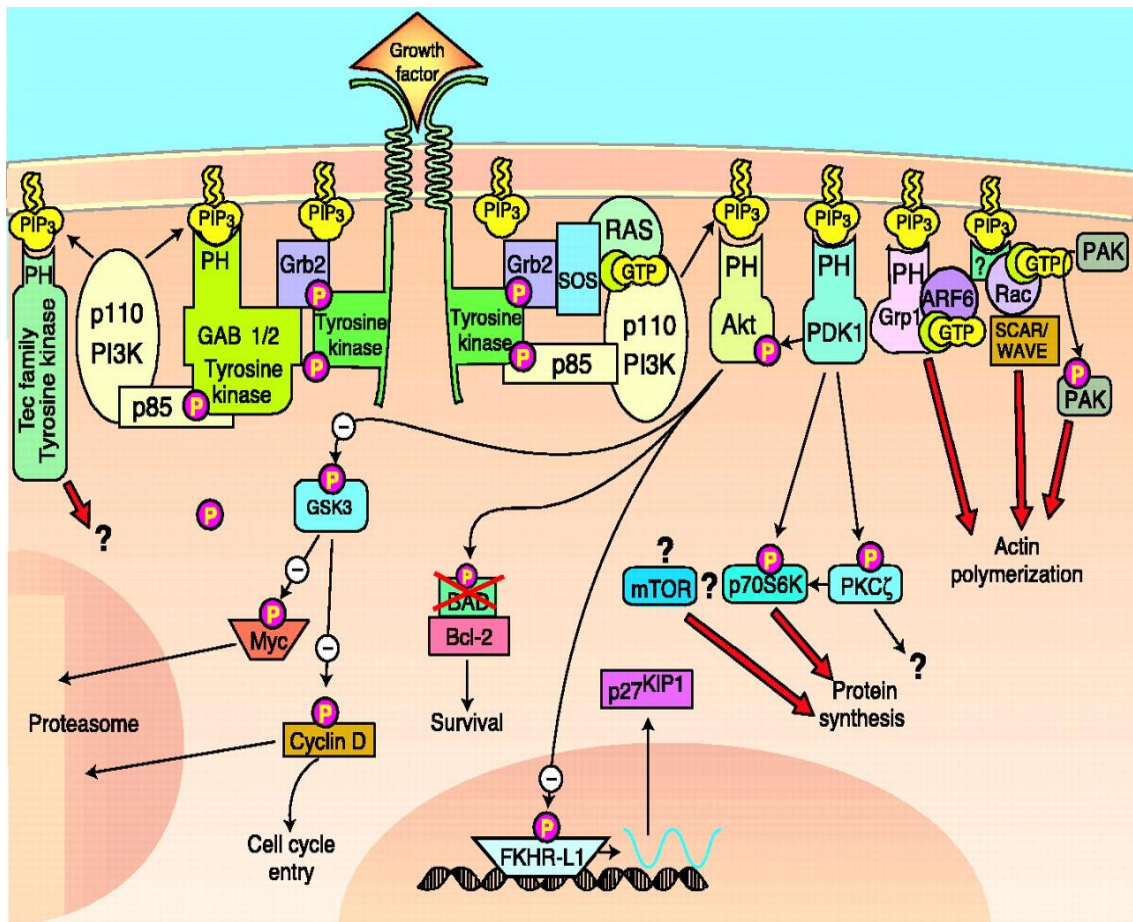


Figure 1.5: Signalling pathways illustrating GSK3 putative protein kinase regulation in mammalian cells.

This is a complex signalling pathway involving many types of proteins which affect cell growth, cell survival and cell movement. Activation of the growth factor receptor protein stimulates PI3K phosphorylation, thus in turn activating signalling molecules such as PKB/Akt. PKB/Akt then triggers many different pathways blocked by GSK3, because GSK3 can be inhibited by PKB/Akt phosphorylation (which is part of the insulin signal transduction). This diagram is an overview of the complex pathway that is regulated throughout the mammalian cells. This image was adapted from Cantley (2002).

In mammalian cells, there are two isoforms of GSK3 encoded by distinct genes: GSK-3 α and GSK-3 β (Woodgett, 1990). GSK-3 α has a mass of 51 kDa, whereas GSK-3 β has a mass of 47 kDa. The main reason for the size difference is due to a glycine-rich extension at the N-terminus of GSK-3 α (Figure 1.6).

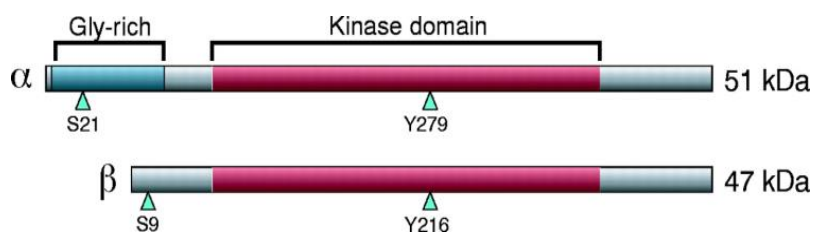


Figure 1.6: The mammalian schematic of GSK-3 α and GSK-3 β .

The site of serine (S21 and S9) and tyrosine (Y279 and Y216) phosphorylation indicated through the blue arrowheads. The N-terminal domain on GSK-3 α and GSK-3 β are unique glycine enriched conserved kinase domains. Adapted from Doble and Woodgett (2003).

GSK-3 is a key regulator in several physiological processes; many pathways that use GSK-3 as a regulator have links to human diseases. In mammalian cells, GSK-3 has been implicated in non-insulin-dependent Diabetes Mellitus and the generation of neurofibrillary tangles (NFTs) that are associated with Alzheimer's disease (Doble *et al.*, 2003). GSK-3 inhibitors can play an important role in treating disease affected by aberrant GSK-3 activity. Inhibitors of GSK-3 are being developed as potential drugs to treat diabetes, stroke, Alzheimer's and other diseases (Cohen and Goedert, 2004). A study found that CT99021 is the most potent and specific inhibitor *in vitro* (Bain *et al.*, 2007). CT99021 inhibits GSK-3 at nanoMolar concentrations and it inhibits CDK2-cyclin A about 50-fold less potency and did not significantly affect other protein kinases tested in the same panel at 1 μ M (Bain *et al.*, 2007). Another inhibitor of GSK-3 is lithium ions; LiCl inhibit GSK-3 at the millimolar level and it has been found to stabilise the mood in patients suffering from bipolar disorder (Geddes *et al.*, 2010). The biochemical actions of lithium have been identified but the mechanisms for its therapeutic action are unknown (Jope, 1999, Phiel and Klein, 2001). Lithium has been shown to be a direct, reversible inhibitor of GSK-3 with an IC_{50} value of approximately 2 mM, acting as a competitive inhibitor of Mg^{2+} (Ryves and Harwood, 2001). The half maximal inhibitory concentration (IC_{50}) represents the concentration of a drug that is required for 50% inhibition *in vitro*. A more recent study found that LiCl inhibited GSK-3 β activity *in vitro* more strongly than any of the other protein kinases tested (Bain *et al.*, 2007). On the other hand, LiCl also inhibits other protein kinases with slightly lower potency, such as MAPK-integrating protein kinase 1 and 2 (MNK1, MNK2), smooth muscle myosin light chain kinase (SmMLCK), phosphate kinase

(PHK), checkpoint kinase 2 (CHK2), NIMA (never in mitosis in *Aspergillus nidulans*)-related kinase 6 (NEK6), elongation-factor-2 kinase (EF2K), homeodomain-interacting protein kinase 3 (HIPK3), inhibitory kB kinase (IKK) and TANK-binding kinase 1 (TBK1) (Bain *et al.*, 2007).

1.8 Putative PI3Ks in *Giardia*

In a report by Cox *et al.* (2006), it was shown that the *G. intestinalis* genome encodes two PI3Ks which share homology with the Class I and Class III PI3Ks. The evidence obtained from bioinformatics showed alignment of *Giardia* PI3Ks and Class I PI3K-kinase domain from *Sus scrofa*, Ss PI3K γ (GenePept: NP_999104), a structurally and functionally characterised PI3K sequence (Figure 1.7).

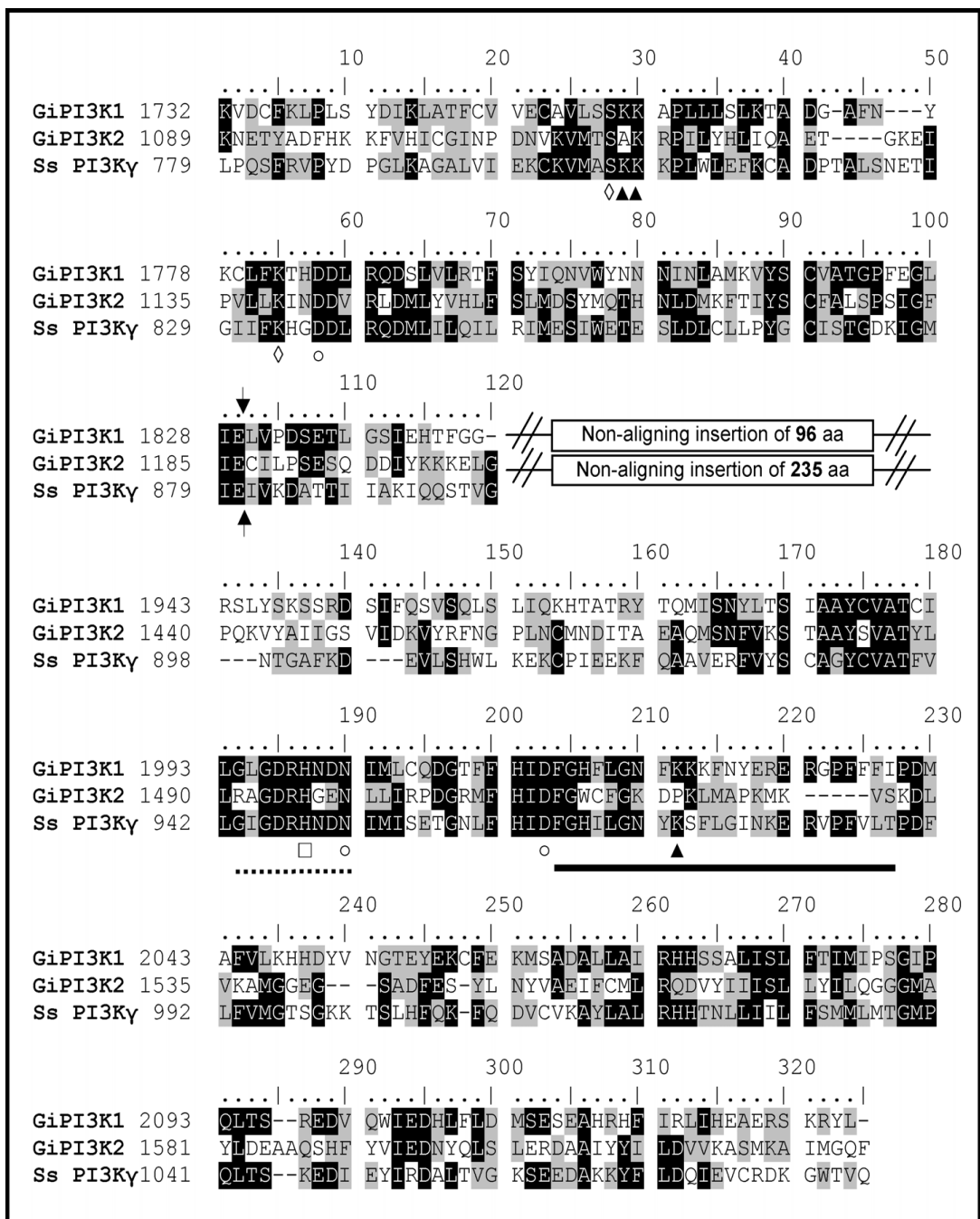


Figure 1.7: Detailed sequence analysis of the kinase domains of GiPI3K1 and GiPI3K2.

This figure illustrates the multiple sequence alignment of the kinase domain of giardial PI3Ks with a structurally characterised Class I PI3K-kinase domain from *Sus scofa*, Ss PI3K γ (GenePept: NP_999104) highlighting the conserved region of functional residues. Sequences were aligned using Clustal W. Arrows indicate the boundary between the N- and C-terminal lobes of the kinase domain for the *S. scofa* sequence. Insertions in the kinase domain of GiPI3K1 and GiPI3K2 are shown in boxes. Solid underlined residues indicate activation loop residues in the *S. scofa* sequence essential for substrate specificity. Dashed underlined residues indicate catalytic loop residues in the *S. scofa* sequence. Key: \diamond , ATP binding residues; \blacktriangle , PI-binding residues; \circ , metal binding residues; \square , possible substrate-activating base/nucleophile to that attack γ -phosphate of ATP. Figure was taken directly from Cox *et al.* (2006).

This detailed multiple alignment analysis of GiPI3K1 and GiPI3K2 kinase domains against PI3K γ (class IB PI3K) shows that all of the residues required for ATP binding and kinase activity in the *S. scrofa* PI3K γ are conserved in both GiPI3K1 and GiPI3K2 (Cox *et al.*, 2006). GiPI3K2 is reported to lack one of the lysine residues that is thought to interact with the I-phosphate of PI substrate (Lys-807 in the *S. scrofa* sequence) and a second lysine thought to act as a ligand for the 5-phosphate of PI(4,5)P₂ (Walker *et al.*, 1999). These features are common to other functional class III PI3K isoforms such as *D. discoideum* DdPIK5, which are also thought to be specific to PI only, since their short activation loops cannot accommodate the 4-phosphate of PI(4)P substrate. Therefore, this analysis highlighted that GiPI3K1 and GiPI3K2 could be functional PI3Ks belonging to the Class I and Class III isoforms, respectively (Table 1.1).

Table 1.1: Analysis of the giardial PI3K domains.

Percentage identity values for the full-length and domain-only sequences of GiPI3K1 and GiPI3K2 with other PI3K isoforms following their sequence alignment. This table was taken directly from Cox *et al.* (2006).

	GiPI3K1	GiPI3K2
Full- length	39% to <i>Dictyostelium discoideum</i> PIK1, a Class I PI3K	34% to <i>Glycine max</i> Vps34-like (Class III) PI3K
Ras Binding Domain (RBD)	41% to <i>Homo sapiens</i> Class IB p110 γ PI3K	Absent
PIK	28% to <i>H. sapiens</i> Class IA p110 α PI3K	27% to <i>Caenorhabditis elegans</i> Vps34-like (Class III) PI3K
Kinase	39% to <i>D. discoideum</i> PIK1	33% to <i>Glycine max</i> Vps34-like (Class III) PI3K

The catalytic domain sequences of Class I, II and III PI3Ks were used to search for sequence similarity to identify giardial genes encoding putative PI3Ks. Table 1-1 shows the open reading frames of sequences that are similar to PI3K genes and are therefore called

GiPI3K1 and *GiPI3K2*. The predicted open reading frames are 6,468 bp and 4,917 bp in length, respectively. *GiPI3K1* is predicted to encode a 2,155 amino acid protein (GenPept: EAA41385) with a molecular mass of 242 kDa and *GiPI3K2* is predicted to encode a 1,638 amino acid protein (GenPept: EAA40923) with a molecular mass of 183 kDa.

The characteristic domains of PI3K are present in the typical conformation for both *GiPI3K1* and *GiPI3K2*, with the former consisting of Ubiquitin/RBD-like, C2, PIK and kinase domains and the latter consisting of C2, PIK and kinase domains. Interestingly, it was found that both putative kinase domains appeared to be interrupted by long insertions compared to other well-studied PI3Ks. This is shown in Figure 1.8.

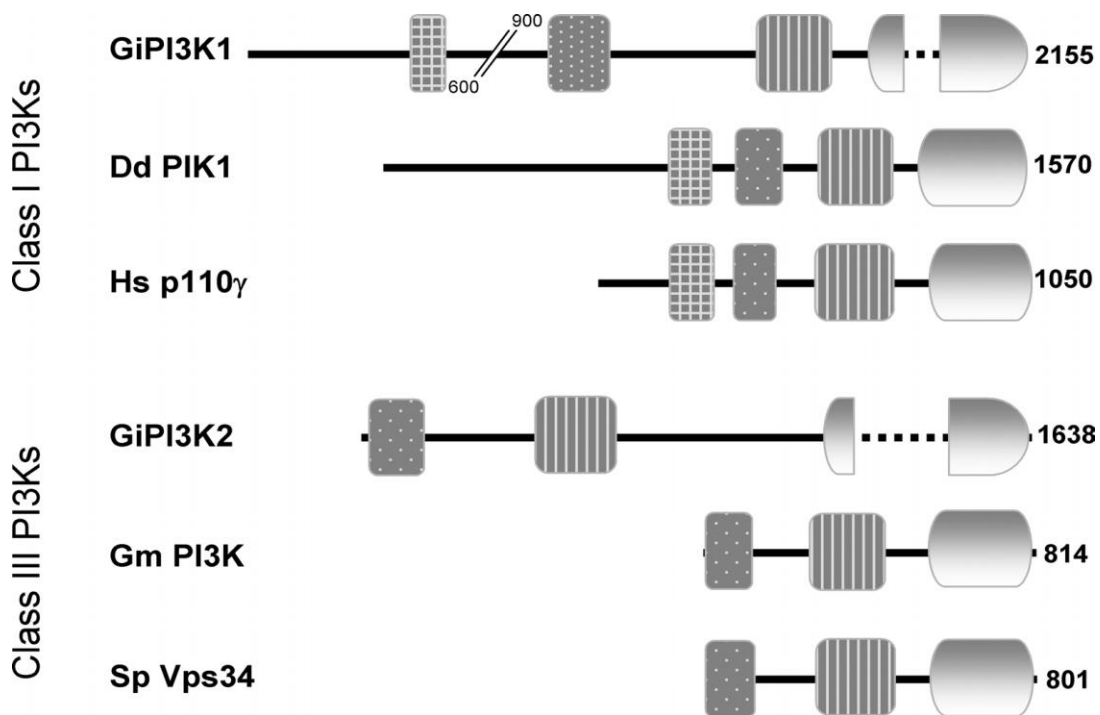


Figure 1.8: Domain structure of *GiPI3K1* and *GiPI3K2* compared to other PI3Ks.

Here, *GiPI3K1* is compared to *Dd PIK I*, *D. discoideum* class I PI3K (GenPept: AAA85721) and to *Hs p110 γ* , *H. sapiens* class I PI3K (GenPept: NP_002640). The *GiPI3K1* sequence is interrupted for the sake of clarity. The second half shows *GiPI3K2* compared to *G. max* class III PI3K (GenPept: AAA64468) and to *Sp Vps 34*, *Schizosaccharomyces pombe* Class III PI3K (GenPept: AAC49133). The number indicates the count of amino acid residues. Different shading illustrates various domains: checked, Ras binding; dotted, C2; striped, PIK; gradient, kinase. Figure taken from Cox *et al.* (2006).

Characterisation of *GiPI3K1* and *GiPI3K2* gene products through RT-PCR analysis provides evidence that both *GiPI3K* genes are expressed in trophozoites and encysting cells (Figure 1.9). This suggests that *GiPI3K* plays an important role during growth and encystation. Long insertions of giardial PI3Ks were highlighted, and appear to separate the two lobes of their putative kinase domains. They are unique to the giardial sequences and it

is possible that they may form part of the protein sequence as they are not intron-derived. These insertions in giardial sequences have been suggested to serve as useful drug targets (He *et al.*, 2005). This would allow the drugs to specifically and effectively select and target giardial PI3Ks on the basis of their insertion sequences because PI3K activity in *G. intestinalis* is important for parasite proliferation.

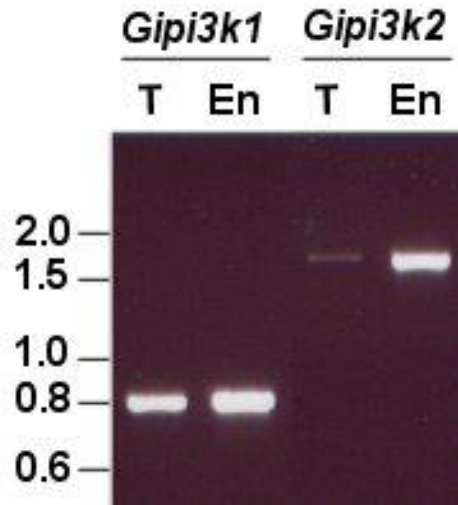


Figure 1.9: The analysis of GiPI3K1 and GiPI3K2 using RT-PCR.

(T) Extracted and purified RNA from trophozoites and (En) 36-hour encysting cells converted to cDNA via a reverse transcriptase (RT) reaction and subjected to PCR to amplify regions encoding the apparent insertions in GiPI3K1 and GiPI3K2. The resulting PCR products were separated on an agarose gel. Negative controls were included to ensure that the products originated from RNA only. Molecular size markers are in kilobases. This figure was taken from Cox *et al.* (2006).

The work of Cox *et al.* (2006) also illustrated the inhibitory effect of LY294002 on exponentially growing trophozoites. The results showed that cells remain approximately constant with no significant growth observed at the concentration of 50 μ M LY294002. This suggests that LY294002 may affect cell proliferation by inducing cell cycle arrest. LY294002 has been the inhibitor of choice when cells are incubated for prolonged periods because wortmannin is unstable in aqueous solutions. When trophozoites were exposed to wortmannin in a range of concentrations (50 – 500 nM) there was no effect observed on cell number relative to the control (Cox and Tovar unpublished work). Moreover, observation in the work of Cox *et al.* (2006) showed that trophozoites treated with LY294002 did not undergo any dramatic changes in their morphology or motility, thus demonstrating the selective effect of LY294002 on the cell cycle of *Giardia*.

When the PI3K inhibitor LY294002 was added to cultured trophozoites, it specifically and significantly inhibited the proliferation of trophozoites at a concentration of 50 μ M. However, the effect of the LY294002 inhibitor is reversible; once the inhibitor is removed, the trophozoites grow exponentially up to equivalent numbers in the untreated control sample. These data (Cox and Tovar, unpublished work) suggest that cell cycling in *G. intestinalis* is controlled by PI3K activity. PI3K-inhibited trophozoites remain stationary through the addition of LY294002. Further observations show increased levels of cyst wall protein 2 (CWP2) mRNA, CWP2 protein and abundance of CWP2 localised to encystation specific vesicles (Cox and Tovar, unpublished data) which suggests that encystation may be regulated by PI3K activity. Conversely, in the control sample, PI3K activity may normally be required to prevent *Giardia* initiating the process of encystation. However, even though exposure to LY294002 may initiate the encystation of trophozoites, cyst maturation failed to complete (Cox and Tovar, unpublished work). Therefore, encystation could not be completed, possibly due to the PI3K activity required for CWP2 processing and/or dispersal to form the cyst wall.

1.9 Aims and objectives

Accumulating evidence suggests that PI3K signalling pathways may operate in *Giardia* and that lipid signalling may be important in the regulation of parasite differentiation. LY294002 has been shown to inhibit PI3K and different kinases, more specifically when *Giardia* trophozoites are exposed to LY294002, where positive inhibition in the cell growth of trophozoites was observed. The study of PI3Ks is important for many types of cells; this knowledge together with work on PI3Ks in *Giardia* may hold the key for future discovery in drug targeting approaches.

This project aims to investigate the range and nature of molecular components involved in *G. intestinalis* intracellular signalling cascade and drug susceptibility. The project has the following specific objectives:

- To identify genes encoding additional proteins that may be involved in lipid signalling cascades through *Giardia* genomic database mining.
- To determine the effect of specific inhibitors of central signalling proteins (such as PI3K and GSK-3 β).
- To develop a reproducible method of quantifying *Giardia* trophozoites using spectrometry.
- To detect and quantify PI(3,4,5)P₃ using a PIP₃ Mass ELISA assay for evidence of PI3K activity in *Giardia*.
- To investigate the effect of PI3K inhibitor LY294002 on *G. intestinalis* cells by using an immunofluorescence labelling technique.
- To quantify and investigate the morphological differences of PI3K-inhibited *G. intestinalis* cells using scanning and transmission electron microscopy.

CHAPTER 2: Materials and Methods

2.1 Bioinformatics

2.1.1 *Giardia intestinalis* genome database search with translation BLAST and pairwise alignment

The *Giardia intestinalis* genome database is available online (<http://giardiadb.org/giardiadb/>) and the National Centre for Biotechnology Information (NCBI) website (<http://www.ncbi.nlm.nih.gov/>). The search for polyphosphoinositide kinases and other proteins was performed using the NCBI “BLAST” (Basic Local Alignment Search Tool) with *G. intestinalis* PI3Ks (*GiPI3K1* and *GiPI3K2*). *GiPI3K1* and *GiPI3K2* (GenPept: EAA41385 and EAA40923) were the PI3K proteins encoded by the *G. intestinalis* genome (Cox *et al.*, 2006). To confirm these findings, the protein query sequences used were representatives of three classes of polyphosphoinositide kinases: Class I *Homo sapiens* p110 α (GenPept: NP_006209), Class II *H. sapiens* PI3K-C2 α (GenPept: NP_002636) and Class III *Saccharomyces cerevisiae* Vps34 (GenPept: NP_013341). Using the kinase domains of PI3K for the search translation, BLAST (tBLASTn) was adopted to search for common sequences in the *G. intestinalis* genome. The setting on the tBLASTn search was the default setting, showing an expectation value of 10. This means that 10 sequence matches are expected to be found only by chance and if the statistical significance in a match is greater than the expectant threshold, the match will not be reported. Five matched sequences of *G. intestinalis* open reading frames (ORFs) were predicted using tBLASTn and these sequences contain detailed information related to translated GenPept entries. The *Giardia* database three best match ORFs were GenPept: GL50803_14855, GL50803_17406 and GL50803_16558; these were submitted to tBLASTn and nucleotide-BLAST searches of non-redundant databases at NCBI to verify the similarity of *Giardia* PI3Ks sequences to the matched PI3K isoforms. The result of the matched PI3K sequences were pairwise aligned with default settings on BioEdit (Hall, 1999) against *Giardia* PI3K sequences for percentage identity and similarity values.

Using the above methods, the identification of other lipid component glycogen synthase kinase-3 (GSK-3) in *G. intestinalis* was achieved with giardial homologue searching and sequence alignments were completed. However, the initial protein query sequences used

were: *H. sapiens* GSK-3 α (GenPept: NP_063937.2) and *H. sapiens* GSK-3 β (GenPept: NP_002084.2). Matching sequence results from GSK-3 protein query search were two giardial homologs: GSKa (GenPept: GL50803_9116) and GSKb (GenPept: GL50803_17625). These two giardial homologs of GSK-3 were pairwise aligned using BioEdit (Hall, 1999) with default settings to access the percentage identity and similarity values to the similar sequences in non-redundant databases at the NCBI. Alignment was visualised using the BioEdit graphic view, which allows the comparison of each sequence with one another, therefore showing the similarities and certain identical residues following alignment. The pairwise alignments were then exported as rich text file formats and annotated manually using Microsoft Word 2010.

2.1.2 Protein analysis and identification of domains

The domain-prediction program SMART (Simple Modular Architecture Research Tool) website (<http://smart.embl-heidelberg.de/>) (Schultz *et al.*, 1998) was used to predict protein domains in giardial PI3K and GSK isoforms. To confirm the identity of the predicted domains, the investigated predicted domains of *Giardia* PI3Ks and GSKs were analysed using sequence-similarity searched against a non-redundant database. Using BioEdit (Hall, 1999), the predicted domains were pairwise aligned in the same way as described in 2.1.1 and was visualised through Graphic view, where identical and similar residues were highlighted after the completion of sequence alignment. The results from Graphic view were then exported as rich text file formats and annotated manually using Microsoft Word 2010.

2.1.3 Protein structure analysis

The protein prediction program PSIPRED version 3.3 (<http://bioinf.cs.ucl.ac.uk/psipred/>) was used to predict the secondary structure protein with the default settings (McGuffin *et al.*, 2000). Constructions of three-dimensional protein structures were carried out using Cn3D version 4.3 downloaded from the NCBI (<http://www.ncbi.nlm.nih.gov/Structure/CN3D/cn3d.shtml>). Cn3D was opened and run on a Microsoft Windows 7 PC. The program initially was used to open the three-dimensional structure of *H. sapiens* GSK-3 β (Protein Data Bank identification: 3SAY opened using Cn3D through the linked from NCBI). The sequence opened was aligned in the Cn3D viewer with the imported Serine/Threonine kinase catalytic domain sequences of either *G.*

intestinalis GSK isoforms GSKa or GSKb. The two *H. sapiens* sequences and giardial GSK sequences were aligned using the BLAST single option in the sequence/alignment viewer. The overlay option was chosen and the alignments were carried out on the three-dimensional visualisation of *H. sapiens* GSK-3 β . The Serine/Threonine kinase catalytic domains in *Giardia* GSKa and GSKb were aligned to *H. sapiens* GSK-3 β ; the colour red represented identity, while blue corresponded to similarity and grey areas denoted non-aligned residues. The images obtained were exported as PNG files, arranged using Microsoft PowerPoint 2010 and presented in Microsoft Word 2010.

2.1.4 Multiple alignments

Sequence alignment using the BioEdit program was previously completed using protein query sequences obtained from the Giardia DB and NCBI. In order to investigate these protein sequences, they were multiple-aligned using the CLUSTALW program with default settings. The complete multiple alignment using CLUSTALW was viewed using Graphic View, exported as a rich text format and opened in Microsoft Word 2010.

2.1.5 Protein subcellular localisation sites

Protein sequences were inputted into PSORTII and iPSORT to predict the subcellular localisation sites of the giardial GSKs. The PSORTII prediction program (<http://psort.hgc.jp/>) (Nakai and Horton, 1999) is a computer-based program which analyses the input sequence and predicts the protein localisation sites in the cells. The iPSORT prediction program (<http://ipsort.hgc.jp/>) (Bannai *et al.*, 2002) is also a computer-based program that predicts the subcellular localisation site for N-terminal sorting signals. Both programs were used with standard settings.

2.2 Cell culture

2.2.1 Trophozoite culture

G. intestinalis WB trophozoites were subcultured every 3 to 4 days and allowed to proliferate at 37°C in axenic filter-sterilised modified YI-S medium as follows: 800 ml YI broth (1.24 g K₂HPO₄, 0.6 g KH₂PO₄, 1.0 g NaCl, 30.0 g yeast extract (Sigma-Aldrich), 0.5 g dehydrated bovine bile (Sigma-Aldrich), 10.0 g glucose, 2.0 g L-cysteine HCL (Sigma-Aldrich), 0.2 g ascorbic acid, 22.8 mg ferric ammonium citrate (Sigma-Aldrich), distilled

H₂O, to 880 ml, pH 7.0-7.1), 20 ml vitamin mixture 18 (Biofluids Inc.) and 100 ml of (10 v/v) bovine serum (Sigma-Aldrich) heat inactivated at 56°C for 30 minutes to inactivate proteins of the complement pathway (Clark and Diamond, 2002). After 3 to 4 days, fully grown trophozoites (estimated population of 1×10^6 cells/ml) were placed in screw-capped borosilicate glass culture tubes containing 13 ml of medium, and 50 or 100 µl was inoculated.

2.2.2 Induction of *Giardia* encystation

After *Giardia* trophozoites were grown, with populations reaching approximately 1×10^6 cells/ml, the culture medium was poured away and replaced with encystation medium, as described in Kane *et al.* (1991); this contained the same components as the modified YI-S medium but with 10 g/L bile and an increased pH of 7.8. Encystation experiments were carried out over 14-168 hours at 37°C; cysts were harvested and counted to determine the time course of the appearance of cysts from 24 to 168 hours.

2.2.3 Cell counts

Cell counts were demonstrated by using a haemocytometer, where the averages were calculated, multiplied by dilution factors and multiplied by 10^4 to account for the volume counted; this was to determine the cells/ml and total cells present. Prior to cell counting, 13 ml tubes containing trophozoites were chilled on ice for 10 minutes and inverted a few times to allow trophozoites to detach from the glass surface. Then, 50 µl aliquots of trophozoite cultures were taken and mixed with the same volume of 4 w/v paraformaldehyde (PFA) for the immobilisation of trophozoites. Once immobilised, trophozoites were then pipetted onto a haemocytometer slide and counted using a light microscope set to 10 x magnification.

2.2.4 Purification and counting of cysts

To purify the cyst from trophozoites and encysting cells and to separate each individual cyst from cyst “islands”, the culture tubes were allowed to recover for 30 minutes at 37°C. The culture tubes were then centrifuged at 500 x g for 5 minutes and the supernatant was removed. The pellet was resuspended in 13 ml chilled double-distilled water and stored at 4°C overnight to lyse encysting cells and trophozoites. The tissue culture tube was then

vortexed for 2 minutes to break up the individual cysts. Following the vortex, a haemocytometer was used to count cysts, as described in 2.2.3.

2.2.5 Colorimetric quantitation of cell growth

2.2.5.1 Standard curve for colorimetric assay

A standardisation experiment was carried out using a known number of trophozoites to determine the linear responsive range of the spectrophotometer. Trophozoites that were grown for 72 hours were counted to reach a population range 2×10^6 cells/ml. Using table-top centrifugation, the cultures were centrifuged at $800 \times g$ for 10 minutes at 4°C . The pellets were concentrated with trophozoites and the supernatant was discarded. The pellets were resuspended with 1.3 ml of Phosphate-Buffered Saline (PBS) to allow cells to be concentrated by 10-fold. The final volume in each of the 96-well cell flat bottom tissue culture plates (Costar 3599) was $300 \mu\text{l}$. The different concentration of cells was calculated and pipetted into each well to reach a final volume of $300 \mu\text{l}$ (Figure 2.1). The blank wells contained PBS only. The cells were then fixed (see 2.2.5.3) and the different concentration of cells in the 96-well tissue culture plate was measured by using a spectrophotometer with an absorbance reading at 655 nm.

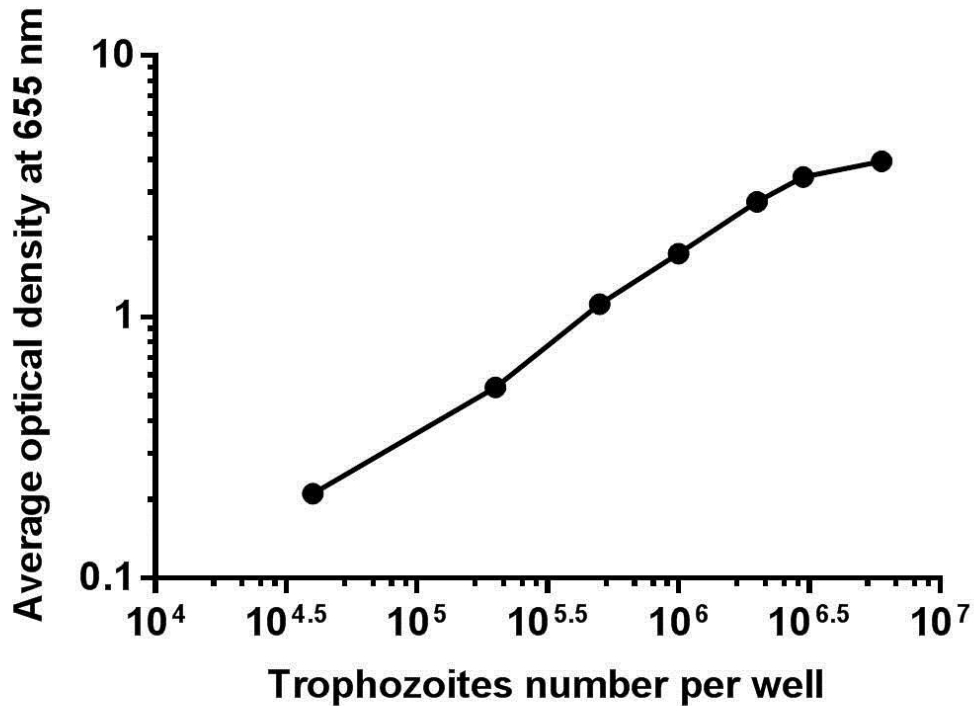


Figure 2.1: Standard curve for colorimetric assay

The standard curve of trophozoite number per well was measured by using the average optical density at 655 nm. Following 72 hours of incubation of trophozoite culture, cells were counted and different concentrations of cells were inoculated into each well, ranging from 4×10^4 cells to 6×10^6 cells in order to generate a standard curve plotted over a logarithmic scale.

2.2.5.2 Standard growth curve

Fully grown trophozoite cultures were placed on ice and counted to reach the population range of 1×10^6 cells/ml (2.2.1). *Giardia* trophozoites were inoculated into 18 borosilicate glass tubes with an individual tube containing 13 ml of fresh culture medium. The borosilicate glass tube was labelled 0, 24, 48, 72, 96, and 120 hours, and treated with inoculums of 0.1×10^6 cells/ml (Figure 2.2). Calculations to inoculate 0.1×10^6 cells/ml were completed using the following equation:

Inoculate trophozoites require/Number of fully grown trophozoites = Amount of inocula needed.

Every 24 hours, the preparation for transferring trophozoite populations into 96 well tissue culture plate was as follow. Culture tubes were place on ice for 10 minutes following the incubation time. Trophozoites were centrifuged to collect the pellet at 800 x g, 4°C for 10 minutes. Then, 10 ml of the supernatant was removed without disturbing the pellet and the rest was gently mixed and pipetted into 15 ml sterile disposable tubes (Sarstedt). Trophozoites were again centrifuged at 800 x g, 4°C for 10 minutes, to collect the pellet using a table-top centrifuge. The supernatant was completely removed without disturbing the pellet. Trophozoites were fixed by adding 100 µl of PBS and 100 µl of 4 w/v PFA and transferring into a 1.5 ml sterile centrifuge tube (Greiner bio-one). The sterile centrifuge tube containing trophozoites was centrifuged with the supernatant removed and then 300 µl of 1 x PBS was pipetted into each sterile centrifuge tube and vortexed. Cells were then fixed and the standard growth curve was determined using absorbance readings at 655 nm on the microplate reader (see 2.2.5.3).

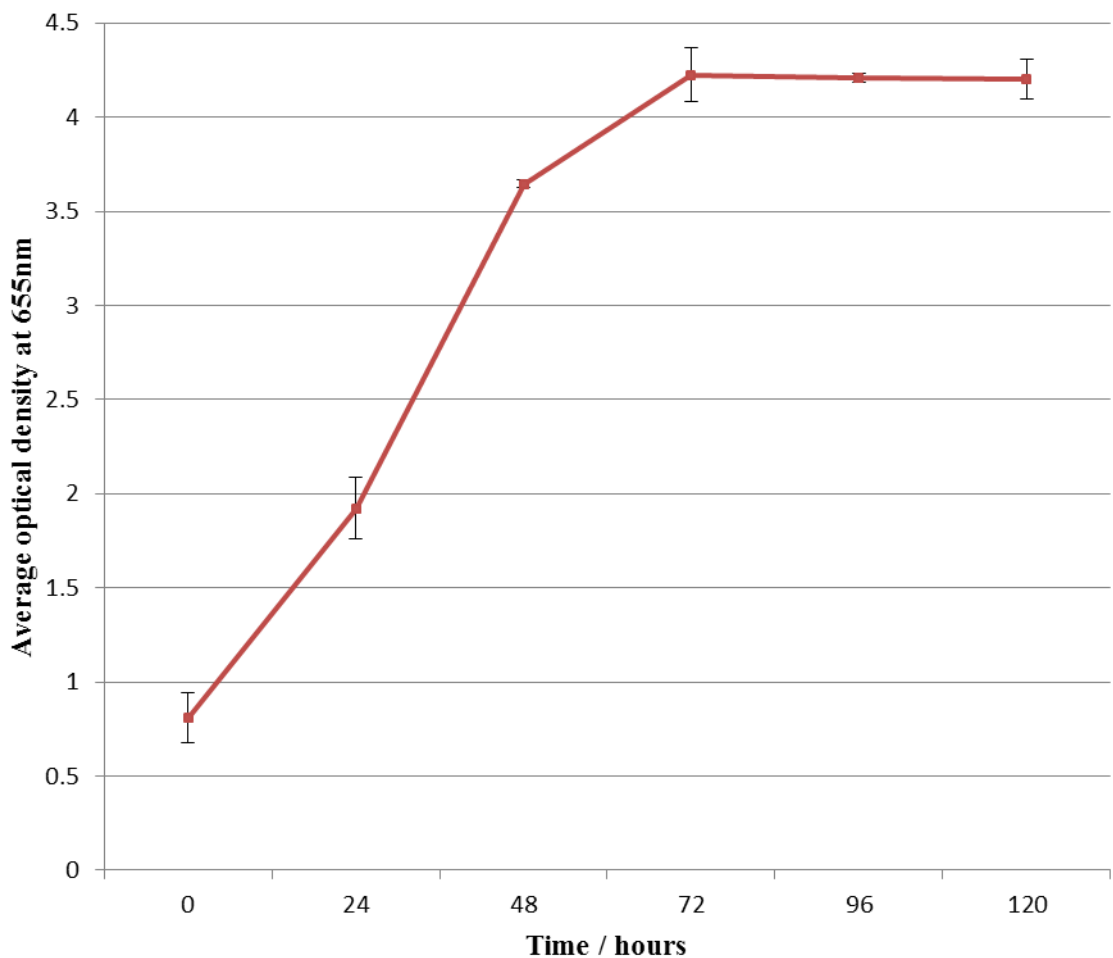


Figure 2.2: Standard growth curve

The numbers of trophozoites were measured using average optical density at 655 nm over a period of 120 hours. Each data point represents 3 readings from a single culture tube of trophozoites. The initial numbers of cells inoculated were 0.1×10^6 cells/ml. The error bars represent standard deviation from the average absorbance reading taken in triplicate.

2.2.5.3 Fixation of trophozoites to tissue culture plate

The tissue culture plate was filled with two-fold dilutions of trophozoites that range from 6×10^6 to 4×10^4 cells/ml in triplicate. The trophozoites in the tissue culture plate were incubated for 2 hours at 37°C. After incubation, the plate was allowed to air-dry overnight. The plate was first dehydrated by adding 300 µl of 70 v/v ethanol before fixing trophozoites with 300 µl of 100 v/v methanol; at each step, the tissue culture plate was allowed to dry. The plate was then stained with 0.1 w/v methylene blue for 10 minutes and washed twice with distilled H₂O. A 300 µl portion of 0.1M hydrochloric acid solution was added to each well to release the dye. The dye extracted was determined with optical density at 655 nm using a microplate reader (E-max plate reader spectrophotometer, Molecular devices, California, USA). The experiments were repeated several times to minimise cell loss.

2.2.6 Statistic representation

The construction of data and graphs through cell counting was first calculated for standard deviation and standard errors. The data were then tested for statistical significance using normal distribution and a paired Student's *t*-test for a confidence level of $p < 0.05$ (using Microsoft Excel 2010).

2.3 Chemical inhibition studies

2.3.1 Inhibitor preparation

LY294002 (2-(4-Morpholinyl)-8-phenyl-4H-1-benzopyran-4-one), CT99021 (6-[2-[[4-(2,4-dichlorophenyl)-5-(5-methyl-1H-imidazol-2-yl)pyrimidin-2-yl]amino]ethylamino]-pyridine-3-carbonitrile), LiCl (Lithium chloride), PI-103 (3-[4-(4-morpholinyl)pyrido[3', 2':4,5]furo[3,2-d]pyrimidin-2-yl]-phenol), Wortmannin (Sigma-Aldrich) and DRB (5,6-Dichloro-1-β-D-ribofuranosylbenzimidazole, Calbiochem) were dissolved in different volumes of sterile dimethyl sulphoxide (DMSO, Sigma-Aldrich) at room temperature to achieve 100 x stock solutions. Inhibitors were prepared for 1/100th of the 13 ml culture

volume of 100 x stock solutions of LY294002, CT99021, LiCl, PI-103, Wortmannin and DRB. Each inhibitor was diluted as appropriate and added to 13 ml of exponentially growing trophozoites to achieve the final concentrations of 25 and 50 μM for LY294002; 0.5, 1 and 2 μM for CT99021; 5, 10 and 20 mM for LiCl; 0.5, 1 and 2 μM for PI-103; 0.1, 0.5, 1, 5, 10 and 15 μM for Wortmannin and 100 μM for DRB. Control cultures were treated with 130 μl of DMSO (1 v/v).

2.3.2 Inhibitor treatment on trophozoites

Freshly subcultured trophozoites in 13 ml screw-capped borosilicate glass culture tubes were incubated at 37°C and grown for 48-72 hours. Once in the exponential phase of growth, the trophozoite culture are ready for the start of treatment. Cultures were chilled on ice for 10 minutes and counted as described in 2.2.3. Trophozoites at 0.1×10^6 cells/ml were subcultured into 13 ml of fresh medium and cultures were treated with inhibitors LY294002, PI-103 and DRB for 48 hours at 37°C. Control cells were treated with equal volumes of concentrated DMSO (final concentration of 1 v/v). All experiments were carried out in triplicate and 50 μl aliquots of each culture were counted every 8 hours, as described in 2.2.3.

For reversible effects, trophozoites treated with LY294002, DMSO and LiCl for 48 hours were prepared in two different ways:

1. Cells were counted after 48 hours, as described in 2.2.3, and equal numbers of cells (0.1×10^6 cells/ml) were inoculated using a pipette to seed treated trophozoites into fresh medium borosilicate glass tube; cells were counted over a 72-96 hour period.
2. Cells were centrifuged at 800 x g for 5 minutes and the supernatant was removed. The treated trophozoites were washed in 13 ml of 1 x PBS and centrifugation was repeated as before. This was followed by another washing step in 5 ml of 1 x PBS and subsequent centrifugation to remove the supernatant. The treated trophozoites are then resuspended in fresh culture medium and counted over a 72 hour period.

2.3.3 Inhibitor treatment of encysting cultures

Giardia intestinalis encysting cultures were prepared, as described in section 2.2.2. The inhibitors LY294002 and DRB were prepared as described in section 2.3 and added to achieve final concentration of 50 μM and 100 μM , respectively. The treatment of

LY294002 and DRB to trophozoites was performed either immediately or 12 hours after the addition of encysting culture medium. The control cultures were treated with equal volumes of concentrated DMSO. All of the experiments were carried out in triplicate with encysting cultures treated with inhibitors for up to 168 hours at 37°C. Once the treatment of inhibitors was completed, encysting cells and trophozoites were collected, fixed and counted as described in section 2.2.3; cysts were purified, harvested fixed and counted as described in section 2.2.4.

2.3.4 Inhibitor treatment of trophozoites

The colorimetric method in this report was improved from the technique described by Hounkong *et al.* (2011). An aliquot of 1×10^4 trophozoites cells/ml taken from a fully grown culture tube, as described in section 2.2, was subcultured into fresh medium. Inhibitors (as described in section 2.2) and puromycin to a final concentration of 100 μ M were added to the fresh medium culture tube containing 1×10^4 trophozoites. The culture tubes with inhibitors were incubated for 16 or 48 hours in separate experiments. After 16 or 48 hours of incubation, the culture tubes were chilled on ice for 10 minutes and trophozoite cells were collected by centrifugation at 800 x g for 5 minutes at 4°C. In all of the culture tubes, the cells were concentrated to a level of around 4.3×10^6 cells per well in 96-well tissue culture plates. After centrifugation, the supernatant was removed, leaving the pellet. The culture tube containing the trophozoite pellet was mixed with 1 ml of PBS (pH 7.2) and transferred into 1.5 ml centrifuge tubes. An aliquot of 300 μ l from each 1.5 ml centrifuge tubes was pipetted into a 96 well-tissue culture plate; each concentration was assessed in triplicate and repeated at least three times. Trophozoites were first dehydrated with 70 v/v ethanol and fixed with methanol; both procedures were allowed to air-dry. Trophozoites were then stained with 0.1 w/v methylene blue for 10 minutes. The plate was washed twice by immersing the whole plate in distilled H₂O. The dye was extracted by adding 300 μ l of 0.1 M hydrochloric acid solution into each well and read at 655 nm (Busatti and Gomes, 2007). The percentage growth inhibition was calculated by comparison with the controls grown without treatment. A graph was plotted of concentration of trophozoites against the optical density at 655 nm.

2.4 Lipids

2.4.1 Extraction of PI(3,4,5)P₃ from *Giardia intestinalis*, *Dictyostelium discoideum* and mouse fibroblast cell lines

Trophozoites were subcultured and grown in 13 ml borosilicate tubes, as described in section 2.2.1, and treated with LY294002 and PI-103. Encysting cells were cultured in 13 ml glass culture tubes, as described in section 2.2.2. NIH 3T3 mouse fibroblast cell lines were grown in Dulbecco's Modified Eagle Media (DMEM). *Dictyostelium discoideum* cells were grown in Axenic medium to reach approximately 3×10^7 cells. *D. discoideum* were harvested and washed with phosphate buffer. Trophozoites and encysting cells were counted (as described in section 2.2.3) and a single lipid extraction experiment required approximately 5×10^6 total cells. Two 13 ml trophozoite cultures tubes were collected by centrifugation at $800 \times g$ for 5 minutes at 4°C to achieve the concentrated trophozoite pellet required. The supernatant was removed by gentle aspiration and cell pellet was washed twice with 1 x PBS. The PBS/cell mix was centrifuged at $800 \times g$ for 10 minutes at 4°C and the supernatant was discarded. The pellet was resuspended in 4 ml cold 0.5 M trichloroacetic acid (TCA) and incubated on ice for 5 minutes. The TCA/cell mix was centrifuged at $500 \times g$ for 5 minutes at 4°C , the supernatant was discarded and the pellet was resuspended in 3 ml cold 5 v/v TCA/1 mM EDTA. The TCA/1 mM EDTA/cell mix was vortexed, centrifuged at $500 \times g$ for 5 minutes at 4°C and the supernatant was discarded. The pellet was then resuspended in 3 ml cold 5% TCA/1 mM EDTA and centrifuged as before. Lipids were extracted by adding 2.25 ml MeOH:CHCl₃:12M HCl (80:40:1) to the pellet, and vortexing 4 times over 15 minutes at room temperature. The mixture was centrifuged at $500 \times g$ for 5 minutes and the supernatant was transferred to a new centrifuge tube. The supernatant was phase-split by the addition of 0.75 ml of CHCl₃ and 1.35 ml 0.1 M HCl, vortexed and centrifuged at $500 \times g$ for 5 minutes to separate the organic and aqueous phases. The lower organic phase was collected and dried in a vacuum dryer. The dried lipid pellet was stored at -20°C .

2.4.2 Detection and quantification of PI(3,4,5)P₃

PI(3,4,5)P₃ dried-down extracted sample was resuspended in 65 μl to 185 μl of PBS-T 3 v/v PS (assay buffer with protein stabiliser provided by PIP₃ Mass ELISA Kit K-2500s, Echelon Biosciences). The resuspended samples were then vortexed for at least 1 minute and centrifuged. Cell extraction samples were then loaded onto an incubation plate

(Echelon Biosciences) in triplicate. Each well, except the blank controls, then had 60 μl /well of diluted PIP₃ detector (Echelon Biosciences) added. The incubation plate was sealed and placed on a shaker at room temperature for 1 hour; 100 μl from each well was transferred to the corresponding wells in the Detection plate (K-1001s, Echelon Biosciences). The Detection plate was then sealed and placed on a shaker at room temperature for 1 hour. The wells were washed 3 times with 200 μl /well of PBS-T (assay buffer, Echelon Biosciences) and 100 μl /well of diluted secondary detector was added. The incubation plate was then sealed and place on a shaker as before. The wells were washed 3 times with 200 μl /well PBS-T. TMB solution (K-TMB1, Echelon Biosciences) was applied to each well and the colour was allowed to develop for 5-10 minutes in the dark. Colour development was then stopped with 50 μl of 1 N H₂SO₄ stop solution (K-STOPl, Echelon Biosciences). The plate was analysed by absorbance reading at 450 nm on a plate reader. The mass of PIP₃ present was estimated by comparison to standard curves constructed by the addition of known amounts of phosphoinositide to the PIP₃ Mass ELISA Kit (Echelon Biosciences) (Figure 2.3).

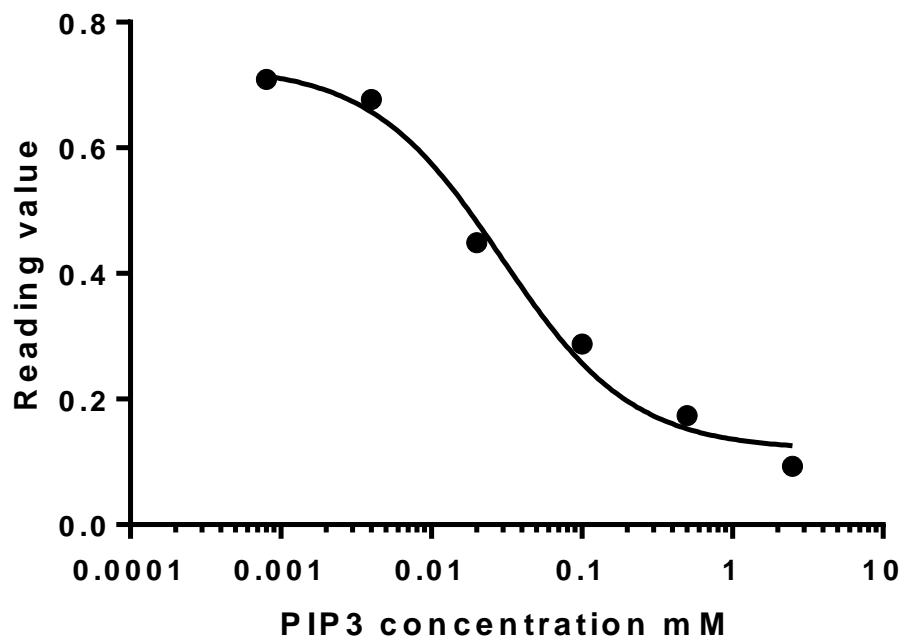


Figure 2.3: PIP₃ Mass ELISA standard curve

The Reading value was measured by the absorbance at 450 nm. There are six standard values from wells containing PIP₃ in a concentration-dose response manner. This standard curve was generated using GraphPad prism software using non-linear regression analysis.

2.5 Imaging

2.5.1 Electron microscopy

2.5.1.1 Scanning electron microscopy

G. intestinalis trophozoites and encysting cells treated with LY294002 and DMSO at different time periods (12, 24, 48 and 72 hours) were harvested by centrifugation at 500 x g for 10 minutes before the pellets were resuspended in 1.5 ml centrifuge tubes. Approximately 100 µl of trophozoites was pipetted onto a 24-well cell culture plate containing a coated poly-L-lysine 13 mm diameter glass coverslip. The 24-well cell culture plate was filled with 2 ml culture medium and placed at 37°C for 60 minutes. Culture medium was then carefully removed and the cell culture plate was washed with 2 ml 1 x PBS and incubated for 15 minutes at 37°C. Then, 1 x PBS was removed and 1 ml of 2.5 w/v glutaraldehyde in 0.1 M sodium cacodylate buffer at 37°C was added to each well in a cell culture plate followed by incubation at room temperature for 1 hour. Cell culture plates were washed twice with 0.2 M cacodylate buffer and stored at 4°C in 0.2 M cacodylate buffer. Trophozoites and encysting cells on the coverslip were osmicated for 40 minutes at 4°C with 1 w/v osmium tetroxide in 0.2 M cacodylate phosphate buffer, followed by a dehydration step in ethanol: 2 x 50 v/v ethanol for 10 minutes each, 3 x 70 v/v ethanol for 10 minutes each, 3 x 95 v/v ethanol for 10 minutes each and 3 x 100 v/v ethanol for 20 minutes each. The coverslips were then transferred to 100 v/v ethanol in critical point drying holders and were critical point-dried using carbon dioxide in a Polaron E3000 critical point dryer with > 3 flushes over a 45 minute soaking period. The coverslips were mounted on stubs (TAAB Laboratories Equipment Ltd) with conductive carbon adhesive discs (TAAB Laboratories Equipment Ltd). The samples were sputter-coated with gold in an Emitech K550 sputter-coater at 45 mA current for 2 minutes. Samples were examined and images collected using an FEI Quanta 200 Field emission scanning electron microscope operated at 12 kV in high vacuum mode.

2.5.1.2 Transmission electron microscopy

Fully grown trophozoites at confluence (approximately 1×10^6 cells/ml) were harvested by centrifugation at 500 x g for 10 minutes before the culture medium was gently removed. The fully grown trophozoites were resuspended in fresh culture medium treated with LY294002 at 50 µM or encystation medium and incubated for different time periods of 24 and 48 hours. Trophozoites were harvested by centrifugation at 500 x g for 10 minutes, the

culture medium was removed and the pellet was washed with 1 x PBS. The centrifugation step was repeated to remove 1 x PBS and then 1 ml of 2.5 w/v glutaraldehyde in 0.1 M sodium cacodylate buffer (fixative) was added to each tube. The resuspended pellet in fixative was transfer to a 1.5 ml centrifuge tube and incubated at room temperature for 3 hours. The pellets of fixed trophozoites were collected by centrifugation at 500 x g for 5 minutes at 4°C and the fixative was removed. The pellets were resuspended in sodium cacodylate buffer and centrifugation was repeated twice every 10 minutes. Samples were post-fixed at 4°C for 1 hour and 30 minutes with 1% osmium tetroxide in 0.15 M sodium cacodylate phosphate buffer. Trophozoites were dehydrated for 10 minutes in 10 v/v ethanol, 30 minutes in 70 v/v ethanol and three times for 20 minutes in 100 v/v ethanol at room temperature. Samples were exposed twice for 10 minutes in propylene oxide at room temperature. Pre-infiltration to the samples for 2 hours and 30 minutes on 1:1 propylene oxide and Resin (TAAB Laboratories Equipment Ltd embedding resin, medium) and complete infiltration into 100 w/v resin over night at room temperature. Cells were then embedded in resin and polymerised for 24 hours at 70°C. Ultrathin sections (70-90 nm) were prepared using a Reichert-Jung Ultracut E ultra-microtome and mounted on 150 mesh copper grids. Ultrathin sections were contrasted using uranyl acetate and lead citrate and observed on an FEI Tecnai 12 transmission microscope operated at 120 kV. Images were taken with an AMT 16000 M digital camera.

2.5.2 Light immunomicroscopy

2.5.2.1 Immunofluorescence analysis

Giardia intestinalis trophozoites incubated with LY294002, DMSO or Encystation medium for 12, 24 and 48 hours or control WB trophozoite cells in normal culture medium for 48 hours were harvested by centrifugation at 500 x g for 10 minutes; pellets were collected. The pellets in each sample were resuspended in approximately 350 µl. Aliquots (100 µl) were loaded into each well in the 24-well tissue culture plate containing poly-L-lysine-coated coverslips per time point in duplicate. Medium (2 ml) was then added to each well and the trophozoites were incubated at 37°C for 1 hour to allow adherence to the coverslip. Cells were washed with 2 ml warm 1 x PBS for 15 minutes at 37°C. The supernatant was gently removed and trophozoites on the coverslip were fixed in 1 ml of 4 w/v PFA in 1 x PBS for 30 minutes at room temperature. After 30 minutes, the supernatant was removed and the cells on the coverslip were washed with 2 ml 1 x PBS. The cells on the coverslip

were permeabilised by adding 1.5 ml of 0.2 v/v Triton-X-100 (Sigma-Aldrich) in 1 x PBS (PBS-T) for 15 minutes. This was followed by repeating the washing step with 1 x PBS as before, and cells on the coverslip were blocked in blocking solution (1 w/v BSA in 1 x PBS) for 1 hour at room temperature with no agitation. This was followed by repeated washing with 1 x PBS as before, but with 5 minutes of gentle agitation at room temperature to remove the blocking solution. PBS washed cells were then incubated overnight at 4°C with primary antibody solution prepared to the following dilutions:

- 1:100 or 1:250 anti-CWP2 mouse monoclonal, fluorescein conjugated 7D2 (kind gift from Professor Theodore Nash)
- 1:1000 mouse monoclonal, anti- α tubulin (Sigma-Aldrich).
- 1:100 or 1:250 rabbit monoclonal, anti-IscS (iron sulphur cluster) (kind gift from Dr. Jorge Tovar)

After overnight incubation, the primary antibody solution was discarded and the wells were washed thrice in 1 x PBS-T at 5 minute intervals, with a final wash in 1 x PBS. After the washes, cells were incubated with 1:500 goat anti-mouse FITC or 1:1000 rabbit anti-mouse Cy3 for 1 hour at room temperature. The wells were washed again thrice in 1 x PBS at 5 minute intervals. The cells on the coverslip were nuclei-stained with DAPI (Sigma-Aldrich) at 10 μ g/ml for 15 minute. The wells were washed again thrice in 1 x PBS-T at 5 minute intervals. These washes were followed by a filter-sterilised 1 x PBS wash for 10 minutes. The coverslips were gently tapped to remove excess fluid and were mounted on glass slides with a drop of Fluorsave (Calbiochem), before being allowed to air-dry for 1 hour. Slides were sealed with nail varnish, covered and stored at 4°C for immunofluorescence microscopy (Nikon TE300).

In co-localisation experiments, trophozoite cells treated with anti-CWP2 antibodies were further incubated with rabbit monoclonal, anti-IscS antibodies overnight, washed with 1 x PBS and then incubated with secondary anti-rabbit IgG-TRITC conjugated for 1 hour at room temperature. Cover slips were washed thrice with 1 x PBS at 5 minute intervals and treated with DAPI. The coverslips were washed again thrice in 1 x PBS-T at 5 minute intervals and followed by a 10 minute wash using filtered-sterilised 1 x PBS. The cover slips were mounted on glass slides using Fluorsave and observed under a confocal microscope.

2.5.2.2 Confocal microscopy

The fluorescence images of trophozoites that were labelled using the FITC and TRITC secondary antibodies were viewed on a Nikon TE300 inverted fluorescence microscope. The microscope had magnification components of 60 x and 100 x oil immersion objectives. For FITC, the excitation wavelength was 488 nm with the emission wavelengths of 515-520 nm; the excitation wavelength for TRITC was 549 nm, with the emission collection wavelength of 595-620 nm employed.

The epifluorescence images were taken using a 60x oil immersion objective lens when the dye lists were chosen to either FITC or TRITC. Images were taken using Z stack at 0.42 μm intervals with 10 slices using the FVI1000 system and collected using the FV10-ASW software (version 1.36). The images collected were saved as *.tif* files and were arranged using Adobe Photoshop (version 7). Co-localised images of FITC and TRITC were presented using RGB merge tools to display both fluorescences.

CHAPTER 3: Bioinformatics sequence analysis of *G. intestinalis* signalling proteins phosphoinositide 3-kinases and glycogen synthase kinases

3.1 Introduction

Giardia genomic resources are an important tool to provide the platform for understanding putative lipid signalling cascades and for identifying additional molecular components of lipid in this research. Genomic data can have a potential effect on research aims and objectives in *G. intestinalis* sequence. In this research it was considered crucial to investigate the identity and confirm the presence of PI3K and GSK gene sequences and the amino acid sequence of *G. intestinalis*.

The *G. intestinalis* genome contains 12 million base pairs distributed over five chromosomes. *G. intestinalis* is different to other parasites in that it contains two identical nuclei in the trophozoite stage. During the active trophozoite stage of the life cycle, each *G. intestinalis* nuclei cycles between a diploid (2N) and tetraploid (4N) state (Bernander *et al.*, 2001). The published *Giardia* genome sequence has enlightened researchers about the nuclear genome organisation, the presence of metabolic signalling pathway components and the molecules involved in the cellular biology of pathogenicity. Data statistics in the *G. intestinalis* Database (GiardiaDB), which is part of the Eukaryotic pathogen Database (EuPathDB), currently show (as of February 2013) that 12.83 mega base pairs of *Giardia* assemblage A isolate WB, clone 6, have been sequenced. The *Giardia* genome was sequenced using whole genome shotgun sequencing where both ends of *G. intestinalis* genomic DNA were sequenced, single reads were assembled into contigs and mapped to chromosomes and cloned in a BAC (bacterial artificial chromosome) vector. The genomic sequence encoding specific proteins can be found directly on the *Giardia* database website (<http://eupathdb.org/eupathdb/>) and all single reads are translated and queried against non-redundant protein databases at NCBI (National Centre for Biotechnology Information).

The *Giardia* gene structure has been reported to show certain eukaryotic features and other prokaryotic features (Adam *et al.*, 2000). *Giardia* regularly shows the pattern of simplified molecular machinery, cytoskeletal structure and metabolic pathways when it is compared to subsequent diverging lineage organisms such as fungi and *Entamoeba*

histolytica (Morrison *et al.*, 2007). This evidence suggests that many specific pathways in *Giardia* are simple in comparison with those of eukaryotic organisms. The similarity in *Giardia* gene structure to yeast and other parasites is shown in Table 3.1. Both *G. intestinalis* nuclei present in trophozoites appear indistinguishable; each has complete copies of the genome and are both transcriptionally active (Kabnick and Peattie, 1990, Yu *et al.*, 2002, Carranza and Lujan, 2010).

The availability of the *Giardia* sequences from the *G. intestinalis* genome project has increased the understanding of protein kinases involved in the intracellular signalling pathways in the parasite. This chapter entails the identification of PI3Ks and GSK homologues in *Giardia* and illustrates the protein sequence coding for these kinases through bioinformatics. The components of the signalling cascade that will be examined in this chapter are PI3K and GSK. In eukaryotic cells, the PI3K signalling cascade has been associated with mechanisms to regulate cell growth, intracellular trafficking and cell motility (Wymann *et al.*, 2003, Marone *et al.*, 2008). Therefore, it is possible to envisage that a failure in PI3K-mediated activity in eukaryotic cells may result in cell cycle arrest that will disrupt cell proliferation and cell growth and consequently lead to cell death. It is important to understand the signalling cascade and the components involved in the PI3K pathway. These components can activate different processes which are important in the regulation of cell proliferation, cell growth, and intracellular trafficking and cell motility. Reported studies illustrate that *G. intestinalis* encodes and expresses two putative PI3Ks (Cox *et al.*, 2006). Once PI3K is activated in the signalling cascade, PI3K phosphorylates PI to generate PIP. An additional phosphorylation reaction adding phosphate to PIP by PI3K generates PIP₂, and then PIP₃ is produced by Class I PI3Ks and recruits proteins with a pleckstrin homology (PH) domain to the plasma membrane; an example of one of these proteins is protein kinase B (PKB). The phosphate from PIP₃ is then transformed to PKB, thereby activating PKB through phosphorylation of the PH domain at the membrane. Once activated, PKB activates or inactivates a series of downstream effector proteins. Thus, PKB acts as a key regulator of important cell processes such as cell survival. PKB has been extensively studied in mammalian cells as a regulator of cell growth, proliferation and survival. Furthermore, PKB has been identified in *Dictyostelium discoideum* (Haribabu and Dottin, 1991), *Trypanosoma cruzi* (Pascucci *et al.*, 1999) and *Entamoeba histolytica* (Que *et al.*, 1993). Work by Kim, *et al.* (2005) showed the identification and characterisation of PKB in *G. intestinalis* (GenPept: AAF06671). Another important

component associated with PPI_n is the PPI_n-metabolising phosphatase. Below is a list of the protein phosphatases in *G. intestinalis* that have been identified to date: serine/threonine protein phosphatase 2A-2 (PP2A-2) catalytic subunit (GenPept: EDO79971), serine/threonine protein phosphatase 5 (GenPept: EDO77915), serine/threonine protein phosphatase 4 (GenPept: EDO76443.1) and serine/threonine protein phosphatase (GenPept: EDO80051.1); all of these may act to dephosphorylate the products of GiPI3K1 (Lauwaet *et al.*, 2007, Morrison *et al.*, 2007). Furthermore, *Giardia* PP2A is needed during the parasite differentiation, as knockdown of *Giardia* PP2A RNA by the expression of antisense RNA under a strong constitutive promoter results in the inhibition of encystation and excystation (Lauwaet *et al.*, 2007).

Table 3.1: *G. lamblia* genome contents in comparison to other eukaryotic species.

A comparison of genome content and organization of common eukaryotic species to *G. lamblia*.

	<i>Saccharomyces cerevisiae</i>	<i>Plasmodium falciparum</i>	<i>Trypanosoma brucei</i>	<i>Leishmania major</i>	<i>Entamoeba histolytica</i>	<i>Encephalitozoon cuniculi</i>	<i>Trichomonas vaginalis</i>	<i>Giardia lamblia</i>
Size (MB)	12.5	22.8	26.1	32.8	~24	2.3	~160	11.7
%G+C content	38.3	19.4	46.4	59.7	~25%	47.6	32.7	49.0
Proteins encoded	5770	5268	9068	8272	9938	1997	25,949	6470
Mean CDS (bp)	1424	2283	1592	1901	1170	1077	929	1283
Mean intergenic distance (bp)	515	1694	1279	2045	1245	129	1165	372
Gene density, per kbp	0.48	0.23	0.32	0.25	0.41	0.97	0.34	0.58
Introns	272	7406	1	0	~2500 predicted	2	65	4
tRNAs	275	44	65	83	Subtelomeric arrays	44	479	63

3.2 Experimental Results

3.2.1 Identification of putative phosphoinositol-3 kinase and glycogen synthase kinase in *G. intestinalis*

G. intestinalis genome searches were executed by using translation BLAST (tBLASTn) to identify genes encoding putative PI3Ks and GSK. First, we searched for validated PI3K and GSK sequences from other organisms representing the three homologues of class I, II and III PI3Ks and homologues of GSK. The protein query sequences chosen for PI3Ks were; 1) *Homo sapiens* p110 α representing class I PI3K (GenPept: NP_006209); 2) *H. sapiens* PI3K-C2 α representing class II PI3K (GenPept: NP_002636); 3) *Saccharomyces cerevisiae* Vsp34 representing class III PI3K (NP_013341). For GSK, the chosen protein query sequences were; 1) *H. sapiens* GSK-3 α (Genpept: NP_063937.2) 2) *H. sapiens* GSK-3 β (GenPept: NP_002084.2).

Using the catalytic domain of PI3Ks and GSK isoforms as query sequences, tBLASTn was performed with query sequences against the *Giardia* genome. The translated sequences of five PI3K and two GSK open reading frames (ORFs) from *G. intestinalis* were identified. The matches of query sequence to *G. intestinalis* probability show significant low E-values in both PI3K and GSK kinase domains (E values refer to the probability of the query sequence getting a matching return from the genome it was compared to; the lower the E values, the higher the number of matched sequences). Also the percentage identity values were moderately high by the kinase domain of PI3K and GSK; this is shown in Tables 3.2 and 3.3.

G. intestinalis PI3K matched sequences in Table 3.2 were analysed and two sequences were removed from the list. The bottom two amino acid sequences excluded from further analysis are GL50803_35180 and GL50803_16805; the former sequence name is GTOR and it is predicted to be involved in the targeting of Rapamycin-related protein kinase, while the latter is predicted to be a hypothetical protein (Morrison *et al.*, 2007). The remaining three matching sequences of PI3K are made up of long sequences: GL50803_14855 is 6,467 bases on chromosome 5, GL50803_17406 is 4,916 bases on chromosome 2 and GL50803_16558 is 6,779 bases on chromosome 4. Furthermore, when these three PI3K sequences are translated into amino acid protein sequences, the molecular weights are 242 kDa, 183 kDa and 254 kDa for GL50803_14885, GL50803_17406 and GL50803_16558, respectively. The two matching GSK sequences from *G. intestinalis* contain 1,112 bases and 1,052 for GL50803_9116 on chromosome 5 and GL50803_17625

on chromosome 3, respectively. *Giardia* GSK protein sequences have a molecular weight of 42.24 kDa and 39.98 kDa and are similar to the putative *Leishmania major* GSK sequence (accession: XP_001682433), which contains 355 amino acid residues and has a molecular weight of 40.72 kDa (Aslett, 2005).

Table 3.2: Percentage identity and probability values of putative *G. intestinalis* PI3K sequences.

Amino acids of PI3K class I, II and III from *H. sapiens* were chosen as query sequences for translational blast to determine the PI3K homologues in *G. intestinalis* genome. Here are the five *Giardia* match sequences with low E-values and moderately high percentage identity. Each sequence identification code can be referred to the *Giardia* Genome Database.

<i>Giardia</i> match		Query sequences		
		<i>H. sapiens</i> p110 α	<i>H. sapiens</i> PI3K-C2 α	<i>S. cerevisiae</i> Vps 34p
GL50803_14855	E-value	4.0 x 10 ⁻⁶⁰	6.5 x 10 ⁻⁴⁶	1.2 x 10 ⁻³⁶
	% identity	44%	33%	31%
GL50803_17406	E-value	5.7 x 10 ⁻¹⁷	3.1 x 10 ⁻¹⁹	1.1 x 10 ⁻³²
	% identity	27%	26%	31%
GL50803_16558	E-value	2.5 x 10 ⁻¹⁵	3.9 x 10 ⁻¹²	6.7 x 10 ⁻¹⁹
	% identity	27%	25%	23%
GL50803_35180	E-value	8.7 x 10 ⁻³	3.5 x 10 ⁻⁴	1.1 x 10 ⁻⁰⁸
	% identity	34%	36%	25%
GL50803_16805	E-value	1.4 x 10 ⁻³	-	4.2 x 10 ⁻⁰¹

	% identity	34%	-	24%
--	------------	-----	---	-----

Table 3.3: Percentage identity and probability values of putative *G. intestinalis* GSK-3 sequences.

Amino acid sequences of GSKs from *H. sapiens* have been chosen as query sequences for translational blast to determine the GSK homologues in the *G. intestinalis* genome. Here are a couple of *Giardia* match sequences with very low E-values and quite high percentage identity. Again, each sequence given below can be referred to the *Giardia* Genome Database.

		Query sequences	
<i>Giardia</i> match		<i>H. sapiens</i> GSK-3 α	<i>H. sapiens</i> GSK-3 β
GL50803_9116	E-value	2.7×10^{-81}	6.8×10^{-83}
	% identity	46%	48%
GL50803_17625	E-value	2.2×10^{-72}	1.7×10^{-72}
	% identity	41%	45%

Three remaining sequences of *G. intestinalis* PI3K and two *G. intestinalis* GSK sequences were translated and were used to search with tBLASTn for similar sequences in a non-redundant database. The top three matches for PI3K in *Giardia* are listed in Table 3.4 and for *Giardia* GSK matches are listed in Table 3.5. Non-redundant database searches for *Giardia* PI3Ks returned matches showing similarity and identity to class IB p110 PI3K, class III PI3K and PI4K kinases. It was decided that further analysis should focus on the putative giardial PI3K enzymes rather than the putative PI4K. PI3K based research has rapidly accelerated in many different cell types together with the knowledge of PI3K structure and cellular function; it was reasoned that there was more to gain in terms of applying known PI3K principles by focusing on the giardial PI3Ks.

Table 3.4:
Probability and percentage identity values of matches from the non-redundant database of nucleotide sequences at NCBI to all three *G. intestinalis* ORF following tBLASTn.
 Percentage identity and probability result from three *Giardia* PI3Ks (GiPI3K1, GiPI3K2 and GiPI4K) that were used to search for similar sequences in the non-redundant sequence in NCBI non-redundant database using tBLASTn tool. E-values are the expected values for the sequence to show up; they are in brackets below.

	Match 1	Match 2	Match 3
GL50803_14855 (GiPI3K1)	39% identity ($2e^{-40}$) to <i>D. discoideum</i> PIK1, that has a roles of p110 PI3K homologs (Zhou <i>et al.</i> , 1995)	41% identity ($1e^{-35}$) to <i>S. scrofa</i> mRNA for p120-PI3K protein, which is highly associated to class IB mammalian p110 γ PI3K (Stephens <i>et al.</i> , 1997).	44% identity ($5e^{-35}$) to <i>H. sapiens</i> class IB p110 α , PI3K. (Sturdivant <i>et al.</i> , 1997)
GL50803_17406 (GiPI3K2)	33% identity ($6e^{-31}$) to <i>G. max</i> PI3K	35% identity ($9e^{-30}$) to <i>S. pombe</i> Vps 34	34% identity ($3e^{-29}$) to <i>A. thaliana</i> Vps 34
GL50803_16558 (GiPI4K)	31% identity ($1e^{-38}$) to <i>A. thaliana</i> PI4K	30% identity ($1e^{-36}$) to <i>H. sapiens</i> PI4K	34% identity ($3e^{-35}$) to <i>D. discoideum</i> PI4K

The search for *Giardia* GSKs against non-redundant proteins returned matches to GSK3 and the GSK3-beta isoforms. The sequences given in the search will now be referred to as GiPI3K1 (GL50803_14855), GiPI3K2 (GL50803_17406) and GiPI4K (GL50803_16558); for GSK sequences, two different isoforms will be referred to as GiGSKa (GL50803_9116) and GiGSKb (GL50803_17625). The term “Gi” represents *G. intestinalis*.

Table 3.5:
Analysis of the putative
G.
intestinalis
GSK
sequences
following
tBLASTn.
 Percentage identity and probability result from two *Giardia* GSKs (GiGSKa and GiGSKb) that were used to search for similar sequences in the non-redundant sequence in NCBI non-redundant database using tBLASTn tool. E-values are in brackets below.

	Match 1	Match 2	Match 3
GL50803_9116 (GiGSKa)	52% identity ($5e^{-104}$) to <i>C. elegans</i> GSK-3 (Schlesinger <i>et al.</i> , 1999)	49% identity ($5e^{-103}$) to <i>D. discoideum</i> (GSKa) (Eichinger <i>et al.</i> , 2005)	48% identity ($6e^{-92}$) to <i>H. sapiens</i> GSK3 (He <i>et al.</i> , 1995)
GL50803_17625 (GiGSKb)	46% identity ($9e^{-97}$) to <i>G. max</i> GSK-3 (Zhang <i>et al.</i> , 2010)	44% identity ($3e^{-94}$) to <i>S. pombe</i> GSK-3 (Wood <i>et al.</i> , 2002)	43% identity ($4e^{-94}$) to <i>C. reinhardtii</i> GSK-3 (Merchant <i>et al.</i> , 2007)

3.2.2 Analysis of the domains in PI3Ks and GSKs in *G. intestinalis*

The domains characteristic of PI3Ks and GSKs in *G. intestinalis* were analysed through the domain-prediction programs SMART (Schultz *et al.*, 1998). *G. intestinalis* GiPI3K1, GiPI3K2 and GiPI4K sequences were entered into SMART and predicted to contain a Ras-binding domain, a C2 domain, a PIK and kinase catalytic domains with a high E-value. The domain predictions were similar to the other PI3Ks which also show Ras binding, C2-like and catalytic domain. Upon activation by external stimuli to cell membrane receptors, the Ras binding domain interacts specifically to effector-proteins, thereby initiating protein-protein interactions. The resulting effector protein activation for example in PI3K, therefore leads to the increased PI3K activity due to translocation of the enzyme to the plasma membrane. C2-like domains have been reported to be important for membrane interaction and binding (Walker *et al.*, 1999). Work reported by Cox *et al.* (2006) illustrated that GiPI3K1 and GiPI3K2 appear to have long insertions in the PIK domains, whereas other well-studied organisms do not. *Giardia* PI3K domains were analysed using sequence-similarity searches where the predicted domains of GiPI3K1 and GiPI3K2 were queried against a non-redundant database, thus confirming the identity of the predicted domains and providing further evidence of the similarity of *Giardia* PI3Ks to class I and III PI3K isoforms (Table 3.6). GiPI4K was also queried and a kinase domain was reported in the region of amino acids 1955-2257. Several matches were reported, with the highest being 12% sequence identity to the *H. sapiens* PI4K kinase domain.

Giardia GSK isoforms were also queried through sequence similarity using the sequence of predicted Serine/Threonine protein kinases, catalytic domain (S_Tkc), against a non-redundant database. S_Tkc was chosen as the query to search for GSK isoforms in *Giardia* because GSK protein sequences in other organisms contain S_Tkc domains. The S_Tkc domain is one of the three main classes of protein kinases that are able to catalyse the transfer of phosphate groups, which result in a conformational change affecting the protein function. The results illustrate that there are several matches to S_Tkc domain in both GiGSKa and GiGSKb; the highest percentage score was 53% to *Caenorhabditis remanei* GSK-3 and 47% to *H. sapiens* GSK-3 β (Table 3.7). In general, GSK-3 homologues in well-studied organisms share significant degrees of homology, especially in the kinase domain; therefore, to further support this, pairwise alignment of the giardial GSK domain S_Tkc was performed against the GSKs sequence, which share the greatest similarity with giardial GSKs.

Research in PI3K cellular signalling has rapidly progressed beyond PI4K-based research. Moreover, the knowledge of PI3K structure and intracellular function in many different cell types is more advanced. Therefore, it was to gain in terms of applying known PI3K principles by focusing on the giardial PI3Ks and GSK.

Table 3.6: Investigation of giardial PI3K domains.

This table shows sequence identity values as a percentage of GiPI3K1, GiPI3K2 and GiPI4K in comparison to other well-studied isoforms of PI3K.

	GiPI3K1	GiPI3K2	GiPI4K
RBD	41% to <i>H. sapiens</i> class IB PI3K	-	-
PIK	29% to <i>H. sapiens</i> PI3K catalytic p110 α	31% to <i>C. elegans</i> Vps34-like PI3K	-
Kinase	39% to <i>D. discoideum</i>	34% to <i>G. max</i> PI3K	12% to <i>H. sapiens</i> PI4K
C2 domain	12% to <i>D. discoideum</i>	13% to <i>G. max</i> PI3K	-

Table 3.7: Investigation of giardial GSK proteins.

Serine/Threonine protein kinase, catalytic domain sequences were used for sequence-similarity search and the percentage identity value of the similar domain sequences were shown following sequence alignment.

	GiGSKa	GiGSKb
S_Tkc	53% to <i>C. remanei</i> GSK-3 protein	47% to <i>H. sapiens</i> GSK-3 β

Giardia PI3K sequence alignments by Cox *et al.* (2006), showed similarities in the domain sequence and provided structural analysis of important domains, such as the Ras binding domain, the C2 domain and the PIK domain. Here, *Giardia* GSK pairwise alignments were carried out (Figure 3.1) for alignment of GiGSKa and GiGSKb against

kinase domains of GSKs from *C. elegans* and *G. max*, respectively. The domain sequences used in the comparison were chosen based on the highest percentage matches in similarity and identity.

Glycogen synthase kinase is from a family that includes cyclin-dependent kinase (CDK), mitogen-activated protein kinase (MAPK), glycogen synthase kinase-3 (GSK-3) and CDC-like kinase (CMGC). Two isoforms are typically found: GSK-3 α and GSK-3 β . In the primitive eukaryote, GSK or GSK-3 has one isoform, GSK-3 α , while an invertebrate would normally have two isoforms of GSK-3. Comparison of the amino acid sequences of the two open reading frames reveals identity of up to 98% in the region containing motifs that are common to all protein kinases (Woodgett, 1990). The differences between the two genes are found in the N-terminal and C-terminal, where the latter share only 36% identity in the last 76 residues.

Structural analysis of the kinase domain S_Tkc, in the well-studied organism *Rattus norvegicus*, has revealed conserved residues that have important features within this domain. For example, key serine residues (Ser-21 in GSK-3 α and Ser-9 in GSK-3 β) have been implicated in phosphorylation and, therefore, play a role in a variety of signalling pathways such as the insulin signalling cascade, cyclic AMP activation and the epidermal growth factor. Two conserved lysine residues, Lys-148/149 in GSK-3 α and Lys-85/86 in GSK-3 β , are important for ATP binding and stabilising γ -phosphate during transfer to the substrate. Initially, the substrate undergoes priming via a phosphorylation mechanism; this is when pre-phosphorylation of the substrate occurs by another kinase at a site four amino acids towards the C-terminal to the GSK-3 phosphorylation site, where the optimal site for GSK-3 is Ser/Thr-x-x-x-Ser/Thr-P (Martinez *et al.*, 2002). In *H. sapiens*, GSK-3 β activity is negatively regulated by phosphorylation of Ser-9 and positively regulated by phosphorylation on Tyr-216. The putative kinase domain sequences of *Giardia* GSKs (GiGSKa and GiGSKb) were analysed using a protein structure prediction server from University College London (program PSIPRED) to reveal their secondary protein structure (Bryson *et al.*, 2005; McGuffin *et al.*, 2000). The S_Tkc domains of GiGSKa and GiGSKb are predicted to fold into 8 and 9 beta strands, respectively (Figure 3.2). The alpha helix of the two sequences analysed show 9 and 8 α -helices from GiGSKa and GiGSKb, respectively. Both the number of alpha helices and beta strands in the S_Tkc domain of *Giardia* GSKa and GSKb are similar to the secondary structure arrangement in *Rattus norvegicus* (Woodgett, 1990).

In addition to the study above, the structure of *Giardia* GSK domain S_TKc was further analysed using the crystal structure of human GSK-3 β as a model (Cheng *et al.*, 2011). The structure of GiGSKa and GiGSKb kinase domains was imported into the Cn3D macromolecular structure viewer and aligned to *H. sapiens* GSK-3 β . The kinase domain from GiGSKa and GiGSKb was blast-searched against the sequence of GSK-3 β and aligned to GSK-3 β (see Figure 3.3). This showed the 3D-structural homology. The structural analysis of the kinase domains revealed that GiGSKa and GiGSKb share similar S_Tkc domains, as illustrated in the alignment with mammalian GSK-3 β . This could be due to the high similarity and conservation of the functional kinase domain reported across the species (see Figure 3.5).

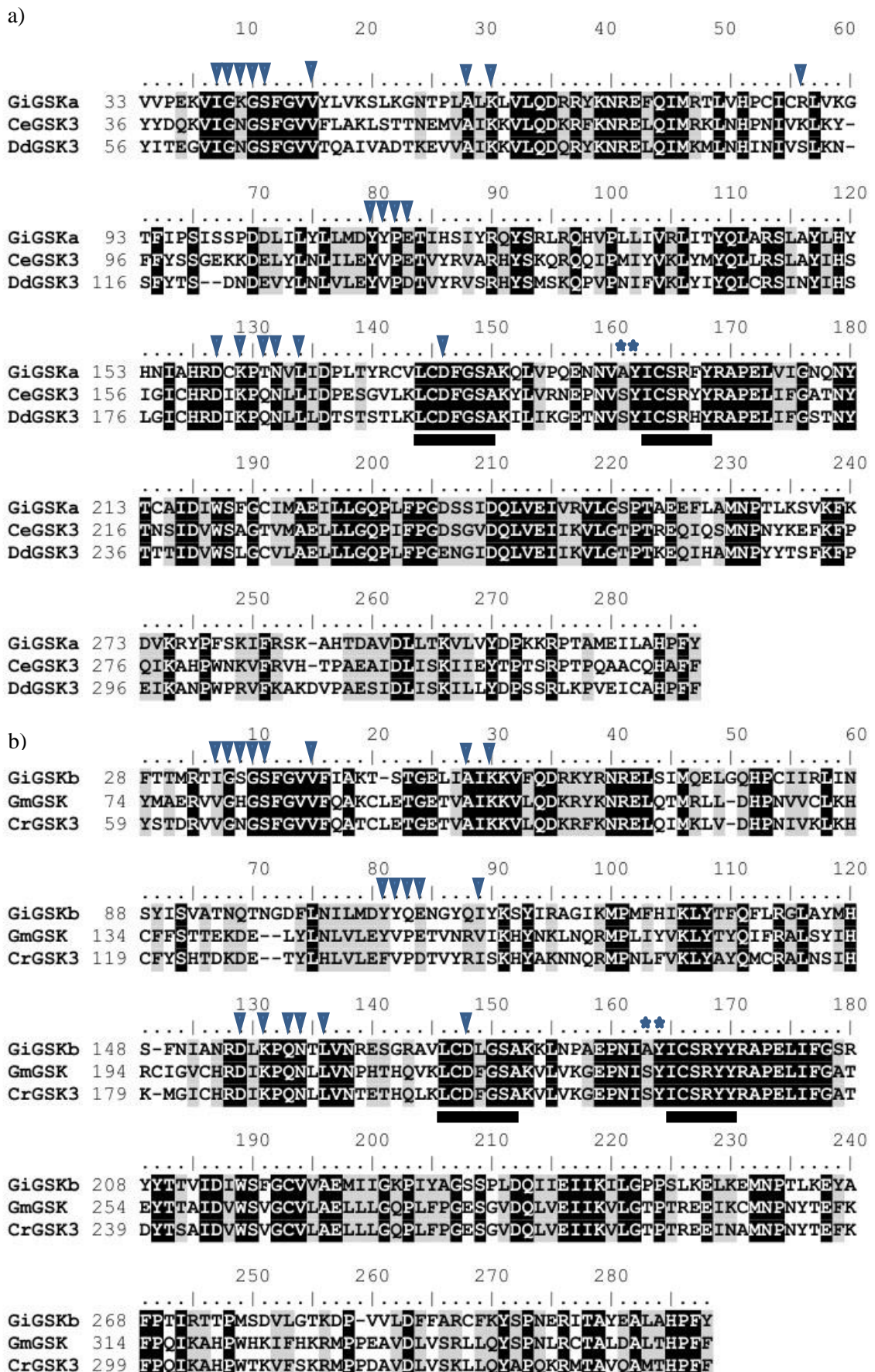
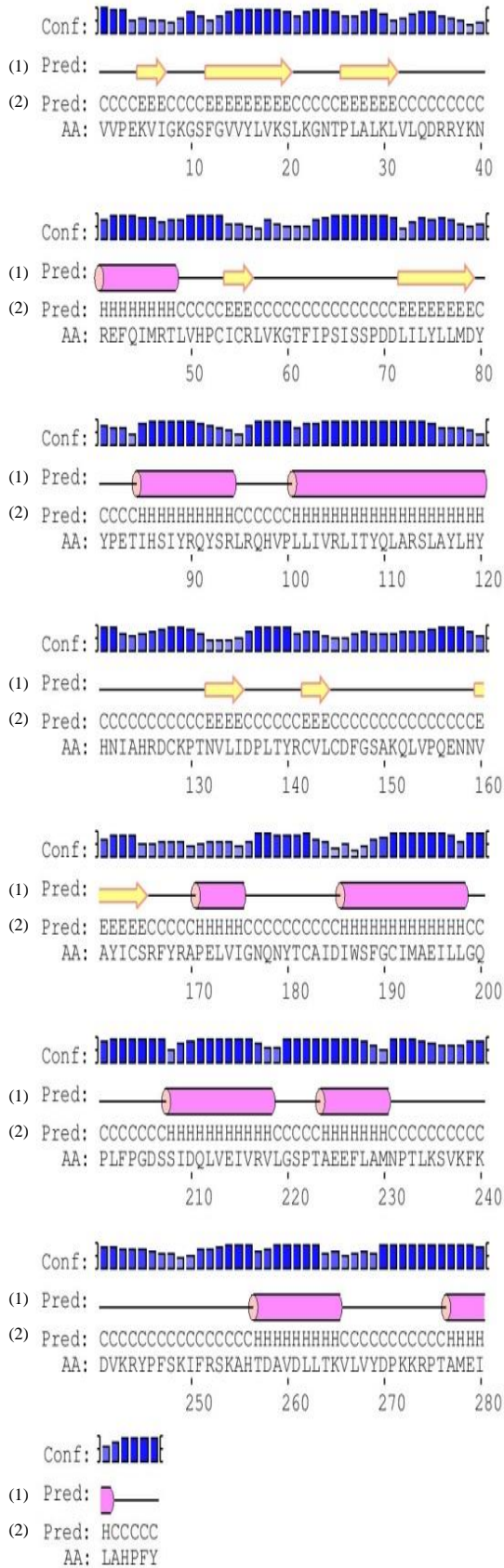


Figure 3.1: GSK domain pairwise alignments for GiGSKa and GiGSKb sequences.

Pairwise sequence alignments of GiGSKa (a) and GiGSKb (b) Serine/Threonine protein kinase, catalytic domain (S_Tkc) using CLUSTAL W multiple alignment (Thompson *et al.*, 1994). Sequences with identical residues are highlighted in black shading and the conserved residues are shaded in grey according to PAM250 matrix (Schwartz and Dayhoff, 1978). Identity and similarity percentages for the sequence alignments of GiGSKa are 53% and 73% with CeGSK3 (Accession: NP_493243), and 49% and 72% with DdGSK3 (Accession: XP_645156). The identity and similarity percentages for sequence alignments of GiGSKb are 47% and 73% with GmGSK (Accession: ACQ91102), 45% and 73% with CrGSK3 (Accession: XP_001690881). ▼ , ATP binding and active sites; ★ , phosphorylation site; Solid line under the residues indicates an activation loop.

GiGSKa



GiGSKb

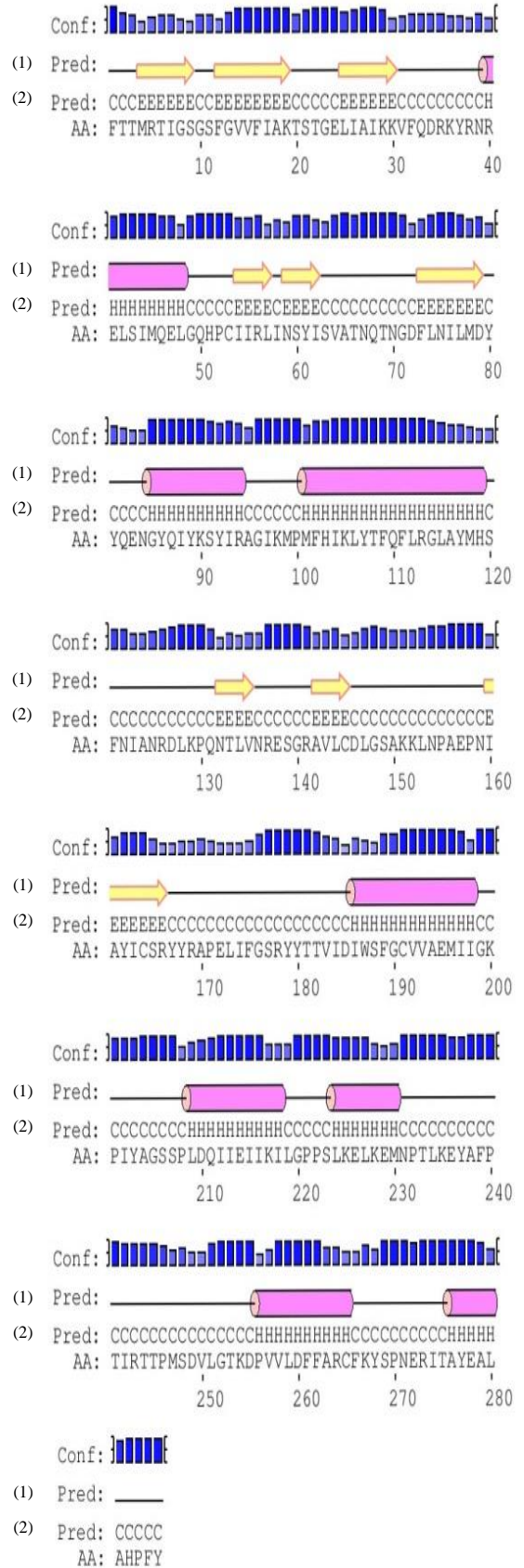

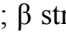



Figure 3.2: Secondary structure prediction of Serine/Threonine protein kinase, catalytic domains in *Giardia* GSKa and GSKb.

The Serine/Threonine protein kinase catalytic domains of GiGSKa and GiGSKb were input to the PSIPRED protein sequence analysis at Bioinformatic group, University College London (Jones, 1999). The PSIPRED show the secondary structure prediction of the input sequence. Legend: Conf, confidence of prediction (the higher the bars, the higher confidence values); (1) Pred, predicted secondary structure in a diagrammatic form; (2) Pred, series of coil (C), helix (H) and strand (E); AA, target sequence (S_Tkc from GiGSKa and GiGSKb); α helix, ; β strand,  and coil, 

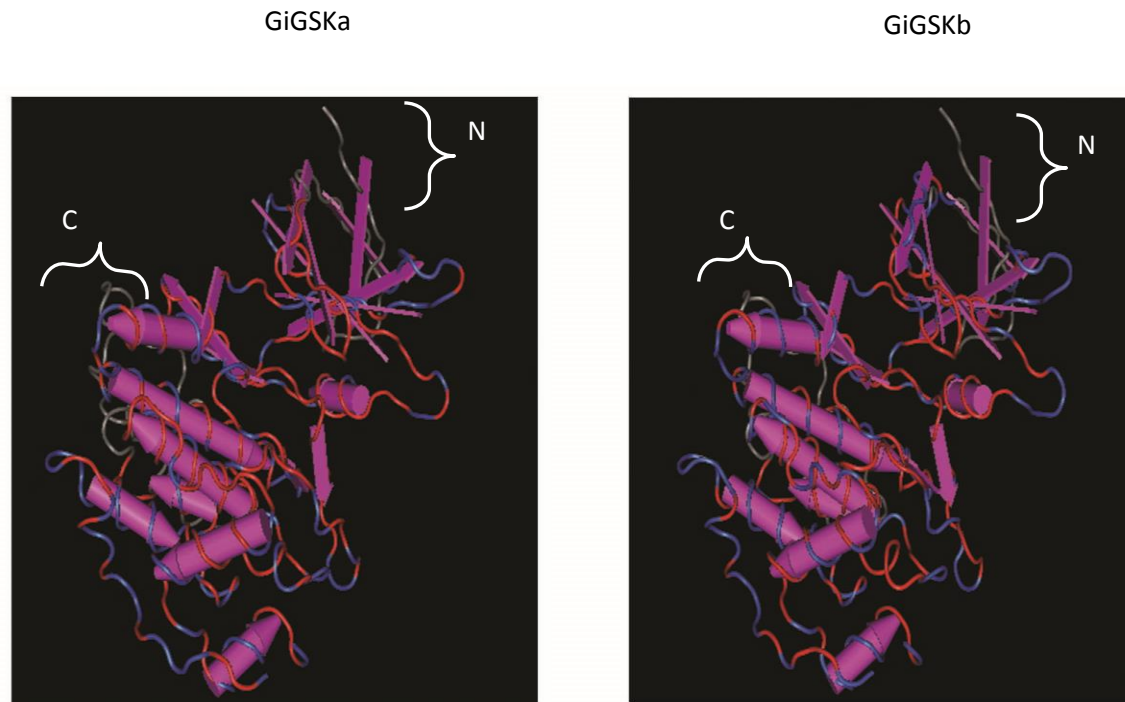


Figure 3.3: GiGSKa and GiGSKb Serine/Threonine kinase catalytic domain alignment on crystal structure of *Homo sapiens* glycogen synthase kinase-3 beta (HsGSK-3 β).

Giardia GiGSKs sequences were aligned onto the three-dimensional crystal structure of Human glycogen synthase kinase beta (Cheng *et al.*, 2011). Cn3D (version 4.1) was used to produce the three-dimensional structures of GSK-3 β and the overlaying alignments were red for identity and blue for similarity. The grey areas are non-aligned residues; the structure is presented in the secondary structure model, and thus consists of: alpha helices, pink cylinder arrows; beta pleated sheets, flat arrows; and coils, intervening loops. The N-terminal and C-terminal are labelled N and C, respectively.

3.2.3 Functional analysis of GiPI3Ks and GiGSKs

It is important to mention the function of the kinases and highlight the residues required to carry out the specific activity. Firstly, the GiPI3K1 and GiPI3K2 kinase domain has been determined against the structurally characterised kinase domain of PI3K γ from *S. scrofa* by Cox *et al.* (2006). The residues required for ATP binding site in *S. scrofa* PI3K γ

are Ser-806 binding to β -phosphate of substrate ATP and Lys-833 binding to α -phosphate of ATP and the PI3K inhibitor wortmannin. Other important residues that feature in *S. scrofa* PI3 γ are metal binding residues (Asp-836, Asn-951 and Asp-964) and the phospholipid substrate binding site that includes Lys-807, Lys-808 and Lys-973. Residues Lys-807 and Lys-808 function as a ligand for the I-phosphate of the substrate; GiPI3K1 shares these residues with *S. scrofa* PI3 PI3K γ , whereas GiPI3K2 shares only Lys-808. Residues Lys-973 acts as a ligand of the 5-phosphate and only GiPI3K1 shares phospholipid binding residues (Walker *et al.*, 1999).

Moreover, the activation loop of GiPI3K2 appears to be shorter than that found in GiPI3K1. GiPI3K2 lacks Lys-807, an important residue that is thought to provide I-phosphate of phospholipid substrate binding, and lacks Lys-973, which is another important residue that acts as a ligand for 5-phosphate of PI(4,5)P₂, as reported in the *S. scrofa* sequence. This suggests that GiPI3K2 belongs to the class III isoforms. Also, due to the similarity between GiPI3K and *S. scrofa* PI3K γ in lysine residues and a similar length in the activation loop, this strongly suggests that GiPI3K1 belongs to class I.

The structural functionality of *Giardia* GSKa and GSKb was also investigated here with comparison to the well-known *R. norvegicus* GSK-3 α structure. The region of the functional kinase domain reveals 72% and 74% similarity when *R. norvegicus* GSK-3 α is aligned to the GiGSKa and GiGSKb sequences, respectively. The residues required for ATP binding and kinase activity in *H. sapiens* and *R. norvegicus* are 88% and 90% conserved in GiGSKa and GiGSKb (Figure 3.4). The conserved residue responsible for tyrosine phosphorylation at Tyr-279 in *R. norvegicus* and the *H. sapiens* kinase domain are also found in GiGSKa and GiGSKb sequences. Moreover, the conserved GSK-3 primed substrate recognition site residues Arg-159, Arg-243 and Lys-268, which are present in *H. sapiens* and *R. norvegicus* kinase domains, are conserved in both GiGSKa and GiGSKb. Priming is important as it involves hierarchical pre-phosphorylation of the substrate by another kinase at a site downstream, towards the C terminus of the GSK-3 phosphorylation site, thus forming the GSK-3 recognition motif Ser/Thr-x-x-x-Ser/Thr-P. The conserved residues mentioned suggest that GiGSKa and GiGSKb are both functional kinase domains, meaning that it is possible to hypothesise that they would operate in the same manner as the well characterised GSK-3.

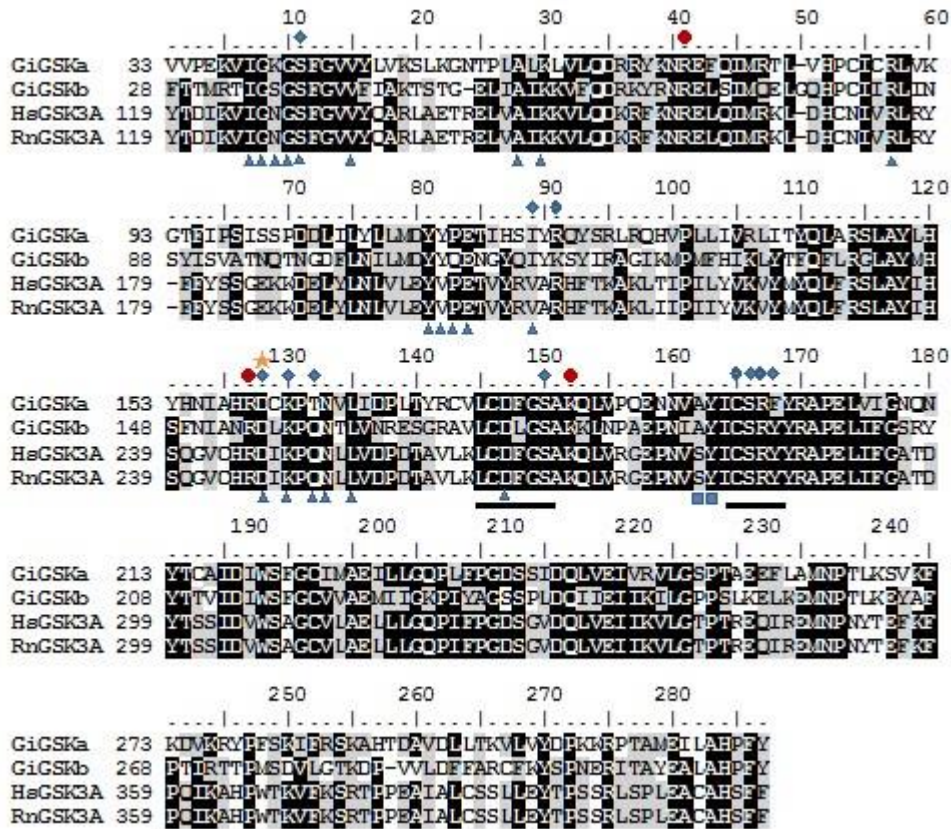


Figure 3.4: Detailed sequence investigation of Serine/Threonine kinase catalytic domain of GiGSKa and GiGSKb.

ClustalW multiple alignments of the kinase domain S_TKc of GiGSKa and GiGSKb with the well characterised GSK-3 α S_TKc domain from *H. sapiens* (HsGSK3A) [Accession: NP_063937.2] and *Rattus norvegicus* (RnGSK3A) [Accession: P18265]. The alignment highlights the similarity of the sequences, and also reveals conserved functional residues. Solid line under the residues indicates an activation loop using the ClustalW multiple alignment between well characterised sequence and GiGSKa and GiGSKb. ●, substrate binding sites; ◆, ATP binding and active sites; ▲, primed substrate recognition site binding sites; ■, possible proton acceptor site; ★, phosphorylation site.


```

          10          20          30          40          50          60          70          80
      ....|....|....|....|....|....|....|....|....|....|....|....|....|....|
GiGSKa 33 VVPEKVIIGKSGFGVVYLVKSLKNGTPLAKLVLQDRRVYKNREQIMR---TLVHPCTCRLVKGTFIPSISSPDD--LILY
GiGSKb 28 FTTMRTIGSGSFGVVFIAKT-STGELIAIKKVFQDRKYRNRELSIMO--ELGOHPCIRILIN-SYISVATNQTN-GDFLN
LmGSK3 20 FQVERMAGOGTFGTVOLGKEKSTGMSVAIKKVLQDPREFRNRELOIMODLAVLHHHPNIVLOQS-YFYTLGERDRR-DIYLN
SpGSK3 32 YTSKVVGSGSFGVVMQVHLIESDKAAIKRVLQDKRKRNRELOIMR---IMKHPNIVDLIA-YYFTTGDNSDE--VYLN
PFGSK3 67 YKLGNIICNGSFGVVYEAICIDTSEOVAIKKVLQDPQYKNRELMIMK---NLNHNINITYLKD-YYFTESFKKNEKNIIFLN
CeGSK3 36 YYDQVVICNGSFGVVFQAKLSTTNEVVAIKKVLQDKRKRNRELOIMR---KLNHPNIVKVKY-FFYSSGEKKDE--LYLN
GmGSK 74 YMAERVVGHGSFGVVFQAKLETGTVVAIKKVLQDKRKRNRELOIMR---LDDHPNIVVCLKH-CFFSTTEK-DE--LYLN
CrGSK3 59 YSTDRVVGNSSFGVVFQATCLETGTVVAIKKVLQDKRKRNRELOIMK---LVDHPNIVKVKH-CFYSHTDK-DE--TYLH
DdGSK3 56 YITEGVICNGSFGVVTQAVADTKGVVAIKKVLQDQRYKNRELOIMK---MLNHNINIVSLKN-SFYT--SDNDE--VYLN
DmGSK3 33 YTDKVVVGNSSFGVVFQAKMVPSEVVAIKKVLQDRRKRNRELOIMR---KLRHONITLKW-FFFSSGEKKDE--VYLN
AtGSK3 82 YIAEHVGTGSFGVVFQAKRETGEVVAIKKVLQDKRKRNRELOIMO---MDDHPNIVVCLKH-SFYSRTE-EE--VYLN
HsGSK3A 119 YTDIKVICNGSFGVVYQARLAETRELVAIKKVLQDKRKRNRELOIMR---KLDHCNIVRLRY-FFYSSGEKKDE--LYLN
SsGSK3A 119 YTDIKVICNGSFGVVYQARLADTRELVAIKKVLQDKRKRNRELOIMR---KLDHCNIVRLRY-FFYSSGEKKDE--LYLN
SsGSK3B 56 YTDKVICNGSFGVVYQAKLDSGEVVAIKKVLQDKRKRNRELOIMR---KLDHCNIVRLRY-FFYSSGEKKDE--VYLN
RnGSK3A 119 YTDIKVICNGSFGVVYQARLAETRELVAIKKVLQDKRKRNRELOIMR---KLDHCNIVRLRY-FFYSSGEKKDE--LYLN
RnGSK3B 56 YTDTKVICNGSFGVVYQAKLDSGEVVAIKKVLQDKRKRNRELOIMR---KLDHCNIVRLRY-FFYSSGEKKDE--VYLN
DrGSK3A 83 YTDIKVICNGSFGVVYQARLIDSEVVAIKKVLQDKRKRNRELOIMR---KLDHCNIVRLRY-FFYSSGEKKDE--VYLN

```

```

          90          100          110          120          130          140          150          160
      ....|....|....|....|....|....|....|....|....|....|....|....|....|....|
GiGSKa 113 ILMDYYPETIHSIYROYSRLRQHVPLLIIVRLITYOLARSLAYLHY--HNTAHRDCKPTNVLIDPLTYRCVLCDFGSAKQL
GiGSKb 108 ILMYYQENGYQIYKSYIRAGIKMFMFHIKLYTFQFLRGLAYMHS--FNIANRDLKPNLTVNRESGRAVLCDLGSAKKL
LmGSK3 100 VMVEYVPTLHRCORNYRROVAPPPIIKVFLFQLRISIGCLHLPVSNVCHRDIKPNVNLVNEADGTLKLCDFGSAKKL
SpGSK3 112 LVLEFMPETIYRASRLYTRQKLSMFMLEVKLYIYQLRSLAYIHA--SGTCHRDIKPONLLDPENGILKLCDFGSAKIL
PFGSK3 147 VMVEYIPQTVHKYMKYYSRNNQALMFLVVKLYSYQLCRALSITHS--KFTCHRDIKPONLLDPERTHLLKLCDFGSAKNL
CeGSK3 116 LILEYVPEVYRVARHYSQRQQIPMIYVKLYMYQLRSLAYIHS--IGTCHRDIKPONLLDPESGVLLKLCDFGSAKYL
GmGSK 154 LVLEYVPEVNRVIKHYKNLQRMPLIYVKLYIYQIFRALSITHRC-IGVCHRDIKPONLLVNPHTHVKLCDFGSAKVL
CrGSK3 139 LVLEFVPTVYRISKHYAKNQRMPNLFVVKLYIYQIMCRALNSIHK--MGTCHRDIKPONLLVNTETHOLKLCDFGSAKVL
DdGSK3 136 LVLEYVPTVYRVSRRHYSMSKQPVENIFVKLYIYQLCRSINYIHS--LGTCHRDIKPONLLDSTSTLKLKLCDFGSAKIL
DmGSK3 113 LVMEFLPETLYKVEROYARAKQTLVNFVRLYMYQLRSMGYIHS--LGTCHRDIKPONLLDSETGVLLKLCDFGSAKQL
AtGSK3 162 LVLEFVPEVNRRTARSYSRNLMPLIYVKLYIYQICRGLAYLHNC-CGLCHRDIKPONLLVNPHTHOLKICDFGSAKVL
HsGSK3A 199 LVLEYVPEVYRVARHFTKAKLTIPIIYVKVVMYQLRSLAYIHS--QGVCHRDIKPONLLVDPDTAVLKLKLCDFGSAKQL
SsGSK3A 199 LVLDYVPEVYRVARHYSRAKQTLPIIYVKLYMYQLRSLAYIHS--QGVCHRDIKPONLLVDPDTAVLKLKLCDFGSAKQL
SsGSK3B 136 LVLDYVPEVYRVARHYSRAKQTLPIIYVKLYMYQLRSLAYIHS--FGTCHRDIKPONLLVDPDTAVLKLKLCDFGSAKQL
RnGSK3A 199 LVLEYVPEVYRVARHFTKAKLTIPIIYVKVVMYQLRSLAYIHS--QGVCHRDIKPONLLVDPDTAVLKLKLCDFGSAKQL
RnGSK3B 136 LVLDYVPEVYRVARHYSRAKQTLPIIYVKLYMYQLRSLAYIHS--FGTCHRDIKPONLLVDPDTAVLKLKLCDFGSAKQL
DrGSK3A 163 LVLDVPEVYRVARHFNKSKTTIPIIYVKVVMYQLRSLAYIHS--QGVCHRDIKPONLLVDPDTAVLKLKLCDFGSAKQL

```

```

          170          180          190          200          210          220          230          240
      ....|....|....|....|....|....|....|....|....|....|....|....|....|....|
GiGSKa 193 VPOENNVAICSRFYRAPELVIIGNONYTCAIDWISFGCIMAELLGQPLFPGDSSIDQOLVEIVRVLGSPTAEELFAMNPT
GiGSKb 188 NPAEPNVAICSRFYRAPELIFGSRYYTVIDWISFGCVVAEMIIGKPIYAGSSPLDQIIEIKILGPPSLKELKEMNPT
LmGSK3 180 SPSEPNVAICSRFYRAPELIFGNQHYTTAVDWISVGCIFAEMLGEPHFRGDNAGOLHEIVRVLGCPSREVLRLKLNPS
SpGSK3 192 VAGEPNVSYICSRFYRAPELIFGATDYTHAIDWISGCVMAELMLGHPHFGPESGIDQOLVEI IKVLGTPSREQIKTMNPN
PFGSK3 227 LAGQRSVSYICSRFYRAPELMGSIYNTTHIDWISLGLIAEMLLGYPHFGSOSSVDQLVRI IQVLGTPTEDQLKEMNPN
CeGSK3 196 VRNEPNVSYICSRFYRAPELIFGATNYTNSIDWISAGVVAELLGQPIFPGDQSGVDQOLVEI IKVLGTPTREQIKSMNPN
GmGSK 234 VKGEPNLSYICSRFYRAPELIFGATBYTTAIDWISVGCVLAELLGQPIFPGESGVQDQOLVEI IKVLGTPTREIKCMNPN
CrGSK3 219 VKGEPNLSYICSRFYRAPELIFGATDYTSAIDWISVGCVLAELLGQPIFPGESGVQDQOLVEI IKVLGTPTREINAMNPN
DdGSK3 216 IKGETNVSYICSRFYRAPELIFGSIYNTTTIDWISLGCVLAELLGQPIFPGENGIDQOLVEI IKVLGTPTKQOIHAMNPN
DmGSK3 193 ISGEPNVSYICSRFYRAPELIFGSDTYTTKIDWISAGCVMSSELLGQPIFPGDQSGVDQOLVEI IKVVMGTPTSEQLHDMNPN
AtGSK3 242 VKGEPNLSYICSRFYRAPELIFGATBYTTAIDWISGCVMAELLGQPIFPGESGVQDQOLVEI IKVLGTPTREIKCMNPN
HsGSK3A 279 VRGEPNVSYICSRFYRAPELIFGATDYTSSIDWISAGCVLAELLGQPIFPGDQSGVDQOLVEI IKVLGTPTREQIREMNPN
SsGSK3A 279 VRGEPNVSYICSRFYRAPELIFGATGYTSSIDWISAGCVLAELLGQPIFPGDQSGVDQOLVEI IKVLGTPTREQIREMNPN
SsGSK3B 216 VRGEPNVSYICSRFYRAPELIFGATDYTSSIDWISAGCVLAELLGQPIFPGDQSGVDQOLVEI IKVLGTPTREQIREMNPN
RnGSK3A 279 VRGEPNVSYICSRFYRAPELIFGATDYTSSIDWISAGCVLAELLGQPIFPGDQSGVDQOLVEI IKVLGTPTREQIREMNPN
RnGSK3B 216 VRGEPNVSYICSRFYRAPELIFGATDYTSSIDWISAGCVLAELLGQPIFPGDQSGVDQOLVEI IKVLGTPTREQIREMNPN
DrGSK3A 243 VRGEPNVSYICSRFYRAPELIFGATDYTSSIDWISAGCVLAELLGQPIFPGDQSGVDQOLVEI IKVLGTPTREQIREMNPN

```

Figure 3.5: Multiple alignment of Serine/Threonine kinase catalytic domain (S_TKc).

The S_TKc domain of several sequences was aligned using ClustalW (Thompson *et al.*, 1994) with GiGSKa and GiGSKb. The accession numbers of the following GSKs sequences are: *L. major* GSK-3, LmGSK3 [Accession: CAJ03501.1], *S. pombe* GSK-3, SpGSK3 [Accession: NP_593134], *Plasmodium falciparum* GSK-3, PfGSK3 [Accession: XP_001351197], *C. elegans* GSK-3, CeGSK3 [Accession: NP_493243], *G. max* GSK, GmGSK [Accession: ACQ91102], *C. reinhardtii* GSK-3, CrGSK3 [Accession: XP_001690881], *D. discoideum* GSK-3, DdGSK3 [Accession: XP_645156], *D. melanogaster* GSK-3, DmGSK3 [Accession: P83101], *A. thaliana* GSK-3, AtGSK3 [Accession: AAG50665], *H. sapiens* GSK-3 α , HsGSK3A [Accession: NP_063937.2], *S. scrofa* GSK-3 α and GSK-3 β , SsGSK3A/SsGSK3B [Accession: NP_063937 and NP_001121915, respectively], *R. norvegicus* GSK-3 α and GSK-3 β , RnGSK3A/RnGSK3B [Accession: P18265 and P18266, respectively] and *D. rerio* GSK-3 α , DrGSK3A [Accession: NP_571465]. The shading threshold was set at 70%, where grey shading refers to similar residues and black shading refers to identical residues. The underline in blue represents ATP binding sites and underline in red represents the activation loop.

3.2.4 Prediction of GiPI3Ks and GiGSKs protein localisation sites in cell through bioinformatics learning algorithms

PSORTII (Nakai, 1999) and iPSORT (Bannai *et al.*, 2002) are bioinformatics programs that were used to predict the subcellular localisation sites of the query protein in the cell. Although the program PSORTII has massive potential, it assumes that all proteins are localised in a single subcellular compartment within the systems; thus, it should not be assumed that all query proteins are assigned to one of the known compartments. Both GiPI3K1 and GiPI3K2 with their kinase domains sequences removed were predicted by PSORTII to localise to the nucleus (see Table 3.8). However, if the GiPI3K1 sequence is entered without the removal of the kinase domain, the protein is predicted to localise to the plasma membrane. This shows that the kinase domain influences the overall prediction, possibly due to bias in the training data used by PSORTII; alternatively, it is possible that GiPI3K1 may localise to multiple known compartments. There were no signal peptides or any mitochondrial targeting signal sequences identified in either of GiPI3K1 or GiPI3K2 using iPSORT prediction.

G. intestinalis GiGSKa and GiGSKb were also submitted for PSORTII prediction as a full sequence and sequences without the serine/threonine kinase catalytic domain (S_TKc). The exclusion of the S_TKc domain was performed to ensure that the domain did not have any influence on the entire PSORTII sequence prediction. In GiGSKb, the prediction of full length sequence was cytoplasmic; however, upon removal of the kinase domain, the result of the prediction was nuclear (see Table 3.9). In mammalian cells, GSK-3 is constitutively active in resting conditions. However, GSK-3 becomes inactivated

through phosphorylation on the N-terminal residue Ser-21 for GSK-3 α and Ser-3, for GSK-3 β , respectively. Wakefield *et al.* (2003) observed accumulation of phospho-GSK-3 at the centrosomes upon entry into mitosis, and further reported that PKB is responsible for phosphorylating and inactivating GSK-3 at the centrosome during mitosis. Therefore, the prediction that GiGSKb would localise in the nucleus seems appropriate to this example. Moreover, the results from PSORTII for GiGSKb show a predicted nuclear localisation of 69.6%, which may be due to the nuclear localisation signals (NLS). NLS sequences are rich in either arginines or lysines. These two residues are required for transporting proteins through the nuclear pore complex into the nucleus (Boulikas, 1993).

Table 3.8: The subcellular localisation of GiPI3K1 and GiPI3K2 prediction using the internet program PSORTII.

PSORTII is a computer-based program that compiles a list of different subprograms which use mathematical algorithms to calculate the probability of the localisation of query sequences. These subprograms identify query sequences for specific localisation; for example, signal sequence recognition, ER retention motif, and peroxisomal targeting signals. The PSORTII program uses the *k*-nearest neighbour algorithm to predict the probability of the subcellular localisation of the query sequence through values of the subprograms and training data. The values of *k*-nearest neighbour predictions are in percentages, where a higher percentage is used for the final prediction.

Protein	PSORTII prediction
GiPI3K1	<p>34.8% plasma membrane; 17.4% nuclear; 17.4% endoplasmic reticulum; 13.0% vacuolar; 4.3% cytoskeletal; 4.3% Golgi; 4.3% mitochondrial; 4.3% cytoplasmic.</p> <p>No significant signal peptides / motifs identified</p> <p>Prediction for sequence is Plasma membrane</p>
GiPI3K1 without kinase domain	<p>56.5% nuclear; 21.7% cytoplasmic; 8.7% cytoskeletal; 8.7% mitochondrial; 4.3% Golgi</p> <p>No significant signal peptides / motifs identified</p> <p>Prediction for sequence is Nuclear</p>
GiPI3K2	<p>69.6% nuclear; 13.0% cytoplasmic; 8.7% mitochondrial; 4.3% vesicles of secretory system; 4.3% endoplasmic reticulum</p> <p>Nuclear localisation signals KKKR at 632; RHRR at 1003; PMRHRI at 1001</p> <p>ER retention motif signal KKXX-like motif in the C-terminus QGFK</p> <p>2nd peroxisomal targeting signal RLDMLYVHL at 1145</p>

	Prediction for sequence is Nuclear
GiPI3K2 without kinase domain	73.9% nuclear; 17.4% cytoplasmic; 4.3% cytoskeletal; 4.3% plasma membrane Nuclear localisation signals KKKR at 632; RHRR at 1003; PMRHRI at 1001 Prediction for sequence is Nuclear

Table 3.9: The subcellular localisation of GiGSKa and GiGSKb prediction using the internet program PSORTII.

PSORTII is a computer-based program that compiles a list of different subprograms which use mathematical algorithms to calculate probability of the localisation of query sequences. These subprograms identify query sequences for specific localisation; for example, signal sequence recognition, ER retention motif, and peroxisomal targeting signals. The PSORTII program uses the *k*-nearest neighbour algorithm to predict the probability of subcellular localisation of the query sequence through values of the subprograms and training data. The values of *k*-nearest neighbour predictions are in percentages, where the higher the percentage is used for the final prediction.

Protein	PSORTII prediction
GiGSKa	69.6% cytoplasmic; 17.4% nuclear; 13.0% mitochondrial No significant signal peptides or protein motifs Prediction for sequence is Cytoplasmic
GiGSKa without Kinase domain	43.5% cytoplasmic; 30.4% nuclear; 17.4% mitochondrial; 4.3% vesicles of secretory system; 4.3% cytoskeletal No significant signal peptides or protein motifs. Prediction for sequence is Cytoplasmic

<p>GiGSKb</p>	<p>60.9% cytoplasmic; 30.4% nuclear; 4.3% vacuole; 4.3% mitochondrial</p> <p>ER membrane retention signal KKXX-like motif in the C-terminus KIRP</p> <p>Prediction for sequence is Cytoplasmic</p>
<p>GiGSKb without kinase domain</p>	<p>69.6% nuclear; 13% cytoplasmic; 13% mitochondrial; 4.3% cytoskeletal</p> <p>ER membrane retention signal KKXX-like motif in the C-terminus KIRP</p> <p>Prediction for sequence is Nuclear</p>

3.3 Discussion

The availability of various bioinformatics tools has paved the way for scientists to identify sequence of interest within the model organism. These analysis tools such as sequence BLAST, ClustalW, secondary protein structure model, three-dimensional structural display through sequence alignment and domain prediction programs have provided relevant information and a platform for experimental work. *G. intestinalis* PI3K isoforms (GiPI3K1 and GiPI3K2) can be found within the giardial genome and it has been shown that the closest class that these isoforms represent is class IB and class III for GiPI3K1 and GiPI3K2, respectively. Indeed, a class II PI3K sequence search did not reveal any homologues of class II PI3K in *G. intestinalis*. However, the reason why there may only be two isoforms of PI3K homologues in *G. intestinalis* could be due to reductive evolution as a result of the parasitic way of life. Mammalian cells may have as many as eight PI3K isoforms (Fry, 2001).

The large insertion in the PI3Ks kinase domain means that GiPI3K1 and GiPI3K2 are much larger than in other organisms containing homologues of PI3K. The study by Cox *et al.* (2006) concluded that the functional significance of the insertion sequence in the kinase domain region of PI3K is still unknown. However, it has been observed that the long insertions in the kinase domain did not interfere with substrate binding and formation of the active site using three dimensional mapping alignments in GiPI3K1. On the other hand, the kinase insertion of GiPI3K2 has the potential to inhibit substrate entry because the insertion residues may fold at its amino and carboxy-terminal, thus affecting the active site of the enzyme.

The bioinformatics analysis indicates that the *G. intestinalis* genome encodes two GSKs from the CMGC group. Initially GSK was described to be a regulator of glycogen metabolism; however, GSK-3 (where the 'three' in GSK-3 derived from is currently unknown) is also an important component of the *Wnt* pathway in many organisms, including humans and *D. melanogaster* (Komiya *et al.*, 2008). Therefore, the name GSK is somewhat of a misnomer because GSK-3 has a variety of other functions, as described in the introduction (Ojo *et al.*, 2011). Sequence analysis in similarity and identity searches within the S_Tkc catalytic domain has shown the presence of highly conserved residues in both GiGSKa and GiGSKb. Although it has been mentioned that the kinase domain between GSK-3 α and GSK-3 β is 98% identical in mammalian cells, between GiGSKa and GiGSKb it is 71%. This indicates that there are two homologues of GSK in *G. intestinalis*

that contain the S_Tkc domain. It has been identified that the GSK-3 α homologue does have a longer N-terminus, with the *H. sapiens* and GSK-3 α having 483 residues compared to the 420 residues in GSK-3 β . GiGSKa contains 370 amino acids, whereas GiGSKb contains 350 amino acids; this means that the difference in the size of GSKs within *G. intestinalis* and mammalian cells is up to one hundred amino acid residues. However, the alignment of the kinase domain sequence using ClustalW has shown that important amino acid residues are highly conserved within the kinase domain of *Giardia* and mammalian cells (Figure 3.4). Identification of threonine phosphorylated proteins was highlighted in the alignment and abundant phosphoserine and phosphothreonine presence within the *Giardia* trophozoites lysate has been detected using western blot (Manning *et al.*, 2011).

The program PSORTII, predicting the localisation of GSKs in *Giardia*, has calculated that GiGSKa is in the cytoplasm whereas GiGSKb may be in the nucleus or cytoplasmic through specialised learning algorithms. Given the background of GSK-3 signalling in mammalian cells, the predicted subcellular localisation of the giardial GSKs matches other GSK-3 proteins in mammalian cells. Therefore, GiGSKa may be phosphorylated by PKB leading to the inactivation of cyclin D and the initiation of proteolytic degradation. On the other hand, nuclear localised GiGSKb may play a role in cell cycle regulation.

In summary, detailed analysis of the *Giardia* genome has revealed the gene sequence that encodes PI3Ks and GSKs. However, due to the divergent nature of *G. intestinalis* as a parasitic organism that is undergoing reductive evolution, kinases in *Giardia* may have lost many of their basic cellular functions. Research presented in the next chapter involving these protein kinases will attempt to understand the cellular functions of PI3Ks and GSKs in *Giardia* trophozoites.

CHAPTER 4: Investigating the effect of PI3K and GSK inhibition on *G. intestinalis*

4.1 Introduction

In this Chapter, a panel of inhibitors has been utilised to study the effect of PI3K and GSK-3 signalling in *Giardia* trophozoites. Previous studies mentioned earlier in the introduction chapter have demonstrated that exposure of trophozoites to LY294002 appeared to initiate the process of encystation (Cox and Tovar, unpublished data). With this in mind, in order to try and understand the molecular basis of this observation, we carried out the work described in this chapter. There were three PI3K inhibitors that used: LY294002, wortmannin and a novel inhibitor PI-103. LY294002 and wortmannin are both commonly used inhibitors of PI3K. Although wortmannin had been shown in the literature to be more potent and specific inhibitor of PI3K than LY294002 (Bain *et al.*, 2007), it was recommended that both of these inhibitors may cause a similar phenotypic effect to inhibit the activity of PI3K (Davies *et al.*, 2000).

LY294002 is a PI3K inhibitor of p110 α , p110 β and p110 δ and was synthesised from the flavonoid quercetin. Quercetin is a PI3K inhibitor marketed by Calbiochem. It can inhibit a number of protein serine/threonine kinases such as AMPK, CKII, MAPKAP-K1/RSK2 and S6K1 with similar concentrations to PI3K. LY294002 has been reported to inhibit the PI3K family and other kinases through competitive inhibition at the ATP binding site (Davies *et al.*, 2000). Moreover, it has been described that LY294002 used at microMolar (μ M) concentrations is effective against protein kinases from humans. Also, LY294002 has been shown to inhibit other kinases such as mTOR, DNA-PK (DNA-dependent protein kinase), GSK-3, CKII and Pim-1 (proto-oncogene serine/threonine-protein kinase) (Bain *et al.*, 2007, Gharbi *et al.*, 2007).

Wortmannin is a commonly used PI3K inhibitor, it has a steroid metabolite structure derived from the fungi *Penicillium funiculosum* and *Talaromyces wortmanni* (Brian *et al.*, 1957). The mode of action of wortmannin is that it inhibits members of PI3K family through irreversible inhibition at nanoMolar (nM) concentrations reported in the mammalian cells study. To interact with the substrate, wortmannin forms a covalent link to a lysine residue in the ATP-binding pocket of PI3K (Lys802 in p110 α and Lys833 in PI3K γ). However, at higher concentrations, wortmannin has been shown to target other

kinases in mammalian cells such as PI4K α/β , mTOR and DNA-PK (Stein and Waterfield, 2000).

PI-103 is a novel synthetic small molecule of the pyridofuropyrimidine class, which has been reported to be both a potent and selective inhibitor of class I PI3K (Raynaud *et al.*, 2007, Westhoff *et al.*, 2009). PI-103 is an ATP-competitive PI3K inhibitor that can also inhibit several other protein kinases such as DNA-PK, mTORC1 and mTORC2, with an IC₅₀ value of 2nM, 20 nM and 83 nM, respectively (Raynaud *et al.*, 2007). PI-103 inhibits mTOR through its morpholine ring, which binds to the adenine pocket, forming two hydrogen bonds; the phenol group binds to the inner pocket to form another two hydrogen bonds. These hydrogen bonds are likely to be important for the affinity of PI-103 for mTOR (Yang *et al.*, 2013). *In vitro* studies have shown that PI-103 inhibits human cancer cell growth and has been observed *in vivo* to have anti-tumour activity in several human tumour xenograft models (Raynaud *et al.*, 2007). Recent studies have reported that PI-103 binds with class I PI3K of the human PI3K α by forming a new hydrogen bond with Lysine residue 802 (Lys802), which is adjacent to the ATP catalytic site, in order to increase binding affinity (Zhao *et al.*, 2013).

The application of LY294002 and wortmannin inhibitors in mammalian cells has contributed toward our understanding of the PI3K signalling pathways. Many researchers have linked LY294002 and wortmannin to cell growth inhibition, apoptosis and cellular proliferation. Since these inhibitors of PI3K were discovered, steps have been taken by scientists to understand the complex cellular signalling pathways that involve the phosphoinositide family and PI3K activity. Early research showed that wortmannin, a known inhibitor of respiratory-burst activity, acts on PI3Ks by inhibiting PIP₃ production at concentrations between 10 and 100 nM (Arcaro and Wymann, 1993). LY294002 was synthesised using the bioflavonoid quercetin as a model compound (Vlahos *et al.*, 1994). Quercetin has been demonstrated to inhibit kinases, including PI3K, other tyrosine and serine/threonine kinases (Matter *et al.*, 1992). Moreover, LY294002 was found to be a selective inhibitor of PI3K with an approximately three-fold greater potency than quercetin (Vlahos *et al.*, 1994). Vps 34 (vacuolar protein sorting 34) was first described to be the sole PI3K in yeast. Vps 34 belongs in class III of the PI3K family, and is the only PI3K that is expressed in all eukaryotic cells. Previous works have indicated that Vps 34 in yeast is relatively resistant to wortmannin with protein structural studies highlighting key differences in residues between human class I PI3K and Vps 34. This may explain the

reason for inhibitor resistance (Backer *et al.*, 2008). The pyridofuopyrimidine PI-103, a novel inhibitor of PI3K, was pharmacologically characterised in 2007 (Hayakawa *et al.*, 2007). This inhibitor of PI3K has been reported not only to be a highly potent inhibitor (IC₅₀ values of 3 nmol/L) but also a selective inhibitor of class I PI3K (Bain *et al.*, 2007, Raynaud *et al.*, 2007).

There are different methods that may be carried out to study the inhibition effect of PI3K *in vivo* and *in vitro*. Experimental designs to detect the activity of PI3K usually start with purified protein (Bain *et al.*, 2007). During *in vivo* testing, cells are labelled directly with radioactive ³²[P]; they are then harvested and the lipid is extracted for radioactive activity after treatment with inhibitors. Comparison between the control cells (cells with ³²[P] but without PI3K treatment) and sample cells (with PI3K inhibitors) were completed using thin layer chromatography (TLC) to measure the level of phosphate in PIP₃ products of PI3K (Zhou *et al.*, 1998).

Downstream of PI3K signalling, protein kinase B acts as the direct effector of PI3K signalling and plays an important role in cell survival, cell proliferation and cell differentiation. Activated PKB will phosphorylate downstream protein effectors which will stimulate cell survival signals, thus preventing the cells from undergoing cell death (Franke *et al.*, 1995). An experiment using anti-phosphorylated PKB was able to reveal the effect of wortmannin and LY294002 on the inhibition of PI3K, as the results show that PI3K inhibition effectively blocks the phosphorylation of PKB (Cheatham *et al.*, 1994).

Inhibitors of PI3K, such as LY294002, wortmannin and PI-103, have contributed towards our understanding of the PI3K pathway. Extensive works in this field have been reported in many different types of cells, most of which are from mammalian cells. In addition, work in *G. intestinalis* by Hernandez *et al.* (2007) reported inhibition of the PI3K signalling pathway by both LY294002 and wortmannin. This contradicts previous findings from this laboratory suggesting that wortmannin did not affect trophozoite growth while LY294002 did (Cox *et al.*, unpublished data). With this in mind, the effects of PI3K inhibition were further investigated in this work. The inhibition of GSK, a downstream effector of PI3K signalling, was also studied.

4.2 Experimental Results

Experiments in this Chapter were demonstrated by utilising two different methods. One approach uses the method of counting the number of cells in each of the subcultured samples. Trophozoites in the sample tube were directly counted visually using a haemocytometer under a light microscope and calculated to give cells per ml (see section 2.2.3). An average number of cells in three counts was collected, standard deviation of the data was calculated and graphs were plotted showing the number of trophozoites per millilitre against either concentration of an inhibitor or time (hours). The second approach demonstrates the use of methylene blue staining of trophozoite cells. The rationale for using this technique is that the methylene blue assay allows a higher throughput of samples under different treatments. Moreover, this quantitative method provides an efficient and effective means of calculating the total number of cells. The absorbance reading was measured on each sample, which correlates to the number of cells in the individual population. The methylene blue staining cannot penetrate viable cells; therefore, cells were initially fixed, and stained with methylene blue, consequently allowing the membrane of the cell to turn deep blue. After the cells were stained, hydrochloric acid was used to de-stain the cells and absorbance was taken in order to quantify how many cells were in each sample. Both of the approaches described above were carried out to monitor the effect of the inhibitor under two different conditions.

4.2.1 Effect of PI3K inhibitor LY294002 on *G. intestinalis*

Here, inhibitors of PI3K are tested to determine the roles of PI3K activity on trophozoite proliferation. Prior to the inhibition experiments, trophozoite growth curves were determined to establish the normal course of vegetative growth. A number of *G. intestinalis* trophozoite log growth curves were found to be reproducible, showing a period of exponential growth following subculture. After the exponential growth, trophozoites enter the stationary phase, displaying constant numbers of cells (Figure 4.1). The concentrations of LY294002 used were reported at 10 - 50 μM to inhibit class I PI3Ks in cell-based assays (Bain *et al.* 2007). Therefore, in this experimental work, trophozoites were treated with LY294002 to a final concentration of 10, 25, 30, 50 and 75 μM . LY294002 was added to exponentially-growing trophozoites to observe any inhibition of growth. If trophozoites were treated with LY294002 at a late exponential or even stationary

phase, the observation of a decrease in cell number could be due to the shortage of nutrients and over-populated cultures (Figure 4.1).

In Figure 4.2, the exponential growing trophozoite cells were treated with the PI3K inhibitor LY294002 for 48 hours. The rate of trophozoite cell proliferation at the end of 48 hours was measured by the average optical density reading at 655 nm following treatment using methylene blue staining (Houk Kong *et al.*, 2011). The effect of LY294002 on trophozoites was dose-dependent because cell proliferation decreased significantly with the increasing concentration of LY294002. At concentrations of 25-30 μM , we were able to observe approximately 50% inhibition of growth in trophozoite cell cultures. Toward higher concentrations of 50 and 75 μM of LY294002, a decrease in trophozoite proliferation of approximately 75% was observed compared to control cells exposed to equal volume of DMSO. The control background absorbance in each experiment was observed by measuring the well containing culture medium with no cells. Any background absorbance was subtracted from both the drug-treated values and the control values.

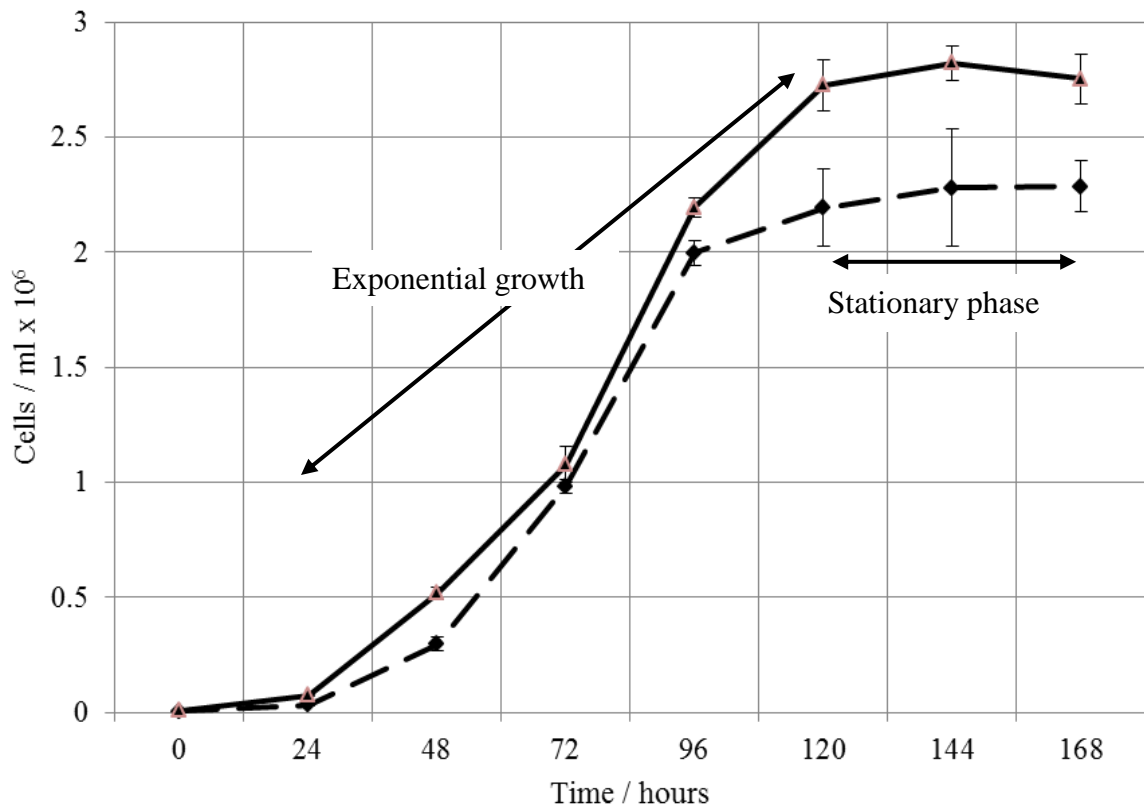


Figure 4.1: *Giardia intestinalis* growth curve over a 168-hour period.

Giardia intestinalis trophozoites were subculture into fresh culture medium and counted over 168 hours. Exponential growth and stationary phases are indicated and the error bars on each time point show the standard deviation of the mean of 3 counts per time point. The solid and dotted lines indicate two individual growth curves by trophozoites; at time zero, solid line starting inoculum: 8.2×10^3 cells/ml and dotted line starting inoculum: 4×10^3 cells/ml.

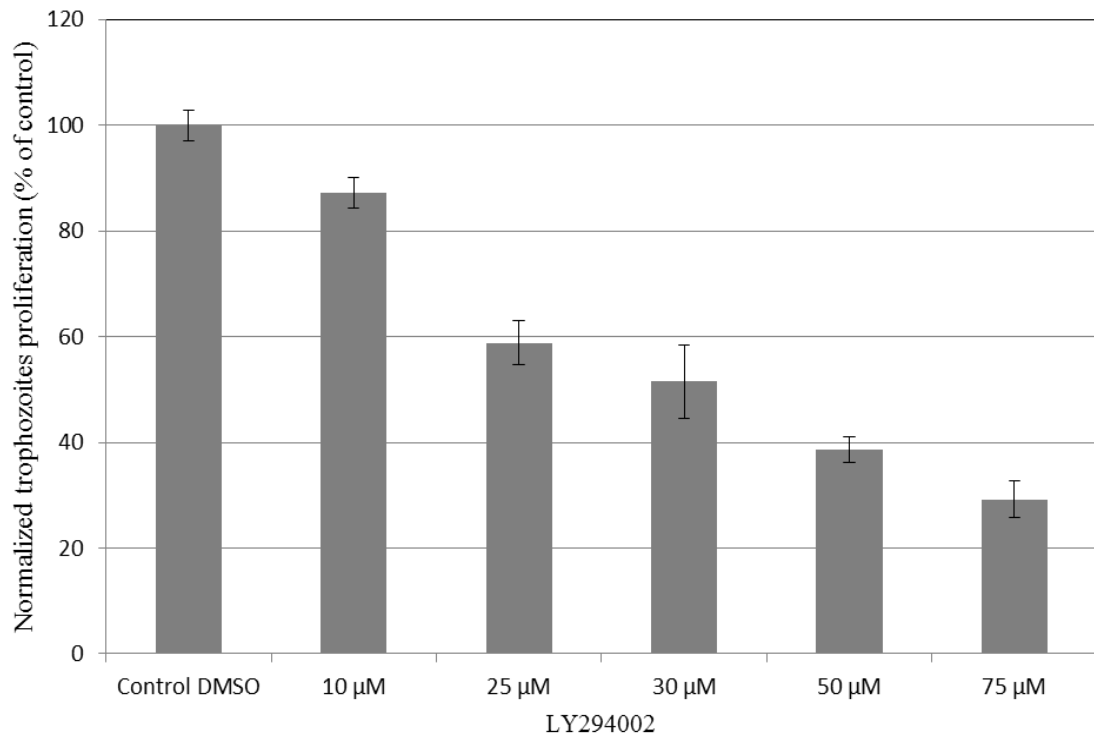


Figure 4.2: Inhibition of trophozoites proliferation by PI3K inhibitor LY294002.

Trophozoites with starting inoculums of 1×10^5 cells/ml were treated with PI3K inhibitor LY294002 to a final concentrations of 0 (DMSO-solvent control), 10 μM, 25 μM, 30 μM, 50 μM and 75 μM. Following 48 hours of incubation, trophozoites were harvested, pipetted into a microplate, fixed, stained with methylene blue, and quantified by measuring absorbance at 655 nm. The data show the average number of cells of three samples measured by absorbance at 655 nm and the error bars represent the standard deviation of the data.

These data suggest that cell growth was reduced due to the effect of LY294002 on PI3Ks intracellular signalling in *Giardia* trophozoites. Another important PI3K inhibitor, wortmannin, was tested to verify this hypothesis. The concentrations of wortmannin experimental work reported by Bain *et al.* (2007) found that wortmannin inhibits class I and II PI3Ks activities at 50-100 nM. Wortmannin can enter *Giardia* trophozoites through the parasite biological membrane. Research by Cox *et al.* (unpublished) tested the inhibitory action of wortmannin against human embryonic kidney-293 cells which resulted in decreased levels of phosphorylated PKB compared to the untreated control. This result

revealed that wortmannin solution was capable of effectively inhibiting the HEK-293 PI3Ks to reduce PKB activation by phosphorylation. Hernandez *et al.* (2007) reported wortmannin to inhibit trophozoite cell growth with $IC_{50} \sim 11 \mu\text{M}$. Therefore, the concentration gradients in the chosen experiment were 0.1, 0.5, 1, 5, 10 and 15 μM . The rationale behind these concentration ranges with the highest concentration being 15 μM was because there was no effect of growth inhibition observed at 1 μM ; therefore, the concentration of 15 μM wortmannin was set to determine whether this excessive concentration showed any effect on PI3K inhibition. The results of the wortmannin experiment are shown in Figure 4.3; here, the number of trophozoites is represented through average optical density at 655 nm against different concentrations of wortmannin and the DMSO control. Compared with the control, no significant different in cell number was observed across the chosen concentrations. The results were found to be reproducible for a further two separate experiments. It may be useful to compare the giardial PI3Ks with wortmannin-insensitive PI3Ks; an example of this is in yeast. Yeast Vps 34 is $\sim 1000\text{x}$ less susceptible to wortmannin inhibition than its human homologue (Stack and Emr, 1994), possibly because of differences in key ATP/wortmannin-binding regions of the respective class III isoforms (Walker *et al.*, 2000). Human Vps 34 compared with yeast Vps 34 differs at Ile-831 and Gly-868 in the *S. scrofa* PI3K sequences (Cox and Tovar, unpublished). Studies of giardial PI3Ks reveal that its residues also differ at the same position described for yeast Vps 34. Therefore, the differences in residue might explain the apparent insensitivity of *Giardia* to wortmannin. Another possible explanation for the lack of a significant difference in the number of cells observed in the result may be due to the inhibitor wortmannin. Previous findings suggest that wortmannin is unstable in cell culture medium (Woscholski *et al.*, 1994). The results of these two experiments have raised questions: 1. was the inhibition of trophozoite proliferation by LY294002 the result of blocking PI3K activity? 2. Could LY294002 affect other intracellular signalling kinases, thus resulting in the inhibition of trophozoite cell growth?

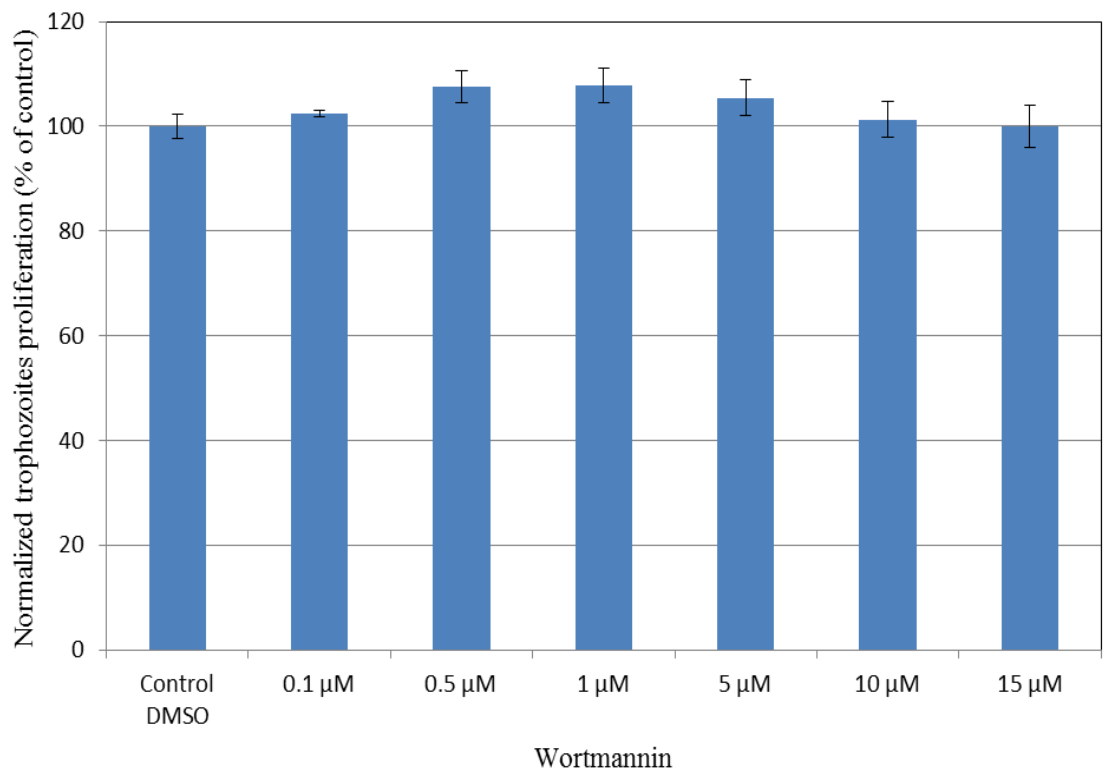


Figure 4.3: Effect of wortmannin on trophozoite proliferation.

Trophozoites at exponential growth were treated with wortmannin at various concentrations: 0 (DMSO-solvent control), 0.1 μM, 0.5 μM, 1 μM, 5 μM, 10 μM and 15 μM. The average bar charts from three samples were measured by absorbance readings at 655 nm after 48 hours of treatment. The error bars represent the standard deviation of the data.

To find out a possible answer to the first question, a novel PI3Ks inhibitor PI-103 was introduced. PI-103 is a potent inhibitor of class I PI3Ks reported by Raynaud *et al.* (2007). PI-103 was selected for this experiment because it can inhibit the PI3K pathway and the proliferation of cancer cells *in vitro*. The concentrations chosen for the inhibitor were based on previous studies by Bain *et al.* (2007). Figure 4.4 shows the absorbance reading at 655 nm over a period of 48-hours for the average trophozoite cell proliferation after treatment with different concentrations of PI-103. The optimal concentration of PI-103 required for PI3K inhibition in mammalian AML cells is 1 μM (Park *et al.*, 2008). When 1 μM PI-103 was applied to *Giardia* trophozoites, however, no significant difference in cell number was observed. At a higher concentration of 2 - 5 μM PI-103, the cell number decreases by about 20-25% compared to the control DMSO cells. However, between the three concentrations of 2, 3 and 5 μM, there was no significant difference in the cell number observed. The range of PI-103 concentrations employed only increased up to 5 μM

because higher PI-103 concentrations that may have an effect on trophozoite proliferation will not be due to the inhibition of PI3K.

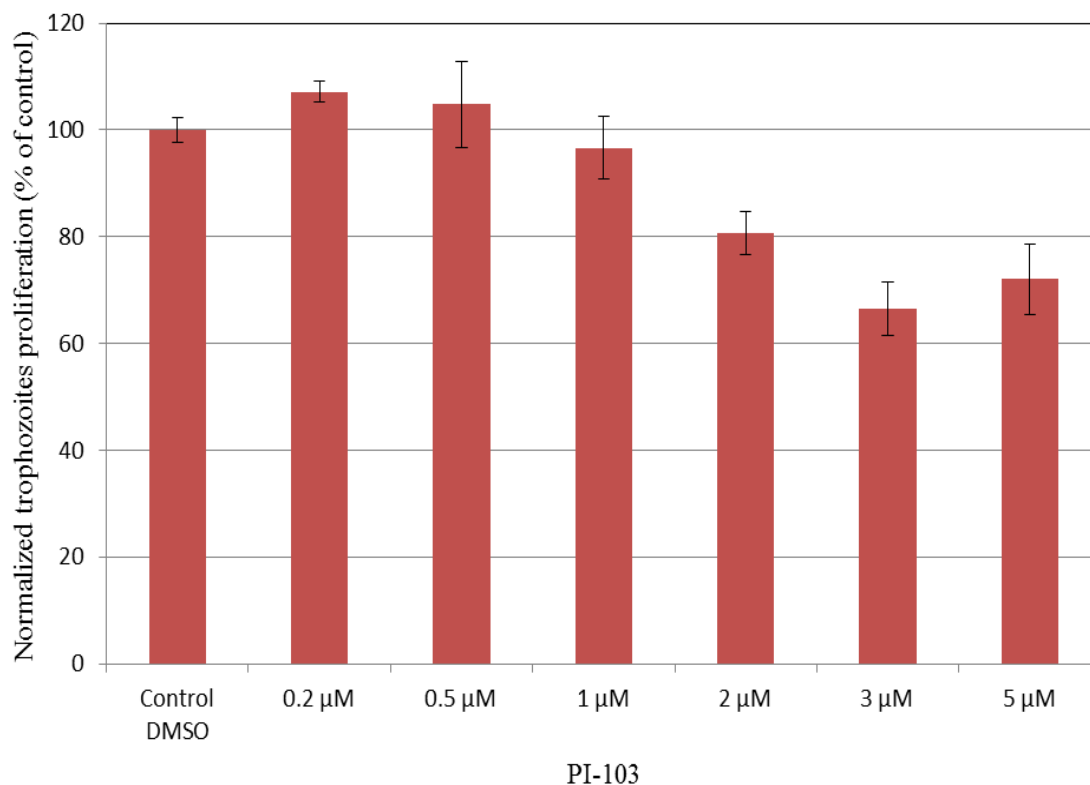


Figure 4.4: Effect of PI-103 treatment on trophozoites proliferation.

Trophozoites with starting inoculums of 1×10^5 cells/ml were treated with PI3K inhibitor PI-103 with various concentrations: 0 (DMSO-solvent control), 0.2 μ M, 0.5 μ M, 1 μ M, 2 μ M, 3 μ M and 5 μ M. Following 48 hours of incubation, trophozoites were harvested, pipetted onto a microplate, fixed, stained, and quantified using a spectrophotometer at 655 nm. The data show the average number of cells of three samples measured by absorbance at 655 nm and the error bars represent the standard deviation of the data.

4.2.2 Effect of known PI3Ks inhibitors LY294002, wortmannin and PI-103 on trophozoite proliferation over time

The predicted outcome of LY294002 inhibition on *Giardia* trophozoites would be the decrease in the overall population of *Giardia* to a certain number of cells per ml through inhibition of the PI3K pathway. When *Giardia* culture is treated with LY294002 at a concentration of 50 μ M, the trophozoite number remains constant for 48 hours under the cell counting approach. The result in Figure 4.5 illustrates that the growth of trophozoites was inhibited in a concentration-dependent manner, because at 25 μ M LY294002, the rate of trophozoites proliferation decreased by approximately 50%. This suggests that there was

an effect of LY294002 on the proliferation of the exponentially growing trophozoites over a period of 48 hours. Therefore, based on these results, one can hypothesise that LY294002 may have an effect on the trophozoite replication pathway, as PI3K plays a major role in the cell proliferation and cell growth. If PI3K is inhibited in the signalling pathway, we predicted that this will cause cell cycle arrest, as trophozoite numbers remain constant, rather than cell death.

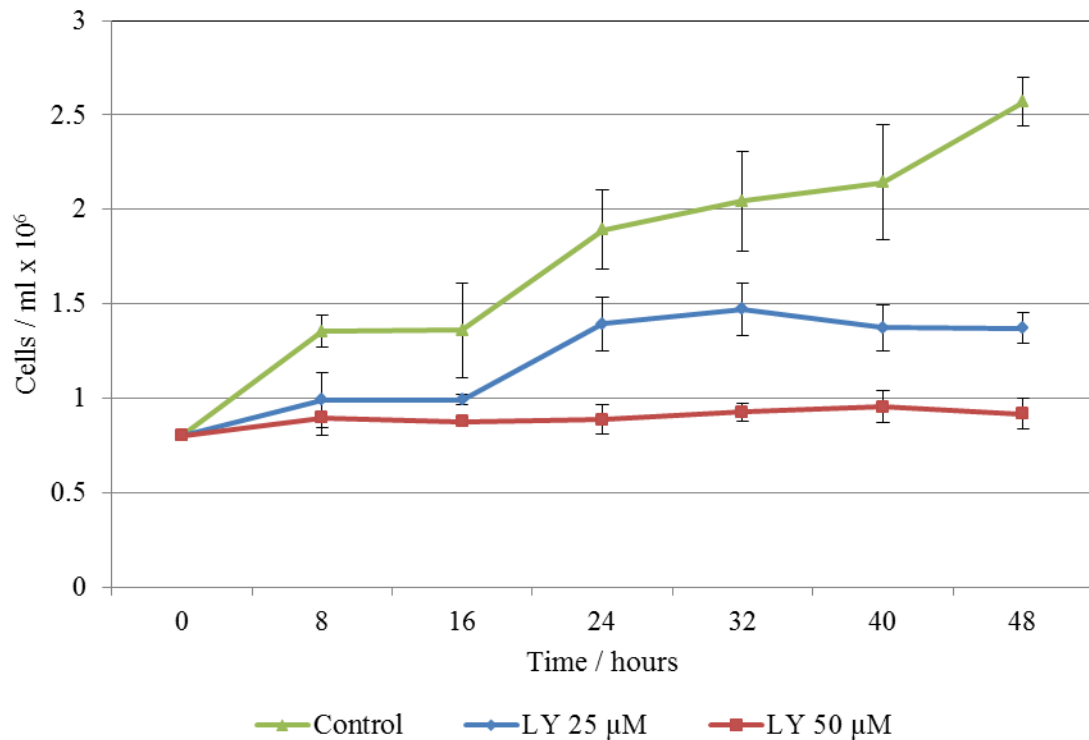


Figure 4.5: Effect of LY294002 inhibition on trophozoites population over a 48-hour period.

The exposure of LY294002 at different concentrations: 25 μM (blue line) and 50 μM (red line) on exponentially growing trophozoites. This was monitored by cell counting every 8 hours over a 48 hour period. The error bars indicate the standard deviation of 3 counts. Standard deviation shows how much variation or, “dispersion” exists from the average. A paired Student’s *t*-Test calculated to 0.007 showed a significant difference between control DMSO and 50 μM LY294002, where $p < 0.05$ for normalised data.

To test this possibility, we investigated whether the effect of LY294002 treatment could be reversed upon the removal of LY294002 from the culture medium. After 48 hours of treatment with LY294002 (25 μM and 50 μM), trophozoite cells in each sample were used to seed new cultures in fresh culture medium without an inhibitor. The growth of subcultured cells was monitored for 96 hours. Figure 4.6 shows subcultured trophozoite cells prior to treatment with LY294002 (25 μM and 50 μM) and DMSO (untreated).

Trophozoite cells show that upon removal of LY294002 inhibitor, they are capable of proliferating to increase the population equal to that of the untreated control cells. Trophozoites in this experiment (Figure 4.6) were no longer resting in culture medium containing different concentration of LY294002 inhibitor; therefore, cell proliferation continued to increase and reached a similar cell density as the control DMSO (untreated sample) upon the removal of PI3K inhibition.

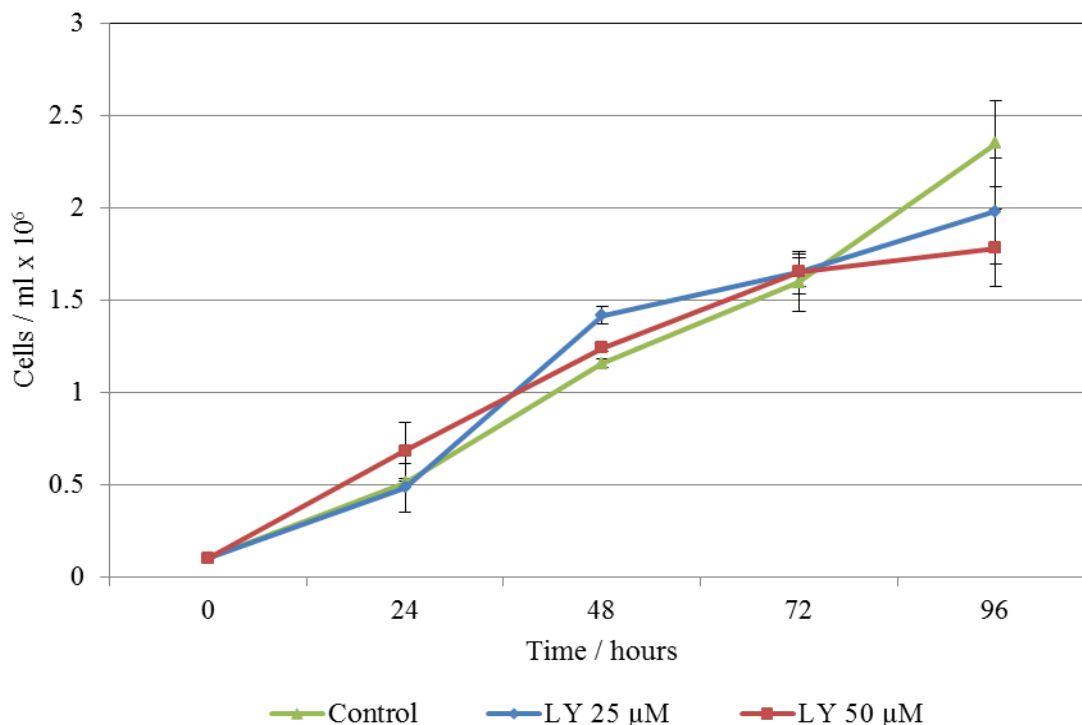


Figure 4.6: The effect of LY294002 inhibitor can be reversed by subculturing in inhibitor-free medium.

Exponentially growing trophozoites treated for 48 hours with DMSO (control) and LY294002 at two concentrations 25 μM and 50 μM were counted and equal numbers (0.1×10^6 cells/ml) were inoculated to seed new cultures. This graph shows the average cell count of 3 samples that are the result of treated samples over a 96 hour period. The bars represent the standard deviation of three counts. Statistical analysis using the paired Student's *t*-Test calculated show no significant difference between the tested samples.

The specificity of the inhibitor LY294002 has been argued to inhibit the activity of other protein kinases. The reported study on protein inhibitors by Davies *et al.* (2000) demonstrated *in vitro*, using purified proteins in a cell-based assay, that the inhibitor LY294002 also inhibits other protein kinases such as CKII at concentrations similar to those that inhibit PI3Ks. The IC_{50} for CKII is 6.9 μM and IC_{50} for PI3K is 10 μM (Davies *et*

al., 2000). CKII is present in the *G. intestinalis* genomic database (McArthur *et al.*, 2000) under the accession numbers XP_766966 (for alpha subunit) and EAA39338 (for the beta subunit). CKII is a serine/threonine selective protein kinase that phosphorylates a range of enzymes and transcriptional factors implicated in cell cycle control, DNA repair, regulation of the circadian rhythm and other cellular processes (Litchfield, 2003). The disruption of genes encoding for CKII catalytic subunits could lead to cell cycle arrest and even apoptosis. For example, CKII has been shown in *D. discoideum* and *S. cerevisiae* to be essential for cell growth and viability, respectively (Kikkawa *et al.*, 1992, Glover, 1998). Therefore, it is reasonable to hypothesise that because the LY294002 inhibitor has an effect on CKII in *Giardia*, the cell cycle arrest of trophozoites when treated with LY294002 inhibitor could be due to the inhibition of *Giardia* CKII and not PI3K. To test this possibility, a specific CKII inhibitor DRB (5,6-Dichloro-1-β-D-ribofuranosylbenzimidazole) (Zandomeni *et al.*, 1986) was examined on trophozoites to compare the growth of LY294002-treated cells against DRB-treated cells.

In this experiment, LY294002 inhibitor concentrations were kept the same at 25 μM and 50 μM. DRB was prepared at a final concentration of 100 μM, which is the standard concentration of DRB used in mammalian studies (Dirac-Svejstrup *et al.*, 2000; Yang and Sale, 2000). It is important to take into account that the LY294002 inhibitor IC₅₀ value for CKII is 6.9 μM whilst that for DRB is 6 μM. Therefore, if a putative CKII was being targeted by LY294002, using DRB at 100 μM should be sufficient to inhibit this enzyme (Cox *et al.*, 2006). Exponentially growing trophozoite samples were counted over 48 hours to determine the effect of DRB and LY294002 inhibitors with a control being DMSO. Figure 4.7 demonstrates that DRB-treated cells continue to grow exponentially compared to LY294002-treated cells for the duration of 48 hours. However, at the 48 hour cell count, the population of LY294002-treated cells at 50 μM was less than 50% of the population of the control DMSO cells. These data demonstrate that LY294002 does not have an inhibitory effect on *Giardia* CKII, because trophozoites exposed to DRB do not show positive growth inhibition. Furthermore, LY294002 also inhibits a number of other kinases such as GSK-3β and Polo-like kinase 1 (Gene id: GL50803_104150), which are present in *G. intestinalis*. The experimental works have been designed and carried out later in this chapter to determine whether LY294002 has an effect on *Giardia* GSK.

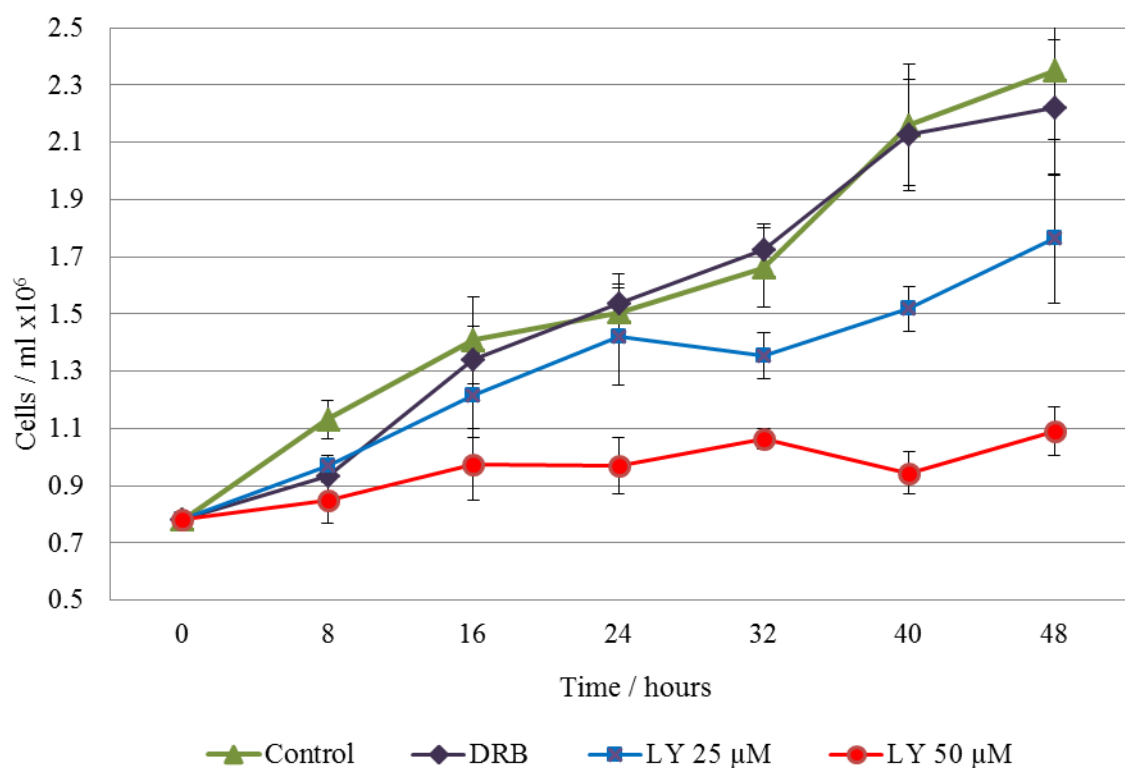


Figure 4.7: The effect of LY294002 and DRB exposure over a 48-hour period.

To test LY294002 specificity, the experiment was repeated with the same concentration of LY294002 in treated cells (25 μM and 50 μM) and DMSO in untreated cells from experiments in Figure 4.5. The addition of DRB at a final concentration of 100 μM aimed to establish whether LY294002 was able to inhibit CKII in trophozoites. Trophozoites were monitored by cell counting over a 48-hour period. The average number of cells in three counts was plotted and the error bar plots show the standard deviation of the data.

The effect of PI-103 was also tested to determine whether its reported specific inhibitions of PI3K activity will have a positive effect on trophozoite growth inhibition. PI-103 is a novel potent PI3K, PKB and mTOR inhibitor (Raynaud *et al.*, 2007, McNamara and Degterev, 2011). Recent work on PI-103 in cell-based assays illustrates that PI-103 blocks Class I PI3Ks completely at only 0.5 μM (Bain, *et al.* 2007). However, Bains *et al.* (2003) reported that at 1 μM PI-103 inhibits very few of the 70 purified protein kinases tested and no more than 30-40% even when assayed *in vitro* at 1 μM (Bains, *et al.* 2003). Therefore, two experiments were designed and completed to expose *Giardia* trophozoites to PI-103 at a final concentration of 0.5, 1 and 2 μM , in triplicate. In Figure 4.8, trophozoite samples were treated with various concentrations of PI-103 (0.5, 1 and 2 μM). The results show trophozoite proliferation at a rate similar to that in the untreated sample over the period of forty-eight hours for all treatments. The results in Figure 4.8 can be interpreted to

show that the PI-103 inhibitor does not inhibit *Giardia* trophozoite proliferation at any concentration; Student's *t*-Test showed no significant difference in the data between the DMSO control and PI-103-treated samples ($P > 0.05$). One could argue that because PI-103 was tested on a purified protein sample by Bains *et al.* (2007), and once it is added into *Giardia* culture medium, the capability for the inhibitor may have failed to enhance any effect on growth inhibition of trophozoite cells. PI-103 functions as a competitive inhibitor of ATP binding, although it is unknown which amino acid residues are important for PI-103 binding and inhibition in giardial PI3Ks. Therefore, one could not rule out the possibility that LY294002 inhibits giardial PI3Ks. In light of this result, it was important to explore other kinases that LY294002 was reported to inhibit, therefore resulting in inhibition of the cell cycle.

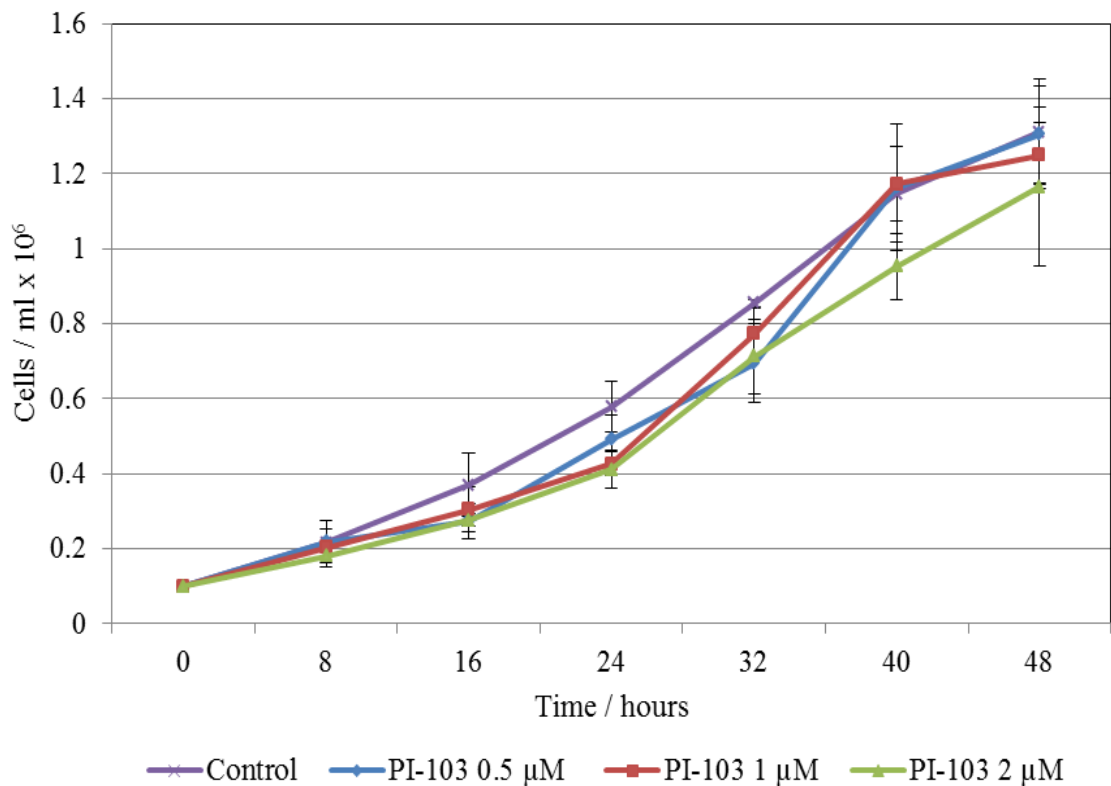


Figure 4.8: Exposure of trophozoites to different concentrations of PI-103.

Trophozoites were counted every 8 hours over a 48 hour period with an initial inoculum of 1×10^5 cells/ml at time zero. The error bars represent the standard deviation of the data. Using a paired student's *t*-test, there was no significant difference ($p > 0.05$). The experiment was conducted in triplicate on at least two different occasions.

4.2.3 Effect of puromycin on *Giardia* trophozoites

To establish whether the inhibition of PI3K activity in LY94002-treated trophozoites was due to cell death or inhibition of cell proliferation, puromycin was introduced into this experimental study as a positive control of cell death. Puromycin is an aminonucleoside antibiotic, which originates from *Streptomyces alboniger*. Puromycin is known to be continuously used as a selective marker in *G. intestinalis* transfection experiments (Yu *et al.*, 2002) and inhibits protein synthesis by binding to RNA, therefore causing premature chain termination during the translation process that takes place in the ribosome. Exponentially growing trophozoites were subcultured and treated with puromycin to a final concentration of 100 μ M at time zero. The samples were collected at 48, 96 and 144 hours for quantitative analysis. The evidence clearly showed that puromycin-treated trophozoite cells under the light microscope appear to be stationary compared to control cells. Furthermore, in Figure 4.9, the number of puromycin-treated trophozoites remained constant from the addition of puromycin (time zero) to 144 hours. Quantitative studies showed a significant increase in the number of trophozoites in the control (untreated) sample measured by the average optical density at 655 nm where cells would reach the absorbance of 4 at 48 hours, which is equivalent to approximately 6×10^6 cells. Moreover with the quantitative analysis technique, Figure 4.10 illustrates cells treated with puromycin and LY294002 to the final concentration of 100 μ M and 50 μ M, respectively. The untreated control trophozoite proliferation over 48 hours was significantly different over three average optimal density readings (where $p \leq 0.005$). After 24 hours, the quantitative analysis detected less than 50% of the cells treated with LY294002 compared to untreated control. On the other hand, puromycin-treated cells were unable to proliferate (see Figure 4.10), resulting in the same number of cells following treatment at time zero to 48 hours.

Furthermore, to determine whether puromycin-treated cells were still functional and to show that the inhibition was temporary, as evidenced by the LY294002-treated cells, puromycin-treated trophozoites had the medium containing puromycin removed and replaced with fresh culture medium. After 48 hours of incubation, Figure 4.11 shows the remaining number of trophozoites that were pre-treated with puromycin through quantitative analysis with the control cultures. The result suggests that pre-treated puromycin cells were non-responsive after changing the medium. Indeed, this also meant

that cells were not moving. However, the inability of puromycin-treated cells to recover upon the removal of puromycin strongly suggests that this is the characteristic of cell death.

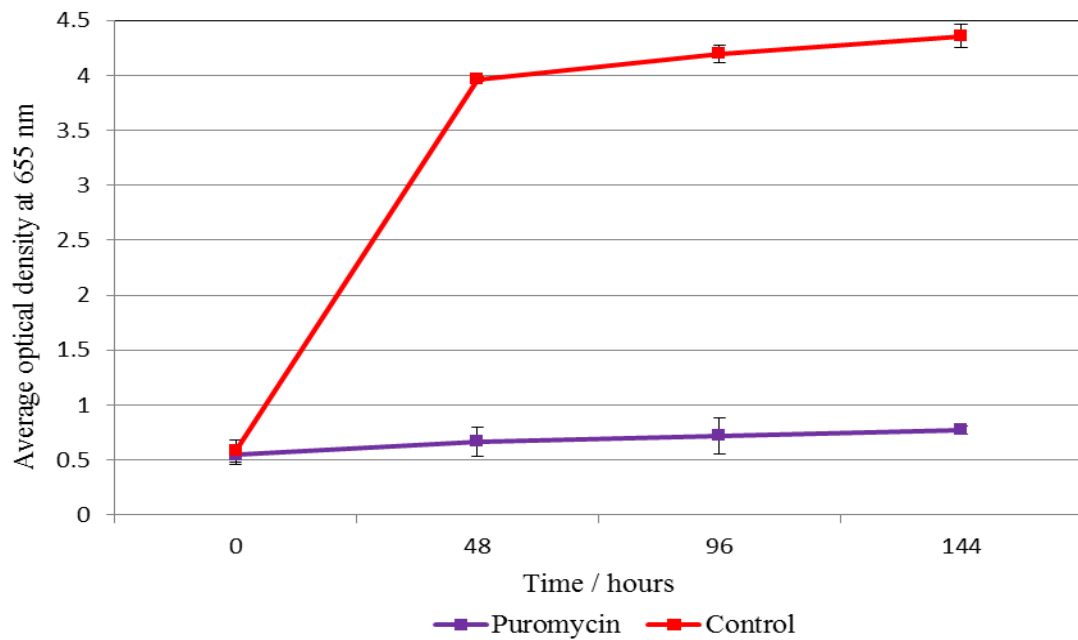


Figure 4.9: The effect of puromycin on *Giardia* trophozoite proliferation over 144 hours. Spectrophotometric quantification of *Giardia* trophozoites after the addition of 100 μ M of puromycin was applied to exponentially growing trophozoites over 144 hours. The average optical density at 655 nm for the triplicate sample was plotted and the error bars represent the standard deviation of the data.

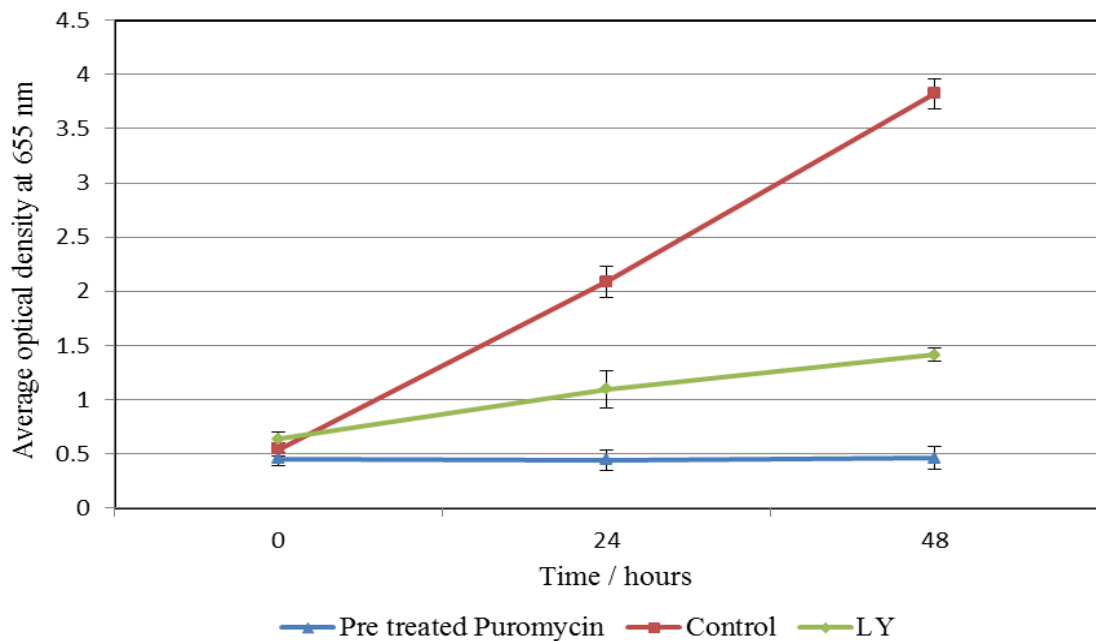


Figure 4.10: The effect of puromycin and LY294002 inhibition over 48 hours.

Inhibitory effect of puromycin (100 μM) and LY294002 (50 μM) on *Giardia* trophozoites was monitored by using a spectrophotometric quantification method over a period of 48 hours compared to the control (distilled water). The triplicate samples were measured by absorbance readings at 655 nm and data were plotted. The error bars represent the standard deviation of the data.

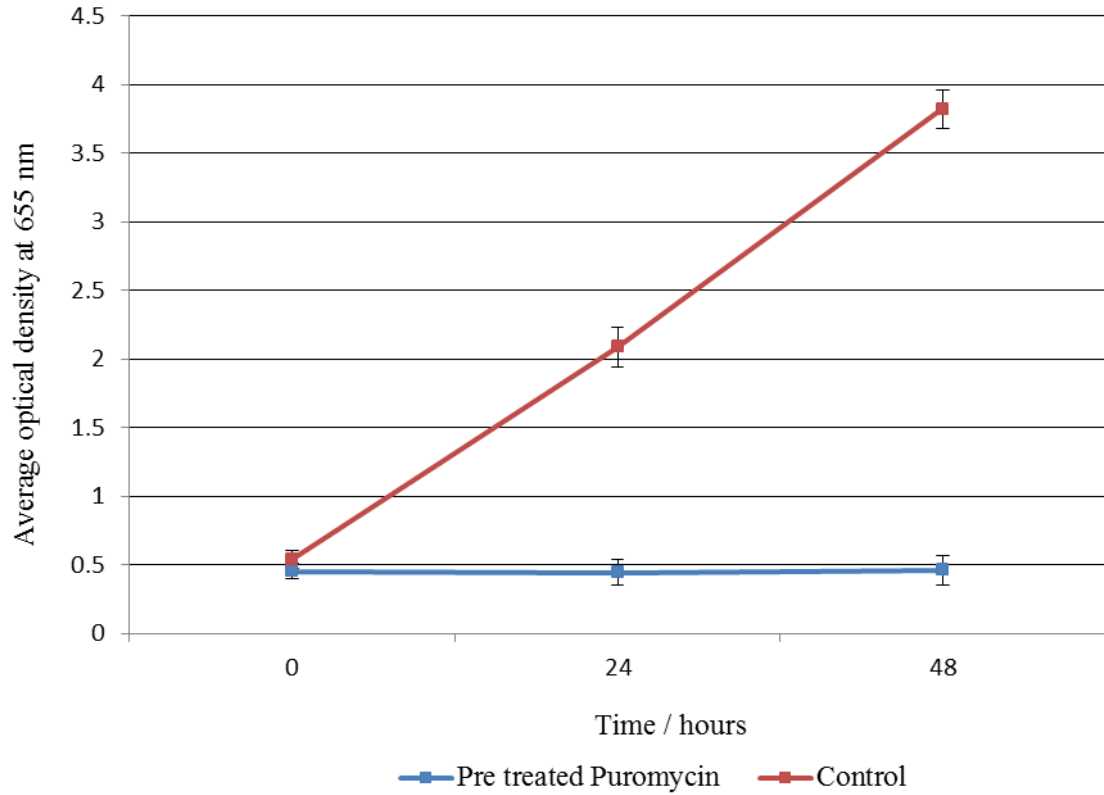


Figure 4.11: Pre-treated with puromycin trophozoite cell proliferation observed after subculturing.

Exponentially growing trophozoites treated for 48 hours with puromycin (100 μM) and control (distilled water); these were washed and 0.1×10^6 cells of the control cells were used to seed new cultures, while puromycin-treated cell cultures were replaced with fresh medium. The graph shows the average triplicate absorbance reading at 655 nm over a 48-hour period. The error bars represent the standard deviation of the data.

4.2.4 Inhibition of Glycogen synthase kinase-3

Glycogen synthase kinase is a well-known downstream effector of PI3K signalling. To determine whether *Giardia* GSK-3 homologues are involved in the regulation of cell proliferation and cell cycle arrest in *G. intestinalis*, two different types of GSK-3 inhibitors reported to inhibit GSK-3 activity were examined: i) CT99021, a highly potent and specific inhibitor of GSK-3, and ii) LiCl, which inhibits GSK-3 β activity more strongly than other protein kinases tested (Bain *et al.*, 2007).

Figure 4.12 (A) shows that CT99021 at final concentrations of 0.5 μ M, 1 μ M, 2 μ M, 5 μ M and 10 μ M had no significant effect on exponentially growing trophozoites. The average optical density measured in the control compared to the average optical density of the samples treated with CT99021 indicated no significant change in cell density. Under normal conditions in mammalian cells, GSK-3 are inactivated (Doble *et al.*, 2003); thus cell growth continues as normal, and we can hypothesise that trophozoites treated with CT99021 will not be inhibited with regard to cell proliferation because the inhibition of GSK-3 by PKB inactivates GSK-3 by inducing phosphorylation (Doble *et al.*, 2003). Therefore, to confirm that CT99021 shows no positive effect in reducing trophozoite proliferation, in Figure 4.12 (B), CT99021 was applied to trophozoites during the exponential phase (trophozoite subculture after 48 hours, see Figure 4.1) to final concentrations of 0.5 μ M, 1 μ M and 2 μ M with control DMSO. Figure 4.12 (B) demonstrates that for the duration of the time course, cell numbers that were counted over a 48 hour period show that CT99021 treated cells continue to grow exponentially and, in comparison to the control DMSO treated cells, no significant difference in trophozoite cell number was observed. This suggests that CT99021 does not have a positive effect on trophozoites growth and supports the hypothesis that GSK-3 may be normally inhibited by PKB phosphorylation, thus maintaining substrate dephosphorylation, allowing the continuation of trophozoite proliferation. In mammalian cells, active GSK-3 would activate phosphorylated cyclin D and deactivate eukaryotic protein synthesis initiation factor -2B (eIF2B), which would lead to cell cycle arrest (Diehl *et al.*, 1998, Quintayo *et al.*, 2012).

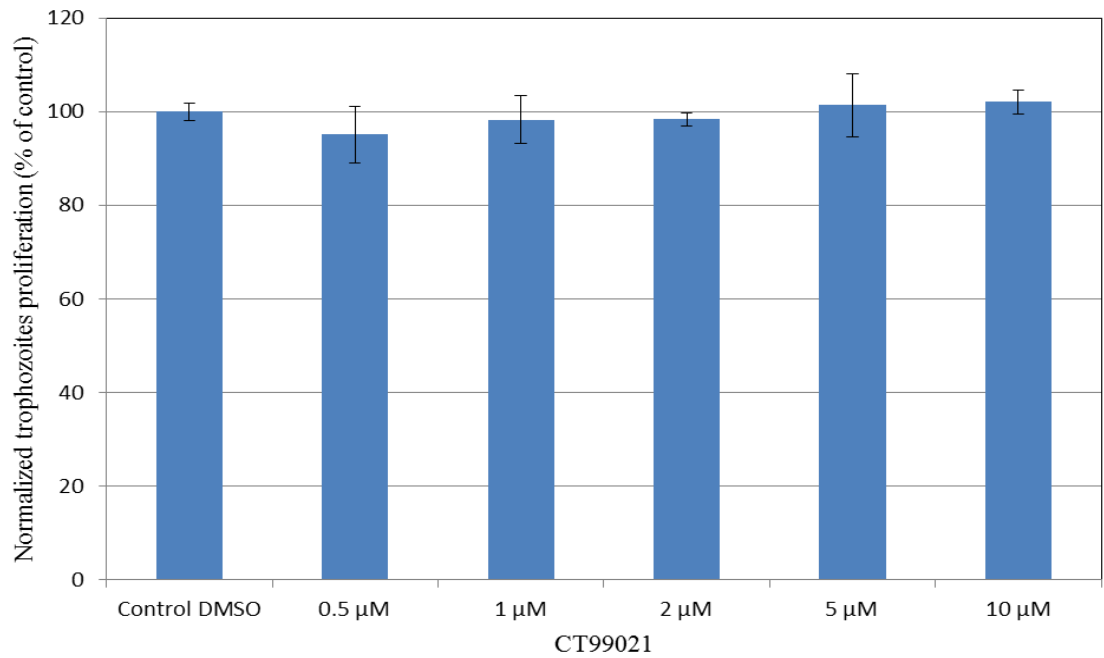
Another experiment was carried out using an inhibitor of GSK-3, lithium chloride (LiCl), to monitor trophozoite growth. The lithium cation (Li⁺) has been shown to inhibit GSK-3 β with an IC₅₀ concentration of 2 mM. Moreover, in mammalian cells, Li⁺ has also been implicated to inhibit other kinases such as: polyphosphate 1-phosphatase, inositol

monophosphatase, casein kinase-II (CKII), MAP kinase-activated protein kinase-2 and p38-regulated/activated kinase (Bhat *et al.*, 2008).

Trophozoite cell numbers of LiCl-treated cultures over a 48-hour period were measured using a spectrophotometer with an optical density of 655 nm to test the effect of LiCl, which is represented in Figure 4.13. Figure 4.13 illustrates that trophozoites treated with LiCl at final concentrations of 1 mM, 2 mM, 5 mM and 10 mM for 48 hours show no significant changes when compared to the control DMSO culture. However, trophozoites treated with LiCl at 20 mM show growth inhibition when compared to control DMSO. This suggests that LiCl treatment at a final concentration of 20 mM may have an effect on trophozoite proliferation. However, using statistical calculations, the results show no significant differences between trophozoites treated with LiCl at 20 mM against the control DMSO and other concentrations employed. Bain *et al.* (2007) reported using a 10 mM concentration of LiCl to inhibit the activity of purified GSK-3 β *in vitro* and describes that, after treatment, only 30% activity remained compared with the control. Figure 4.13 describes trophozoites treated with different concentrations of LiCl (5 mM, 10 mM and 20 mM) and control DMSO. The numbers of cells from different cultures were counted over a 48-hour period to determine the effect of LiCl on trophozoite cultures when different concentrations of LiCl were used. At 8 to 32 hours, the population of LiCl- and the control-treated cells are not significantly different from one another when calculated using a paired Student's *t*-Test. However, at 40 hours and 48 hours, LiCl-treated trophozoites at 20 mM demonstrated the same number of trophozoites when compared to a previous time point at 32 hours. LiCl is reported to inhibit GSK-3 β activity more strongly than any of the protein kinases tested *in vitro* by Bain *et al.* (2007); at higher concentrations of 20 mM, it may also inhibit other protein kinases in trophozoites (as mentioned above). This is because the inhibition of GSK-3 leads to inactive/phosphorylated GSK-3; therefore, downstream signalling would permit the cell cycle to continue.

The concentration ranges of CT99021 and LiCl suggested in the literature were used in the experimental work on purified proteins (Jope, 2003, Bain *et al.*, 2007). Therefore, it is important when working with *Giardia* as the model organism to determine the concentrations of these two inhibitors of GSK.

A.



B.

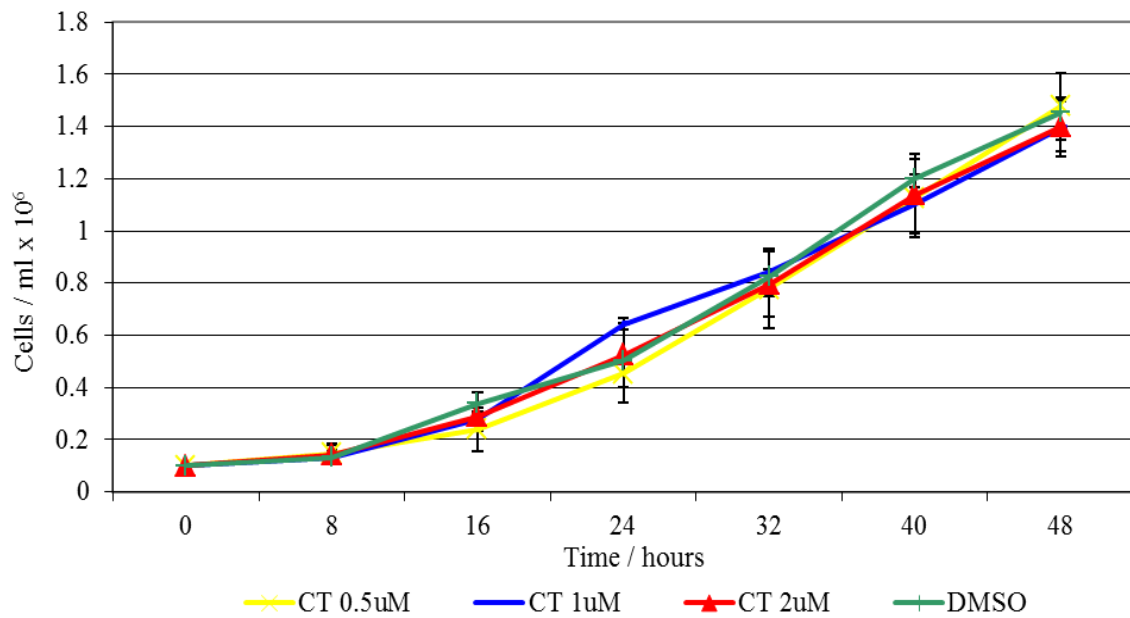


Figure 4.12: Effect of CT99021 over a 48-hour period.

CT99021, inhibitor of GSK3 was applied to trophozoites (at exponential growth). A, Trophozoites with starting inoculums of 1×10^5 cells/ml were treated with various concentrations: 0 (DMSO-solvent control), 0.5 μ M, 1 μ M, 2 μ M, 5 μ M and 10 μ M. The trophozoites were quantified using spectrophotometer at 655 nm, where the bars show the average number of cells of three samples. B, CT99021-treated trophozoites at concentrations of 0.5 μ M, 1 μ M and 2 μ M were observed by cell counting over a 48-hour time period. The samples exposed to each concentration of CT99021 are

the average number of cells in triplicate samples. The error bars represent the standard deviation of the data. Using a paired Student's *t*-Test, no significance was detected between each concentration.

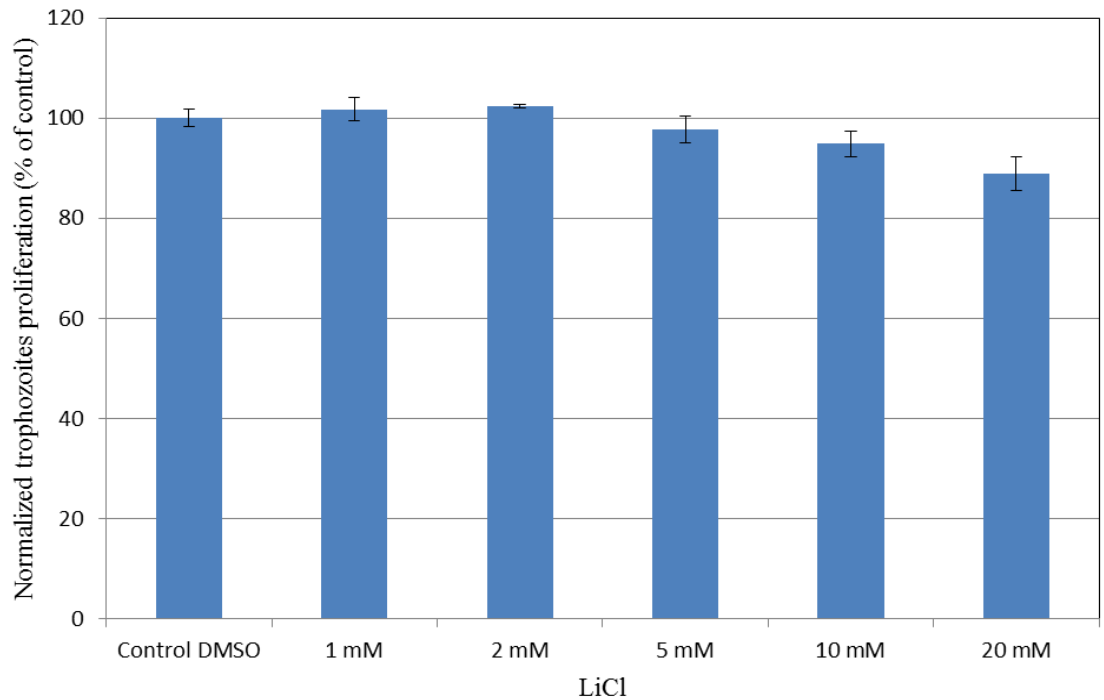


Figure 4.13: Effect of Lithium chloride over 48-hour period.

Lithium chloride, a common inhibitor of GSK-3 β , was applied to exponentially growing trophozoites. Trophozoites with starting inoculums of 1×10^5 cells/ml were treated with LiCl at various concentrations: 0 (DMSO-solvent control), 1 mM, 2 mM, 5 mM, 10 mM and 20 mM. Following 48 hours of incubation, trophozoites were harvested, pipetted onto a microplate, fixed, stained, and quantified using a spectrophotometer at 655 nm. The data show the average number of cells of three samples measured by absorbance at 655 nm. The error bars represent the standard deviation of the data.

A summary of all of the inhibition studies performed so far is shown in Figure 4.14. Here, trophozoites were treated with a range of inhibitors at time zero: LY294002 to a final concentration of 25 and 50 μ M; PI-103 to a final concentration of 0.5, 1 and 2 μ M; CT99021 to a final concentration of 0.5, 1 and 2 μ M; LiCl to a final concentration of 5, 10 and 20 mM; and DRB to a final concentration of 100 μ M. These concentrations have been reported to be within the range as being effective for most mammalian cell types (Cohen, 2003). Positive controls of the experiment were wild type cells and DMSO-treated trophozoites. Alternatively, the negative control in this experiment was three wells in a 96-well tissue culture plate with no wild type trophozoite.

Figure 4.14 illustrates trophozoites that were treated and untreated with inhibitors at two different time intervals (16 and 40 hours) following subculture and treatment with

inhibitors. The number of trophozoites was quantified through the quantitative method; at 16 hours the DMSO-treated control and wild type trophozoite cells had average optical density (at 655 nm) readings of 1.25 and 1.1, respectively. When the controls were compared to trophozoite-treated samples at 16 hours, the data showed no significant difference. However, LY294002-treated trophozoites (50 μ M) at 40 hours highlighted the effect on *Giardia* proliferation, as it reported that approximately 50% of the population was reduced compared to the DMSO-treated and wild type control. Moreover, it is worth noting that trophozoites treated with 25 μ M LY294002 also showed positive inhibition of cell proliferation and the cell number was reduced by approximately 40% compared to the controls. LiCl-treated trophozoites at 20 mM also showed an approximately 25% decrease in the number of cells when compared to controls. It is unclear as to why this occurs, because there were no changes in cell number observed across LiCl-treated sample after 16 hours. Only when *Giardia* trophozoites were incubated with LiCl (20 mM) for over 40 hours was a decrease in the number of cells observed compared to the controls.

It is unlikely that a reduction in the number of trophozoite demonstrated in the LiCl-treated sample was due to the inhibition of GSK-3 or the inhibition of PI3K, as PI3K-inhibited trophozoite cell cultures would demonstrate a decrease in cellular proliferation at a concentration dose-dependent manner. It is important to distinguish in an experiment whether the inhibition of PI3K activity by LY294002 hampered growth due to cell death or a block in the cell cycle. This experimental study will be re-visited later on in this Chapter.

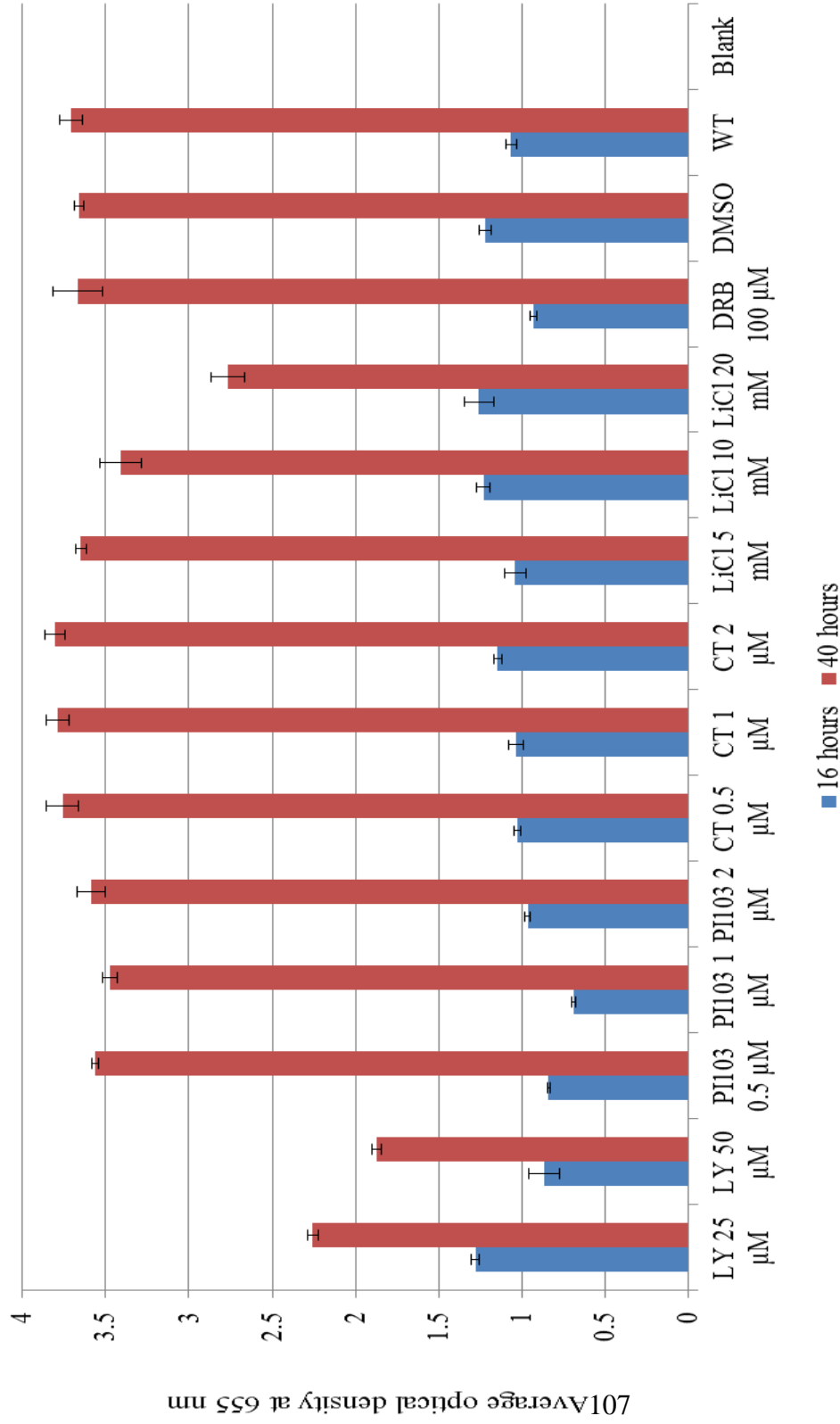


Figure 4.14: Overall result of inhibitors treatment on *Giardia* trophozoites.

Trophozoites were subcultured into fresh culture medium with starting inoculums of 1×10^5 cells/ml and treated with various concentrations of LY294002 (25 μM and 50 μM), PI-103 (0.5 μM , 1 μM and 2 μM), CT99021 (0.5 μM , 1 μM and 2 μM), LiCl (5 mM, 10 mM and 20mM), DRB (100 μM) and control (DMSO). Cells were treated at time zero and processed for analysis at time intervals of 16 and 40 hours. Once the treatments were completed, trophozoites were harvested, pipetted on to microplate, fixed, stained, and quantified using spectrophotometer with average optimal density at 655 nm. The bars show the average number of cells in three wells (blue bars: cells were processed at 16 hours; red bars: cells were processed at 40 hours). The error bars represent the standard deviation of the data.

4.2.5 Effect of co-exposure to PI3K and GSK-3 inhibitor on *Giardia* trophozoites

Experiments were carried out with two inhibitors to investigate the downstream signalling pathway of PI3K and GSK-3. The mammalian intracellular signalling pathways involving PI3K and GSK-3 show that when GSK-3 is phosphorylated it is inactive under normal growth conditions allowing the cell cycle to progress. The effect of blocking PI3K from phosphorylating phosphatidylinositol will result in no phosphorylated PKB; thus, downstream GSK-3 will not be phosphorylated. GSK-3 will become active and therefore lead to blocking of the cell cycle. The inhibition experiment used purified protein in a cell-based assay, which showed that LY294002 can partially inhibit GSK-3 activity directly (Bain *et al.*, 2007). The rationale for these experiments is that although theoretically one does not expect the GSK-3 inhibitor to affect the cell cycle due to the inactive state of GSK-3 under normal growth, given what had been published, it was important to demonstrate this using an inhibitor of GSK-3 on trophozoite culture (Bain *et al.*, 2007). One possibility is that the inhibition of trophozoite growth caused by LY294002 may not be the result of PI3K activity inhibition but rather of LY294002-mediated GSK-3 inactivation. If this was the case, based on the GSK-3 inhibition studies reported above (section 4.2.4), the prediction would be that the cell cycle should continue unimpeded (as GSK-3 is normally kept inactivated by PKB-mediated phosphorylation during normal cell growth) and parasite culture growth would be observed.

To investigate this hypothesis, two inhibitors, LY294002 and CT99021, were used for the double inhibitor experiments. The first experiment (Figure 4.15) demonstrated the double inhibitor experiment initially with constant CT99021 at a final concentration of 2 μM and in addition, an increasing concentration of LY294002 at a final concentration of 10 μM , 25 μM or 50 μM . Inhibitors were added at the same time, each treatment was completed in triplicate and trophozoites in the treated cultures were counted over a 48-hour period. The control culture samples contained a single inhibitor of CT99021 with a final concentration of 2 μM . The observation of trophozoites through cell counting showed that control culture CT99021-treated samples proliferate as seen in previous experiments (see Figure 4.12). On the other hand, cultures treated with CT99021 and LY294002 begin to affect cell numbers 16 hours into treatment. The experiment showed that increasing the concentration of LY294002 in a constant CT99021 concentration (2 μM) affected cell number in a concentration-dependent manner. This has been shown previously in LY294002-treated cells (see Figure 4.5). For the duration of the time course in LY294002-

treated cultures at 50 μM with CT99021 (2 μM), cell numbers remained constant from time zero. This evidence strongly suggests that LY294002 is likely to inhibit PI3K and not GSK-3. LY294002 might not affect GiGSKs, possibly because GSK-3 in *Giardia* does not contain specific residues required to bind to the inhibitor. Furthermore, the missing serine residues in the GiGSK N-terminus may affect the binding of an inhibitor complex, because in mammalian cells, Serine 21 on GSK-3 α and Serine 9 on GSK-3 β have been shown to be essential residues for the phosphorylation of GSK-3 (Zhang *et al.*, 2010).

The second double inhibitor experiment examined the hypothesis that if LY294002 was inhibiting PI3K, we would not expect to see a reversal of the mutant growth phenotype upon addition of increasing concentrations of GSK inhibitor. Alternatively, if LY294002 was inhibiting GSK, then further inhibition with CT might possibly exacerbate the growth phenotype. However, because there is no abnormal growth phenotype in CT99021-treated trophozoites (see Figure 4.12 and Figure 4.14), then no change in growth phenotype would be expected. Exponentially growing trophozoites were treated with two inhibitors, LY294002 and CT99021. Trophozoite cell cultures were set up with an increasing CT99021 at a final concentration of 0.2 μM , 1 μM and 3 μM , with the second inhibitor LY294002 added at 50 μM added to all of the samples. The controls for this experiment LY294002 and CT99021 were applied to trophozoites to a final concentration of 50 μM and 1 μM , respectively. The former represent a control for positive growth inhibition, whereas the latter was a control for positive trophozoite cell proliferation. Figure 4.16 shows cell numbers of CT99021-treated control cultures grown exponentially from time zero to 48 hours. In contrast, the number of LY294002-treated trophozoite cell cultures appeared to be constant for the duration of the time-course. The effect of LY294002 on trophozoite number was observed 8 hours into the treatment. Furthermore, from 16 hours to the final count of trophozoites at 48 hours, there were no significant changes in cell number from all double inhibitor treated samples. These data strongly suggest that LY294002 inhibits PI3K and that the inhibition of PI3K activity indirectly leads to the activation of GSK through a lack of PKB-mediated phosphorylation. This leads to cell cycle arrest.

The results of two double inhibitor experiments were as expected. LY294002 inhibits PI3K, which leads to a lack of downstream phosphorylation of PKB and GSK-3, leading to cell cycle arrest.

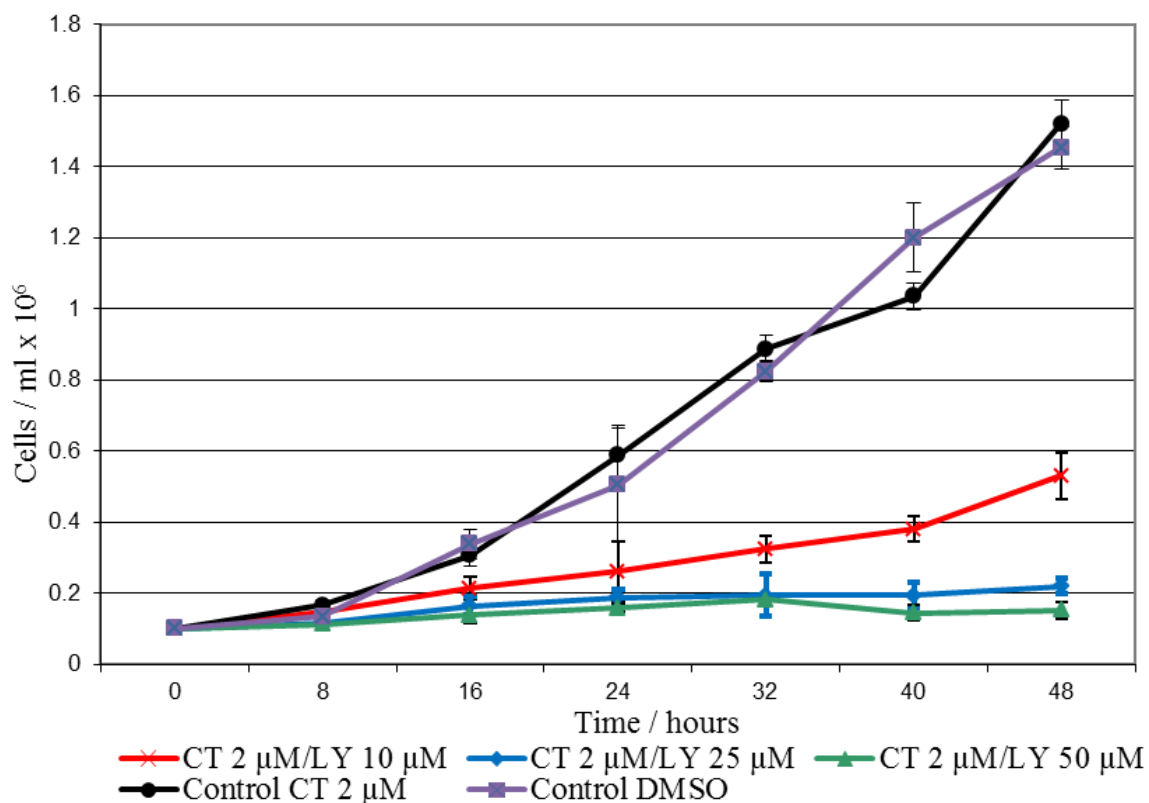


Figure 4.15: Effect of double inhibitor treatment on trophozoite proliferation.

Inhibitor CT99021 and LY294002 was applied to exponentially growing trophozoite culture starting at 0.1×10^6 cells/ml, where the CT99021 concentration remained constant with increasing LY294002 concentrations (10 μ M, 25 μ M and 50 μ M). Control samples were individually treated with CT99021 and DMSO to a final concentration of 2 μ M and 100 μ M, respectively. Trophozoites were counted over a period of 48 hours following the treatment. This graph shows the average number of cells from three counts and the error bars represent the standard deviation of the data.

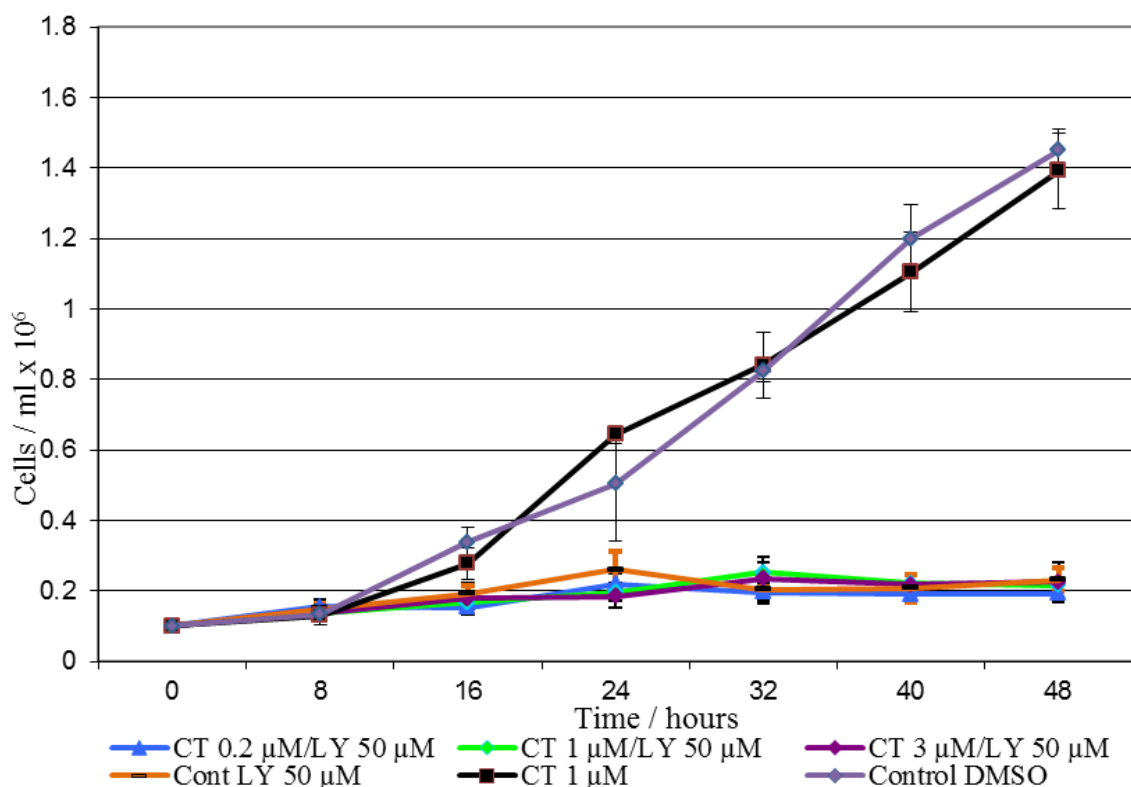


Figure 4.16: Effect of double inhibitor treatment to monitor trophozoite proliferation.

Exponentially growing trophozoites were treated in the presence of LY294002 at a concentration of 50 μM together with increasing CT99201 concentrations (0.2 μM , 1 μM and 3 μM). Control samples were individually treated with LY294002, CT99021 and DMSO to a final concentration of 50 μM , 1 μM and 100 μM , respectively. Trophozoites were harvested every 8 hours over a 48-hour period and counted. The line plotted shows the average number of cells from three counts and the error bars represent the standard deviation of the data.

4.2.6 The importance of PI3K activity during encystation process

The relevance of PI3K activity during *G. intestinalis* trophozoite vegetative growth is described above. *Giardia* encystation is an important mechanism that allows the parasite to differentiate from trophozoite cells into resistant cysts. During trophozoite replication within the host intestinal surface, the initiation of encystation occurs in the jejunum after exposure to biliary secretions (Adam, 2001). *Giardia* relies on the formation of environmentally-resistant cysts for transmission to a new host, thus ensuring the survival of the parasite. With this in mind, it is important to further investigate the impact of the PI3K inhibitor LY294002 on trophozoites under the process of encystation.

Here, we determined whether the inhibitor LY294002 would affect the *Giardia* encystation process. The differences between the normal culture and encysting culture medium are in the concentration of bile. Normal trophozoite culture medium contains low-

bile content, whereas the encysting medium contains high-bile content in the complex medium. *Giardia* trophozoites, in the presence of high-bile culture medium, will initiate the process of encystation (Gillin *et al.*, 1987 and Lujan *et al.*, 1997). The process of encystation was described in the introduction chapter as an adaptive process where an extracellular signal is perceived (for example changes in the concentration of bile), which activates the processes of parasite encystation. Within approximately 10 hours, the first phase of encystation begins in response to the change in environment. This includes the expression of encystation-specific genes (such as cyst wall proteins) and the complete synthesis of these cyst wall proteins together with packaging and intracellular transportation in encystation-specific vesicles (ESVs) to the target site. Subsequently, the second phase, referring to the cyst wall being assembled by exocytosis of ESVs, is complete after 16 hours, with zero hour being the time at which the encystation medium is added (Lujan *et al.*, 1997, Adam, 2001).

Before the start of encystation experiments, it is vital to distinguish the differences between trophozoite, encysting cell and cyst cell morphology. Initially, cysts may be the obvious candidate to discriminate from trophozoites and encysting cells. Cysts are ovoid in shape and rounder than trophozoites and encysting cells. A cyst is approximately 8 – 10 μM in diameter with the composition of cyst wall proteins that may appear like a fibrous coat on the outer layer. Once the formation of cysts is complete, the disappearance of trophozoite flagella has been suggested to be because they were disassembled during the encystation process (Roxstrom-Lindquist *et al.*, 2006). In addition, a previous study illustrated images of flagella internalisation during encystation process, thus rendering them immotile (Middlej and Benchimol, 2009). Trophozoites are pear-shaped cells with four pairs of flagella; these are known as the anterior flagella, caudal flagella, posterior lateral flagella and ventral flagella. Each trophozoite cell contains two nuclei that can be found on the dorsal side at the anterior lobe. The length of a trophozoite cell is approximately 10 – 15 μM ; this is also approximately the same as an encysting cell. The morphology of encysting cells appears rounder than trophozoites, but with shorter posterior. Not every trophozoite undergoes the encystation process at the same time; therefore, encystation is divided into two phases: early and late. In the early phase, encysting cells contain two nuclei, similar to trophozoites. The flagella on encysting cells appear shorter in length and disappear completely at the completion of encystation. Adhesive discs become dysfunctional and can no longer be detected; thus, encysting cells are not able to attach to a surface (Adam, 2001).

The early phase of encysting cells may display ESVs carrying cyst wall material proteins; these are apparent on the body of encysting cells as granulated structures.

It is important to investigate PI3K signalling activity for trophozoites at the beginning of encystation, because trophozoites will need to respond quickly to changes in the surrounding environment by modifying the extracellular morphological structures. PI3K signalling might play an important role during the whole period of *Giardia* encystation process because PI3K activity was demonstrated to be crucial for the proliferation of vegetative trophozoites. Therefore, one can expect that PI3K activity may be essential in the differentiation of trophozoite cells. The inoculated exponentially growing trophozoites are transferred to fresh encystation medium supplemented with LY294002 to a final concentration of 100 μ M. This meant that trophozoite exposure to LY294002 was at time zero, during which trophozoites were also under the chemical signal in the encystation medium. The number of trophozoites, encysting cells and cysts were then counted. Trophozoite cells were treated instantly with LY294002 after the changes in trophozoite conditions under encysting culture medium. Previously in this chapter, the concentration of LY294002 was kept at 50 μ M; however, it has been suggested that inhibitor degradation for 120 to 168 hours may affect the result. Therefore LY294002 at a final concentration of 100 μ M was adopted to maintain the potency of the inhibitor. Equally, PI3K activity may not only be important at the beginning of encystation; to test this hypothesis, trophozoites were treated with LY294002 to a final concentration of 100 μ M and incubated in encysting medium for 12 hours. This was to allow the parasite to perceive and respond to the chemical signals in the encystation medium for 12 hours before exposing them to an inhibitor of PI3K (LY294002).

The total numbers of *Giardia* cells were counted in Figure 4.17 under encysting medium. The treated cultures show decreases in the total number of cells in all of the samples under encysting medium (inhibitor added immediately and 12 hours later). The encysting cultures that were treated immediately in Figure 4.17 (A) illustrate that the cell number of the control-DMSO and DRB-treated cells decreased by 40% and 50%, respectively, from the start to 168 hours. LY294002 treated cell population also decreased by 72%. Cells treated 12 hours after exposure to encysting medium showed decreases in the number of cells of the controls DMSO- and DRB-treated cells by approximately 16% and 23%, respectively, when compared with the population at time zero. LY294002-treated cells had a 68% decrease in the cell population, as shown in Figure 4.17 (B). A reason for

this overall decline in cell numbers could be due to the effect of the DMSO solvent in each of the samples. The studies by Trubiani *et al.* (1996) have shown that a DMSO concentration above 0.5% may cause G1 cell cycle arrest in cell types such as human lymphoid cells. At higher concentrations, DMSO can reduce cell viability in human hepatoblastoma cells and cause apoptosis in the developing mouse brain cells (Vesey *et al.*, 1991, Hanslick *et al.*, 2009). Generally, an increase in the number of cells between 48 to 72 hours was followed by a marked decrease in the number of cells under all conditions. However, the number of cells was always lower in LY294002-treated than in DRB-treated and control trophozoites. The reason for the overall decrease in the number of cells could be because of the effect of DMSO solvent that is present in all of the inhibitors added at a concentration of 1%.

DMSO is widely used in cell biology and its mode of action employed at low concentration is to induce membrane thinning, which results in increasing permeability of the membrane. However, at higher concentrations, DMSO may induce transient water pores into the membrane and can disintegrate the bilayer structure of the cell (Gurtovenko and Anwar, 2007). Cox and Tovar (unpublished work) showed that at a concentration of 1%, after two days, DMSO can decrease the cell number of trophozoite in normal culture medium by approximately 50%.

Observations in the experimental work earlier with LY294002 suggest that this PI3K inhibitor has a cytostatic effect on trophozoite cells suggesting that a block in the cell cycle for up to 48 hours was responsible (see Figure 4.5). During the encystation process, however, LY294002-treated trophozoite cultures demonstrated a decrease in the number of cells that was significantly higher ($P < 0.05$) than that observed for the control-DMSO and DRB-treated cells (see Figure 4.17). This trend of decline in cell number suggests that it is not only due to the effect of DMSO solvent or the cytostatic effect on trophozoite cells by LY294002. A possible explanation is that LY294002 not only has a cytostatic effect on trophozoite cells, but may also trigger the encystation process upon the treated cells. However, this does not explain why the total number of cells suddenly declines but what if LY294002-treated cells do not complete encystation process, due to the inhibition of PI3K activity therefore resulting in a halt the cell cycle. Additionally, during encystation, trophozoites that were treated after 12 hours with LY294002, DRB and control (DMSO), all to a final concentration of 100 μM , revealed an increase in total cells in DRB- and control-treated cells. However, at 48 hours, LY294002 retains approximately the same

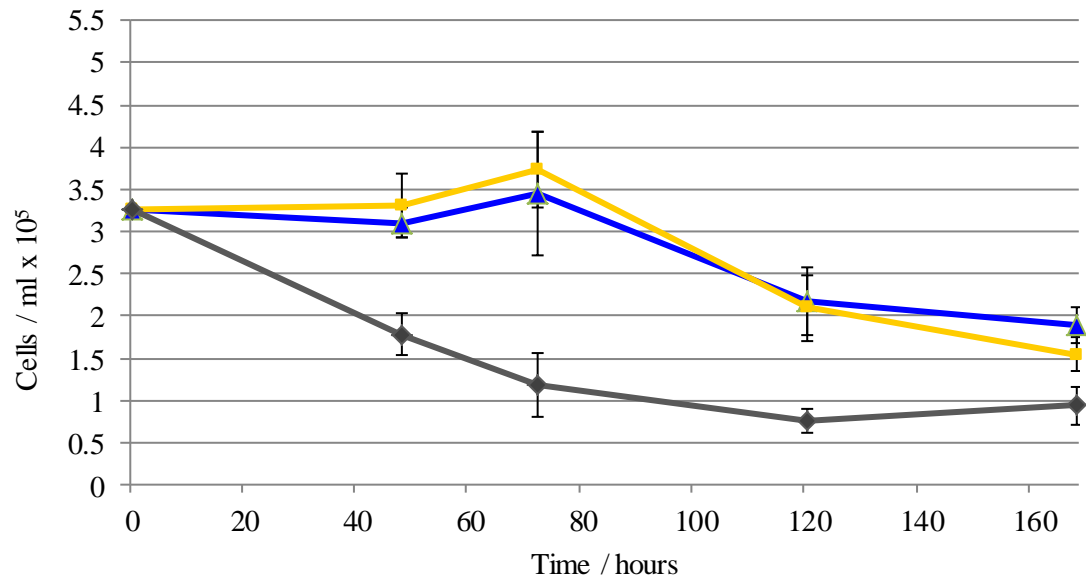
number of cells that it had started with (see Figure 4.17 (B)). In Figure 4.17 (A), the number of LY294002-treated cells could be seen to decrease by 50% at 48 hours and 42% at 72 hours. This result illustrates that trophozoite cells under encysting medium for 12 hours prior to the treatment may influence cells to enter encystation under normal conditions, thus initiating an early phase of the encystation process. In comparison to Figure 4.17 (A), the addition of treatment 12 hours following encysting medium in Figure 4.17 (B) may allow cells to adjust to the encysting medium giving cells the advantage of initiating the process of encystation that may aid in protection from LY294002 inhibitor.

It was challenging to accurately measure the number of encysting cells and cysts because of the morphology and the positioning of individual cells. Therefore, using a vortex after the hypotonic lysis of cysts, “island” allows better distinction between each cell. These limitations could be the reason for errors, therefore cysts and encysting cells were placed in the same category. The number of cysts and encysting cells were calculated through total cell count subtracting trophozoite cell count in each of the treated and untreated samples.

In the process of encystation, one may expect trophozoites to stop cell proliferation; however, because of the nature of *Giardia* trophozoites, each individual cell does not divide and replicate at the same time in the cell cycle. Besides, not every trophozoite enters encystation and differentiates into a cyst. In reality, some trophozoites will continue to proliferate under encysting medium. Therefore, to ensure that the results under these circumstances are reliable, the number of trophozoites, encysting cells and cysts were represented as a percentage of the total number of cells in Figures 4.18 and 4.19. Figure 4.18 shows that in the cultures treated immediately following the onset of encystation, the number of trophozoites is significantly higher than the number of encysting/cyst cells in LY294002-treated samples at 24, 72 and 120 hours. At 168 hours, LY294002 treated samples display similar numbers of trophozoites and encysting/cysts cells. When this is compared to the other sample treated at 168 hours, the pattern shows a very high number of encysting/cyst cells against trophozoites. Compared with the control-treated cultures, the significant differences in trophozoites and encysting/cysts cells observed in the LY294002-treated sample could be because inhibitor LY294002 compromises PI3K cell signalling; thus, the process of encystation in LY294002-treated samples is interrupted. Furthermore, Figure 4.19 with the addition of treatment 12 hours after the beginning of encystation with DMSO, DRB or LY294002 illustrate that LY294002-treated cells were able to reach a

similar pattern compared to other treated samples towards 168 hours. Again, the result may suggest that once trophozoites initiate encystation, changes in morphology can reduce the effect of LY294002, thus allowing a normal encystation process. Finally, the similarity between the number of cells treated with DRB and DMSO in encysting cultures exposed to inhibitors immediately and after 12 hours across the timeline indicates that the effect by the LY294002 inhibitor may be PI3K-mediated.

A.



B.

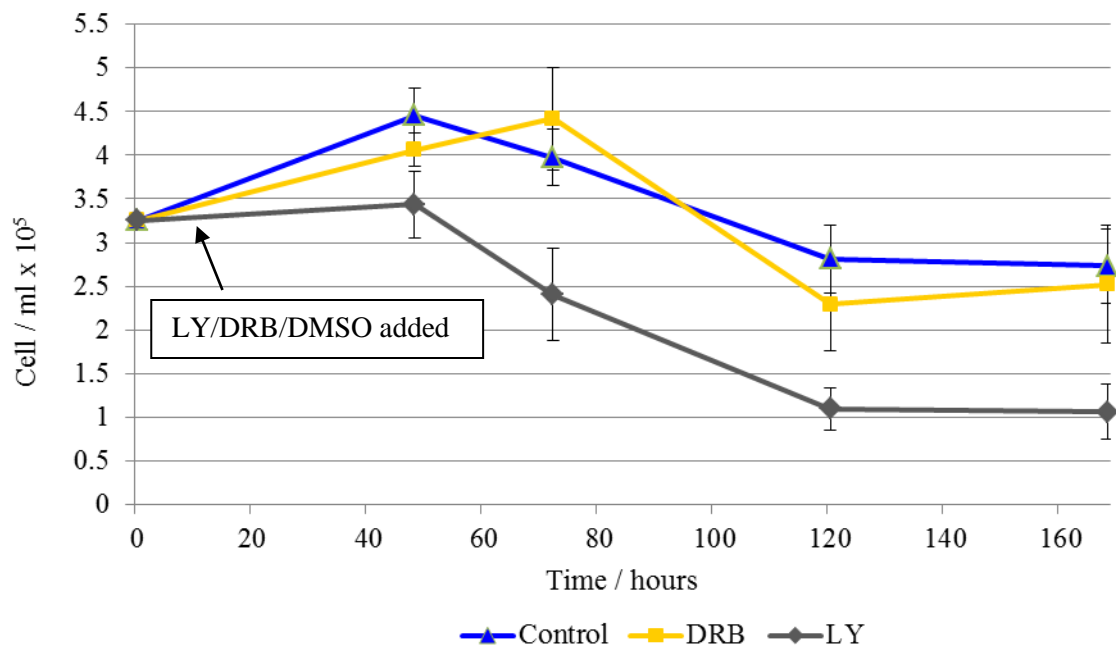
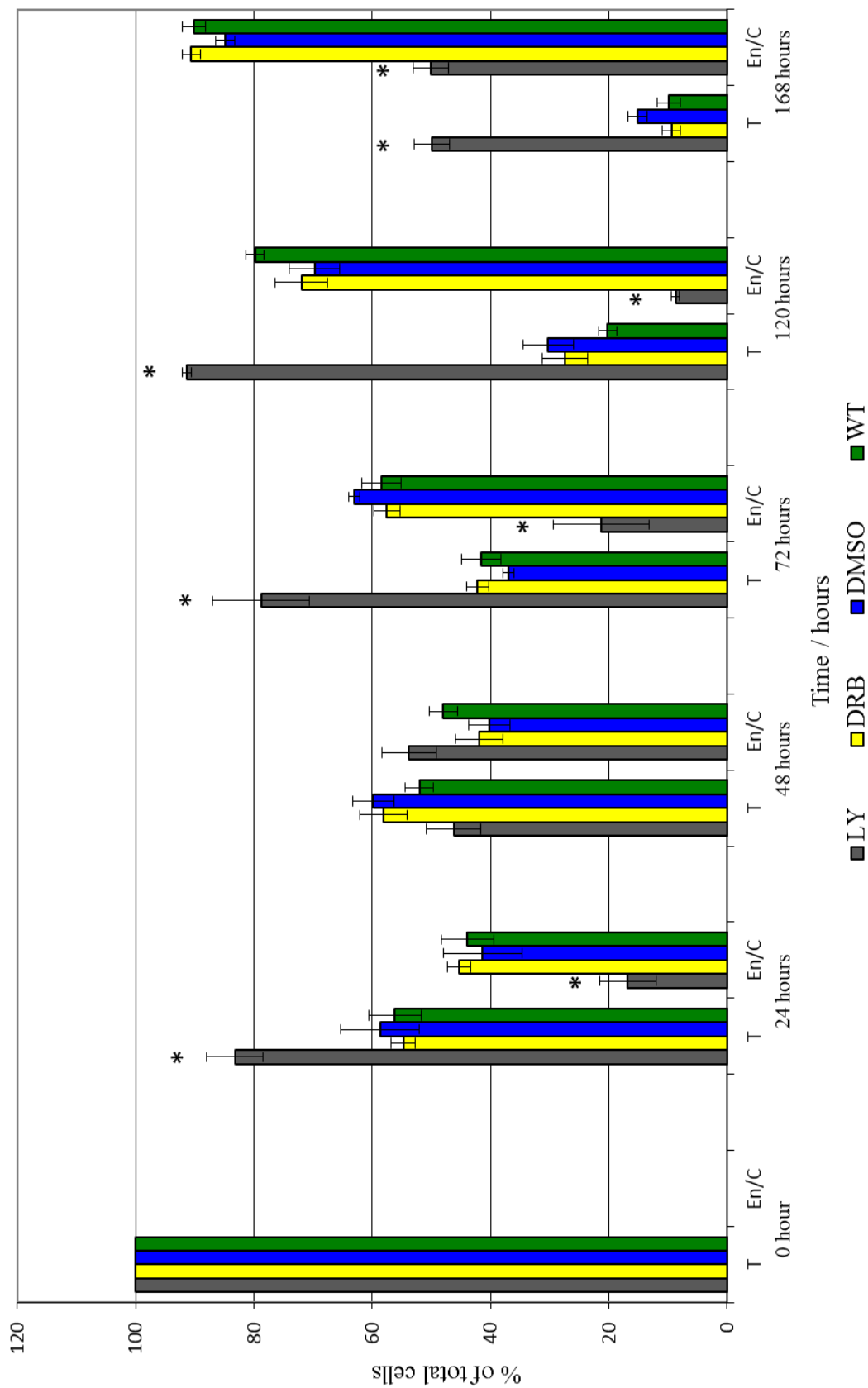


Figure 4.17: Total cell number under encystation.

Encysting cultures were treated immediately (A) or 12 hours later (B) with LY294002 or DRB or DMSO control, all at a final concentration of 100 μ M. The total number of cells per ml was counted over 168 hour period following the initiation of encystation. The total number of cells of three counts was averaged and plotted. The bars represent the standard errors of the data.



B.

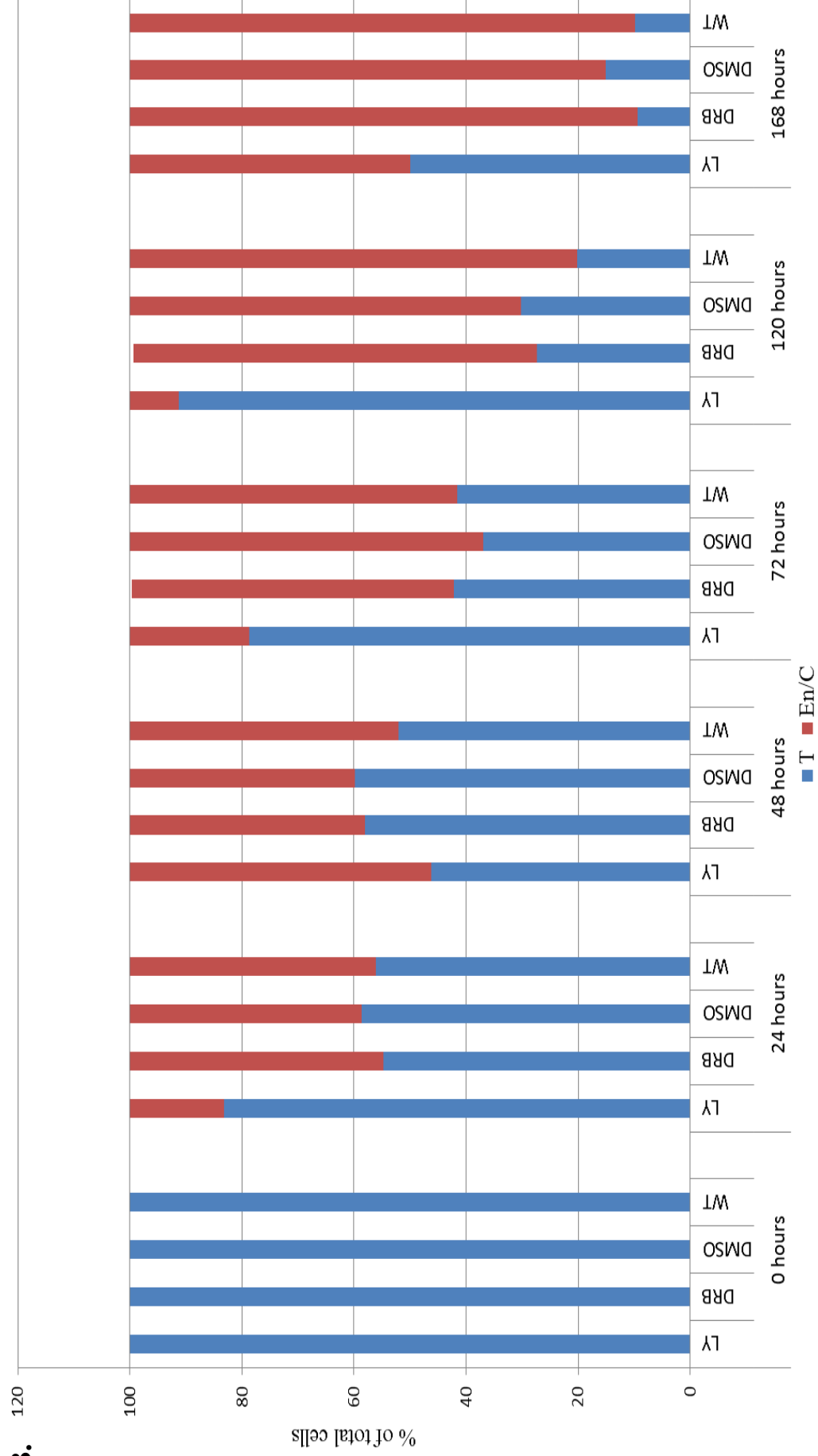
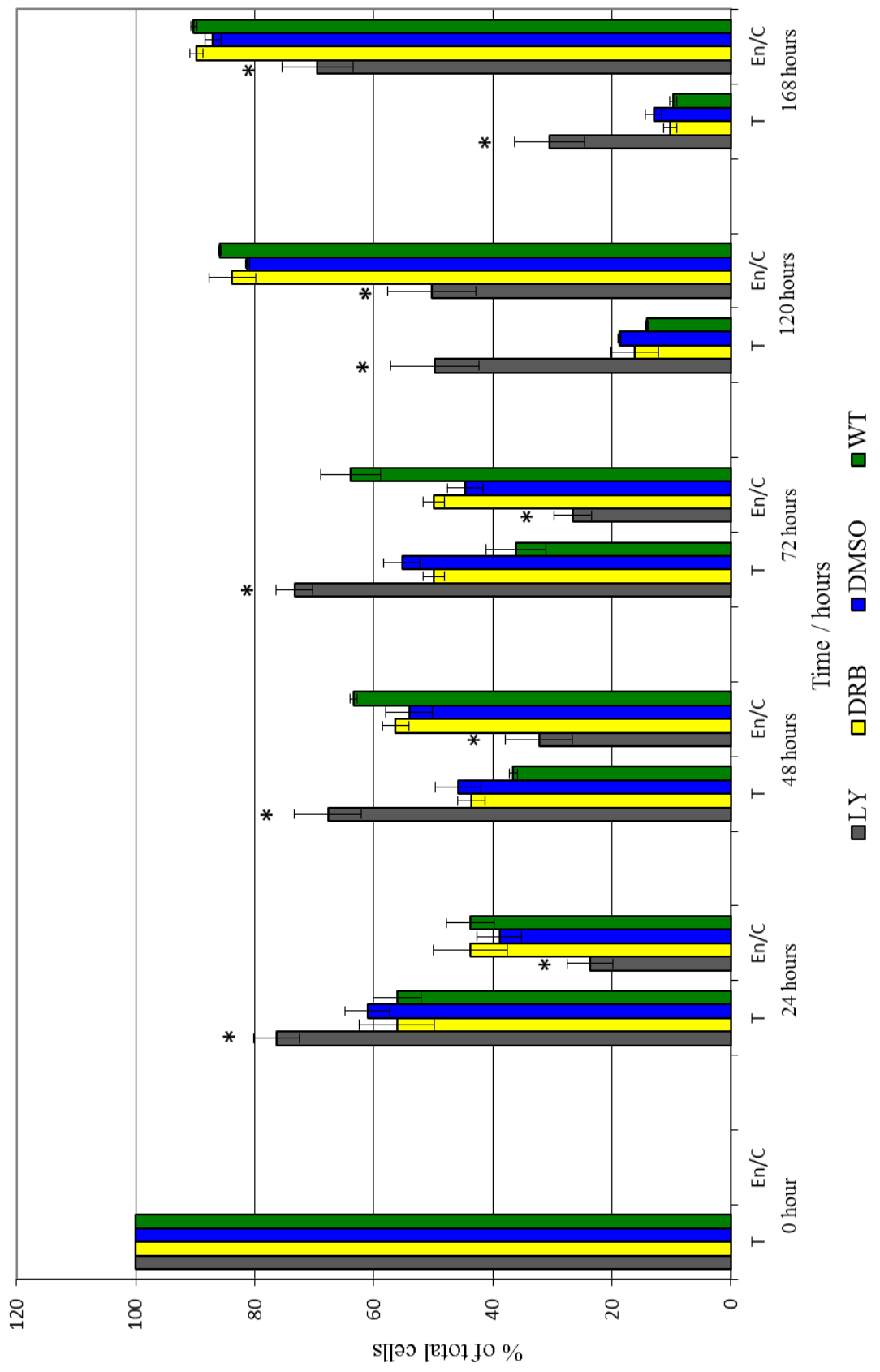


Figure 4.18: Effect of PI3K inhibition in encysting cultures.

Trophozoites were induced to encyst and immediately treated with LY294002 (100 μ M final concentration), DRB (100 μ M final concentration) or DMSO (control). A. Untreated trophozoites in encystation medium were labelled wild type (WT). Trophozoites (T), encysting cells (En) and cysts (C) were then counted over a 168-hour period. The average number of cells from three counts was calculated and the counts are shown as a percentage of the total number of cells at a given time point. The bars represent the standard error of mean of the data. Paired Student's *t*-Test calculated to determine significance at $p < 0.05$ in the average cell counts (asterisks) B. Trophozoites (T) with encysting cells and cysts (En/C). B. Presented in this Figure to facilitate the viewing of the data, it represents the same data as shown in A.



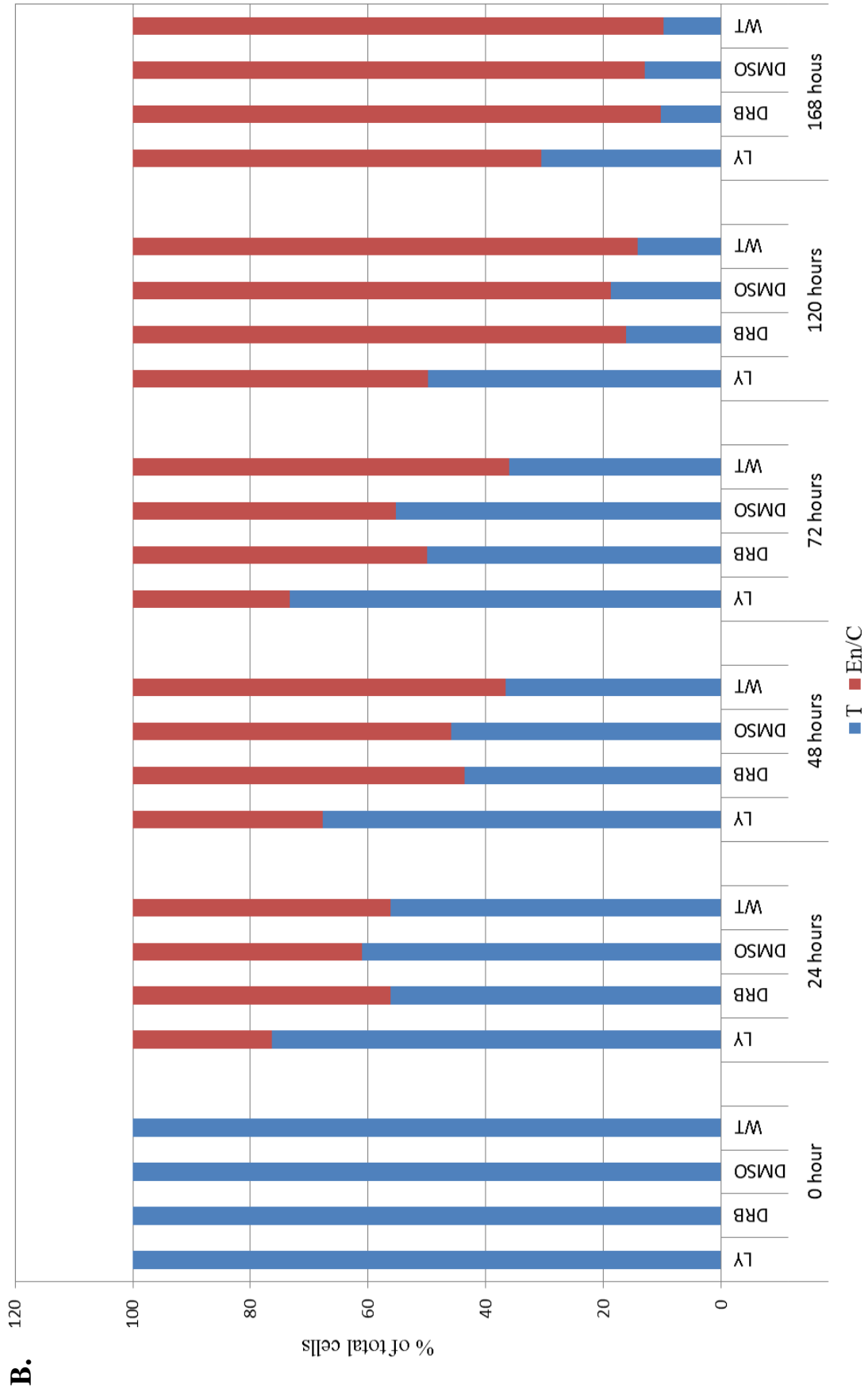


Figure 4.19: Effect of PI3K inhibition in encysting cultures.

Trophozoites were induced to encyst and treated with LY294002 (100 μ M final concentration), DRB (100 μ M final concentration) or DMSO (control) twelve hours following the addition of encystation medium (at 0 hour). A. Untreated trophozoites in encystation medium were labelled wild type (WT). Trophozoites (T), encysting cells (En) and cysts (C) were then counted over 168-hour period. The average number of cells from three counts was calculated and the counts are shown as a percentage of the total number of cells at a given time point. The bars represent the standard error of the mean of the data. Paired Student's *t*-Test was calculated to determine significance at $p < 0.05$ in the average cell counts (asterisks). B. Trophozoites (T) with encysting cells and cysts (En/C). B. Presented in this Figure to facilitate the viewing of the data; it represents the same data as shown in A.

4.2.7 Detection and quantitation of phosphatidylinositol (3,4,5)-trisphosphate in cell cultures

To determine the presence of PI3K activity in *G. intestinalis*, the product of class I PI3K, phosphatidylinositol (3,4,5)-trisphosphate (PIP₃), was quantified using PIP₃ Mass ELISA assay. It has been widely accepted that PIP₃ is the product of class I PI3Ks; therefore, the detection of PIP₃ may provide evidence of class I PI3K activity in *Giardia* trophozoites and encysting cell cultures. Experiments were carried out to detect PIP₃ in *G. intestinalis*, NIH-3T3 mouse fibroblast cells and *D. discoideum*. Lipid samples were extracted from cell cultures and incubated with a PIP₃ detector protein. Individual samples were then added to the PIP₃-coated plate for competitive binding. A peroxidase-linked secondary detection reagent and colorimetric substrate were applied to detect the level of PIP₃ which corresponds to the detector protein bound to the plate. The colorimetric absorbance was read at 450 nm in which the absorbance reading is inversely proportional to the amount of PIP₃ extracted from cell samples. The PIP₃ standards were pre-applied to the assay and used as a comparison to allow one to determine the signal of PIP₃ in the cell extract. The amount of PIP₃ quantified in trophozoites is 0.355 picomoles per 1×10^7 cells, which is lower than the amount detected in mammalian mouse fibroblast cells, of 2.324 pmol per 1×10^7 cells (Table 4.1). This observation was consistent over two independent repeat experiments. *Giardia* trophozoite cells were collected after 48 hours incubation in normal culture medium following initial subculture, it is possible that a higher concentration of growth factors in *Giardia* culture medium may lead to an increased amount of PIP₃ extracted from the trophozoite cells. Nevertheless, the outcome of this result adds further evidence for the presence of functional PI3K activity in *G. intestinalis*; because PIP₃ is the product of class I PI3Ks, it is possible to hypothesise that class I PI3Ks is present within the intracellular signalling activity of *G. intestinalis*.

Given that PIP₃ is the product of class I PI3Ks and class I PI3K isoforms have been identified in *G. intestinalis* (Cox *et al.*, 2006), it was hypothesised that the level of PIP₃ in trophozoite cells would reduce if trophozoite cells were treated with PI3K inhibitor. However, trophozoite cultures exposed to specific PI3K inhibitor PI-103 (Figure 4.8) did not show growth inhibition in trophozoite cell cultures. Therefore, it was not expected to be able to see a reduction in the level of PIP₃ in trophozoite cell cultures exposed to PI-103. The level of PIP₃ in *Giardia* cells exposed to encystation medium over 48 hours was established here to examine whether there were any changes in the level of extracted PIP₃ in trophozoites under encystation medium. The level of PIP₃ detected using an ELISA assay in normal trophozoite cell cultures, encysting cell cultures, PI-103-treated trophozoites and LY294002-treated trophozoites is presented in Figure 4.20. The level of PIP₃ in trophozoites under normal culture medium was used as a control. The three samples, PI-103-treated cells, LY294002-treated cells and encysting cells, were normalised against the control to obtain the percentage PIP₃ level across the graph plotted (Figure 4.20). The control PIP₃ level and cells under encystation medium show no significant difference in the amount of PIP₃ detected. This was also true in the PI-103 treated trophozoites, as statistical analysis using ANOVA indicated no significant difference in the amount of PIP₃ between PI-103-treated trophozoites and the control and encysting cell cultures. On the other hand, the PI3K inhibited trophozoite cells treated with LY294002 illustrated an approximately 60% decrease in the level of PIP₃ when compared to the level of PIP₃ in the control cells. These data support the evidence that Class I PI3Ks activity is present in *G. intestinalis* and that LY294002 inhibits PI3K activity in trophozoites, leading to a significantly reduced level of PIP₃ in trophozoite cells.

Table 4.1: Quantification table showing amount of PIP₃ detected in different species.

PIP₃ level quantified in three different species are presented here per 1 x 10⁷ cells. These values were obtained using a lipid extraction method and applied to a competitive ELISA assay where the signal given is inversely proportional to the amount of PIP₃ produced. The experiment was repeated in triplicate, where the PIP₃ value is an average ± standard deviation.

Species	PIP ₃ level in 1 x 10 ⁷ cells (pmol)
NIH-3T3 mouse fibroblast	2.324 ± 0.194
<i>D. discoideum</i>	0.410 ± 0.097
<i>G. intestinalis</i> (trophozoite)	0.355 ± 0.131

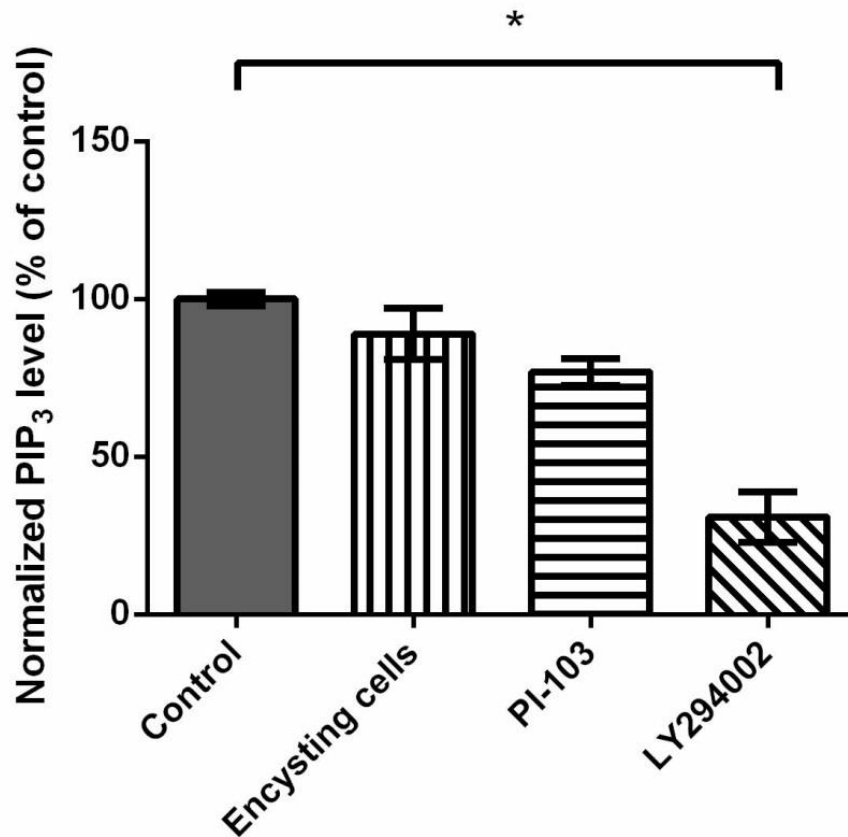


Figure 4.20: Investigation on phosphatidylinositol (3,4,5)-triphosphate (PIP₃) level in *G. intestinalis*.

Giardia trophozoites were treated with PI-103 and LY294002 (48 hours following initial subculture) to a final concentration of 2 μ M and 50 μ M, respectively. Encysting medium was exposed to trophozoite culture 48 hours after the initial subculture. The control of this experiment was a non-treated trophozoite culture. Forty-eight hours following treatment, treated trophozoites and encysting cells were collected, PIP₃ was extracted and analysed by direct PIP₃ ELISA mass assay. The graph shows normalised PIP₃ level in triplicate sample and the error bar represents the SEM. Statistical analysis was performed by post-hoc Tukey test, following ANOVA (*p < 0.001).

4.3 Discussion

Different inhibitors targeting kinases of the lipid signalling pathway have been tested in this chapter to observe the effect on *G. intestinalis* cells proliferation. The importance of the PI3K activity in the lipid signalling pathway of trophozoites has been reported here. The potent inhibitor of PI3K, LY294002, has been commonly used for over 20 years to investigate the mechanisms in the intracellular pathways involving PI3K. In order to confirm that putative PI3Ks in *G. intestinalis* cells are involved in many cellular processes, trophozoite cultures were treated with several PI3K inhibitors. The compound LY294002 was shown to inhibit trophozoite cell proliferation in a concentration-dependent manner. At a final concentration of 25 μM , the trophozoite population was reduced by approximately 50%, while LY294002 at a final concentration of 50 μM lowered the number of trophozoite cells by 65% compared to the control. In contrast, wortmannin and PI-103 did not show any effect on trophozoite population as compared to the control. Wortmannin and PI-103 experiments were completed using a range of concentrations; wortmannin was reported to inhibit PI3K with an IC_{50} of 1 μM (Davies *et al.*, 2000). However, the highest concentration that was experimented in this study was 15 μM . PI-103 was reported to inhibit PI3K with an IC_{50} of 1 μM in the purified protein sample (Bain *et al.*, 2007). Here, various concentrations of PI-103 were examined (0.2 – 5 μM) on trophozoite cells with no effect. The result of the PI-103 experiment did not show any significant effect on growth inhibition. Wortmannin has been known to inhibit PI3K for many years; however, the inhibitory effect seems to not function towards *Giardia* trophozoites. There are a few suggestions as to why wortmannin may not have a positive inhibition effect on trophozoite proliferation. First of all, structural differences between wortmannin and LY294002 suggest that GiPI3Ks may be missing key lysine residues or sequences required for ATP binding (Ward *et al.*, 2003). Additionally, wortmannin insensitivity in class III isoforms in GiPI3Ks could suggest the difficulty in binding through covalent modification as an irreversible inhibitor (Walker *et al.*, 2000). Previous work on PI-103, a novel inhibitor of PI3Ks that target class IA PI3Ks and mTOR, also does not demonstrate positive trophozoite growth inhibition in *Giardia* cell cultures (Workman *et al.*, 2006). To demonstrate that the effect of LY294002 on trophozoite cell proliferation was not CKII-mediated, an inhibitor of CKII was used to treat trophozoite cells. Interestingly, the phenotypes reported from the experimental work using CKII inhibitor showed that

trophozoite cultures behave in the same pattern of proliferation to the untreated control. In light of this result it was concluded that LY294002 is unlikely to affect giardial CKII but does not rule out the possibility that other kinases downstream of PI3K may be affected by the inhibitor (see Table 4.2).

Table 4.2: A brief summary showing specificities of PI3Ks inhibitors.

Values shown represent the percentage of catalytic activity remaining when the corresponding purified kinases were incubated in the presence of PI3K inhibitors as compared with control incubations. The experiment was repeated in triplicate to obtain results with each value as an average \pm standard deviation. The concentrations of each compound were determined by carrying out the experiment at ten different concentrations. Figure summarised from Bain *et al.* (2007).

Kinase	LY294002 (10 μ M)	Wortmannin (1 μ M)	PI-103 (1 μ M)
GSK-3 β	37 \pm 3	65 \pm 1	84 \pm 11
CKII	23 \pm 5	96 \pm 7	83 \pm 6
PLK1	26 \pm 1	64 \pm 1	79 \pm 10
PI3K	13 \pm 0	0 \pm 0	0 \pm 0

Due to the highly specific and potent ability of wortmannin and PI-103 to inhibit PI3Ks in mammalian cells, it was important to verify whether the effect of LY294002 on trophozoites proliferation was indeed because of the downstream inhibition of other kinases (such as GSK-3 β or PLK1). This creates a hypothesis that LY294002 may be inhibiting other kinases thus causing a block in the cell cycle. Glycogen synthase kinase-3 is another essential protein kinase involved in signal transduction, cell survival and protein synthesis. To ascertain this hypothesis, trophozoites were treated with GSK-3 inhibitors LiCl and CT99021. The results show that CT99021-treated trophozoites at various concentrations (Figure 4.9) do not show a positive growth inhibition effect on *Giardia* cells, after observing that the number of treated cells was similar to the untreated control. Following CT99021 treatment, trophozoites with LiCl at the recommended concentration also did not demonstrate the inhibition of growth with five different concentrations treated and compared with the control. Under normal growth, one can hypothesise the two GSK-3 inhibitors applied to trophozoites may facilitate in the phosphorylation of GSK-3; therefore,

the cell cycle would continue, leading to an increase in the number of cells. However, this assumes that these inhibitors actually work in *Giardia* as in other organisms.

The level of PLK1 activity in mammalian cell is regulated during the cell cycle and involves in multiple functions during mitosis (Liu *et al.*, 2005). Small-molecule inhibitors developed to target this kinase have reported that PLK1 inhibitor has a cytotoxic effect on mammalian cancer cells (Sanhaji *et al.*, 2013). This may rule out the possibility of PLK1 being an LY294002 target in *Giardia*, as LY294002 demonstrates a cytostatic effect on trophozoites. However, it is important to note that a specific inhibitor of PLK1 should be investigated on the exponentially growing trophozoite culture to observe any effect on trophozoite cell proliferation.

The result of using double inhibitor treatment on *Giardia* trophozoites showed that LY294002-treated cultures with the addition of GSK-3 inhibitor continues to show growth inhibition. Moreover, increasing the concentration of LY294002 treatment in CT99021-treated trophozoites at a constant concentration affects trophozoite cell number in a concentration-dependent manner. Based on this evidence, this strongly suggests that LY294002 does not inhibit GiGSKs. An explanation could be that GiGSKs lack crucial residues needed for binding to form phosphorylated GSK (inactive form). The second double inhibitor experiment result found that increasing the concentration of CT99021 together with trophozoites treated with fixed levels of LY294002 did not demonstrate an increase in the number of trophozoite cells. Therefore, it was concluded that the effect of LY294002 was due to PI3K inhibition.

LY294002-treated cells inhibit trophozoite proliferation through blocking the activity of PI3K, alleviating this effect with the removal of this compound from cultures; consequently, trophozoites are able to proliferate. To confirm that LY294002 treatment has a cytostatic effect on trophozoites, experiments using puromycin were carried out. The results illustrated that puromycin has a cytotoxic effect on trophozoites. This was confirmed by attempt to reverse the condition through removing the culture medium containing puromycin and replaced with fresh culture medium. Trophozoites pre-treated with puromycin did not show a reversible effect upon removal of puromycin, unlike trophozoites pre-treated with LY294002. This strongly suggests that puromycin kills cells, whereas LY294002 treatment reversibly blocked cell proliferation.

Evidence from previous studies suggests that LY294002-treated trophozoites initiate the process of encystation. Inhibition of PI3K activity may cause trophozoites to initiate expression and translation of CWP2 and package into ESV-like vesicles reminiscent of early encystation cells. This evidence has been shown by Cox and Tovar (unpublished). Therefore, this outcome suggests that trophozoites treated with PI3K inhibitor promote cells to enter cell differentiation, similar to an encystation process.

Experimental work on LY294002-treated cells following encystation induction discovered that it could yield reduced numbers of cysts. However, this may raise an important question that trophozoite cells following encystation induction treated with LY294002 could initiate the process of encystation, but these cells resulted in incomplete cyst formation. Under normal conditions, the percentage of encysting cells and cysts in cell culture should reach approximately 45% within 24 hours (Figure 4.18 and Figure 4.19). In this work, however, approximately 82% of the LY294002-treated cells in encysting medium in the first 24 hours were still showing trophozoite morphology, with the remaining appearing as encysting cells and cysts. This evidence supports the hypothesis that PI3K inhibition at the early phase of encystation delays the differentiation of trophozoites to encysting cells and cysts; as a result, this may lead to cell death (see Figure 4.18). An experiment to increase the accuracy of detecting initiation of the encystation process could use markers of encystation. Encystation markers such as monoclonal antibodies against ESV-specific calcium binding proteins of *G. intestinalis* can detect the changes from trophozoite to encysting cell as it is only present in secretory vesicles of encysting trophozoite (Touz *et al.*, 2002). These findings may be interpreted further by taking a closer look at the *Giardia* cell cycle in relation to the parasite's ability to differentiate into cysts, the PI3K signalling cascade in mammalian cells and initiation of the encystation process involving ESVs and the production of CWPs.

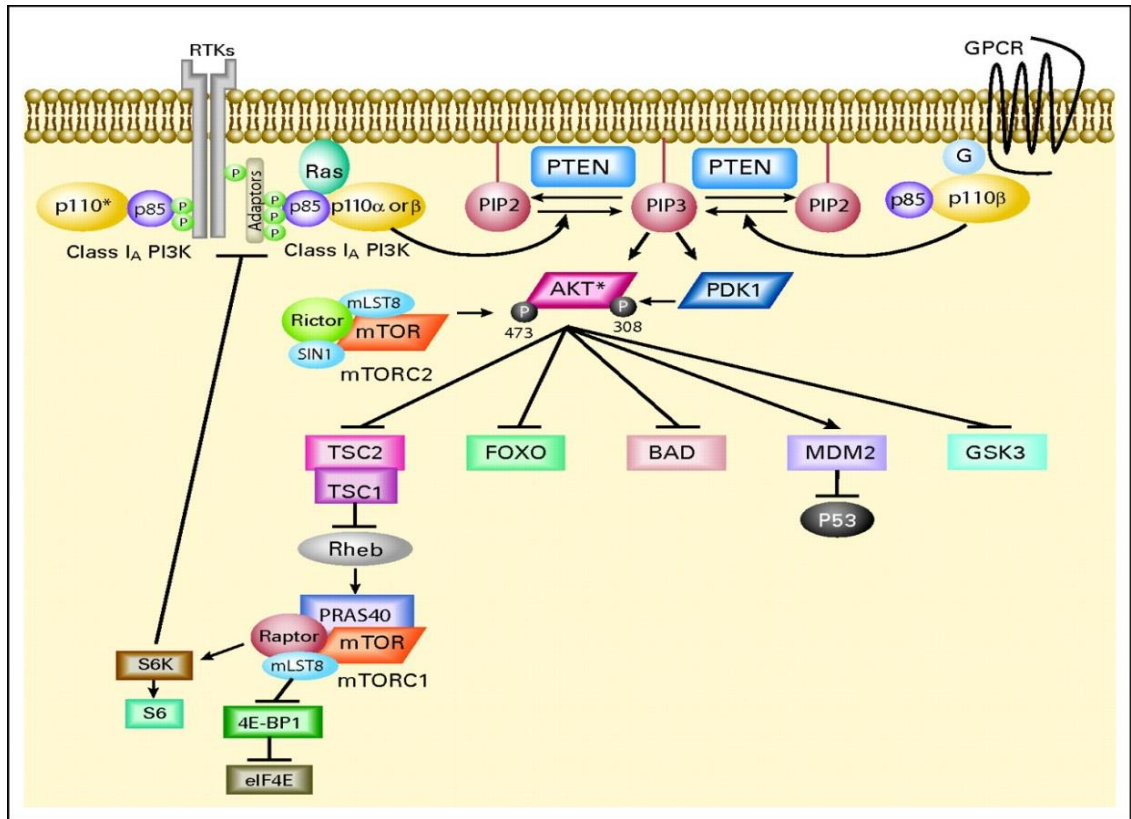


Figure 4.21: Mammalian class IA PI3K signalling pathway impacts on cell growth, survival and metabolism.

Arrows represent activation, while bars reflect inhibition. A negative feedback loop has been described from the downstream target S6 kinase (S6K) to the adaptor protein IRS-1. RTK, receptor tyrosine kinase; GPCR, G-protein coupled receptor; P, phosphate; G, G protein; PTEN, phosphatase and tensin homolog; IRS-1, insulin receptor substrate 1; eIF4E, eukaryotic initiation factor 4E; S6, ribosomal S6 protein; PIP₂, phosphatidylinositol 4,5-bisphosphate; mTORC2, rapamycin (mTOR) – containing protein complex 2. (*) p110 alpha, beta, or delta. Figure taken from Courtney *et al.* (2010).

The PI3K signalling cascade is an important regulator of cell growth and cell survival. Many studies have highlighted the crucial roles that PI3K activity has in mammalian intracellular signalling pathways (Figure 4.21). A central component of this signalling cascade is PKB. While PI3K phosphorylates PIP₂ to PIP₃, this anchoring PIP₃ migrates the two PH domain containing component PDK1 and PKB. PDK1 activates PKB through phosphorylation at threonine 308, thus promoting cell growth and several mechanisms that are involved in cell survival such as GSK-3, Forkhead transcription

factors (FOXO), Bcl-XL-antagonist, causing cell death (BAD), mouse double minute 2 (MDM2) and tuberous sclerosis complex 2 (TSC2). However, a vital component in the regulation of cell growth in the PI3K signalling cascade is mammalian target of rapamycin (mTOR). Phosphorylation of TSC2 by PKB inhibits Rheb (ras homolog enriched in brain) GTPase, therefore activating Rheb. The Rheb component stimulates mTOR which initiates translation by activating ribosomal S6 protein and eukaryotic initiation factor 4E (eIF4E). Activation of the ribosomal S6 protein promotes translation of the ribosome and components of the translation mechanism. Conversely, mTOR also controls cell growth via negative feedback through its protein complex mTORC1 to reduce PI3K activation (Hresko *et al.*, 2005).

Cell growth in *Giardia* during an infection *in vivo* is currently not fully understood; however, *in vitro* studies from cultivation using the extremely versatile TYI-S-33 medium were able to sustain *Giardia* growth. A reversible inhibitor of eukaryotic nuclear DNA replication, aphidicolin, blocks the cell cycle at the S-phase. Flow cytometric analysis was then used to determine the length of time in each of the cell cycle phases and duration in *Giardia* cell cycle (Reiner *et al.*, 2008). *G. intestinalis* cell division involves an unusual number of two nuclei. During vegetative growth, each trophozoite nucleus cycles between a diploid (2N) or tetraploid (4N) genome, therefore resulting in the cellular ploidy of 4N or 8N (Bernander *et al.*, 2001). The starting point of *Giardia* trophozoite cell division begins at G1 stage of the cell cycle, when two nuclei with a total of 4N undergo DNA replication to produce trophozoites with two nuclei, making a total of 8N. Progressing to G2 phase, trophozoites with two nuclei and 8N undergo nuclear division to form trophozoites with four nuclei (8N; $4N \times 2 = 8N$). Following nuclear division, trophozoites containing four nuclei (8N) reach the M phase (mitosis phase), and two trophozoite daughter cells emerge from a single trophozoite parent cell, with each daughter cell possessing two nuclei (4N) (Svard *et al.*, 2003). At what point in the cell cycle the inhibition of PI3K activity could have an effect on *Giardia* cell cycling is currently unknown. However, one would assume that PI3K activity is required in both G1 and G2 stages of the cell cycle. As PI3K-inhibited trophozoites were unable to proliferate and failed to complete cell division, the inhibition of cell growth cause by LY294002 may block cell cycle at G1 or G2. Upon removal of LY294002, if the inhibitory effect does take place in the G1 phase, this may result in a slight delay in the recovery of the trophozoites growth, but should eventually reach the same number of cells as the control. Alternatively, if the inhibitory effect takes place at G2

phase, upon removal of the inhibitor LY294002, the expected outcome would be that there should be no delay in the recovery of the trophozoite growth. Furthermore, an increase in trophozoite number should occur compared to the control because G2 arrest cells are already prepared for the M phase with each trophozoite having four nuclei 8N. However, the results in Figure 4.6 illustrate that there was no significant difference between the number of trophozoites between the treated and control cells at 96 hours upon removal of the PI3K inhibitor. Therefore, it is likely that LY294002 stimulates G1 arrest in trophozoites. Having concluded that, it would be ideal to follow the different stages of cell replication which will pinpoint the specific stage at which PI3K activity is no longer functional. Fluorescence-activated cell sorting (FACS) techniques can provide a tool for identifying *Giardia* differentiation or a stop in cell growth (Bernander *et al.*, 2001). A complication of this could be the fact that *Giardia* trophozoites in cell culture are not synchronised and do not all go through the same stages of the cell cycle at any one time (Bernander *et al.*, 2001).

Given that inhibition of PI3K activity affects trophozoites under normal conditions at the G1 stage, therefore causing cell cycle arrest, under normal conditions, *Giardia* during the encystation process would differentiate from the G2 stage (Bernander *et al.*, 2001). The cyst wall material (CWP) would be transported by ESVs and deposited to the outer cell membrane of *Giardia*. The *Giardia* nuclei then divide, giving a single encysting cell composed of four nuclei (8N). Continuation of cell replication takes place and a mature cyst will have complete 16N cellular ploidy with four nuclei. However, during initiation of the encystation process, trophozoites are likely to differentiate from G2 stage of the cell cycle. Addition of a PI3K inhibitor at this stage may interrupt the encystation signalling pathway, therefore inhibiting cell differentiation. One way of detecting cell differentiation is the use of an antibody to label CWPs carried by encystation-specific secretory vesicles (ESVs) that are made from ER, which may be an important tool in identifying the process of encystation (see Figure 4.22). Further observation of the impact of PI3K inhibition in *Giardia*, the morphology of *Giardia* within cells and the overall ultrastructure will be presented in the next chapter using scanning and transmission electron microscopy.

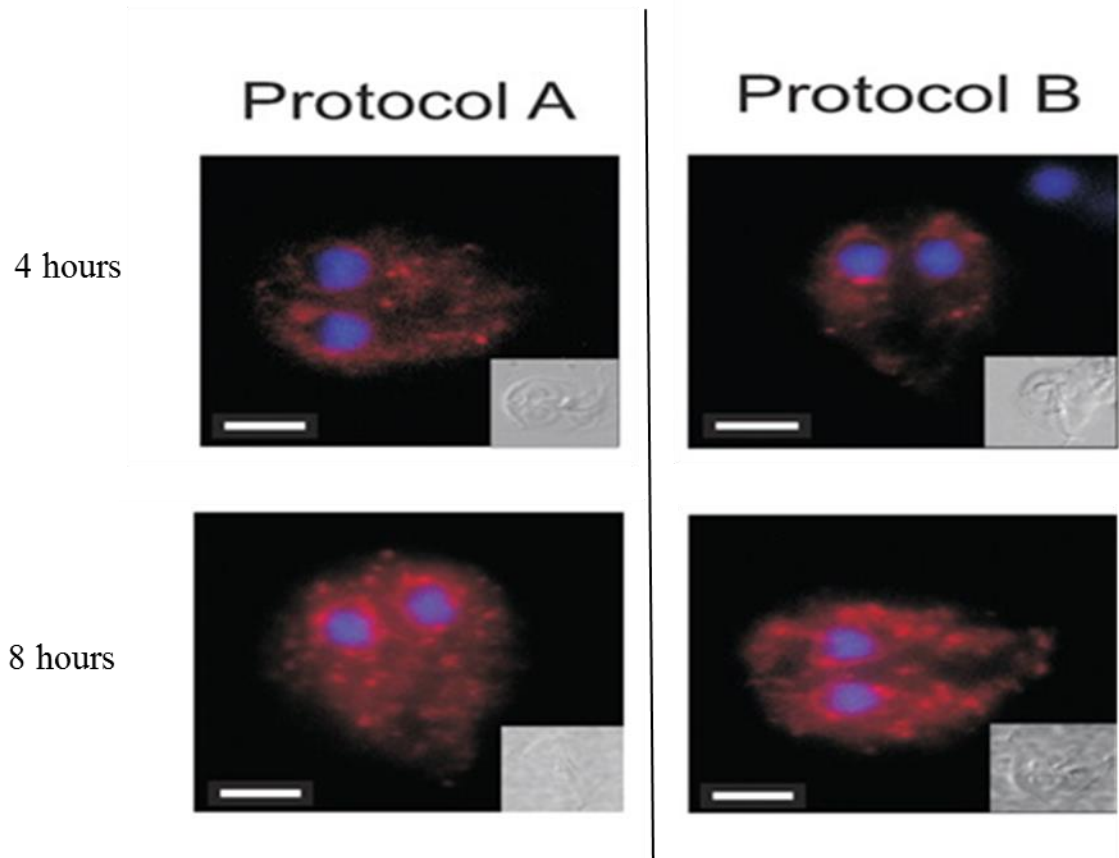


Figure 4.22: Encystation process images at 4 hours and 8 hours.

The two different encystation protocols at time points 4 and 8 hours with insets images of bright-field. Protocol A proceeds with two-step encystation; the first step is pre-encysting medium (bile-free medium) to incubate trophozoite for 44 hours. The second step is using pre-warmed encystation medium with a pH to 7.85 and the addition of porcine bile together with lactic acid. Protocol B initiate lipid starvation using bile-free medium containing delipidated foetal calf serum at a pH of 7.85 to induce differentiation of cells grown in standard trophozoite medium. Scale bars 3 μm , red indicates CWP-labelled cells and blue shows two nuclei labelled by DAPI. Images are taken directly from Morf *et al.* (2010).

CHAPTER 5: Using scanning and transmission electron microscopy to investigate the effect of LY294002 on *G. intestinalis*

5.1 Introduction

The research so far has suggested that components of PI3K intracellular signalling pathway and downstream GSK signalling pathways do exist in *G. intestinalis*. The previous chapter reported the use of PI3Ks and GSK inhibitors on *Giardia* trophozoites to examine the impact that these have on parasite intracellular signalling pathways. The research presented in this chapter was carried out in an attempt to study the ultrastructure of vegetative trophozoites, to investigate the ultrastructural modifications of trophozoites treated with the PI3K inhibitor LY294002 and to examine differentiation of trophozoites into cysts, in a process known as encystation. The different techniques and tools required to address this work lie within the field of electron microscopy.

The first scanning electron microscope (SEM) was introduced by Manfred Von Ardenne in 1937; however, one of the first articles on *G. intestinalis* using SEM was published in 1964 by Cheissin. The exterior morphology of *Giardia* trophozoites are approximately 12-15 µm in length and 5-9 µm wide, and *Giardia* cysts measure about 8-12 µm in length and 7-10 µm in width (Adam, 2001). There are many advantages of using SEM to study the morphology of *Giardia*. Previous SEM studies reported the detailed ultrastructure of the cell and presented high magnification images of the morphology of the cell. Powerful magnification combined with the high resolution of SEM means that each individual flagellum in *Giardia*, the ventral disk used for adherence and the lateral flange that surrounds the whole cell can be clearly examined (Lanfredi-Rangel *et al.*, 1999).

Transmission electron microscopy (TEM), in contrast to ordinary light microscopy, uses electron beams instead of light beams. A beam of electrons is transmitted through the ultra-thin sample that has been cut following resin embedment. The first TEM was built in 1931 by Max Knoll and Ernst Ruska, but this type of microscopy continues to be further developed to the present day. The developments in TEM led to one of the first publications in 1980 using this equipment to investigate *G. intestinalis* cysts (Luchtel *et al.*, 1980). The nature of TEM allows observation of the ultrastructure of the inner layers of trophozoite and cyst cells; together with its high magnification and resolution capability, TEM has been

a useful technique to study the impact of cellular signalling in *Giardia* cells. For example, encystation in *G. intestinalis* has been examined and images of trophozoites differentiating into cysts were presented using electron microscopy (Adam, 2001, Midlej and Benchimol, 2009, Hausen *et al.*, 2009, Castillo-Romero *et al.*, 2009). All of the knowledge of encystation at present could not have been accomplished without the visual aid of TEM. Furthermore, immunolocalisation of cyst wall protein 1 (CWP1) in *Giardia* under TEM clearly shows evidence of the ESVs within encysting cells through electron-dense vesicles (Midlej *et al.*, 2012).

In the present study, SEM and TEM were selected to study *G. intestinalis* cells from the outer layer structural pear-shaped trophozoites to the internal cytoplasmic structures of *Giardia* cells. The aim of this chapter was to utilise SEM and TEM to further explore the suggestion that LY294002-treated trophozoites initiate an encystation-like processes. Taken together our data suggest that trophozoites treated with the PI3K inhibitor LY294002 halt trophozoite proliferation in the G1 phase of the cell cycle in normal growth medium. Inhibition of GiPI3K1 and/or GiPI3K2 under encystation medium also halts in the G2 stage of the cell cycle, preventing the formation of cysts in the encystation process.

5.2 Experimental Results

5.2.1 Scanning electron microscopy images of *G. intestinalis* trophozoites

Using SEM to view exponentially growing *Giardia* trophozoites was crucial to the understanding of trophozoite ultrastructure and cell morphology. Initially, trophozoite exponential growth was reached after 48 hours and the cells were allowed to attach to a coverslip and taken for SEM viewing. It was important to establish these normal untreated pear-shaped trophozoites (Figure 5.1, panel a) showing four pairs of flagella; the anterior flagella (shown closest to the scale bar), posterior lateral flagella, ventral flagella (on the ventral side) and caudal flagella (tail section). The flagella are essential for trophozoite motility and their functional role was reviewed by Elmendorf *et al.* (2003). Here, trophozoites were measured and found to be approximately 15 μm in length and 7 μm in width (Figure 5.1). A general view (see Figure 5.1, panel b) displays single random fields of view that demonstrate the distribution of trophozoites in untreated culture. The anterior side of trophozoites (see Figure 5.1, panel a) shows a smooth surface surrounded by the cell plasma membrane.

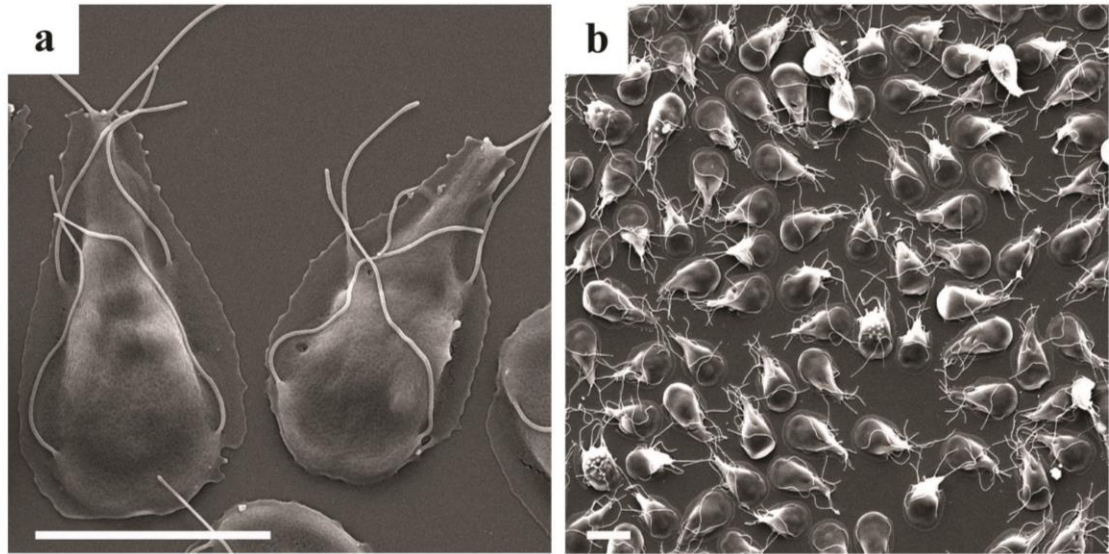


Figure 5.1: *Giardia intestinalis* trophozoites morphology.

SEM images of control trophozoites showing **a**, pear-shape-like cell morphology and **b**, overview of one random field of view under normal conditions. Scale bars, 10 μm .

The results in Chapter 4 show that the PI3K inhibitor LY294002 inhibits exponentially growing *Giardia* trophozoite proliferation in a concentration-dependent manner. Upon removal of the inhibitor LY294002, trophozoite cell cultures recovered back to normal. Therefore, it is important to investigate what had occurred to trophozoite ultrastructure under the PI3K inhibitor that enabled this reversible effect on its growth. Exponentially growing trophozoites were treated with LY294002 at a final concentration of either 15 μM or 50 μM . The selected concentrations were the lowest effected potency and the IC_{50} value for LY294002 concentrations, respectively (Chapter 4). Figure 5.2 illustrates exponentially growing trophozoites treated with LY294002 at 50 μM . After forty-eight hours of incubation, trophozoites were fixed and prepared for SEM. The resulting micrographs detected several differences between the DMSO-control trophozoites and LY294002-treated cells. The general view in a random field shows differences in the number of cells present (later quantify). More importantly, almost all of the cells had altered shapes (Figure 5.2, panel b) and the appearance of vesicular protrusion spots on the body of the trophozoites (Figure 5.2, panel d) compared to the smooth surface of the DMSO-control trophozoite (Figure 5.2, panel c).

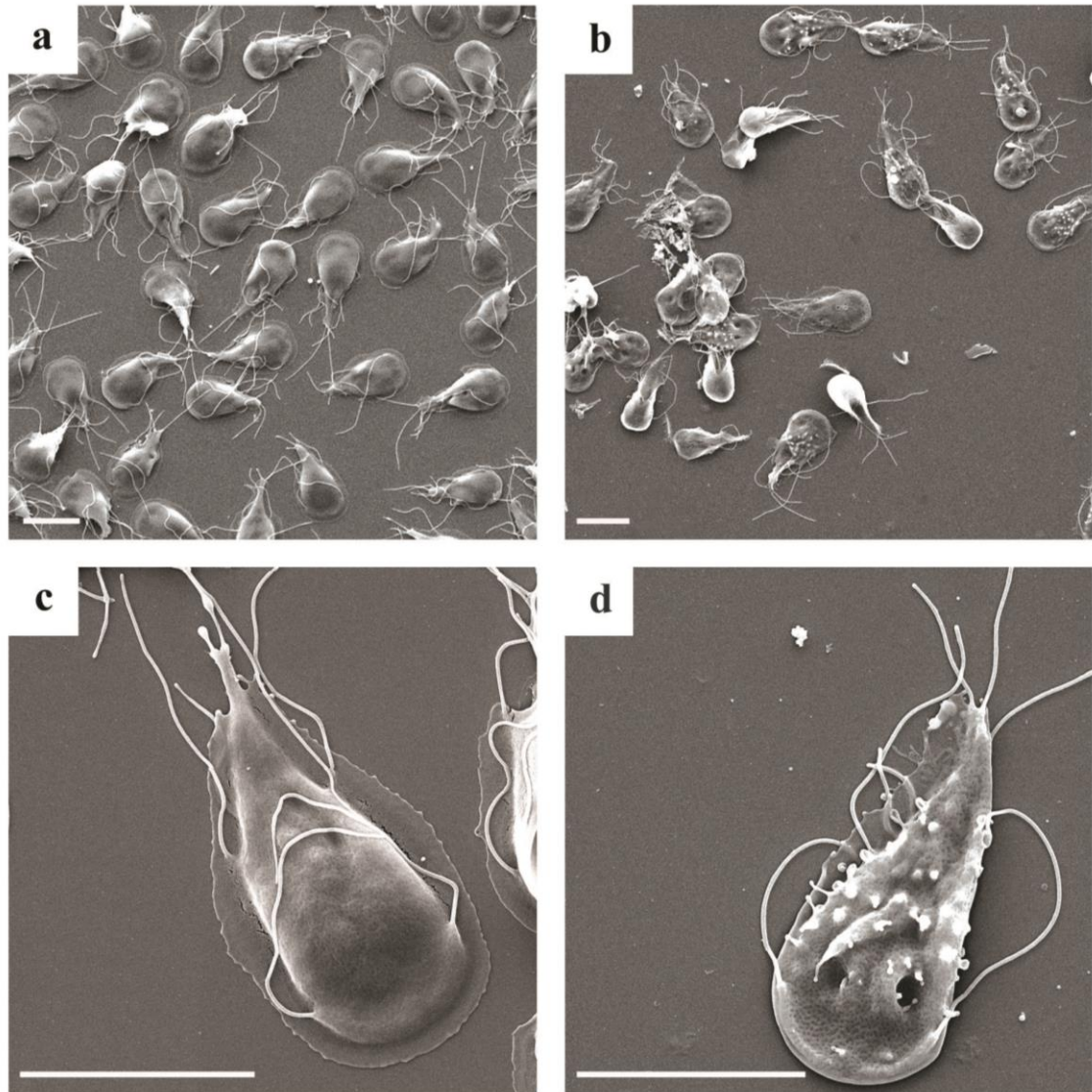


Figure 5.2: Trophozoites cells treated with LY294002 cell morphology.

SEM images showing **a** and **c** control trophozoites treated with DMSO in a random field of view and a single DMSO-control trophozoite cell morphology, respectively. **b** and **d**, trophozoites treated with LY294002 in a single random field of view and morphological changes to a trophozoite structure under the treatment of a PI3K-inhibitor. Scale bars, 10 μm .

To further characterise the morphological changes during LY294002 treatment to trophozoites at concentration of 15 μM and 50 μM , Figure 5.3 shows a general observation in a single field of view where treated and untreated cultures were incubated for 24 hours and 48 hours (left panel and right panel, respectively). Trophozoites exposed to 15 μM of LY294002 over 24 hours display lower numbers of trophozoites in a single random field of view where some *Giardia* cells exhibit unusual morphology compared to the control

trophozoites (see Figure 5.3, panel c). The morphological changes to trophozoites can be categorised into shortened cells, vesicular spots, elongated cells, doublet cells (dividing cells) and membrane blebs. This is also observed in Figure 5.3, panel e; however, at higher concentrations of LY294002, the number of abnormally-shaped trophozoites increases. At 48 hours incubation in Figure 5.3, panel d and f, almost all of the cells show remarkable alterations in cell morphology, cells become more elongated, the cell plasma membranes display thin blebs and the appearance of small vesicular features on the surface of the trophozoite can be observed.

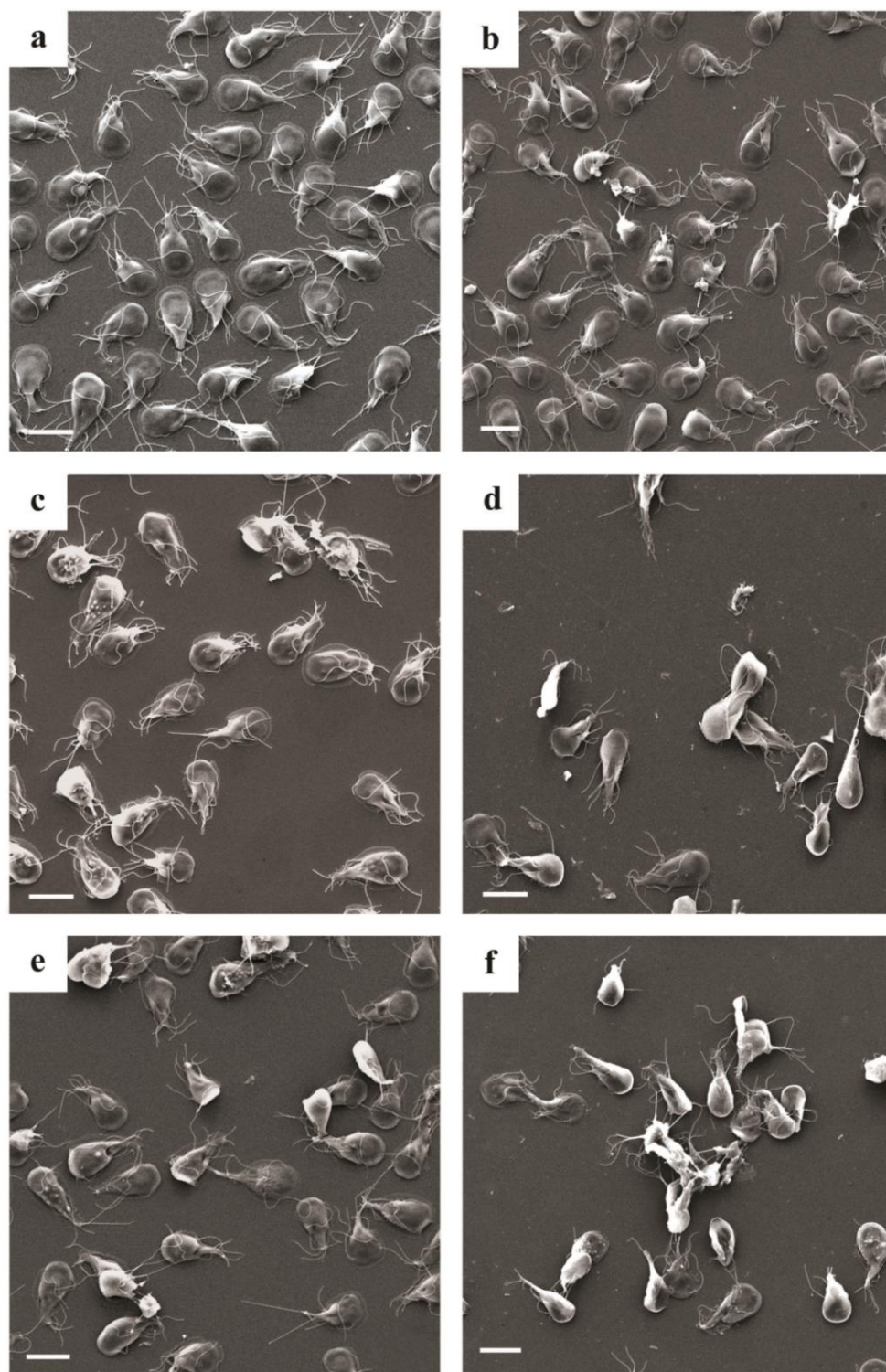


Figure 5.3: Comparison of *Giardia* trophozoite cells treated with LY294002 over 24 hours and 48 hours.

SEM images showing 24 hours (left panel) and 48 hours (right panel) incubation of **a** and **b** control DMSO-treated trophozoites. **c** and **d**, trophozoites treated with LY294002 at 15 μ M. **e** and **f**, trophozoites treated with LY294002 at 50 μ M. Scale bars, 10 μ M.

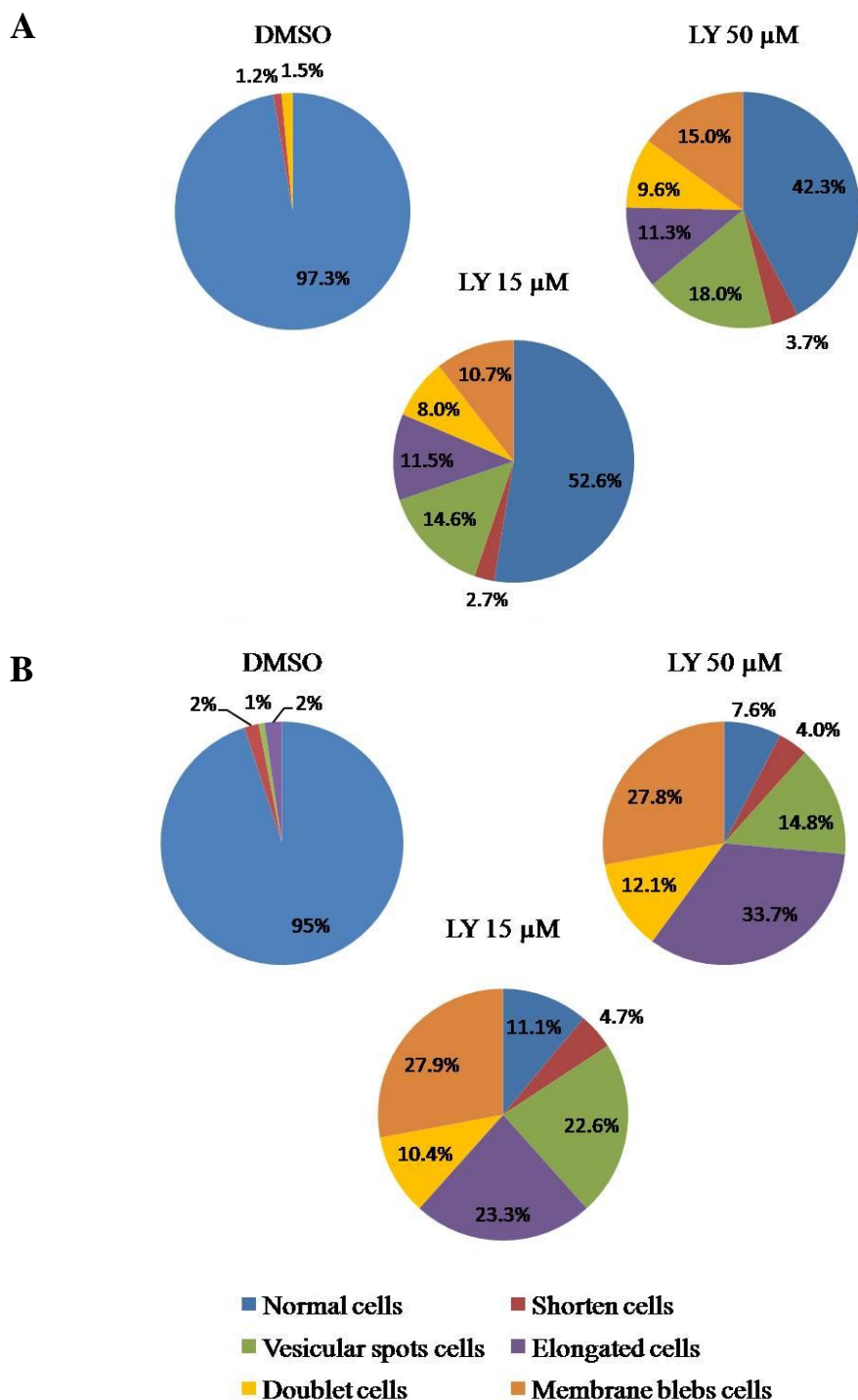


Figure 5.4: Proportion of morphologically-altered trophozoite cells in groups of PI3K-inhibited cells treated with LY294002 and control-treated trophozoites.

SEM was used to view disfigured trophozoites which can be divided into six categories: normal cells, shortened cells, vesicular spots, elongated cells, doublet cells (dividing cells) and membrane blebs. **A** shows the group of cells incubated for 24 hours and **B** shows trophozoites that were incubated for 48 hours. This data are from a single experimental treatment. Data presented as percentages of the total cells counted in a maximum of seven random fields of view in each incubation period. The minimum number of cells counted per treatment was 100 cells.

Total cell numbers of LY294002-treated cultures at final concentrations of 15 μM and 50 μM were counted using micrographs taken from SEM. Figure 5.4 shows a comparison of the treated-trophozoites at different concentrations of LY294002 and the control DMSO-treated cells. The number of morphological changes was calculated by counting the number of cells exhibiting abnormal characteristics and determines the percentage given to each of the categories. The percentage of normal cells in LY294002-treated cells was 52.6% and 42.3% in the first 24 hours with concentrations of 15 μM and 50 μM , respectively. The highest percentage of abnormal characteristics over 24 hours appears to be accounted for by the vesicular spots and plasma membrane blebs. Vesicular spots are irregular protrusions of the cell surface membrane. At 48 hours incubation with LY294002, almost all of the trophozoites appear to become totally distorted; this was evident in Figure 5.4, where LY294002-treated trophozoites at 15 μM and 50 μM indicate 11.1% and 7.6% of normal cells, respectively. There were no major changes in the number of vesicular spots cells or the number of plasma membrane blebs; however, the number of elongated cells in LY294002-treated cells increased. Elongated trophozoites are seen as thinner, 'torpedo-like' in shape, and the area between the median body to caudal flagella is lengthened (Figure 5.5, panel h and i). Figure 5.4 indicates that LY294002-treated cells at 50 μM show an increase in the average percentage of elongated cells from 11.3% after 24 hours incubation to 33.7% in 48 hours exposure to a PI3K-inhibitor. Furthermore, the average percentage of doublet cells has also increased in LY294002-treated cells, where it shows that 10.4% and 12.1% of cells are doublet cells (Figure 5.5, panel d) in cells exposed to LY294002 at 15 μM and 50 μM , respectively. These observations suggest that LY294002 affects trophozoite cell growth and may stimulate G1 cell cycle arrest, thus leading to incomplete cell division of the trophozoites.

Close observation of individual trophozoites following exposure to different concentrations of LY294002 for 24 and 48 hours were completed using SEM. Images taken in Figure 5.5 show abnormal cells that were counted and presented in Figure 5.4. These cells are examples of the morphology of trophozoites that were under the treatment of LY294002. Some trophozoites change morphology from a pear-shaped-like cell (Figure 5.5, panel b) into round shapes with the length of the cell shortened (Figure 5.5, panel c) and doublet cells with a heart-shape-like appearance suggest incomplete cell division (Figure 5.5, panel d). Cell adhesive disks bleb when attached to the coverslip (Figure 5.5, panel e to i), protrusion of vesicles on the cell dorsal surface (Figure 5.5, panel c, d and j),

elongated, torpedo-like cells (Figure 5.5, panel h and i) and flattened cells with loss of normal morphology shown in Figure 5.5, panel k, were also observed.

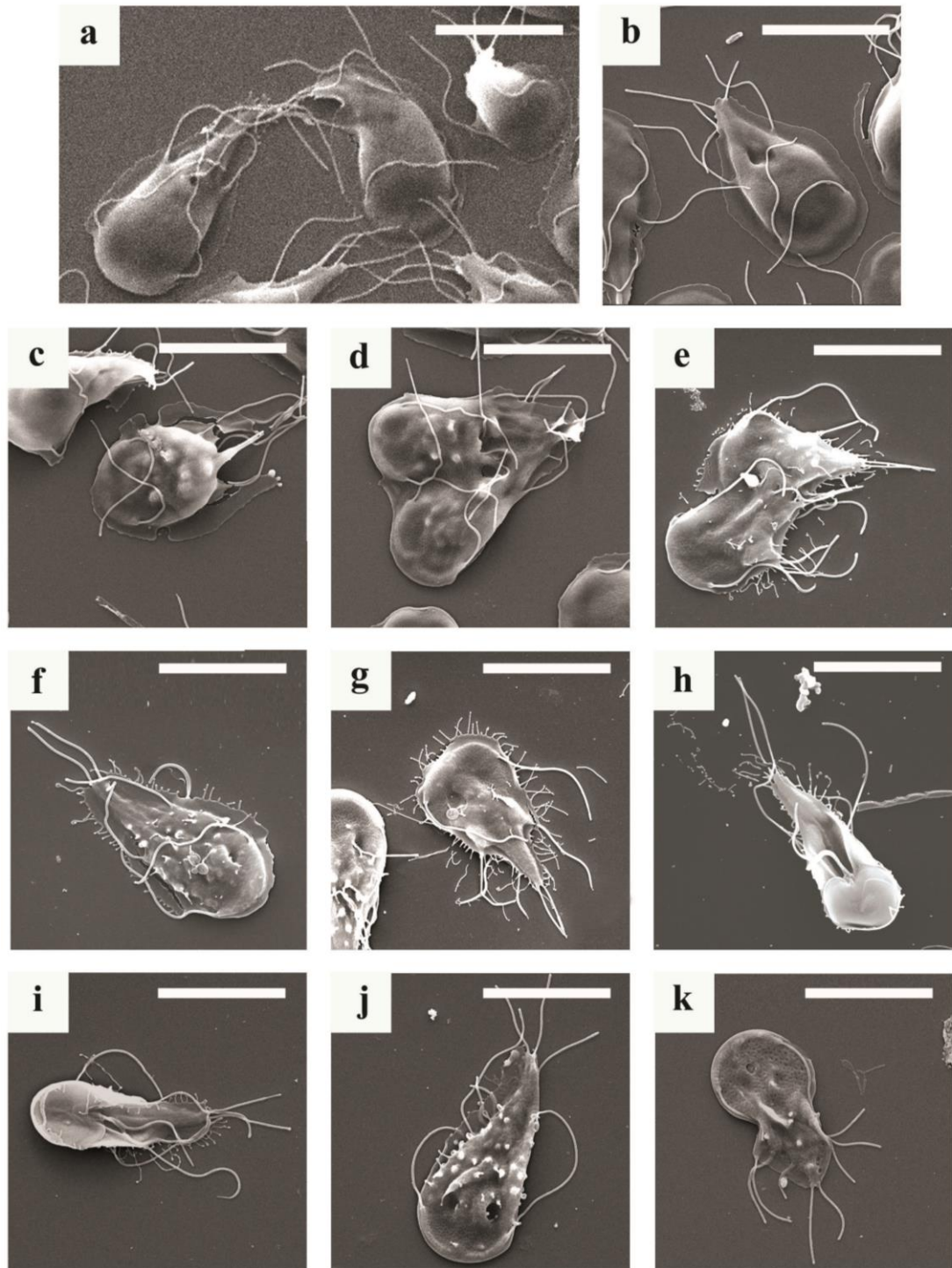


Figure 5.5: *Giardia intestinalis* trophozoites under LY294002 treatment.

SEM images of **a** and **b** control trophozoite cells untreated with a pear-shape appearance. **c** and **d** trophozoites treated with LY294002 at 50 μM after 24 hours. **e** – **h**, trophozoites treated with LY294002 at 15 μM after 48 hours. **i** – **k**, trophozoites treated with LY294002 at 50 μM after 48 hours. Scale bar 10 μm .

5.2.2 SEM images of *G. intestinalis* encysting cells

The observation of *Giardia* trophozoites under SEM was continued to monitor the organism as the encystation process is stimulated through the introduction of encysting medium. Experiments were carried out to study changes in the morphology of *Giardia* during encystation and to examine cell modifications under the exposure of LY294002. Under normal encystation, the introduction of encysting medium will trigger the process of encystation *in vitro*. It was mentioned in Chapter 4 that encystation can be divided into two phases: the earlier phase and the late phase. More importantly, not all *Giardia* trophozoites differentiate into cysts; also, cells within a population do not all enter encystation at the same time (Adam, 2001).

To establish the standard wild type *Giardia* cell morphology during encystation, Figure 5.6 shows *Giardia* cells incubated in encysting medium for 48 hours with SEM images taken every 12 hours after the initial introduction of the medium. Initially, the earlier phase of encystation should complete within the first 10 hours of the introduction of encysting medium. The earlier phase mentioned before in Chapter 4 includes the intracellular synthesis of cyst wall component proteins required for encystation (Reiner *et al.*, 1990). ESVs become visible to allow transportation of the cyst wall components to the outer layer of the cell (Adam, 2001). In Figure 5.6, the left panel a, c, e and i show the general view of *Giardia* in a single random field of view, where the organism was under encysting medium for 12, 24, 36 and 48 hours, respectively. The result highlights that the number of trophozoites, encysting cells or cysts decreases the longer they are under encysting medium. This observation was supported by the percentage of normal cells, which decreases from 61.3% in the first 12 hours to 37.3% at the end of the 48 hour incubation period. Therefore, stimulation of the encystation process may effectively become a stressful environment for the growth of trophozoites. Upon closer inspection, there were signs of morphological change that indicate the initiation of encystation; for example, shortening cells increased from 0.7% in the first 12 hours to 7.5% by 48 hours (see Figure 5.6). Other morphological changes were observed by TEM; these will be discussed later on in this chapter.

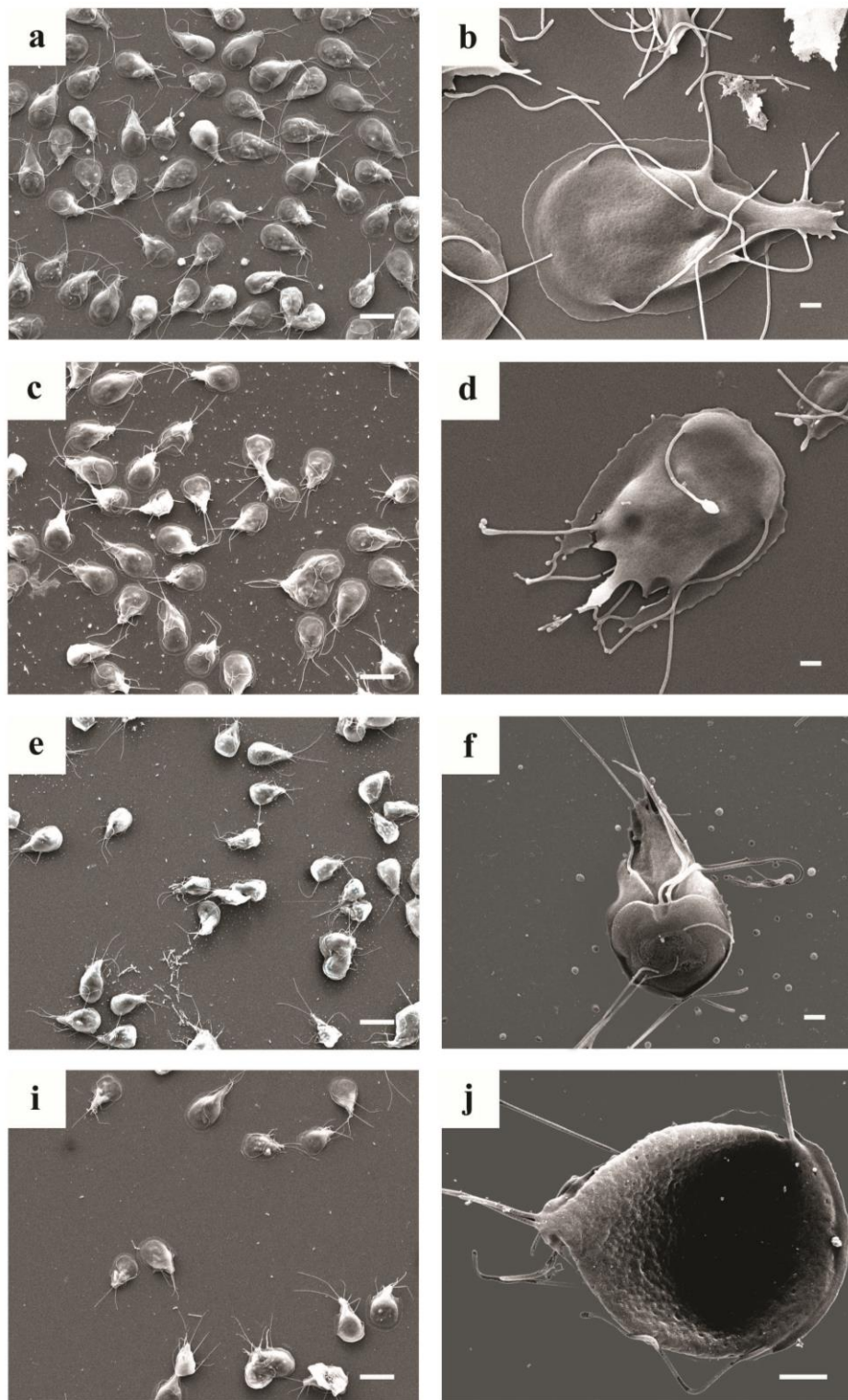


Figure 5.6: *Giardia intestinalis* under encysting medium over 48 hours.

SEM images of **a** and **b** *Giardia* under encysting medium after 12 hours. **c** and **d**, *Giardia* under encysting medium after 24 hours. **e** and **f**, *Giardia* under encysting medium after 36 hours. **i** and **j**, *Giardia* under encysting medium after 48 hours. **a**, **c**, **e** and **i** represent the general view of *Giardia*. **b**, **d**, **f** and **j** display the detailed morphology appearance of the cell. Scale bars **a**, **c**, **e** and **i**, 10 μm ; **b**, **d**, **f** and **j**, 1 μm .

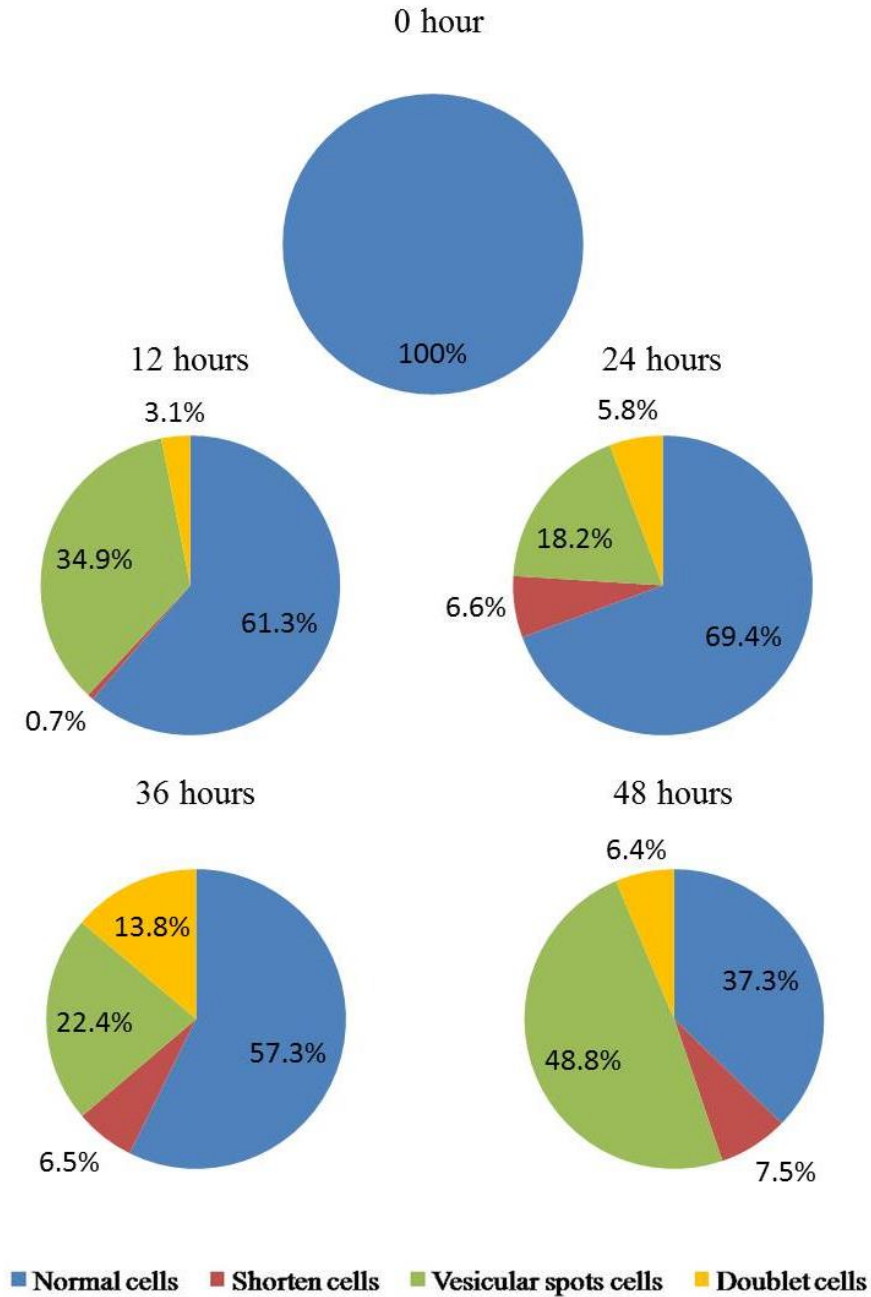


Figure 5.7: Encystation experiment with *G. intestinalis* over a period of 48 hours.

Using SEM images showing the general view of wild type cells exposure to encysting medium, the total number of cells were counted and placed in to different categories of different cell morphology; normal cells, vesicular spotted cells, doublet cells and shortening cells. Data are presented as the number of cells counted in different categories/the total number of cells counted in the group. Percentages are also given and represent the proportion of cells in that category within each time period. These data were from a single experimental work with a minimum of 100 cells analysed per treatment.

To determine the effect of LY294002 on *Giardia* cell morphology using SEM during encystation, encysting cultures were treated with LY294002. *Giardia* cultures were incubated for 24, 48, 72 and 96 hours. The positive control of the experiment was encysting cultures treated with DMSO. Referring back to Chapter 4 during encystation, the total cell number decreases under both control-DMSO- and LY294002-treated encysting cultures over a period of 168 hours. However, the number of cells in control-DMSO encysting cultures did not decrease until after 72 hours. Therefore, this suggests that in the general view, similar numbers of cells are expected at 24 hours and 48 hours.

Observation of SEM images illustrates that the loss of normal morphology continues under encystation conditions when exponentially growing trophozoites were under encysting medium and immediately treated with DMSO (control) and LY294002 (Figure 5.8). Interestingly, Figure 5.8 illustrates that both LY294002-treated samples and the control-DMSO show *Giardia* cells with abnormal morphological changes. In the first 24 hours, the appearance of vesicular protrusions on the cell surface membrane were common to both LY294002-treated and control-DMSO *Giardia* cells. The proportion of vesicular protrusions on an average percentage count was 21.2% and 25.6% in control-DMSO and LY294002-treated cultures, respectively. At 48 hours, the effect of LY294002 treatment showed a significant increase by an average of 60.2% in the number of cells with vesicular protrusions, with the control-DMSO reaching 39.3% (Figure 5.9 A and B). Moreover, flagella were positioned at irregular locations in both conditions and after incubation times of both 24 and 48 hours (Figure 5.8). The SEM images used for analysis show a total decrease in the average percentage of normal cells in both LY294002-treated and control-DMSO treated cells over the course of 72 hours. Initially, LY294002-treated cultures at 24 hours show an average of 49.6% of normal pear-shaped cells, similar to control-DMSO, with an average of 50%. However, after 48 hours of incubation, the proportion of normal cells in the control-DMSO decreased to 32% while, LY294002-treated samples averaged only 12% (Figure 5.9 B). The abnormal appearances of LY294002-treated cells were predominately due to a large number of protrusions distributed on the cell surface membrane. These protrusions can be seen following closer inspection in Figure 5.10, panel b and c; on average, the proportion of cells with vesicular spots appearance was as high as 67.6%. Previous studies have suggested that these protrusions on the encysting cell surface membrane may represent the increasing number of encystation vesicles below the surface of the cell differentiating plasma membrane, as

previously characterised in replicas of freeze-fractured encysted cells (Lanfredi-Rangel *et al.*, 2003 and Bittencourt-Silvestre *et al.*, 2010).

The other important changes in cell morphology were doublet and shortened cells. In LY294002-treated cells, an increase of doublet cells from 11.2% to 15% was observed after 24 hours and 48 hours, respectively. In the control-DMSO-treated culture, doublet cells decreased from approximately 9.7% after 24 hours to 4.5% after 48 hours. This suggests that some of the LY294002-treated cells were not able to complete the process of cell division. Accumulating results lead to the direction that cell cycle is blocked due to inhibition of the PI3K signalling pathway by LY294002. On the other hand, *Giardia* with characteristic shortened cells in both LY294002 and control-DMSO treated cultures under encysting medium shows that both treatments resulted in increased shortened morphology after 24 hours and 48 hours, with LY294002-treated cultures reaching 12.7% and the control-DMSO cultures reaching 24.2%. However, both cultures displayed decreases in shortened cell morphology after a 72 hour incubation period.

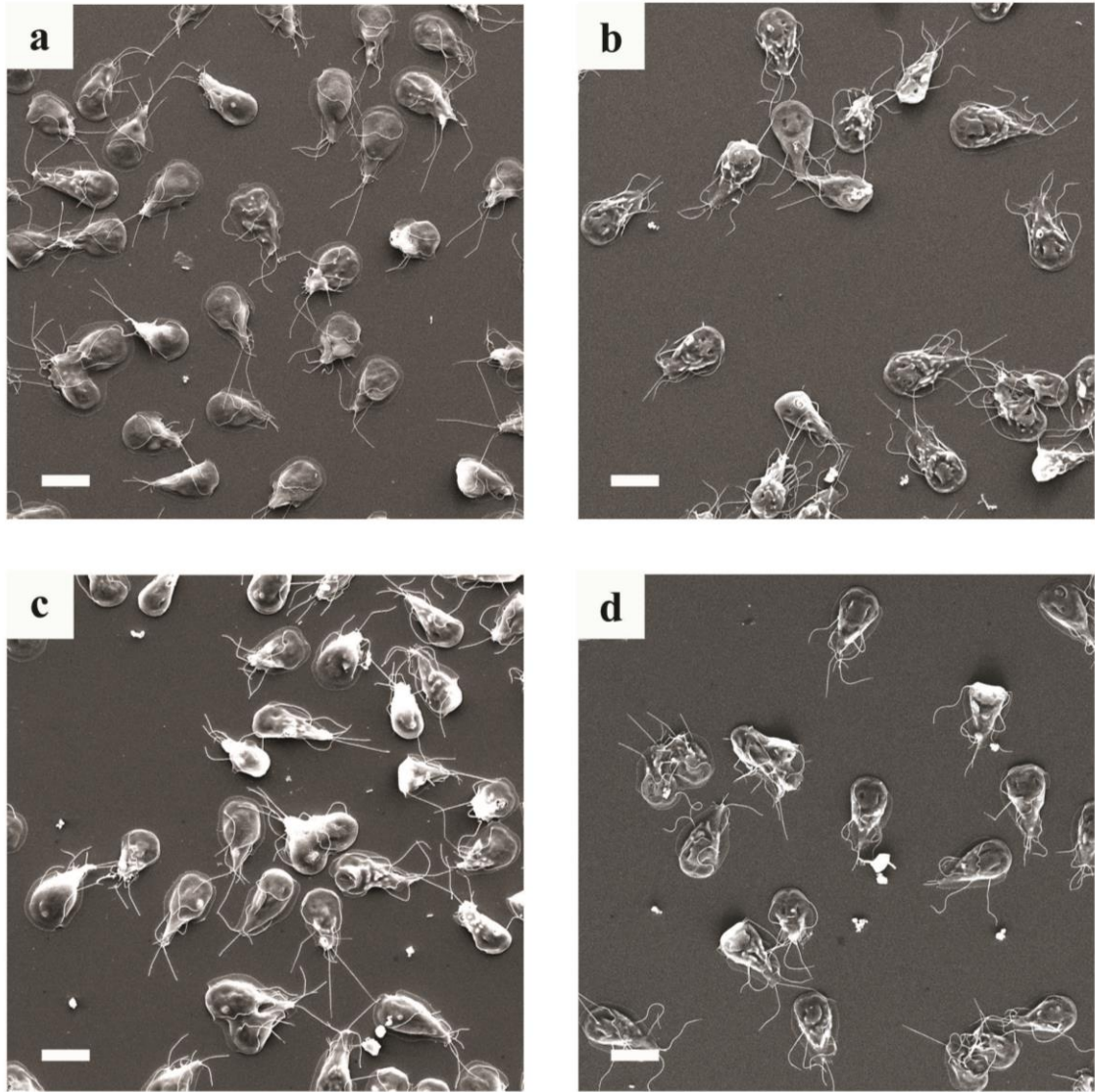


Figure 5.8: General view of *Giardia* under encysting medium and LY294002 treatment. SEM images of **a** and **c**, control *Giardia* cells with DMSO treatment after 24 and 48 hours, respectively. **b** and **d**, *Giardia* cells under LY294002 at 50 μ M after 24 and 48 hours, respectively. Scale bar 10 μ m.

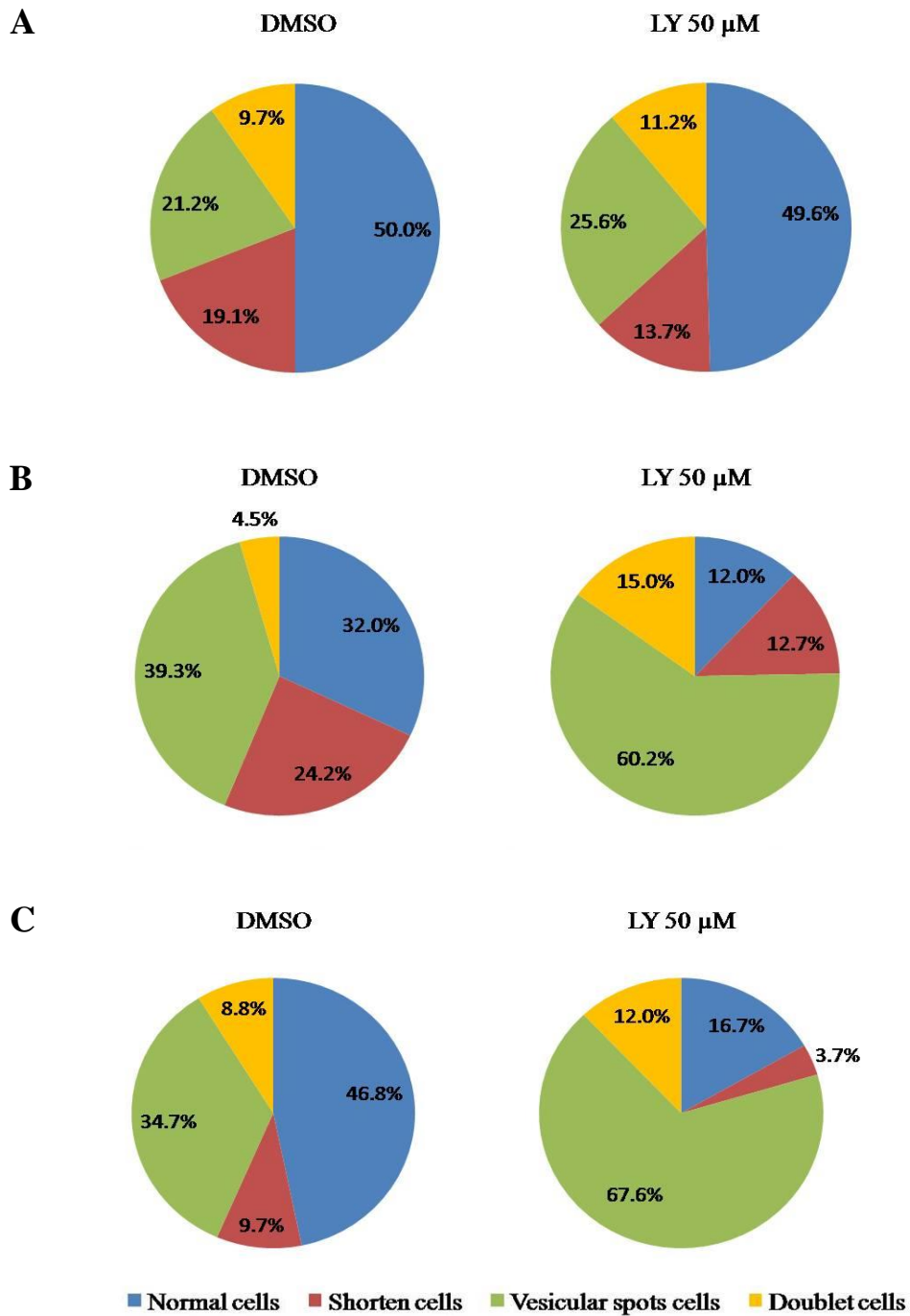


Figure 5.9: Encystation experiment with LY294002 and DMSO treatment.

The general view of *Giardia* cells exposed to encysting medium treated with LY294002 and DMSO (control) was observed under SEM. The total number of cells was counted and they were placed in to different categories of different cell morphology; normal cells, vesicular spotted cells, doublet cells and shortening cells. **A** shows the cells that were incubated for 24 hours, **B** represents the incubation time of 48 hours and **C** show cells that were incubated for 72 hours. Data are presented as the number of cells counted in different categories/the total number of cells counted in the group. Percentages are also given and represent the proportion of cells in that category within each time period.

Encystation in *G. intestinalis* has been well-recorded in previous investigations using light microscopy and electron microscopy (Lujan *et al.*, 1997, Lanfredi-Rangel *et al.*, 2003, Benchimol, 2004, Midlej and Benchimol, 2009, Bittencourt-Silvestre *et al.*, 2010). Although it was not possible to pinpoint the exact time at which each stage of encystation occur in trophozoites under encysting medium *in vitro* in the first 10 hours, trophozoites remained predominately pear-shaped (Midlej and Benchimol, 2009). After 12 hours some trophozoites begin to show alterations in their structure, and the emergence of small protrusions on the cell plasma membrane can be seen. Further transformation of the trophozoite outline takes place from a flattened pear-shaped structure into a rounded form, with an increasing flange size and shortening of the flagella (Bittencourt-Silvestre *et al.*, 2010). The small protrusions were observed again at 18 hours, and after 24 hours they were larger but lower in number on the plasma membrane of the organism. Within the final hours of encystation, Bittencourt-Silvestre *et al.* (2010) reported no surface protrusions and the mature cyst surfaces were demonstrating a homogeneous rough appearance. Under LY294002 treatment, a substantial proportion of cells with protrusions on the surface plasma membrane were observed between 24 and 48 hours, as mentioned earlier. At closer examination in Figure 5.10, the appearance of a large number of protrusions was seen in control-DMSO after 48 hours of incubation (Figure 5.10, panel a). Interestingly, LY294002-treated samples in encysting medium after 72 hours continued to show protrusions distributed throughout the surface of the plasma membrane of the cell (Figure 5.10, panel b and c). This suggests that LY294002-treated cells were held at the stage of encystation. Further investigation into the protrusions in LY294002 treated cells was required in order to confirm these findings in view of the accumulation of encystation vesicles below the surface membrane after 72 hours in LY294002-treated cells.

It was necessary to analyse the work completed by other research groups on *Giardia* under the encystation process. This was because in the wild type encystation experiment, it was not possible to locate any mature cysts images under SEM. Attempts were carried out with *Giardia* trophozoites grown to 72 hours with approximately 1×10^6 cells/ml, and the growth medium was replaced with encysting medium, as described in Kane *et al.* (1991). After the addition of encysting medium, *Giardia* trophozoites were incubated for a further 48 hours. Parasites were washed and, in order to obtain cysts alone, distilled water was added to remove trophozoites through hypotonic lysis overnight. This was completed to increase the efficiency of mature cyst production. However, after processing the cells for

electron microscopy, Figure 5.11 shows images of wild type cells after attempts to obtain cysts. Although in Figure 5.11, panels a and b show characteristics of round and oval-shape encysting cells, it was noticeable that the cells were damaged and distorted. While under the light microscope, more rounded cells and oval cyst shapes were detected contrary to images under SEM. Utilising the SEM high resolution, closer examination of this experiment shows round cells that may look like cysts (Figure 5.11 panel e and f), but they were remnants of the incomplete formation of cysts. An example of non-encysting trophozoites in distilled water can be seen in Figure 5.11, panel c and d. The plasma membrane was removed, allowing observation of the *Giardia* cytoskeleton. An important feature such as the spiral disc is shown in Figure 5.11, panel c and d. This is one of the features observed in the early stages of encystation reported by Midlej *et al.* (2009). At the latter stage of encystation, the spiral disc structure changes into a horse-shaped structure observed on SEM and then a fragmented structure shown by TEM images in the mature cysts (Midlej *et al.*, 2009).

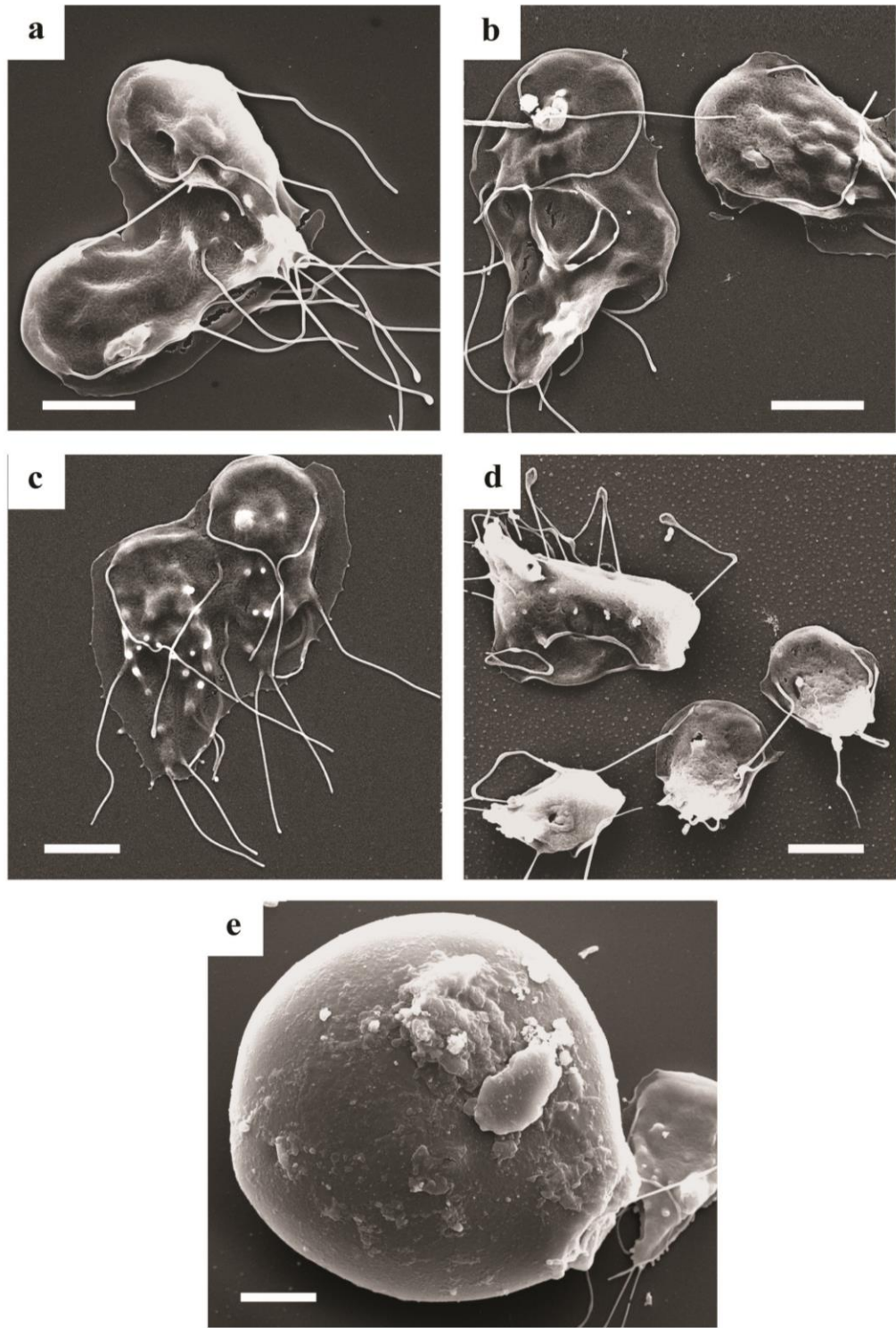


Figure 5.10: *Giardia intestinalis* cells in encysting medium under LY294002 treatment at different concentration.

SEM images of **a** control *Giardia* cell with DMSO treatment after 48 hours. **b** and **c**, *Giardia* cells under LY294002 at 50 μM treatment after 72 hours. **d** and **e**, *Giardia* cells under LY294002 at 50 μM treatment after 96 hours. Scale bars 5 μm .

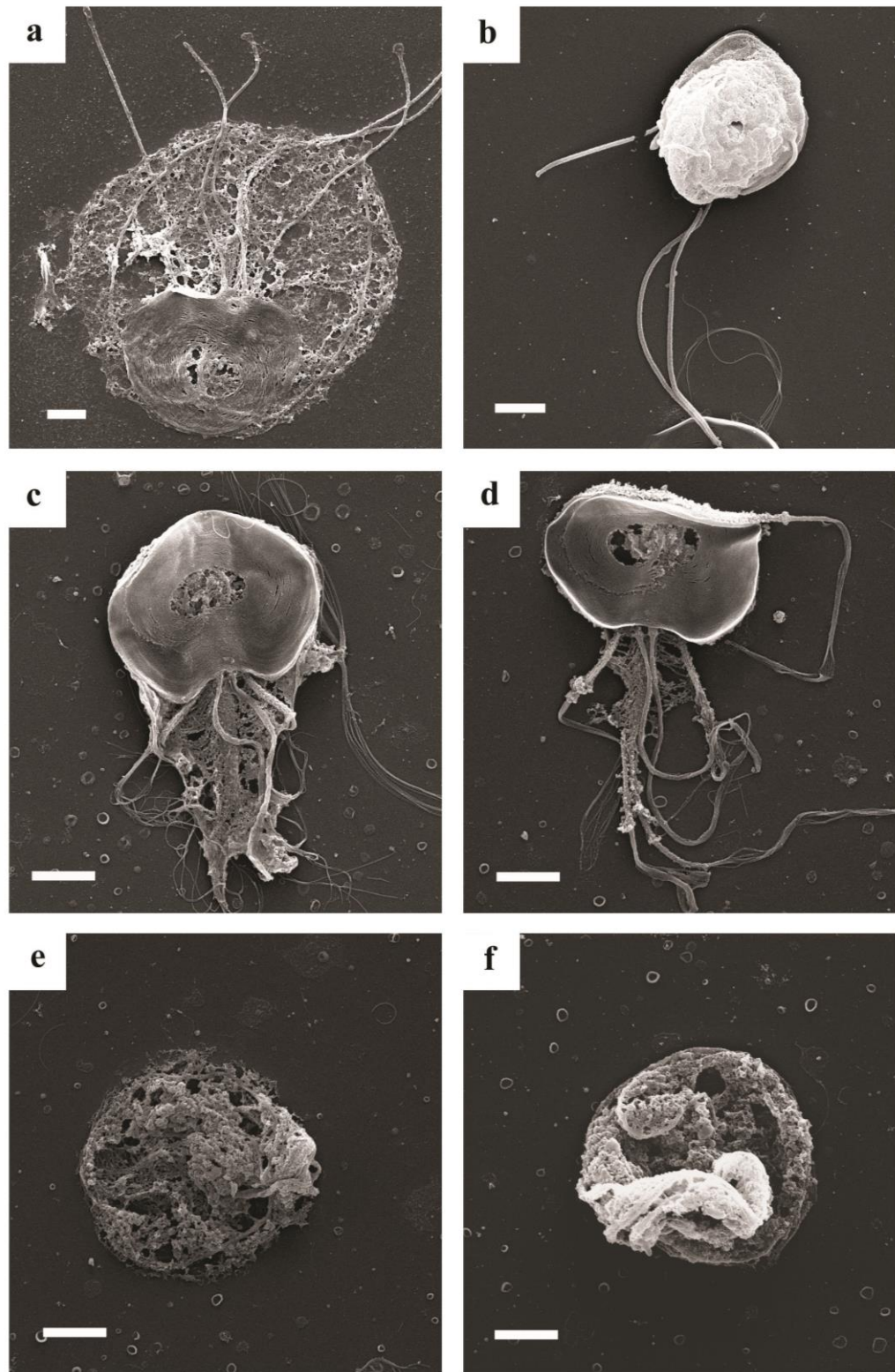


Figure 5.11: Encystation experiment to harvest cysts after 48 hours of trophozoites incubation in encysting medium.

SEM images of **a** ovoid appearance encysting cell with shortened flagella. **b**, round encysting cells. **c** and **d**, trophozoites that did not initiate encystation process. **e** and **f**, round-shape cells that may be misinterpreted as cysts under the light microscope. Scale bars 2 μ m.

5.2.3 Transmission electron microscopy images of *G. intestinalis* trophozoites

The first set of trophozoite images under TEM were cells under normal growth medium incubated over 48 hours at 37°C. The ultrastructure of *Giardia* infective trophozoites in Figure 5.12, panel a, shows a transverse section of the cytoskeleton that includes two nuclei, flagellar axonemes, median body, endoplasmic reticulum, peripheral vacuoles and flagella. The two oval nuclei revealed by TEM images show nearly identical ultrastructure appearance. Peripheral vesicles are located below the cell plasma membrane and are present in both trophozoites and cysts.

A coronal section in Figure 5.12, panel b, highlighted other structures such as the ventral adhesive disk, which allow trophozoites to attach to the intestinal wall of their hosts *in vivo*, and also to the surface of the borosilicate glass culture tubes *in vitro*. The concave ventral disk structure is essential for the survival of trophozoites because it allows adherence to the host and combats against peristalsis (Elmendorf *et al.*, 2003). The median body is located in the midline and dorsal to the caudal flagella. It is made up of a group of microtubules in a tight bundle (Adam, 2001). It has been suggested that the median body is the site responsible for the assembly of microtubules to be incorporated into the ventral disk (Meng *et al.*, 1993 and Adam, 2001). The endoplasmic reticulum (ER) within the cytoplasm of the cell plays an important role in protein folding and translocation. The confirmation of the ER existence in *Giardia* came about through the cloning and characterisation of signal recognition particle receptor α (SR α) and the identification of an extensive membrane system labelled with antibody to the HSP70 homologue found in the ER (BiP). BiP is a chaperonin that aids in folding and the further transport of SR α and SR β (Soltys *et al.*, 1996 and Adam, 2001). Figure 5.12, panel c, displays the general view of ultrathin sections on a gold grid where different slices were taken to allow quantitative studies of the ultrastructure of *G. intestinalis*.

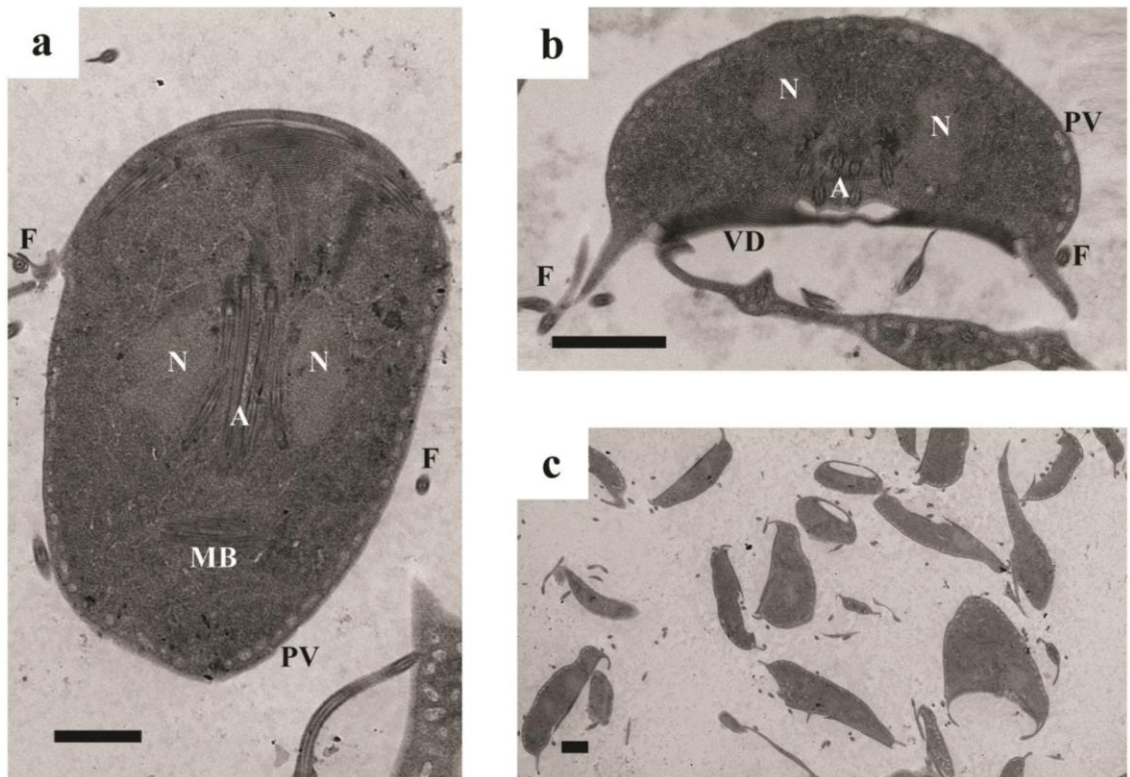


Figure 5.12: *Giardia intestinalis* trophozoite cells.

An untreated control TEM images of **a** cross section of a trophozoite cell with two eye-like nuclei (N), flagella (F), flagellar axonemes (A), median body (MB), surrounded by peripheral vesicles (PV). **b**, A coronal section of trophozoites with visible ventral disk (VD). **c**, A general view showing one random field of view. Scale bars **a** 3 μm ; **b** and **c** 2 μm .

5.2.4 TEM images of *G. intestinalis* encysting cells

The process of encystation in *G. intestinalis* has been investigated by TEM and documented in the literature. Here, trophozoites were induced to encyst *in vitro* following the protocol established by Kane *et al.* (1991). Increasing pH and bile in encystation medium stimulates *Giardia* trophozoites to initiate encystation. One possible approach to identify trophozoites that may have initiated encystation is the development of ESVs that cannot be observed in normal non-encysting trophozoites (Benchimol, 2004). Initiation of the encystation process begins with external stimulation leading to encystation-specific gene expression. ESV appearances in encysting trophozoites were often detected after 6-12 hours filled with an amorphous and electron-dense material in the matrix. These ESVs are responsible for transporting CWPs to the cell membrane where the CWPs will be released at the assembly site of the cell wall (Lujan *et al.*, 1997, Lanfredi-Rangel *et al.*, 2003). In

accordance with previous research, four structural CWPs have been identified: CWP1, CWP2, CWP3 and a high cysteine non-variant cyst protein (HCNCp) (Davids *et al.*, 2006).

Experiments were carried out to investigate the ultrastructure of trophozoites under encystation medium. Trophozoite cultures were grown to approximately 1×10^6 cells/ml confluence and had the growth medium replaced with encystation medium as described in Kane *et al.* (1991). After 24, 48 and 72 hours of incubation in the encystation medium, *Giardia* cells were harvested and prepared for TEM (Figure 5.13). An example of a single random field of view was taken from trophozoite cell culture following a 24 hour incubation period (Figure 5.13, panel a) and a closer image of doublet cells during the process of cell division (Figure 5.13, panel b). It was possible to identify the doublet cells due to double ventral discs; the presence of three nuclei suggested that this was not a single *Giardia* cell but a cell undergoing cell division. Moreover, the peripheral vesicles also surrounded the doublet cell, which displays characteristics of a single cell during the early stages of cell division. After 48 hours of incubation, Figure 5.13, panel c and d, show a general picture at low magnification of *Giardia* TEM sections during encystation and a higher magnification image of two individual cells, respectively. In the general view of the TEM image (Figure 5.13, panel c), normal visible organelles were present and many were labelled such as nuclei, adhesive disk, peripheral vesicles and flagella. Upon closer inspection, unfamiliar vesicular structures in a parasite were observed using TEM. These unknown vesicular structures are labelled with an arrowhead (Figure 5.13, panel d) and they are identical to cleft structure reported by Lanfredi-Rangel *et al.* (2003). These cleft structures can be considered nascent ESVs because they eventually get completely filled with the amorphous electron-dense material and these mature ESVs transport CWPs to peripheral regions of the cell (Lanfredi-Rangel *et al.*, 2003). Cleft structures derived from the dilation of some regions of the cisternae of the rough ER in the early stages of encystation; at this point, these dilations area were empty. This cleft structure appeared as an electron-lucent area within the ER cisternae (Lanfredi-Rangel *et al.*, 2003).

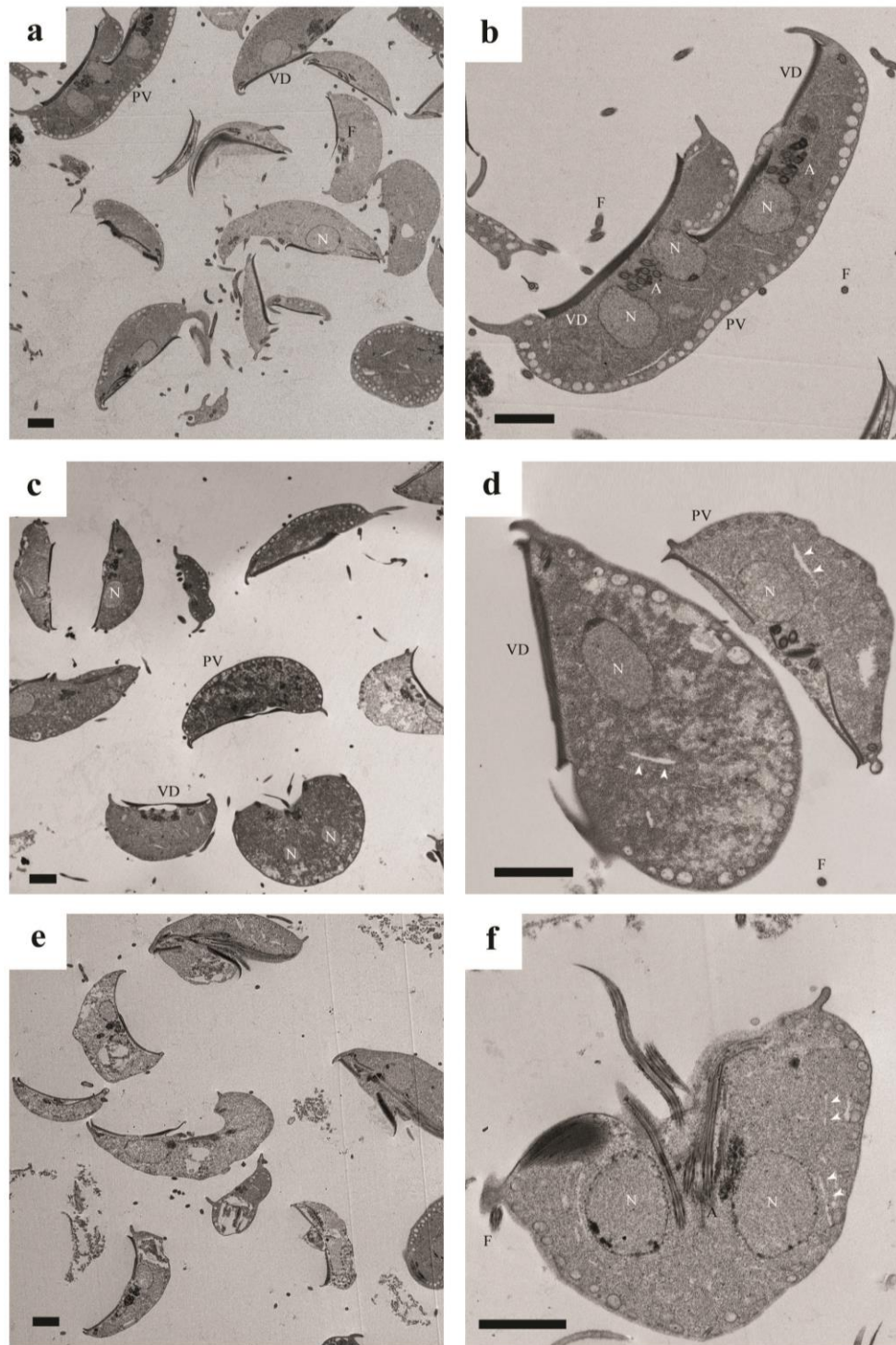


Figure 5.13: *Giardia intestinalis* under encystation medium for a period of 72 hours. TEM image of **a** and **b** *Giardia* cells incubated in encystation medium for 24 hours. **c** and **d**, cells were incubated in encystation medium for 48 hours. **e** and **f**, cells were incubated in encystation medium for 72 hours. The left panel shows a general view of one random field of view and the right panel shows a cross-section or a coronal section of *Giardia* cells. These panels show that *Giardia* cells have surrounding the inner membrane the peripheral vesicles (PV), ventral disk (VD), nascent ESVs (arrowhead), flagella (F) and typically two nuclei (N) per cell. Scale bars 2 μ m.

Recent studies using TEM to investigate vesicle structures in encysting *Giardia* have identified the cleft structure as electron lucent vesicles (ELVs) (Midlej *et al.*, 2012). These ELVs were distinct from other vesicles and organelles in the ultrastructure of encysting *Giardia*. They were shown to contain a different composition from ESV through a monoclonal antibody, anti-CWP1 labelling experiment, which resulted in only ESVs being labelled. Interestingly, both ESVs and the ELVs were found budding from ER membranous profile (Midlej *et al.*, 2012). Upon closer inspection, Figure 5.14 illustrates *Giardia* cells under encysting medium after 24 and 48 hours in Figure 5.14, panel a, b and c, d, respectively. Arrowheads depict cleft structure and electron-lucent vesicles in *Giardia* under encystation medium after 24 and 48 hours (Figure 5.14). Two different structures were identified (labelled with arrowheads): elongated cleft structural features that may be associated with ER cisternae (Figure 5.14, panel a) and the other structure showed a more round enlargement vesicle with an electron lucent area (inset, Figure 5.14, panel b and Figure 5.14, panel d). It was important to analyse the changes in the ultrastructure of *Giardia* cells during transformation under encysting medium, as this may improve our understanding of specific details of this encystation process and act as a control experiment to investigate the effect of LY294002 on *G. intestinalis*. Figure 5.15 shows analysis of each individual *Giardia* population harvested from encystation media; the emergence of a significant ultrastructure that was not present in the non-encysting cells are analysed here in cells fixed at different time of encystation. A rapid was observed increase in the number of *Giardia* cells containing clefts and ELVs in both categories from time zero to the first 24 hours during encystation. The percentage of cells containing these clefts and ESV morphologies was quantified by counting; approximately 82.3% of the cells fixed at 24 hours had the appearance of clefts or ELV structures. The dilated region of the ER (clefts) and round electron-lucent vesicles are approximately 1 to 2.2 μm and 1 to 1.4 μm , respectively. The reported size of the average ELVs in a recent study is 1.02 μm , this measurement is in agreement with this findings. The structures are found throughout the cytoplasm (Midlej *et al.*, 2012). After 48 and 72 hours of encystation, the number of cells containing these clefts and ELVs decreased to 53.8% and 51.7%, respectively, in the population of cells observed. It is important to mention that the ELVs observed (inset, Figure 5.14, panel b) were different from the peripheral vesicles surrounding *Giardia* cells. The peripheral vesicles are smaller, ovoid in shape with measuring approximately 300 nm (inset, Figure 5.14, panel b) and are present throughout the life cycle of *G. intestinalis*.

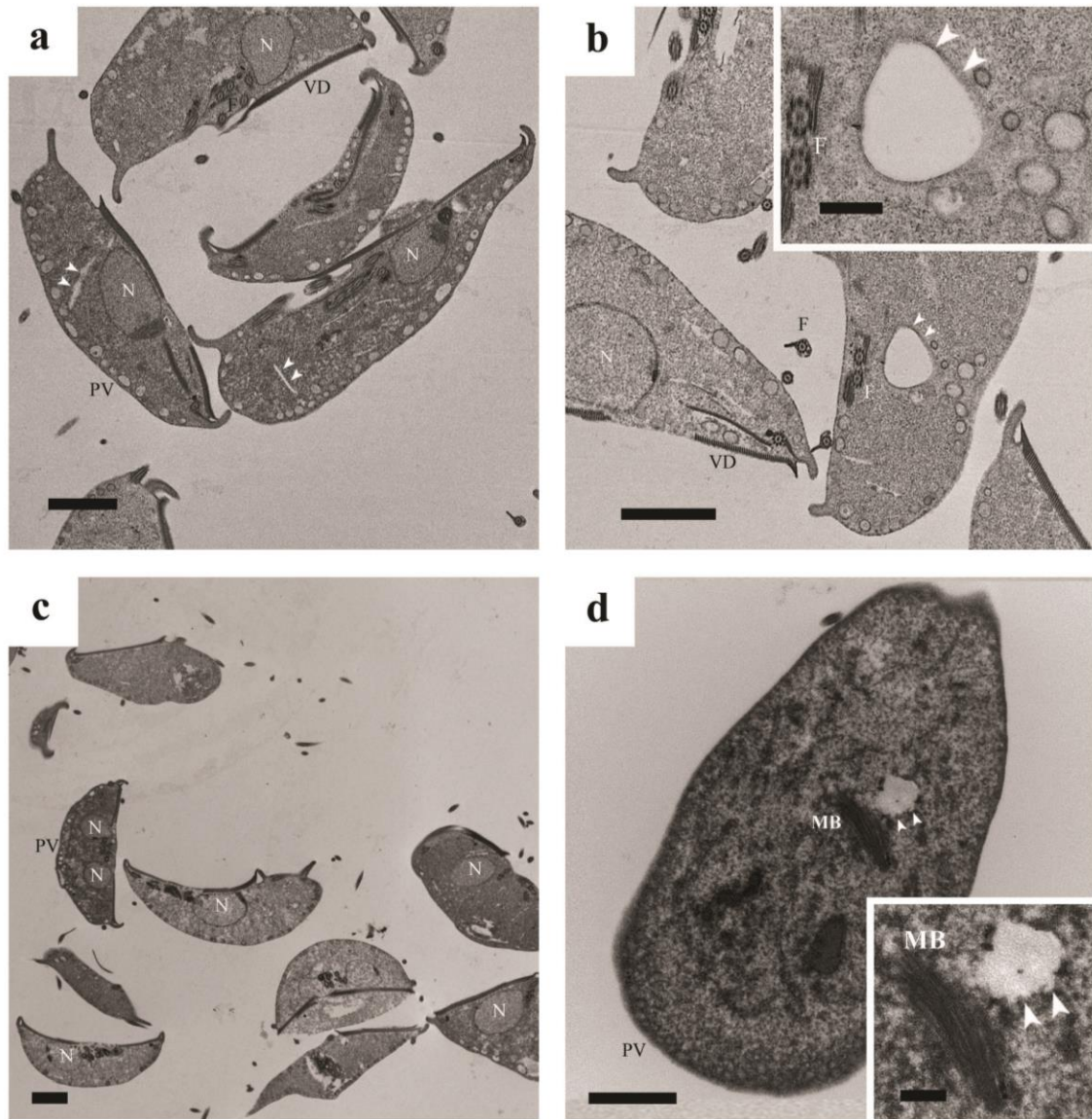


Figure 5.14: *Giardia* cells incubated in encystation medium for 24 and 48 hours. TEM images of **a** and **b** encysting cells after 24 hours; **a** shows a general view of one random field of view displaying nuclei (N), ventral disk (VD), elongated ‘cleft’ (arrowhead). The large granules in **b** (arrowhead) inset is the size of normal encystation specific vesicles. **c** and **d**, Encysting cell after 48 hour incubation; **c**, general view of one random field of view; the peripheral vesicles (PV) are located surrounding the cell; **d**, cross-section area highlighting a granule (arrowhead) adjacent to the median body (MB). Scale bars **a – d** 2 μ m; inset **b** and **d** 500 nm.

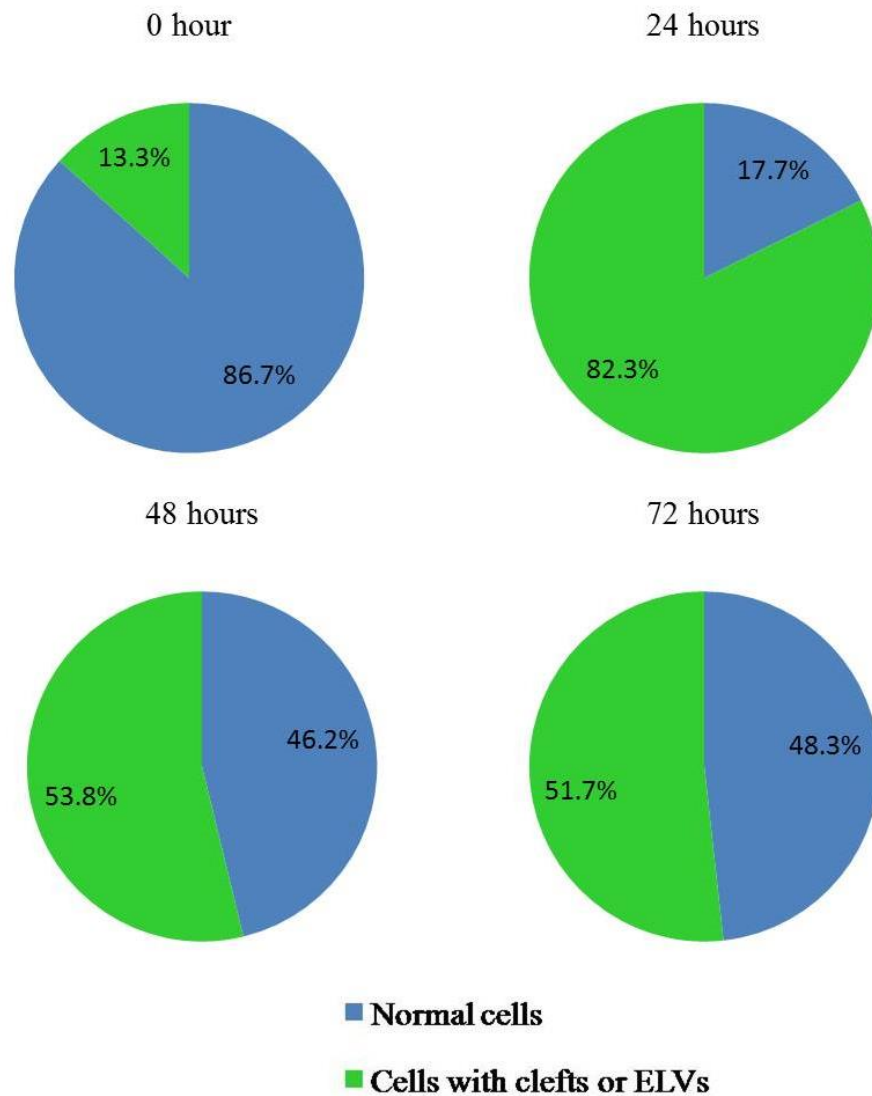


Figure 5.15: Ultrastructure studies of *G. intestinalis* under encystation process.

Analysis of morphological changes in the appearance of clefts or ELVs in *Giardia* cells exposed to encysting medium under transmission electron microscope. The total numbers of cells were counted from a single experimental work; each individual cell was examined to record the presence of clefts or electron lucent vesicles. A minimum of 100 cells was analysed per incubation period under encystation. Data are presented as different Pie charts representing incubation time; within individual charts, there are percentages which represent the average proportion of cells with the number of clefts or ELVs.

5.2.5 Ultrastructural investigation on *G. intestinalis* trophozoites under the effect of LY294002

Experiments were carried out to investigate the effect of LY294002 on ultrastructure of *G. intestinalis* trophozoites. In the results section of Chapter 4, the effect of LY294002, a PI3K inhibitor, was shown to induce growth inhibition of trophozoites under growth medium. Here, the ultrastructures of trophozoites under LY294002 treatment were

observed under TEM. LY294002-treated trophozoites display substantial changes in the morphology of the ultrastructure of the cells over the period of 24 hours. The morphology of the cells shows disorientated peripheral vesicles and the peripheral structures were abnormal in comparison to normal trophozoites (Figure 5.16, panel a-c). Peripheral vesicles in trophozoites treated with LY294002 display an increase in size of the vesicles throughout the cytoplasm of the cell (Figure 5.16, panel a and b), when compared to untreated control (Figure 5.12). Trophozoite morphology and the organisation of vesicles throughout the cytoplasm was significantly altered after a 48 hour incubation period in LY294002. These changes include the appearance of peripheral vesicles forming double layers of vesicles in some areas of trophozoites adjacent to the surface of the plasma membrane (Figure 5.16, panel d). This can be compared to untreated control shown in Figure 5.12. In Figure 5.16, panel e, large and pleomorphic cells were observed upon close inspection. Similar findings in the appearance of *Giardia* cells were also observed recently when LY294002 was added during encystation, viewed using electron microscopy (Bittencourt-Silvestre *et al.*, 2010). An increase in the size of peripheral vesicles has been described in trophozoites incubated with sterol biosynthesis inhibitors on growth EPI (24(R,S),25-epiminolanosterol) (Maia *et al.*, 2007). The diameters of peripheral vesicles in *Giardia* trophozoites after EPI treatment were reported to be within the range of 2.3 to 3.7 μm compared with the average size of 1.54 μm in a number of trophozoite peripheral vesicles treated with LY294002 over a period of 48 hours (Figure 5.16, panel b and e). These peripheral vesicles are the essential component of the endosomal/lysosomal system of the protozoan and it is possible that inhibition of PI3K by LY294002 caused interference in membrane lipid composition, trafficking and permeability (Lanfredi-Rangel *et al.*, 1998, Maia *et al.*, 2007).

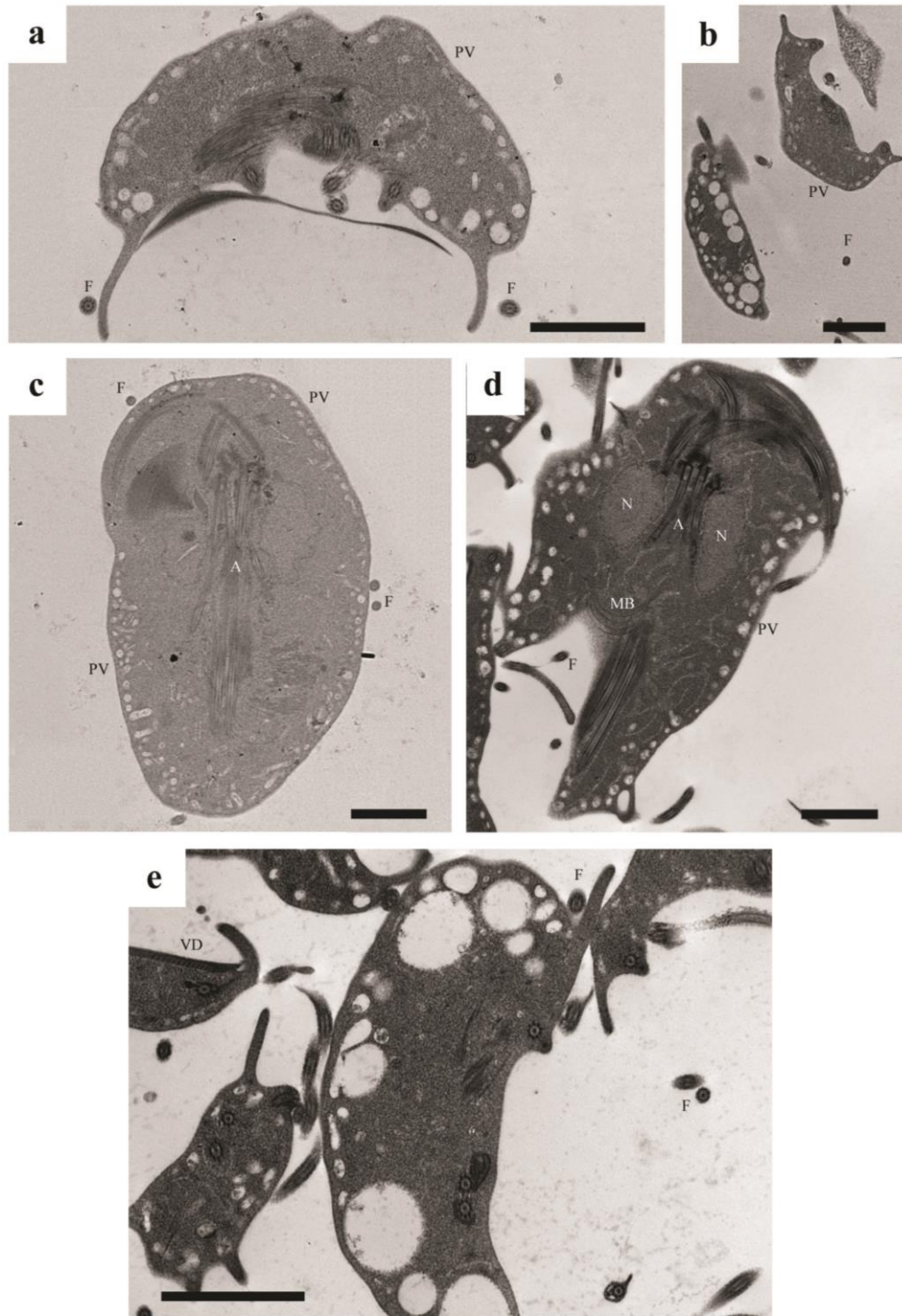


Figure 5.16: *Giardia* trophozoites incubated for 24 and 48 hours in the presence of LY294002. TEM images showing (panel **a** and **c**) trophozoites treated with LY294002 at 50 μ M after 24 hours; **a** displays a coronal section of trophozoite surrounded with peripheral vesicles (PV) and **c** displays a cross-section of trophozoite cells with flagellar axonemes (A), flagellar (F). The presence of LY294002 alters the appearance of PV in **b**, **d** and **e** *Giardia* trophozoite cells treated with LY294002 at 50 μ M after 48 hours. Disorganised PV can also show that enlargement of PV is common in some cells. VD, ventral disk; MB, median body; N, nucleus. Scale bars 2 μ m.

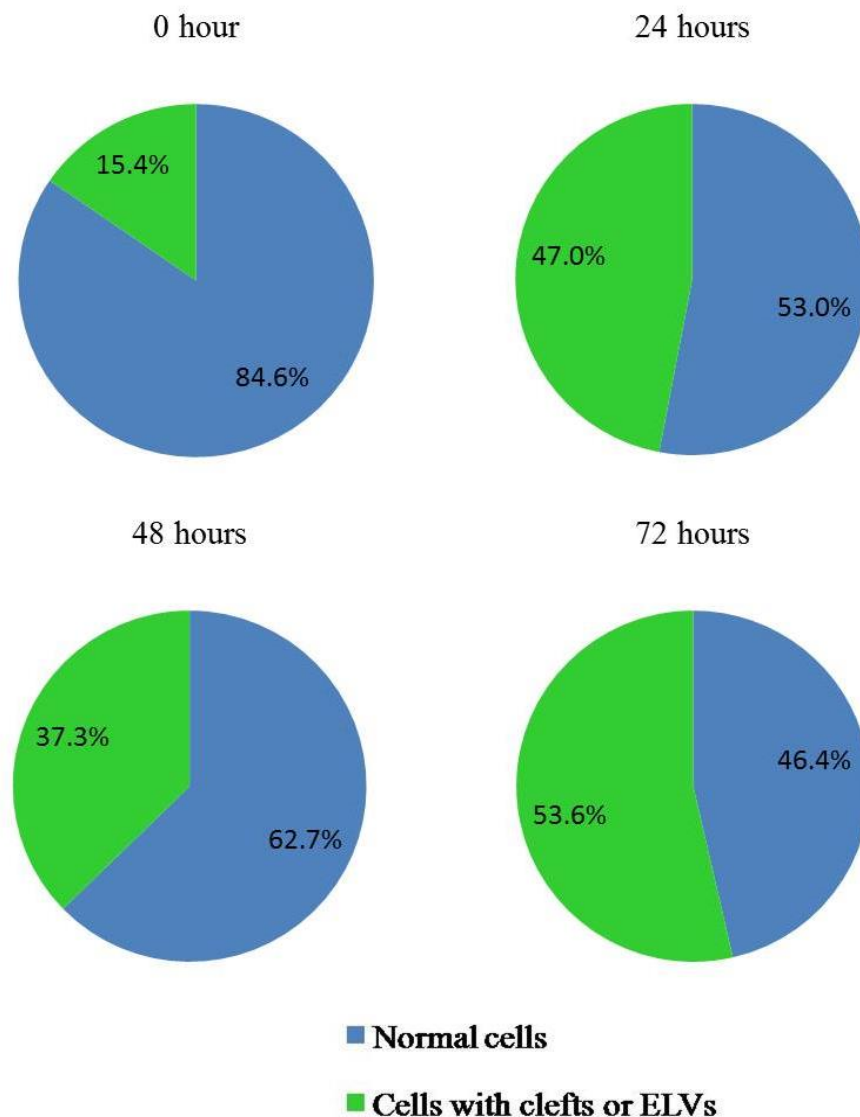


Figure 5.17: Ultrastructural studies of *G. intestinalis* treated with LY294002.

Analysis of morphological changes in the appearance of clefts or ELVs in *Giardia* cells treated with LY294002 under a TEM. The total numbers of cells were counted in a single experimental work and each individual cell was examined to record the presence of cleft or ELV. Minimum of 100 cells were analysed per incubation period with LY294002 treatment. Data are presented as different Pie charts representing incubation time; within individual charts, there are percentages which represent the average proportion of cells with the number of clefts or ELVs.

Another important finding to add to the evidence that trophozoites treated with LY294002 initiate encystation-like processes are described here through the increased number of clefts or prolonged appearance of clefts in the cytoplasm. The general view of *Giardia* LY294002-treated trophozoites under normal growth medium is illustrated here and the number of clefts/ELVs were counted using TEM (Figure 5.18). Ultrastructure of many trophozoites treated with PI3K inhibitor over 24 hours in Figure 5.17 has shown an

average of 47% of cells with clefts or ELVs. The percentage of cells with clefts or ELVs decreased down to 37% after 48 hours of incubation; however, this increases up to 54% after a 72 hour incubation period (Figure 5.17). Upon close inspection, Figure 5.18, panel b, shows ELVs in the central region of the protozoan adjacent to the nucleus and others distributed near the peripheral vesicles. This is in contrast to the control sample in Figure 5.12, where untreated control cells show no presence of ELVs. Due to the effect of LY294002-treatment after 48 hours, changes in peripheral vesicles pattern were shown. In this micrograph, an increase in cytoplasmic space between the peripheral vesicles was observed throughout the cell (Figure 5.18, panel d). Internalisation of the flagella shown in Figure 5.18, panel d, suggests that *Giardia* treated with LY294002 may have initiated an encystation-like process. Concomitant with internalisation of the flagella and the formation of ESVs, an important observation shows ESV-like vesicles in trophozoites after 72 hours of LY294002 treatment (Figure 5.18, panel f inset).

Experimental results of *G. intestinalis* after 72 hours of incubation with LY294002 treatment in growth culture medium, and trophozoites under encysting medium, were compared using micrographs taken from TEM (Figure 5.19). Unfortunately, it was not possible to observe any cyst formation in *Giardia* cultures under encysting medium after 72 hours. However, previous studies indicated that under encystation conditions, only about 4% of trophozoites in culture showed morphological indication of encystation (Maia *et al.*, 2007). Figure 5.19, panel b and e, highlight *Giardia* cell death by the disruption of cell membrane under encysting medium, it was possible to confirm that this might be a natural consequence of encystation under *in vitro* conditions. Control-DMSO cells illustrated the normal shape of trophozoites, complete with the regular organelles within the cytoplasm after 72 hours of incubation (Figure 5.19, panel a and d). LY294002-treated cells on the other hand demonstrate disorganisation of the peripheral vesicles surrounding trophozoite cells. The numbers of trophozoites with these enlarged peripheral vesicles reached an average of 45% of the total number of cells counted in multiple single random fields of view after trophozoites were treated with LY294002 for 72 hours. It is important to mention that in one TEM image, you may or not see the translucent clefts or ELVs, but this does not mean that the cell did not contain any clefts or ELVs. This is because it was a thin slice of the sample in one particular image. Therefore, many fields of views on TEM were taken and a population of cells were quantified for clefts or ELVs.

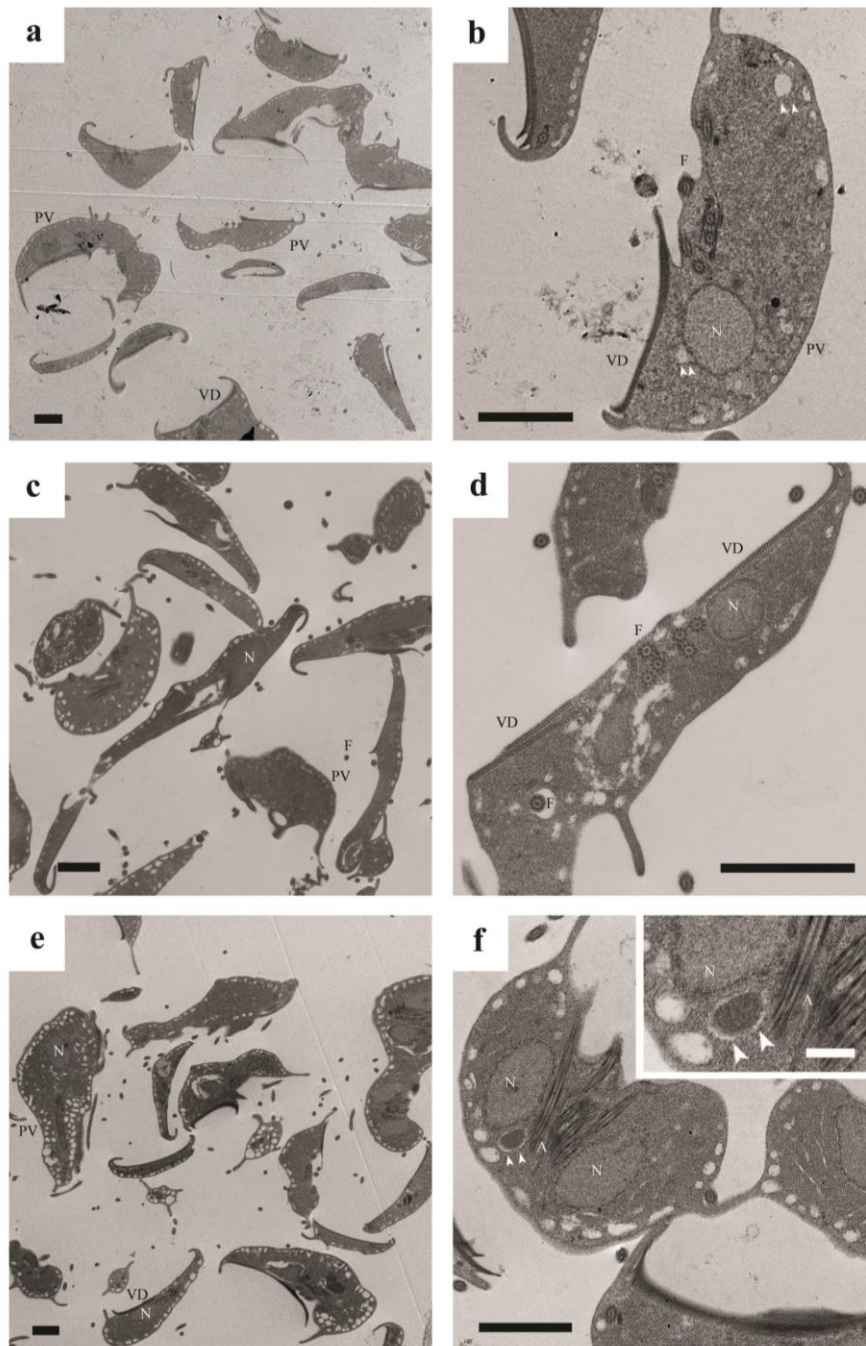


Figure 5.18: *Giardia intestinalis* treated with LY294002 over a period of 72 hours.

TEM images of *Giardia* trophozoites treated with LY294002 for: 24 hours **a** and **b**, 48 hours **c** and **d**, 72 hours **e** and **f**. The left panel display a general view over a random field of view and the right panel shows a coronal section of a single cell within that population. **a**, overview of 24 hours LY294002 incubation of trophozoites showing peripheral vesicles (PV) and a ventral disk (VD). **b** and **d** highlight morphological changes in ventral disk structure, arrowheads in **b** show the presence of ELVs and the appearance of large and pleomorphic cells, **c** and **e**. **f** shows a structure that is similar to ESV-like vesicles with electron dense material embedded within; inset **f** with arrowheads highlighting ESV-like vesicles. F, flagellar; N, nucleus; A, flagellar axonemes. Scale bars 2 μ m; inset **f** 500 nm.

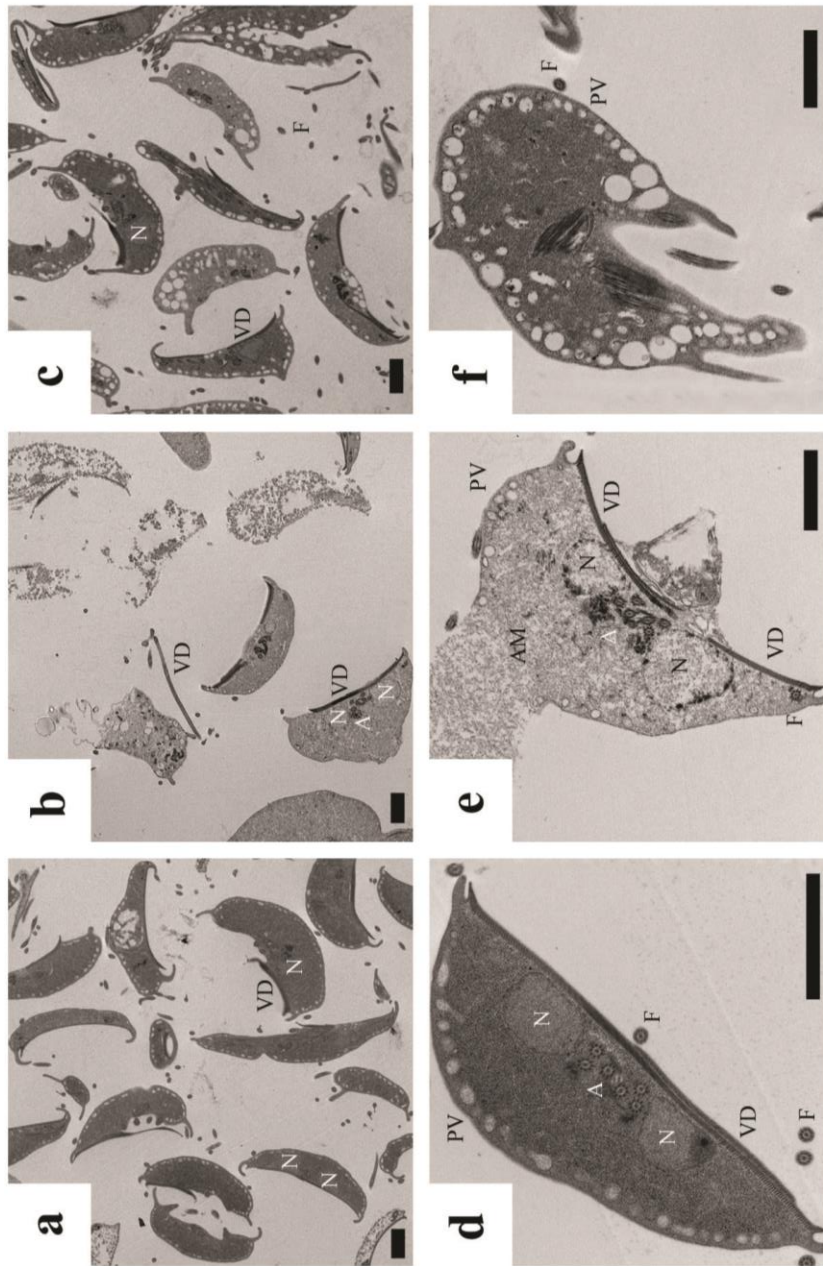


Figure 5.19: Comparison of *Giardia* trophozoites treated with LY294002 against *Giardia* trophozoites incubated in encystation medium.

TEM images of **a** and **d** control-DMSO treated trophozoites over 72 hours, **b** and **e** *Giardia* incubated in encystation medium over 72 hours, **c** and **f** trophozoite cells treated with LY294002 at 50 μ M over 72 hours. **a** The control DMSO outline normal characteristic of trophozoites in the general view with several nuclei (N) presence in some sections. **d** display a coronal section surrounded by peripheral vesicles (PV), two nuclei (N) and flagellar axonemes (A) within the cell. **b** and **e** have shown that encystation medium is toxic to encysting cells over a period of time. The general view on trophozoites treated in **c** highlight significant changes with the appearance of large and disorganised peripheral vesicles surrounding the cell **f**. AM, amorphous material; VD, ventral disk; F,

5.2.6 CWP2 immunofluorescence study in *G. intestinalis*

The previous study using SEM and TEM approaches presented evidence to suggest that trophozoite cells under normal growth medium can be seen to trigger the early stage of encystation-like process after they were treated with PI3K inhibitor LY294002 within 48 hours. With this in mind, anti-Cyst Wall Protein 2 (CWP2) antibodies were used to label the LY294002-treated cells. This should allow the detection of the early triggering of encystation process. The positive control for this experiment was *Giardia* trophozoites incubated in encysting medium over a period of 48 hours and stained with CWP2 antibody (Figure 5.20). The immunofluorescence images of encysting cells exhibit both nuclei and abundant CWP2 staining within encystation-specific secretory vesicles (ESVs). 4',6-diamidino-2-phenylindole (DAPI) was used to label the nuclei by binding to A-T rich regions in DNA (Figure 5.20, panel c-f). The negative control in this experiment was established as exponentially growing trophozoites under normal growth medium, which were fixed and membrane permeable. Results in Figure 5.20, panel a and e, illustrated that control treatment did not display CWP2 antibody labelling on trophozoite cells.

Immunofluorescence images in Figure 5.21 revealed that trophozoites treated with PI3K inhibitor LY294002 exhibit positive CWP2 fluorescence signals when trophozoites have been incubated with anti-CWP2 antibody. The proportion of LY294002-treated trophozoites demonstrated that CWP2 was on average 95% compared to none observed on positive CWP2 staining in the control-DMSO treated with anti-CWP2 antibody (see Figure 5.21, panel e). This result of LY294002-treated trophozoites positive CWP2 staining resembles the positive appearances of CWP2 staining in *Giardia* incubated in encysting medium over 48 hours (Figure 5.20, panel e). Furthermore, the specific CWP2 staining is similar to the observation of ESVs under SEM micrographs represented by membrane surface protrusion. Quantification of the specific ESVs staining using anti-CWP2 varies from one trophozoite to another with approximately 20 – 45 ESVs in each LY294002-treated trophozoite. The ESVs staining in both LY294002-treated cells and *Giardia* cells under encysting medium appear to be distributed throughout the cell.

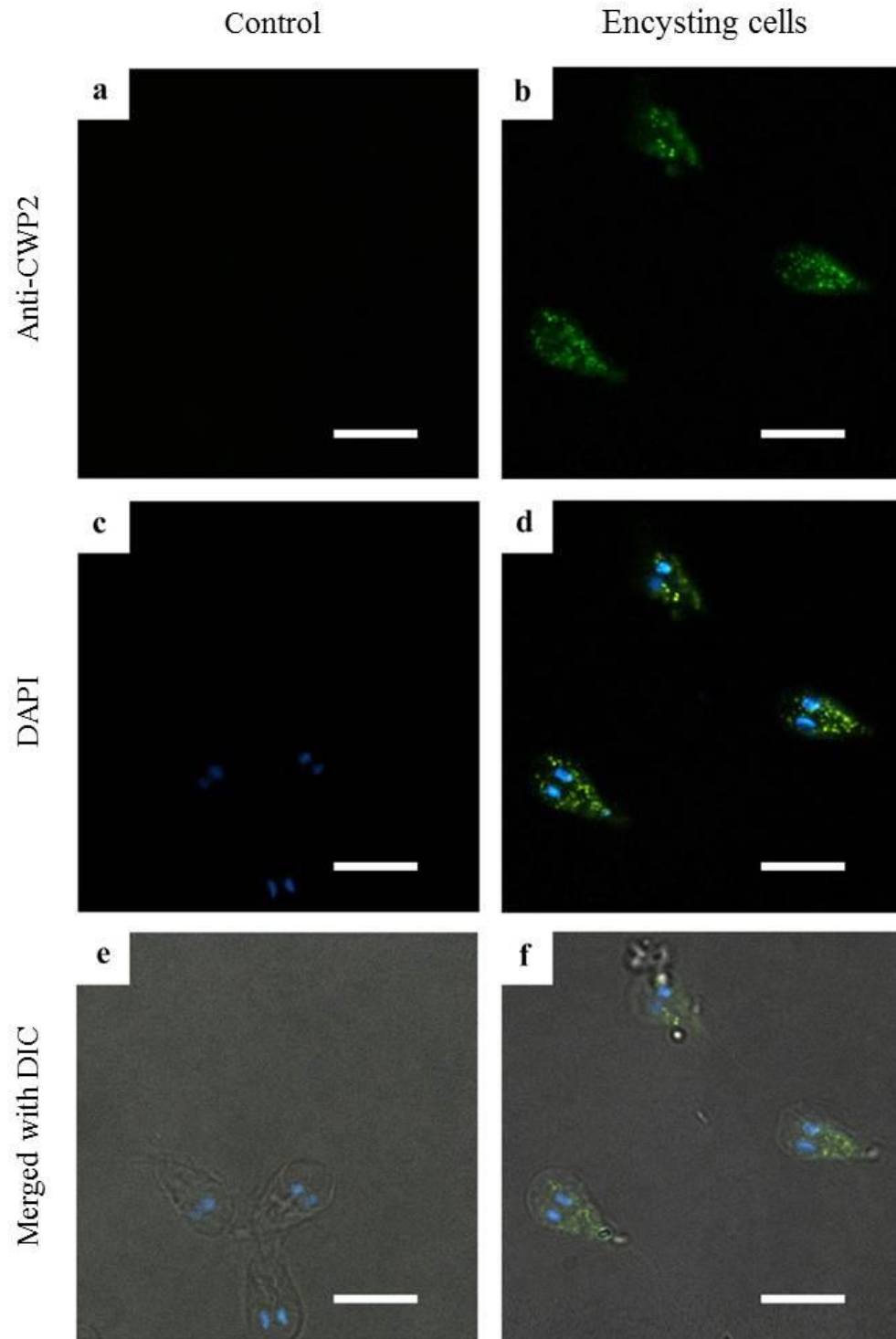


Figure 5.20: Immunofluorescence microscopy of *G. intestinalis* encysting cells stained with anti-CWP2.

Microscopic images showing (a, c and e) control trophozoites under normal growth medium. a, 1:250 anti-CWP2 fluorescence staining. c, 10 µg/ml Dapi staining in the nuclei of trophozoite and e, Dapi staining merged with DIC image showing the outline of each cell. b, d and f represent encysting cells incubated over 48 hours and stained using 1:250 anti-CWP2 fluorescence antibody with Dapi staining. f, represent merged images of both staining used and DIC. Scale bars are all 10 µm.

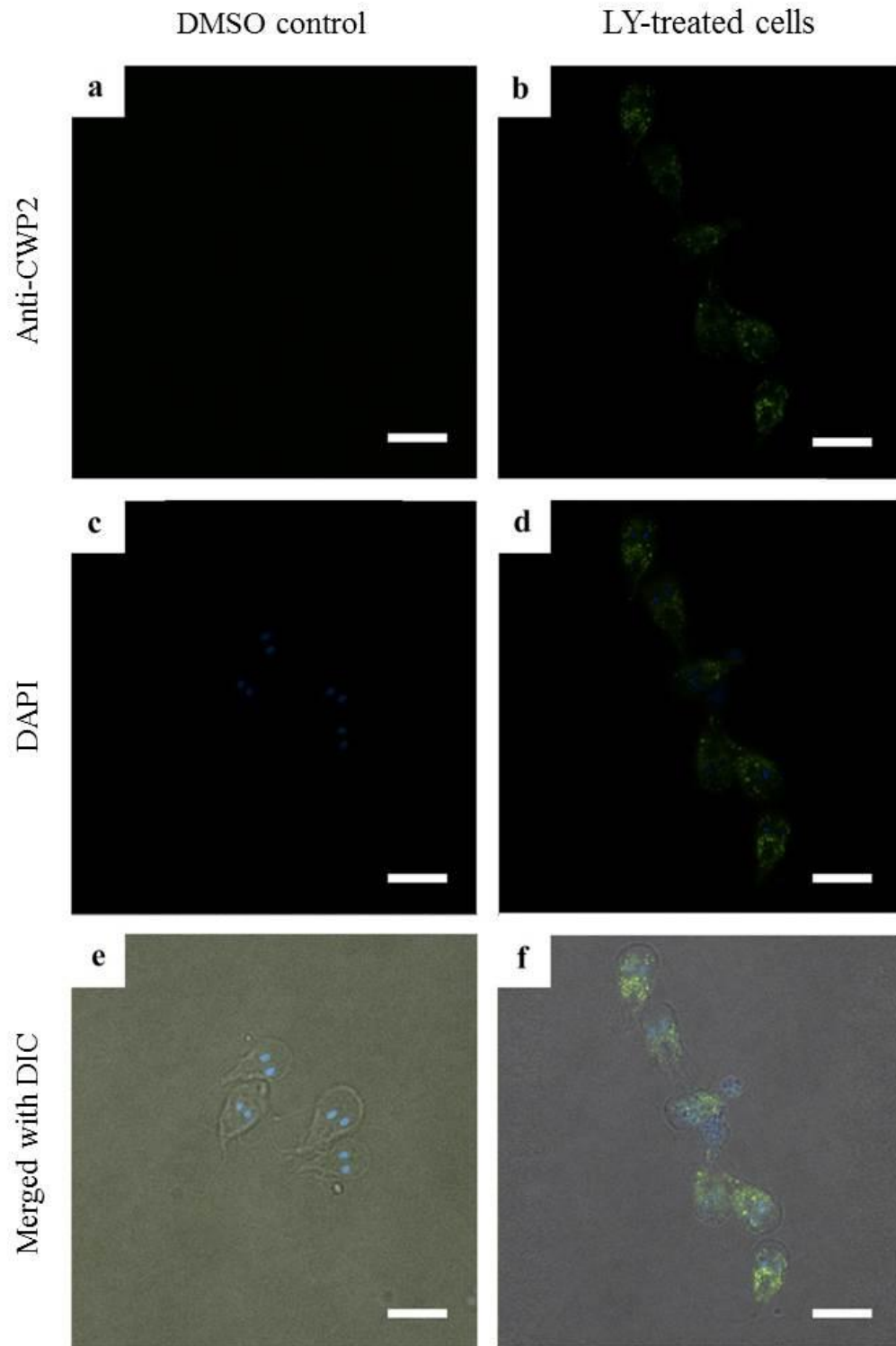


Figure 5.21: CWP2 staining in LY294002-treated cells.

Immunofluorescence microscopy images showing: **a, c, e** - control-DMSO treated trophozoites and **b, d, f** LY294002-treated trophozoites incubated over 48 hours. **a – f** cells were stained with 1:250 primary mouse anti-CWP2 antibody followed by 1:500 secondary goat anti-mouse FITC antibody. **c** and **d** illustrate 10 $\mu\text{g/ml}$ DAPI staining of control-DMSO and LY-treated trophozoite, respectively. **e** and **f** show merged image with DIC. Scale bars are 10 μm .

5.3 Discussion

The aim of using scanning and transmission electron microscopy in this Chapter was to investigate whether the inhibition of PI3K in *Giardia* trophozoite cell cultures leads to the initiation of the stage encystation. SEM and TEM experiments were carried out to analyse, compare and count *G. intestinalis* cells. Moreover, electron microscopes are a powerful tool that can be used to investigate the effect of LY294002 on *Giardia* trophozoites ultrastructure *in vitro*. In an attempt to differentiate trophozoites to form complete cysts, the encystation experimental procedure used was reported to produce up to 50% of cysts that resemble type I cysts, which have characteristics of a smooth oval-shape, described by Gillin *et al.* (1989) (Kane *et al.*, 1991). The trophozoites were grown to confluence in growth medium containing 0.5 mg/ml of bovine bile at pH 7.1 at 37°C and had their medium replaced with encystation medium containing 10 mg/ml of bovine bile, at pH 7.8. The incubation time with encystation medium for maximum numbers of cysts was reported to be 96 hours at 37°C (Kane *et al.*, 1991).

Encystation experiments to produce *G. intestinalis* cysts were attempted with the aim of studying the ultrastructure of this protozoan using SEM and TEM. The morphology studied concentrated on the differentiation from trophozoites to encysting cells followed by the formation of mature cysts. Obtaining mature cysts from cultures containing trophozoites incubated with encystation medium proved difficult, with the apparent loss of a large number of cells after 72 hours incubation and any round oval-shaped *Giardia* cells appear to be non-viable under SEM. If the complete encystation process was to be achieved, it is recommended that the original encystation medium is used (Gillin *et al.*, 1989). The initial experiment on encystation did show the appearance of encysting and cyst cells in the previously reported chapter 4 under the light microscope. When scanning electron microscopy was used, however, all of the samples were fixed and prepared for observation under electron microscopy; therefore, time was an important factor in completing this experimental work.

However, it was still possible to detect modification of the protozoan shape from trophozoites to encysting cells, small surface protrusions and shortening of cells were observed in images taken by SEM. This may indicate that encystation had been triggered through incubation of trophozoites in encysting medium. It has been shown that the appearance of a large number of protrusions was distributed throughout the protozoan surface during encystation process by scanning electron microscopy (Bittencourt-Silvestre

et al., 2010). These surface protrusions or membrane blebs have been reported to represent the ESVs that are under the cell plasma membrane, although still little is known about the process of ESVs releasing their cyst wall materials to be deposited extracellularly (Benchimol, 2004). Within the ultrastructure of *Giardia* cells incubated in encystation medium, the observation under TEM illustrated the appearance of clefts and ELVs over a period of 72 hours. In the first 24 hours, *Giardia* cell populations containing clefts and ELVs under encystation medium reached approximately 82% of the total number of cells. However, the observations at 48 and 72 hours showed a lower percentage of cells containing clefts and ELVs with values of 54% and 52%, respectively. Nonetheless, these structures suggest *Giardia* cells were undergoing differentiation; these results are in agreement with previous studies showing cells at different phases of the encystation process (Lanfredi-Rangel *et al.*, 2003). Furthermore, early immuno-microscopic studies of encystation proposed that ESVs arise from a, “flattened cisterna”. With this in mind, the ultrastructural and histochemical kinetic analyses suggest that the ESVs arise from clefts, which are dilated ER cisternae (Lujan *et al.*, 1997, Lanfredi-Rangel *et al.*, 2003). However, no mature ESVs were observed in our experimental work. Another characteristic showing that trophozoite ultrastructural changes were taking place during the process of differentiation was the internalisation of the flagella. Under TEM, it was apparent that after 24 hours of trophozoites incubated in encystation medium, one flagellum is in the process of internalization, as shown by TEM (Luchtel *et al.*, 1980, Midlej *et al.*, 2009).

The data in this chapter focus on the fact that the PI3K inhibitor LY294002 alters the appearance of trophozoites under normal growth medium. Some of the characteristic morphological alterations were observed after LY294002 treatment; these included the presence of cell surface membrane protrusions, elongated cell shape, inhibition of cytokinesis, irregular flagella beating, presence of large vacuoles in the cytoplasm, disorganisation of the peripheral vesicles in number of cells, internalisation of the flagella and initiation of the encystation-like process. Some of these observations are in agreement with the findings when trophozoites were treated with the LY294002 inhibitor of PI3K. The experimental work on ultrastructural studies on the effect of PI3K inhibitor found that LY294002 causes disorganisation of the peripheral vesicles throughout the cytoplasm and observed large and pleomorphic cells in cells treated with PI3K inhibitor (Bittencourt-Silvestre *et al.*, 2010). Additionally, trophozoite cultures treated with LY294002 appear to

initiate the early stages of encystation in terms of the appearance of ESVs and cyst wall protein (CWP) up-regulation due to the inhibition of PI3K (Tovar, unpublished data).

It was important to report that during the preparation of *Giardia* cells for electron microscopy, after fixing the cells and series of washes, LY294002-treated cells were found to be short in numbers compared to control-DMSO treated cells. An explanation for this could be that LY294002-treated cells are unable to attach onto the glass coverslip like the untreated cells. The attachment of *Giardia* trophozoites treated with LY294002 may have been dysfunctional; therefore, unattached trophozoites treated with PI3K inhibitor were washed away and discarded. Treatment with LY294002 may initiate an encystation-like process that would lead to the initiation of cellular differentiation, which may affect the mechanism of attachment as cysts do not need to have adhesive ability. However, the mechanism of attachment in *G. intestinalis* trophozoites remains unclear and only hypotheses have been proposed. The ventral disc component was identified to contain contractile proteins involved in adherence for the contraction of the disk (Adam, 2001). This component is distinctive and it covers the entire ventral surface of the trophozoites and is crucial to the structure of *Giardia* pathology. Several reported microtubule targeting drugs tested on *Giardia* affect the ventral disc structures; these include benzimidazoles, metronidazole and nitazoxanide, and emphasises the importance of the *Giardia* ventral disk as a focus point as a target for the treatment of giardiasis (Oxberry *et al.*, 1994, Cedillo-Rivera *et al.*, 2002, Mariante *et al.*, 2005).

The early stages of encystation, explained in previous chapters, starts when external signals trigger the synthesis, processing and transport of cyst wall components and ESVs are assembled to the surface of encysting cells forming cyst wall (Lujan *et al.*, 1997). SEM images illustrated approximately 18.2% of *Giardia* cells showing cell surface vesicular spots/protrusion after 24 hours of incubation under encysting medium. After 24 hours of incubation, LY294002-treated cells showed 14.6% and 18.0% of cells with surface vesicular spots/protrusions at a LY294002 concentration of 15 μ M and 50 μ M, respectively. Both conditions continue to show *Giardia* cells with surface protrusions/spots after 48 hours incubation period. These protrusions of vesicles on the cell surface membrane have been suggested to represent the number of encystation vesicles below the surface of the cells (Lanfredi-Rangel *et al.*, 2003, Bittencourt-Silvestre *et al.*, 2010). The images from TEM show that *Giardia* cells treated with LY294002 under normal growth medium and *Giardia* cells under encystation medium display cleft structures within the

cytoplasm. These examples of clefts and ELVs under normal growth culture medium were approximately 8.6% in cells with one cleft or ELV and 4.7% in cells with more than two clefts or ELV structures. LY294002-treated cultures display 29.4% and 17.6%; *Giardia* under encysting medium displays 55.4% and 26.9% of cells with one cleft or ELV and cells with two or more clefts or ELVs after 24 hours incubation. Ultrastructure analysis in recent findings have identified that ELVs were only observed in cells undergoing the encystation process. The same encysting cells could have both ELVs and ESVs present; these two vesicles appear to be distinctively different and were verified by using an anti-CWPI antibody that specifically labels both a constitutive cyst wall protein and labels the ESVs (Gillin *et al.*, 1989, Midlej *et al.*, 2012). Moreover, the peripheral vesicles were measured and compared to ELV to ensure that they were not the observed ELVs in the encysting cells.

Experimental work describing *Giardia* cells when PI3K inhibitor LY294002 was added at the beginning of the encystation process were carried out to examine the effect of LY294002-treated cells under encysting medium with the control being DMSO-treated cultures. Initially, after 24 hours, both LY294002-treated cultures and control-DMSO-treated cultures displayed less than 26% of visible vesicular protrusions of the cell surface membrane and less than 12% of dividing *Giardia* treated cells. After 48 hours of incubation, however, LY294002-treated cultures reached 60.2% of cells showing vesicular cell surface protrusions and 15% of dividing *Giardia* treated cells, but more than 80% of these counted displayed irregular flagella beating and overall abnormal morphology. The control-DMSO treated cells on the other hand show 39.3% of cells with surface protrusions and less than 5% of dividing *Giardia* treated cells. This suggests that PI3Ks are important in trophozoites under normal conditions and differentiating cells during encystation. Recent findings have shown that there is an increase in the expression of PI3Ks during the encystation process in *Giardia* cells and that LY294002 demonstrates an inhibitory effect on encysting cells after the encystation process was launched. This indicates that PI3Ks may be the key regulator during the process of encystation (Hernandez *et al.*, 2007, Bittencourt-Silvestre *et al.*, 2010).

The results show that both SEM and TEM have provided significant data and important information on the effect of the PI3K inhibitor LY294002 in *G. intestinalis* cultures. Evidence such as the appearance of clefts and ELV structures, which may suggest that LY294002-treated cells under normal growth medium trigger the initiation of

encystation-like process; however, no mature cysts were identified in LY294002-treated cultures. Therefore, the addition of PI3K inhibitors to trophozoite cell cultures can block the *Giardia* cell cycle and even though encystation process is initiated through CWPs production, cell differentiation is not completed due to the inhibition of PI3Ks. These observations are in agreement with Cox *et al.* (2006), who stated that *Giardia* PI3Ks play an important role in extracellular-initiated signalling (class I PI3K) and intracellular vesicle trafficking (class II PI3K). Due to the difficulty in obtaining the ultrastructure of cysts from encystation medium, it was not possible to compare the effect of LY294002 on encysting cultures. Future work should assess whether CWP2 was expressed and transported to the surface of the cells by ESV in both control (untreated cultures) and LY294002-treated cultures. The difficulty encountered in this experimental work was the need to use electron microscopy to analyse many *Giardia* cells to search for alterations in morphology that may have occurred during the addition of LY294002 or encysting medium, as the latter process is not synchronised and thus consumes time.

CHAPTER 6: Discussion

6.1 Research hypothesis

This research concentrates on phosphoinositide 3-kinase (PI3K) signalling pathways in *Giardia intestinalis*. PI3Ks are a family of enzymes with a crucial role in the regulation of cellular mechanisms that have been extensively studied in mammalian and yeast cells. The studies of PI3Ks have provided an abundance of knowledge at which one can build on to examine in other cellular systems. The diplomonad *G. intestinalis* parasitises the gastrointestinal tract of humans and mammals causing giardiasis present as an interesting prospect as a model organism to study. Important findings show that *Giardia* processes such as cell growth, proliferation, differentiation and vesicle trafficking, all of which are essential for parasite survival and disease transmission, may involve the PI3K signalling mechanism. Additional work to further characterise PI3K genes is required to identify and characterise putative ancillary components of lipid signalling cascades. Identifying a number of such components in the *Giardia* genome by homology searching could augment this knowledge. Investigating the putative functionality of these lipid signalling kinases in *Giardia* would confirm and provide evidence of the existence of these lipid signalling kinases. Moreover, previous work has identified and characterised two putative PI3K genes in *G. intestinalis* called *GiPI3K1* and *GiPI3K2*, which represent homology to class I and class III PI3K isoforms, respectively. Therefore various reported inhibitor of PI3Ks and other inhibitors of the lipid signalling cascades were tested to provide further insights into the cellular signalling pathway and the regulatory pathways that involve parasite differentiation. Furthermore, attempting to determine whether PI3Ks in *Giardia* play an important role in cell growth and proliferation is essential and may provide insights when searching for new treatment of giardiasis.

6.2 Summary of findings

The bioinformatics results in chapter 3 primarily established that the *G. intestinalis* genomes encodes at least two PI3Ks (*GiPI3K1* and *GiPI3K2*) and two GSKs (*GiGSKa* and *GiGSKb*). The two *Giardia* PI3K isoforms, *GiPI3K1* and *GiPI3K2*, have been shown to share homology to the class I and III PI3Ks, respectively. The two homologues of GSK

isoforms in the giardial genome have been shown as the closest homologues to GSK-3 α and GSK-3 β , respectively. *Giardia* GSKs are likely to be functional proteins, since their sequence alignments with functionally characterised GSK-3 using ClustalW highlighted important conserved functional residues between the sequences. The presence of substrate binding sites, ATP binding sites, active sites are all conserved in the sequence alignments between *Giardia* GSKs and structurally known GSK-3. Furthermore there is evidence of conserved primed substrate recognition binding site within the serine/threonine kinase catalytic domain in *Giardia* GSKs that is required for specific binding with substrates that need priming phosphorylation.

Subcellular localisation in *Giardia* GSKs suggests that GiGSKa may localise in the cytoplasmic space, whereas GiGSKb is likely to be localised in the nucleus or cytoplasm. These findings are in agreement with the localisation of other GSK-3s in mammalian cells; therefore, GiGSKa may be involved in a phosphorylation reaction by PKB which will activate cyclin D downstream leading to cell cycle arrest. GiGSKb is nuclear localised and may be involved in cell cycle regulation.

The experimental results in chapter 4 began by presenting the effect of various inhibitors that have been reported to inhibit PI3K and GSK-3. Of these inhibitors experimented to inhibit PI3K activity, only one PI3K inhibitor exhibits a cytostatic effect on *G. intestinalis*. The PI3K inhibitor LY294002 was shown to inhibit *Giardia* trophozoite proliferation in a concentration-dependent manner when trophozoites were treated with LY294002 ranging from 10 – 75 μ M. The concentration of LY294002, approximately 25 – 30 μ M. can significantly inhibit *Giardia*, with an up to 50% decrease in population of trophozoites compared to the DMSO-treated control culture. Trophozoite culture expose to 50 μ M of LY294002 almost completely stopped cell proliferation over a period of 48 hours. Interestingly, upon the removal of LY294002, a reversible effect was observed whereby *Giardia* trophozoites previously exposed to LY294002 continued to proliferate after fresh culture medium was added to replace the culture medium with a PI3K inhibitor. Therefore, the PI3K inhibitor may stimulate cell cycle arrest at G1 in trophozoites. With all of this evidence, it is possible to suggest that PI3K activity in *G. intestinalis* plays an important role in control of the parasite cell cycle. Another plausible argument could be that some of the PI3K-inhibited trophozoites remain stationary as the result of the parasite initiating encystation process. Therefore, G2 arrested cells may start encystation but not necessarily complete encystation process. Encystation experimental work highlighted the

low yield in encysting/cysts cells culture treated with PI3K inhibitor LY294002 with a high percentage of these cells resulted in an incomplete cyst formation after 48 hours. This result suggests that PI3K activity in *G. intestinalis* is not only important in trophozoite proliferation but also crucial in the differentiations stage during the encystation process. PIP₃ data show that the level of PIP₃ in normal trophozoites is in the same range as the cells under encystation medium for 48 hours. This may provide further evidence that the presence of PI3K activity is active in both cell grown trophozoites and differentiating trophozoites under the encysting process.

The other two PI3K inhibitors examined were wortmannin and PI-103. Both wortmannin and PI-103 did not show any effect on trophozoite proliferation compared to the control. The latter was reported to specifically inhibit PI3K with an IC₅₀ of 1 μM *in vitro* using mammalian purified protein (Bains *et al.*, 2007). PI-103 specific inhibitor of PI3K may be specific for PI3Ks in mammalian cells and may not inhibit *Giardia* PI3Ks due to the differences in amino acids important for the enzyme functionality of *Giardia* PI3Ks. These important differences in amino acids may be vital for substrate and inhibitor binding. This speculation is based on the observation that in trophozoite culture, a concentration up to 5 μM of PI-103 treated to these parasite failed to show any significant effect on positive growth inhibition when compared to DMSO-treated control cultures. The common inhibitor of PI3K, wortmannin, which was reported to inhibit PI3K with an irreversible reaction (Walker *et al.*, 2000) shows no effect on trophozoite proliferation. This finding is consistent with that of Cox *et al.* (2006), who made attempts by testing the activity of the stock solutions on mammalian cells to detect phosphorylated PKB levels and repeated the addition of wortmannin to ensure that it was not due to instability of the inhibitor. In contrast, studies by Hernandez *et al.* (2007) illustrated that overnight incubation of *Giardia* trophozoite treated with wortmannin at concentration of 2.5 – 20 μM showed a significant decreased in the number of trophozoite proliferation. The significant effect on trophozoite proliferation in this study is probably due to the non-specific effect of wortmannin on trophozoite culture. Since the recommended treatment is between 0.05 – 0.5 μM, non-specific effects is likely to be the explanation for the decreased in the number of cells in *Giardia*. Moreover, it is known that wortmannin-insensitive PI3K have been found in yeast. It has been reported that yeast Vps34 is 1200x less susceptible to wortmannin inhibition than its human homologue (Walker *et al.*, 2000 and Cox *et al.*, 2006). It is important to note that key residues within the ATP/wortmannin binding regions are different in yeast Vps 34

to class III isoforms. Giardial PI3Ks demonstrate that they too have residues differ at the same positions shown for yeast Vps 34; thus, this may be another explanation for wortmannin insensitivity (Cox *et al.*, 2006).

To further investigate whether LY294002 has an effect on trophozoite proliferation was a result of the downstream inhibition of glycogen synthase kinase-3 (GSK-3). The inhibitors of GSK-3 examined were lithium chloride (LiCl) and CT99021. Both inhibitors had no effect on trophozoite proliferation when various concentrations ranging from 0.5 – 10 μ M for CT99021 (with reported IC₅₀ of 1 μ M) and 1 – 20 mM for LiCl (with reported IC₅₀ of 5 mM). Using the double inhibitor experimental study, it was possible to conclude that LY294002 does not inhibit GiGSKs. This conclusion is based on the experiment that in trophozoite cultures with increasing LY294002 treatment in constant concentration of CT99021; the numbers of trophozoite cells appears to decrease in a concentration dependent manner. Moreover the second double inhibitor experiment result found that increasing the concentration of CT99201 and treatment with LY294002 did not release the block caused by PI3K inhibition. Therefore, this double inhibitor experiment concluded that the effect of LY294002 on trophozoites culture was due to PI3K inhibition.

Encystation experimental work exposing trophozoites under encysting medium to PI3K inhibitor LY294002 resulted in a small number of encysting/cyst cells. It is important to investigate whether PI3K is indeed required during the beginning of the encystation process. Evidences gathered in chapter 4 highlighted significant differences in the number of cells with trophozoites morphology after 24 hours of incubation period in control culture (DMSO-treated) compared to LY294002-treated culture. The cultures treated with PI3K inhibitor LY294002 show approximately 82% of cells with trophozoites morphology in comparison to 45% of trophozoites that should be observed. This result suggests that PI3K activity is required at least during initiation of the encystation process and that it may be due to the inhibition of PI3K as *Giardia* culture in encysting medium resulted in inefficient encystation process.

To further investigate the effect of PI3K inhibitor LY294002 on *G. intestinalis*, scanning and transmission electron microscope approaches were utilised. These two techniques would address the observation of *Giardia* cells at the ultrastructural level. A scanning electron microscope (SEM) was use to examined *Giardia* cells under high magnification and resolution, which provides detailed observations on all of the morphological changes at the ultrastructural level. The second technique, transmission

electron microscopy (TEM) was used to monitor within the inner layers of trophozoites and encysting cells to provide ultrastructural images of the internal morphological changes that may have taken place. The images of vegetative trophozoites were examined using both techniques and showed the expected appearance of trophozoite cell morphology both within the inner layers of the cell and the round pear-shape-like ultrastructure. The process of encystation *in vitro* to observe *Giardia* trophozoite differentiating into a cyst was attempted, but no cyst morphology was detected under the encysting culture. An explanation into this difficulty of cyst production could be that subcultures of *Giardia in vitro* may cause deficits in the parasite virulence over time; in this particular case, *Giardia* trophozoites differentiate into mature cysts. It is well-known that the laboratory usually obtained the parasite once it has been passage through animal *in vivo*. A recently reported experiment using *Leishmania infantum* demonstrated that virulence deficit caused by successive *in vitro* passages results from an inadequate capacity to differentiate into amastigote forms (Moreira *et al.*, 2012).

However evidence of trophozoite initiating the process of encystation was successful under both SEM and TEM approaches. This conclusion is based on the observation of electron-lucent vesicles (ELVs) and clefts. These clefts which are dilated endoplasmic reticulum cisternae then eventually transformed into encystation specific vesicles (ESVs) (Lujan *et al.*, 1997, Lanfredi-Rangel *et al.*, 2003). Moreover the observed ELVs have been reported to only be identified in cells undergoing encystation process. SEM images have provided evidence of vesicular spots cells showing protrusion on the surface of *Giardia* cells. These vesicular protrusions have been reported to represent the increasing number of ESVs below the surface of the cell differentiating plasma membrane (Lanfredi-Rangel *et al.*, 2003, Bittencourt-Silvestre *et al.*, 2010). These evidence demonstrate that both SEM and TEM have provided confirmation that some of the trophozoites in cell culture have entered the initiation stage of the encystation process. Trophozoite culture exposed to the PI3K inhibitor LY294002 for 24 and 48 hours displayed vesicle protrusion on the cell surface membrane. As mentioned before, this characteristic surface membrane protrusion identified using SEM, and suggests that there are ESVs underneath the surface of the differentiating plasma membrane. Moreover, data from SEM images demonstrate LY294002-treated cells remains stationary over the period of 24 and 48 hours. This observation is based on the increasing number of doublet cells compared with the control culture, which could be due to the inhibition of PI3K activity that is

required to complete cell division. Evidence that LY294002-treated cells may initiate the process of encystation were observed through TEM images, as an increased number of clefts and ELVs were counted and compared to the control cells under encysting medium. This conclusion suggests that trophozoites entering the process of encystation may be regulated by PI3K, as PI3K could have a block on normal trophozoites initiating encystation; once this block is released, the process of encystation is initiated. The block on encystation may be released due to reduced PI3K activity.

6.3 Limitations of approaches used and ideas for improvement

The first improvement required in this project which unfortunately failed is the *in vitro* production of mature cysts through the process of encystation. It is known that not all *Giardia* trophozoites differentiate once triggered to initiate process of encystation differentiate to form cysts. Moreover, the attempt to use different encystation medium protocol for example, as reported by Gillin *et al.* (1989), may prove be successful in producing cysts cells. Alternatively, the reason why *Giardia* trophozoites may not complete the formation of cysts could be due to the loss of structural virulence due to continuous passage *in vitro*, as previously mentioned. This approach could be improved by using a fresh passage of the *in vivo* isolate of *Giardia* trophozoites because the *Giardia* encystation process is completed *in vivo* inside the gut and intestine, which is where the natural niche of trophozoites differentiates into cysts.

The immunofluorescence experimental approach encountered difficulty when attempts were made to use antibodies against iron-binding protein, and the anti-iron sulphur cluster S (anti-IscS). These are two of the mitochondrial marker proteins required for iron sulphur cluster biosynthesis to a labelled double membrane-bound structure within *Giardia* cells. However, this approach was unsuccessful and it was not possible to reproduce the IscS labelling in *Giardia* cell due to strong background signals that labelled the whole cell. It was not possible to detect any specific localized staining signal within the cellular compartment of trophozoite cell. Primary antibodies, anti-IscS, were diluted in an attempt to remove background unspecific binding; the following dilutions were made: 1:250, 1:500, 1:1000, 1:1500, 1:2000, 1:3000 and 1:5000. The concentration of primary antibody anti-IscS in the reported paper was 1:250, however even after x20 the concentration use in the previous paper, the whole cell still has background staining but no specific staining signal labelling the small cellular structures were observed after 1:5000 dilutions. Other

approaches to reduce background labelling were completed by increasing the number of washes between the incubation periods with gentle agitations and washing with PBS-Triton to remove non-specific binding. However, it is important to obtain a balance between the number of washes and the number of cells remaining attached to the coverslip as detachment of *Giardia* cells often takes place after a series of washes using PBS-T.

As an alternative approach to detect the localisation of IscS, transmission electron immunomicroscopy may allow possible detection under thawed frozen cryosections of glutaraldehyde-fixed *Giardia*, as previously reported by Tovar *et al.* (2003). Furthermore, double-labelling of anti-IscS and anti-CWP2 can be incorporated for their viewing under TEM immunomicroscopy and further quantitative techniques can be more effective as the specific labelling of the antibodies use will be clearly visible.

6.4 Implications of research and future work

This research on the study of phosphoinositide 3-kinase in *G. intestinalis* allows the continuous building of intracellular signalling pathways in *Giardia* that regulate the proliferation of trophozoites and differentiation in the cell during encystation process. The finding in the first chapter focuses on the components of the functional intracellular signalling pathway PI3Ks (GiPI3K1 and GiPI3K2 resemble class I and class III, respectively) and GSKs (GiGSKa and GiGSKb are similar to GSK-3 α and GSK-3 β , respectively), which have been shown to exist in *G. intestinalis*. It is likely that the latter GiGSKa regulates its activity with PKB and cyclin D in the cytoplasm whilst GiGSKb may be localised in nuclei that are involved in cell cycle regulation. Together with works done on the existence of a functional PI3K signalling pathway component in *Giardia*, it is a challenge to further contribute to an understanding of *Giardia* signalling pathways.

The cytostatic effect of the PI3K inhibitor LY294002 on trophozoite culture has provided many opportunities to further investigate the role of PI3Ks in *G. intestinalis*. The intracellular signalling pathway in *G. intestinalis* involving PI3Ks has been linked to other *Giardia* genes encoding phosphoinositide-metabolising enzymes, for example phosphatase and tensin homologue deleted on chromosome 10 (PTEN) and PI4K. Moreover, in addition to PKB involvement in phosphorylating other signalling components that are central to the intracellular signalling pathway (Hers *et al.*, 2011), PKB can further phosphorylate the downstream enzymes of GSK-3 that are responsible for many cellular processes, for example cell cycle arrest in mammalian cells. The study of PI3K intracellular signalling in

mammalian cells provided a platform to further investigate other signalling components, starting with PI3K in *G. intestinalis*. To verify whether the product of PI3K class I in *Giardia* is present, PIP₃ mass ELISA assay was utilised. The results revealed that there are measurable amount of PIP₃ in both *Giardia* trophozoites and encysting cells. However, improvements in the future experiments on the identification of this PIP₃ and other polyphosphoinositol family members can be detected through using a liquid chromatography-mass spectrometry approach. Although this method requires time and sample preparation, this technique will identify the phosphoinositol family and there will be an improved understanding of PI3Ks activity in *Giardia*.

To further expand the study of intracellular signalling in *G. intestinalis*, investigation into proteomics studies may contribute to provide a list of protein content in *Giardia*. Using a tandem mass spectrometry approach described by Faso *et al.* (2013), this may identify a number of proteins responsible for the *Giardia* intracellular signalling pathway. More importantly, quantitative analysis of *G. intestinalis* proteome using tandem mass spectrometry could identify the changes in protein abundance before and after the addition of LY294002. This mass spectrometry approach can further provide evidence together with scanning and transmission electron microscopy that supports the hypothesis that the inhibition of PI3K in trophozoites leads to the initiation of the encystation process. This method can be applied to study of the encystation process in *Giardia* cells, in the experiment using PI3K inhibitor LY294002 to observe the changes in protein content that may be involved in PI3K signalling.

It is important to consider that not all trophozoite cells are at the same stage in the cell cycle. Therefore, experiments are required to examine whether GiPI3K1 or GiPI3K2 affect the vegetative trophozoite by potentially blocking the process of encystation at the Gap 2 phase of the cell cycle (Bernander *et al.*, 2001). This is due to the hypothesis indicating that by inhibiting PI3Ks, the block at the G₂ phase of the cell cycle is released, thus initiating trophozoites to differentiate into cysts. Using fluorescence-activated cell flow cytometry, analysis of trophozoite cultures can distinguish whether cell cycle arrest takes place at G₂ (contains 8N cellular ploidy) or Gap 1 or S phase (contain newly divided trophozoites with 4N cellular ploidy) (Bernander *et al.*, 2001). Furthermore it is essential to accurately know that the majority of these cells are at the G₂ phase; the same can be said about the trophozoites under encyst medium. The flow cytometry approach can determined

by assessing at what stage the majority of these cells are within the cell cycle phase (Reaume *et al.*, 2013).

6.5 Conclusion

In conclusion, this research project shows the overall observation of *G. intestinalis* intracellular signalling pathways surrounding PI3K and GSK. LY294002, an inhibitor of PI3K, has shown the importance of PI3K activity in *Giardia* for controlling both the trophozoite proliferation process and the early stages of the encystation process in *Giardia* cellular cycle. The data shown have ruled out the possibility that LY294002 is inhibiting GSK activity in *Giardia* trophozoite cell. Also it has shown that PI3K activity is present in both vegetative trophozoite and encysting cells of *G. intestinalis* through the detection of the production of PIP₃. Scanning electron microscopy and transmission electron microscopy examined vegetative trophozoites that had been exposed to PI3K inhibitor; it was shown that inhibition of PI3K in trophozoites leads to initiation of the early stages of the encystation process in *G. intestinalis*. Furthermore, the activity of PI3K may be involved in the development of a cyst wall in encysting cells through the regulation of CWP2 expressions.

Overall, the current work should not only expand our knowledge of PI3K studies but should also assist researchers in the future work regarding the PI3K signalling cascade. Moreover, this research has the potential to branch out into drug targeting work and further expand the study of parasitology in intracellular signalling research.

BIBLIOGRAPHY

- Adam, R.D. (2001). Biology of *Giardia lamblia*. *Clin Microbiol Rev* **14**, 447-475.
- Allende, J.E., and Allende, C.C. (1995). Protein kinases. 4. Protein kinase CK2: an enzyme with multiple substrates and a puzzling regulation. *FASEB J* **9**, 313-323.
- Arcaro, A., and Wymann, M.P. (1993). Wortmannin is a potent phosphatidylinositol 3-kinase inhibitor: the role of phosphatidylinositol 3,4,5-trisphosphate in neutrophil responses. *Biochem J* **296** (Pt 2), 297-301.
- Arcaro, A., Zvelebil, M.J., Wallasch, C., Ullrich, A., Waterfield, M.D., and Domin, J. (2000). Class II phosphoinositide 3-kinases are downstream targets of activated polypeptide growth factor receptors. *Mol Cell Biol* **20**, 3817-3830.
- Backer, J.M. (2000). Phosphoinositide 3-kinases and the regulation of vesicular trafficking. *Mol Cell Biol Res Commun* **3**, 193-204.
- Backer, J.M. (2008). The regulation and function of Class III PI3Ks: novel roles for Vps34. *Biochem J* **410**, 1-17.
- Baggiolini, M., Dewald, B., Schnyder, J., Ruch, W., Cooper, P.H., and Payne, T.G. (1987). Inhibition of the phagocytosis-induced respiratory burst by the fungal metabolite wortmannin and some analogues. *Exp Cell Res* **169**, 408-418.
- Bain, J., McLauchlan, H., Elliott, M., and Cohen, P. (2003). The specificities of protein kinase inhibitors: an update. *Biochem J* **371**, 199-204.
- Bain, J., Plater, L., Elliott, M., Shpiro, N., Hastie, C.J., McLauchlan, H., Klevernic, I., Arthur, J.S., Alessi, D.R., and Cohen, P. (2007). The selectivity of protein kinase inhibitors: a further update. *Biochem J* **408**, 297-315.
- Bannai, H., Tamada, Y., Maruyama, O., Nakai, K., and Miyano, S. (2002). Extensive feature detection of N-terminal protein sorting signals. *Bioinformatics* **18**, 298-305.
- Barwick, R.S., Levy, D.A., Craun, G.F., Beach, M.J., and Calderon, R.L. (2000). Surveillance for waterborne-disease outbreaks--United States, 1997-1998. *MMWR CDC Surveill Summ* **49**, 1-21.
- Benchimol, M. (2004). The release of secretory vesicle in encysting *Giardia lamblia*. *FEMS Microbiol Lett* **235**, 81-87.
- Bernander, R., Palm, J.E., and Svard, S.G. (2001). Genome ploidy in different stages of the *Giardia lamblia* life cycle. *Cell Microbiol* **3**, 55-62.
- Bittencourt-Silvestre, J., Lemgruber, L., and de Souza, W. (2010). Encystation process of

- Giardia lamblia*: morphological and regulatory aspects. *Arch Microbiol* **192**, 259-265.
- Bosc, D.G., Luscher, B., and Litchfield, D.W. (1999). Expression and regulation of protein kinase CK2 during the cell cycle. *Mol Cell Biochem* **191**, 213-222.
- Boulikas, T. (1993). Nuclear localization signals (NLS). *Crit Rev Eukaryot Gene Expr* **3**, 193-227.
- Bryson, K., McGuffin, L.J., Marsden, R.L., Ward, J.J., Sodhi, J.S., and Jones, D.T. (2005). Protein structure prediction servers at University College London. *Nucleic Acids Res* **33**, W36-38.
- Burda, P., Padilla, S.M., Sarkar, S., and Emr, S.D. (2002). Retromer function in endosome-to-Golgi retrograde transport is regulated by the yeast Vps34 PtdIns 3-kinase. *J Cell Sci* **115**, 3889-3900.
- Buret, A., denHollander, N., Wallis, P.M., Befus, D., and Olson, M.E. (1990). Zoonotic potential of giardiasis in domestic ruminants. *J Infect Dis* **162**, 231-237.
- Busatti, H.G., and Gomes, M.A. (2007). A simple colourimetric method to determine anti-giardial activity of drugs. *Parasitol Res* **101**, 819-821.
- Cantley, L.C. (2002). The phosphoinositide 3-kinase pathway. *Science* **296**, 1655-1657.
- Carranza, P.G., and Lujan, H.D. (2010). New insights regarding the biology of *Giardia lamblia*. *Microbes Infect* **12**, 71-80.
- Castillo-Romero, A., Leon-Avila, G., Perez Rangel, A., Cortes Zarate, R., Garcia Tovar, C., and Hernandez, J.M. (2009). Participation of actin on *Giardia lamblia* growth and encystation. *PLoS One* **4**, e7156.
- Cedillo-Rivera, R., Chavez, B., Gonzalez-Robles, A., Tapia, A., and Yopez-Mulia, L. (2002). *In vitro* effect of nitazoxanide against *Entamoeba histolytica*, *Giardia intestinalis* and *Trichomonas vaginalis* trophozoites. *J Eukaryot Microbiol* **49**, 201-208.
- Cheatham, B., Vlahos, C.J., Cheatham, L., Wang, L., Blenis, J., and Kahn, C.R. (1994). Phosphatidylinositol 3-kinase activation is required for insulin stimulation of pp70 S6 kinase, DNA synthesis, and glucose transporter translocation. *Mol Cell Biol* **14**, 4902-4911.
- Cheng, H., Woodgett, J., Maamari, M., and Force, T. (2011). Targeting GSK-3 family members in the heart: a very sharp double-edged sword. *J Mol Cell Cardiol* **51**, 607-613.
- Chiarini, F., Fala, F., Tazzari, P.L., Ricci, F., Astolfi, A., Pession, A., Pagliaro, P., McCubrey, J.A., and Martelli, A.M. (2009). Dual inhibition of class IA phosphatidylinositol 3-kinase and mammalian target of rapamycin as a new therapeutic option for T-cell acute lymphoblastic leukemia. *Cancer Res* **69**, 3520-

3528.

- Chu, E.C., and Tarnawski, A.S. (2004). PTEN regulatory functions in tumor suppression and cell biology. *Med Sci Monit* **10**, RA235-241.
- Ciaraldi, T.P., Carter, L., Mudaliar, S. and Henry, R.R. (2010). GSK-3beta and control of glucose metabolism and insulin action in human skeletal muscle. *Mol Cell Endocrinol* **315**, 153-158.
- Cohen, P., and Goedert, M. (2004). GSK3 inhibitors: development and therapeutic potential. *Nat Rev Drug Discov* **3**, 479-487.
- Courtney, K.D., Corcoran, R.B., and Engelman, J.A. (2010). The PI3K pathway as drug target in human cancer. *J Clin Oncol* **28**, 1075-1083.
- Cox, S.S., van der Giezen, M., Tarr, S.J., Crompton, M.R., and Tovar, J. (2006). Evidence from bioinformatics, expression and inhibition studies of phosphoinositide-3 kinase signalling in *Giardia intestinalis*. *BMC Microbiol* **6**, 45.
- Das, S., Stevens, T., Castillo, C., Villasenor, A., Arredondo, H., and Reddy, K. (2002). Lipid metabolism in mucous-dwelling amitochondriate protozoa. *Int J Parasitol* **32**, 655-675.
- Davids, B.J., Reiner, D.S., Birkeland, S.R., Preheim, S.P., Cipriano, M.J., McArthur, A.G., and Gillin, F.D. (2006). A new family of giardial cysteine-rich non-VSP protein genes and a novel cyst protein. *PLoS One* **1**, e44.
- Davies, S.P., Reddy, H., Caivano, M., and Cohen, P. (2000). Specificity and mechanism of action of some commonly used protein kinase inhibitors. *Biochem J* **351**, 95-105.
- Diehl, J.A., Cheng, M., Roussel, M.F., and Sherr, C.J. (1998). Glycogen synthase kinase-3beta regulates cyclin D1 proteolysis and subcellular localization. *Genes Dev* **12**, 3499-3511.
- Dirac-Svejstrup, A.B., Shorter, J., Waters, M.G., and Warren, G. (2000). Phosphorylation of the vesicle-tethering protein p115 by a casein kinase II-like enzyme is required for Golgi reassembly from isolated mitotic fragments. *J Cell Biol* **150**, 475-488.
- Djordjevic, S., and Driscoll, P.C. (2002). Structural insight into substrate specificity and regulatory mechanisms of phosphoinositide 3-kinases. *Trends Biochem Sci* **27**, 426-432.
- Doble, B.W., and Woodgett, J.R. (2003). GSK-3: tricks of the trade for a multi-tasking kinase. *J Cell Sci* **116**, 1175-1186.
- Domin, J., Gaidarov, I., Smith, M.E., Keen, J.H., and Waterfield, M.D. (2000). The class II phosphoinositide 3-kinase PI3K-C2alpha is concentrated in the trans-Golgi network and present in clathrin-coated vesicles. *J Biol Chem* **275**, 11943-11950.

- Dominguez, I., Itoh, K., and Sokol, S.Y. (1995). Role of glycogen synthase kinase 3 beta as a negative regulator of dorsoventral axis formation in *Xenopus* embryos. *Proc Natl Acad Sci U S A* **92**, 8498-8502.
- D'Orazi, G., Cecchinelli, B., Bruno, T., Manni, I., Higashimoto, Y., Saito, S., Gostissa, M., Coen, S., Marchetti, A., Del Sal, G., *et al.* (2002). Homeodomain-interacting protein kinase-2 phosphorylates p53 at Ser 46 and mediates apoptosis. *Nat Cell Biol* **4**, 11-19.
- Eichinger, L., Pachebat, J.A., Glockner, G., Rajandream, M.A., Sucgang, R., Berriman, M., Song, J., Olsen, R., Szafranski, K., Xu, Q., *et al.* (2005). The genome of the social amoeba *Dictyostelium discoideum*. *Nature* **435**, 43-57.
- Elmendorf, H.G., Dawson, S.C., and McCaffery, J.M. (2003). The cytoskeleton of *Giardia lamblia*. *Int J Parasitol* **33**, 3-28.
- Fan, Q.W., Knight, Z.A., Goldenberg, D.D., Yu, W., Mostov, K.E., Stokoe, D., Shokat, K.M., and Weiss, W.A. (2006). A dual PI3 kinase/mTOR inhibitor reveals emergent efficacy in glioma. *Cancer Cell* **9**, 341-349.
- Faso, C., Bischof, S. and Hehl, A.B. (2013). The proteome landscape of *Giardia lamblia* encystation. *PLoS One* **8**, e83207.
- Foster, F.M., Traer, C.J., Abraham, S.M., and Fry, M.J. (2003). The phosphoinositide (PI) 3-kinase family. *J Cell Sci* **116**, 3037-3040.
- Franke, T.F., Yang, S.I., Chan, T.O., Datta, K., Kazlauskas, A., Morrison, D.K., Kaplan, D.R., and Tsichlis, P.N. (1995). The protein kinase encoded by the Akt proto-oncogene is a target of the PDGF-activated phosphatidylinositol 3-kinase. *Cell* **81**, 727-736.
- Fraser, D., Bilenko, N., Deckelbaum, R.J., Dagan, R., El-On, J., and Naggan, L. (2000). *Giardia lamblia* carriage in Israeli Bedouin infants: risk factors and consequences. *Clin Infect Dis* **30**, 419-424.
- Fruman, D.A., Meyers, R.E. and Cantley, L.C. (1998). Phosphoinositide kinases. *Annu Rev Biochem* **67**, 481-507.
- Fry, M.J. (1994). Structure, regulation and function of phosphoinositide 3-kinases. *Biochim Biophys Acta* **1226**, 237-268.
- Fry, M.J. (2001). Phosphoinositide 3-kinase signalling in breast cancer: how big a role might it play? *Breast Cancer Res* **3**, 304-312.
- Gao, Y., and Wang, H.Y. (2006). Casein kinase 2 is activated and essential for Wnt/beta-catenin signalling. *J Biol Chem* **281**, 18394-18400.
- Geddes, J.R., Goodwin, G.M., Rendell, J., Azorin, J.M., Cipriani, A., Ostacher, M.J.,

- Morriss, R., Alder, N., and Juszczak, E. (2010). Lithium plus valproate combination therapy versus monotherapy for relapse prevention in bipolar I disorder (BALANCE): a randomised open-label trial. *Lancet* **375**, 385-395.
- Gharbi, S.I., Zvelebil, M.J., Shuttleworth, S.J., Hancox, T., Saghir, N., Timms, J.F., and Waterfield, M.D. (2007). Exploring the specificity of the PI3K family inhibitor LY294002. *Biochem J* **404**, 15-21.
- Gillin, F.D., Boucher, S.E., Rossi, S.S., and Reiner, D.S. (1989). *Giardia lamblia*: the roles of bile, lactic acid, and pH in the completion of the life cycle in vitro. *Exp Parasitol* **69**, 164-174.
- Gillin, F.D., Reiner, D.S., Gault, M.J., Douglas, H., Das, S., Wunderlich, A., and Sauch, J.F. (1987). Encystation and expression of cyst antigens by *Giardia lamblia* in vitro. *Science* **235**, 1040-1043.
- Giraud, S., Diaz-Latoud, C., Hacot, S., Textoris, J., Bourette, R.P., and Diaz, J.J. (2004). US11 of herpes simplex virus type 1 interacts with HIPK2 and antagonizes HIPK2-induced cell growth arrest. *J Virol* **78**, 2984-2993.
- Glover, C.V., 3rd (1998). On the physiological role of casein kinase II in *Saccharomyces cerevisiae*. *Prog Nucleic Acid Res Mol Biol* **59**, 95-133.
- Gurtovenko, A.A., and Anwar, J. (2007). Modulating the structure and properties of cell membranes: the molecular mechanism of action of dimethyl sulfoxide. *J Phys Chem B* **111**, 10453-10460.
- Hanslick, J.L., Lau, K., Noguchi, K.K., Olney, J.W., Zorumski, C.F., Mennerick, S., and Farber, N.B. (2009). Dimethyl sulfoxide (DMSO) produces widespread apoptosis in the developing central nervous system. *Neurobiol Dis* **34**, 1-10.
- Haribabu, B., and Dottin, R.P. (1991). Identification of a protein kinase multigene family of *Dictyostelium discoideum*: molecular cloning and expression of a cDNA encoding a developmentally regulated protein kinase. *Proc Natl Acad Sci U S A* **88**, 1115-1119.
- Harwood, A.J., Plyte, S.E., Woodgett, J., Strutt, H., and Kay, R.R. (1995). Glycogen synthase kinase 3 regulates cell fate in *Dictyostelium*. *Cell* **80**, 139-148.
- Hausen, M.A., de Oliveira, R.P., Gadelha, A.P., Campanati, L., de Carvalho, J.J., de Carvalho, L., and Barbosa, H.S. (2009). *Giardia lamblia*: a report of drug effects under cell differentiation. *Parasitol Res* **105**, 789-796.
- Hayakawa, M., Kaizawa, H., Moritomo, H., Koizumi, T., Ohishi, T., Yamano, M., Okada, M., Ohta, M., Tsukamoto, S., Raynaud, F.I., *et al.* (2007). Synthesis and biological evaluation of pyrido[3',2':4,5]furo[3,2-d]pyrimidine derivatives as novel PI3 kinase p110alpha inhibitors. *Bioorg Med Chem Lett* **17**, 2438-2442.
- He, D., Wen, J.F., Chen, W.Q., Lu, S.Q., and Xin, D.D. (2005). Identification,

- characteristic and phylogenetic analysis of type II DNA topoisomerase gene in *Giardia lamblia*. *Cell Res* **15**, 474-482.
- He, X., Saint-Jeannet, J.P., Woodgett, J.R., Varmus, H.E., and Dawid, I.B. (1995). Glycogen synthase kinase-3 and dorsoventral patterning in *Xenopus* embryos. *Nature* **374**, 617-622.
- Hernandez, Y., Zamora, G., Ray, S., Chapoy, J., Chavez, E., Valverde, R., Williams, E., Aley, S.B., and Das, S. (2007). Transcriptional analysis of three major putative phosphatidylinositol kinase genes in a parasitic protozoan, *Giardia lamblia*. *J Eukaryot Microbiol* **54**, 29-32.
- Houkong, K., Sawangjaroen, N., and Phongpaichit, S. (2011). A colorimetric method for the evaluation of anti-giardial drugs in vitro. *Exp Parasitol* **127**, 600-603.
- Hresko, R.C., and Mueckler, M. (2005). mTOR.RICTOR is the Ser473 kinase for Akt/protein kinase B in 3T3-L1 adipocytes. *J Biol Chem* **280**, 40406-40416.
- Jaber, N., Dou, Z., Chen, J.S., Catanzaro, J., Jiang, Y.P., Ballou, L.M., Selinger, E., Ouyang, X., Lin, R.Z., Zhang, J., *et al.* (2012). Class III PI3K Vps34 plays an essential role in autophagy and in heart and liver function. *Proc Natl Acad Sci U S A* **109**, 2003-2008.
- Jones, D.T. (1999). Protein secondary structure prediction based on position-specific scoring matrices. *J Mol Biol* **292**, 195-202.
- Jope, R.S. (1999). Anti-bipolar therapy: mechanism of action of lithium. *Mol Psychiatry* **4**, 117-128.
- Jope, R.S. (2003). Lithium and GSK-3: one inhibitor, two inhibitory actions, multiple outcomes. *Trends Pharmacol Sci* **24**, 441-443.
- Kabnick, K.S., and Peattie, D.A. (1990). *In situ* analyses reveal that the two nuclei of *Giardia lamblia* are equivalent. *J Cell Sci* **95** (Pt 3), 353-360.
- Kane, A.V., Ward, H.D., Keusch, G.T., and Pereira, M.E. (1991). *In vitro* encystation of *Giardia lamblia*: large-scale production of in vitro cysts and strain and clone differences in encystation efficiency. *J Parasitol* **77**, 974-981.
- Kihara, A., Noda, T., Ishihara, N., and Ohsumi, Y. (2001). Two distinct Vps34 phosphatidylinositol 3-kinase complexes function in autophagy and carboxypeptidase Y sorting in *Saccharomyces cerevisiae*. *J Cell Biol* **152**, 519-530.
- Kikkawa, U., Mann, S.K., Firtel, R.A., and Hunter, T. (1992). Molecular cloning of casein kinase II alpha subunit from *Dictyostelium discoideum* and its expression in the life cycle. *Mol Cell Biol* **12**, 5711-5723.

- Kim, H.R., Kim, K., Lee, K.H., Kim, S.J., and Kim, J. (2008). Inhibition of casein kinase 2 enhances the death ligand- and natural killer cell-induced hepatocellular carcinoma cell death. *Clin Exp Immunol* **152**, 336-344.
- Kim, K.T., Mok, M.T., and Edwards, M.R. (2005). Protein kinase B from *Giardia intestinalis*. *Biochem Biophys Res Commun* **334**, 333-341.
- Kim, Y.H., Choi, C.Y., and Kim, Y. (1999). Covalent modification of the homeodomain-interacting protein kinase 2 (HIPK2) by the ubiquitin-like protein SUMO-1. *Proc Natl Acad Sci U S A* **96**, 12350-12355.
- Komiya, Y., and Habas, R. (2008). Wnt signal transduction pathways. *Organogenesis* **4**, 68-75.
- Lanfredi-Rangel, A., Attias, M., Reiner, D.S., Gillin, F.D., and De Souza, W. (2003). Fine structure of the biogenesis of *Giardia lamblia* encystation secretory vesicles. *J Struct Biol* **143**, 153-163.
- Lanfredi-Rangel, A., Diniz, J.A., Jr., and de Souza, W. (1999). Presence of a protrusion on the ventral disk of adhered trophozoites of *Giardia lamblia*. *Parasitol Res* **85**, 951-955.
- Laporte, J., Blondeau, F., Buj-Bello, A., and Mandel, J.L. (2001). The myotubularin family: from genetic disease to phosphoinositide metabolism. *Trends Genet* **17**, 221-228.
- Lauwaet, T., Davids, B.J., Reiner, D.S. and Gillin, F.D. (2007). Encystation of *Giardia lamblia*: a model for other parasites. *Curr Opin Microbiol* **10**, 554-559.
- Lauwaet, T., Davids, B.J., Torres-Escobar, A., Birkeland, S.R., Cipriano, M.J., Preheim, S.P., Palm, D., Svard, S.G., McArthur, A.G., and Gillin, F.D. (2007). Protein phosphatase 2A plays a crucial role in *Giardia lamblia* differentiation. *Mol Biochem Parasitol* **152**, 80-89.
- Litchfield, D.W. (2003). Protein kinase CK2: structure, regulation and role in cellular decisions of life and death. *Biochem J* **369**, 1-15.
- Liu, Y., Shreder, K.R., Gai, W., Corral, S., Ferris, D.K., and Rosenblum, J.S. (2005). Wortmannin, a widely used phosphoinositide 3-kinase inhibitor, also potently inhibits mammalian polo-like kinase. *Chem Biol* **12**, 99-107.
- Lopez, A.B., Sener, K., Jarroll, E.L., and van Keulen, H. (2003). Transcription regulation is demonstrated for five key enzymes in *Giardia intestinalis* cyst wall polysaccharide biosynthesis. *Mol Biochem Parasitol* **128**, 51-57.
- Luchtel, D.L., Lawrence, W.P., and DeWalle, F.B. (1980). Electron microscopy of *Giardia lamblia* cysts. *Appl Environ Microbiol* **40**, 821-832.

- Lujan, H.D., and Diamond, L.S. (1997). Cholesterol requirement and metabolism in *Entamoeba histolytica*. *Arch Med Res* **28** Spec No, 96-97.
- Lujan, H.D., Mowatt, M.R., and Nash, T.E. (1996). Lipid requirements and lipid uptake by *Giardia lamblia* trophozoites in culture. *J Eukaryot Microbiol* **43**, 237-242.
- Lujan, H.D., Mowatt, M.R., and Nash, T.E. (1997). Mechanisms of *Giardia lamblia* differentiation into cysts. *Microbiol Mol Biol Rev* **61**, 294-304.
- MacDougall, L.K., Domin, J., and Waterfield, M.D. (1995). A family of phosphoinositide 3-kinases in *Drosophila* identifies a new mediator of signal transduction. *Curr Biol* **5**, 1404-1415.
- MacDougall, L.K., Gagou, M.E., Leever, S.J., Hafen, E., and Waterfield, M.D. (2004). Targeted expression of the class II phosphoinositide 3-kinase in *Drosophila melanogaster* reveals lipid kinase-dependent effects on patterning and interactions with receptor signaling pathways. *Mol Cell Biol* **24**, 796-808.
- Maffucci, T., Cooke, F.T., Foster, F.M., Traer, C.J., Fry, M.J., and Falasca, M. (2005). Class II phosphoinositide 3-kinase defines a novel signaling pathway in cell migration. *J Cell Biol* **169**, 789-799.
- Maia, C., Attias, M., Urbina, J., Gilbert, I., Magaraci, F., and de Souza, W. (2007). Azasterols impair *Giardia lamblia* proliferation and induces encystation. *Biochem Biophys Res Commun* **363**, 310-316.
- Manning, G., Reiner, D.S., Lauwaet, T., Dacre, M., Smith, A., Zhai, Y., Svard, S., and Gillin, F.D. (2011). The minimal kinome of *Giardia lamblia* illuminates early kinase evolution and unique parasite biology. *Genome Biol* **12**, R66.
- Mariante, R.M., Vancini, R.G., Melo, A.L., and Benchimol, M. (2005). *Giardia lamblia*: evaluation of the *in vitro* effects of nocodazole and colchicine on trophozoites. *Exp Parasitol* **110**, 62-72.
- Marone, R., Cmiljanovic, V., Giese, B., and Wymann, M.P. (2008). Targeting phosphoinositide 3-kinase: moving towards therapy. *Biochim Biophys Acta* **1784**, 159-185.
- Martinez, A., Castro, A., Dorronsoro, I., and Alonso, M. (2002). Glycogen synthase kinase 3 (GSK-3) inhibitors as new promising drugs for diabetes, neurodegeneration, cancer, and inflammation. *Med Res Rev* **22**, 373-384.
- Matter, W.F., Brown, R.F., and Vlahos, C.J. (1992). The inhibition of phosphatidylinositol 3-kinase by quercetin and analogs. *Biochem Biophys Res Commun* **186**, 624-631.
- McArthur, A.G., Morrison, H.G., Nixon, J.E., Passamaneck, N.Q., Kim, U., Hinkle, G., Crocker, M.K., Holder, M.E., Farr, R., Reich, C.I., *et al.* (2000). The *Giardia* genome project database. *FEMS Microbiol Lett* **189**, 271-273.

- McElhinny, J.A., Trushin, S.A., Bren, G.D., Chester, N., and Paya, C.V. (1996). Casein kinase II phosphorylates I kappa B alpha at S-283, S-289, S-293, and T-291 and is required for its degradation. *Mol Cell Biol* **16**, 899-906.
- McEntagart, M., Parsons, G., Buj-Bello, A., Biancalana, V., Fenton, I., Little, M., Krawczak, M., Thomas, N., Herman, G., Clarke, A., *et al.* (2002). Genotype-phenotype correlations in X-linked myotubular myopathy. *Neuromuscul Disord* **12**, 939-946.
- McGuffin, L.J., Bryson, K., and Jones, D.T. (2000). The PSIPRED protein structure prediction server. *Bioinformatics* **16**, 404-405.
- McNamara, C.R., and Degterev, A. (2011). Small-molecule inhibitors of the PI3K signaling network. *Future Med Chem* **3**, 549-565.
- Meng, T.C., Aley, S.B., Svard, S.G., Smith, M.W., Huang, B., Kim, J., and Gillin, F.D. (1996). Immunolocalization and sequence of caltractin/centrin from the early branching eukaryote *Giardia lamblia*. *Mol Biochem Parasitol* **79**, 103-108.
- Meng, T.C., Hetsko, M.L., and Gillin, F.D. (1993). Antigenic switching of TSA 417, a trophozoite variable surface protein, following completion of the life cycle of *Giardia lamblia*. *Infect Immun* **61**, 5394-5397.
- Merchant, S.S., Prochnik, S.E., Vallon, O., Harris, E.H., Karpowicz, S.J., Witman, G.B., Terry, A., Salamov, A., Fritz-Laylin, L.K., Marechal-Drouard, L., *et al.* (2007). The Chlamydomonas genome reveals the evolution of key animal and plant functions. *Science* **318**, 245-250.
- Michell, R.H., Heath, V.L., Lemmon, M.A., and Dove, S.K. (2006). Phosphatidylinositol 3,5-bisphosphate: metabolism and cellular functions. *Trends Biochem Sci* **31**, 52-63.
- Midlej, V., and Benchimol, M. (2009). *Giardia lamblia* behavior during encystment: how morphological changes in shape occur. *Parasitol Int* **58**, 72-80.
- Midlej, V., Meinig, I., de Souza, W., and Benchimol, M. (2013). A new set of carbohydrate-positive vesicles in encysting *Giardia lamblia*. *Protist* **164**, 261-271.
- Mitra, P., Zhang, Y., Rameh, L.E., Ivshina, M.P., McCollum, D., Nunnari, J.J., Hendricks, G.M., Kerr, M.L., Field, S.J., Cantley, L.C., *et al.* (2004). A novel phosphatidylinositol(3,4,5)P3 pathway in fission yeast. *J Cell Biol* **166**, 205-211.
- Moreira, D., Santarem, N., Loureiro, I., Tavares, J., Silva, A.M., Amorim, A.M., Ouaiissi, A., Cordeiro-da-Silva, A., and Silvestre, R. (2012). Impact of continuous axenic cultivation in *Leishmania infantum* virulence. *PLoS Negl Trop Dis* **6**, e1469.
- Morf, L., Spycher, C., Rehrauer, H., Fournier, C.A., Morrison, H.G., and Hehl, A.B. (2010). The transcriptional response to encystation stimuli in *Giardia lamblia* is restricted to a small set of genes. *Eukaryot Cell* **9**, 1566-1576.

- Morrison, H.G., McArthur, A.G., Gillin, F.D., Aley, S.B., Adam, R.D., Olsen, G.J., Best, A.A., Cande, W.Z., Chen, F., Cipriano, M.J., *et al.* (2007). Genomic minimalism in the early diverging intestinal parasite *Giardia lamblia*. *Science* **317**, 1921-1926.
- Nakai, K., and Horton, P. (1999). PSORT: a program for detecting sorting signals in proteins and predicting their subcellular localization. *Trends Biochem Sci* **24**, 34-36.
- Nakanishi, S., Kakita, S., Takahashi, I., Kawahara, K., Tsukuda, E., Sano, T., Yamada, K., Yoshida, M., Kase, H., Matsuda, Y., *et al.* (1992). Wortmannin, a microbial product inhibitor of myosin light chain kinase. *J Biol Chem* **267**, 2157-2163.
- Nicot, A.S., and Laporte, J. (2008). Endosomal phosphoinositides and human diseases. *Traffic* **9**, 1240-1249.
- Ojo, K.K., Arakaki, T.L., Napuli, A.J., Inampudi, K.K., Keyloun, K.R., Zhang, L., Hol, W.G., Verlinde, C.L., Merritt, E.A., and Van Voorhis, W.C. (2011). Structure determination of glycogen synthase kinase-3 from *Leishmania major* and comparative inhibitor structure-activity relationships with *Trypanosoma brucei* GSK-3. *Mol Biochem Parasitol* **176**, 98-108.
- Oxberry, M.E., Thompson, R.C., and Reynoldson, J.A. (1994). Evaluation of the effects of albendazole and metronidazole on the ultrastructure of *Giardia duodenalis*, *Trichomonas vaginalis* and *Spironucleus muris* using transmission electron microscopy. *Int J Parasitol* **24**, 695-703.
- Park, S., Chapuis, N., Bardet, V., Tamburini, J., Gallay, N., Willems, L., Knight, Z.A., Shokat, K.M., Azar, N., Viguie, F., *et al.* (2008). PI-103, a dual inhibitor of Class IA phosphatidylinositide 3-kinase and mTOR, has antileukemic activity in AML. *Leukemia* **22**, 1698-1706.
- Pascuccelli, V., Labriola, C., Tellez-Inon, M.T., and Parodi, A.J. (1999). Molecular and biochemical characterization of a protein kinase B from *Trypanosoma cruzi*. *Mol Biochem Parasitol* **102**, 21-33.
- Pendaries, C., Tronchere, H., Plantavid, M., and Payrastre, B. (2003). Phosphoinositide signaling disorders in human diseases. *FEBS Lett* **546**, 25-31.
- Phiel, C.J., and Klein, P.S. (2001). Molecular targets of lithium action. *Annu Rev Pharmacol Toxicol* **41**, 789-813.
- Pierantoni, G.M., Bulfone, A., Pentimalli, F., Fedele, M., Iuliano, R., Santoro, M., Chiariotti, L., Ballabio, A., and Fusco, A. (2002). The homeodomain-interacting protein kinase 2 gene is expressed late in embryogenesis and preferentially in retina, muscle, and neural tissues. *Biochem Biophys Res Commun* **290**, 942-947.
- Que, X., Samuelson, J., and Reed, S. (1993). Molecular cloning of a rac family protein kinase and identification of a serine/threonine protein kinase gene family of *Entamoeba histolytica*. *Mol Biochem Parasitol* **60**, 161-170.

- Quintayo, M.A., Munro, A.F., Thomas, J., Kunkler, I.H., Jack, W., Kerr, G.R., Dixon, J.M., Chetty, U., and Bartlett, J.M. (2012). GSK3beta and cyclin D1 expression predicts outcome in early breast cancer patients. *Breast Cancer Res Treat* **136**, 161-168.
- Raynaud, F.I., Eccles, S., Clarke, P.A., Hayes, A., Nutley, B., Alix, S., Henley, A., Di-Stefano, F., Ahmad, Z., Guillard, S., *et al.* (2007). Pharmacologic characterization of a potent inhibitor of class I phosphatidylinositide 3-kinases. *Cancer Res* **67**, 5840-5850.
- Reaume, C., Moore, B., Hernandez, P., Ruzzini, A., Chlebus, M., Wasserman, M. and Yee, J. (2013). Evaluation of drugs and stationary growth on the cell cycle of *Giardia intestinalis*. *Mol Biochem Parasitol* **187**, 72-76.
- Reiner, D.S., Ankarklev, J., Troell, K., Palm, D., Bernander, R., Gillin, F.D., Andersson, J.O., and Svard, S.G. (2008). Synchronisation of *Giardia lamblia*: identification of cell cycle stage-specific genes and a differentiation restriction point. *Int J Parasitol* **38**, 935-944.
- Ren, R., Mayer, B.J., Cicchetti, P., and Baltimore, D. (1993). Identification of a ten-amino acid proline-rich SH3 binding site. *Science* **259**, 1157-1161.
- Roxstrom-Lindquist, K., Palm, D., Reiner, D., Ringqvist, E., and Svard, S.G. (2006). *Giardia* immunity--an update. *Trends Parasitol* **22**, 26-31.
- Ryves, W.J., and Harwood, A.J. (2001). Lithium inhibits glycogen synthase kinase-3 by competition for magnesium. *Biochem Biophys Res Commun* **280**, 720-725.
- Sanhaji, M., Louwen, F., Zimmer, B., Kreis, N.N., Roth, S., and Yuan, J. (2013). Polo-like kinase 1 inhibitors, mitotic stress and the tumor suppressor p53. *Cell Cycle* **12**, 1340-1351.
- Sasaki, A.T., and Firtel, R.A. (2006). Regulation of chemotaxis by the orchestrated activation of Ras, PI3K, and TOR. *Eur J Cell Biol* **85**, 873-895.
- Sayas, C.L., Ariaens, A., Ponsioen, B., and Moolenaar, W.H. (2006). GSK-3 is activated by the tyrosine kinase Pyk2 during LPA1-mediated neurite retraction. *Mol Biol Cell* **17**, 1834-1844.
- Schlesinger, A., Shelton, C.A., Maloof, J.N., Meneghini, M., and Bowerman, B. (1999). Wnt pathway components orient a mitotic spindle in the early *Caenorhabditis elegans* embryo without requiring gene transcription in the responding cell. *Genes Dev* **13**, 2028-2038.
- Schultz, J., Milpetz, F., Bork, P., and Ponting, C.P. (1998). SMART, a simple modular architecture research tool: identification of signaling domains. *Proc Natl Acad Sci U S A* **95**, 5857-5864.
- Siegfried, E., Chou, T.B., and Perrimon, N. (1992). Wingless signalling acts through zeste-

- white 3, the *Drosophila* homolog of glycogen synthase kinase-3, to regulate engrailed and establish cell fate. *Cell* **71**, 1167-1179.
- Soltys, B.J., Falah, M., and Gupta, R.S. (1996). Identification of endoplasmic reticulum in the primitive eukaryote *Giardia lamblia* using cryoelectron microscopy and antibody to Bip. *J Cell Sci* **109** (Pt 7), 1909-1917.
- Spankuch-Schmitt, B., Bereiter-Hahn, J., Kaufmann, M., and Strebhardt, K. (2002). Effect of RNA silencing of polo-like kinase-1 (PLK1) on apoptosis and spindle formation in human cancer cells. *J Natl Cancer Inst* **94**, 1863-1877.
- Stack, J.H., and Emr, S.D. (1994). Vps34p required for yeast vacuolar protein sorting is a multiple specificity kinase that exhibits both protein kinase and phosphatidylinositol-specific PI 3-kinase activities. *J Biol Chem* **269**, 31552-31562.
- Stack, J.H., Herman, P.K., Schu, P.V., and Emr, S.D. (1993). A membrane-associated complex containing the Vps15 protein kinase and the Vps34 PI 3-kinase is essential for protein sorting to the yeast lysosome-like vacuole. *EMBO J* **12**, 2195-2204.
- Stack, J.H., Horazdovsky, B., and Emr, S.D. (1995). Receptor-mediated protein sorting to the vacuole in yeast: roles for a protein kinase, a lipid kinase and GTP-binding proteins. *Annu Rev Cell Dev Biol* **11**, 1-33.
- Stefanic, S., Palm, D., Svard, S.G., and Hehl, A.B. (2006). Organelle proteomics reveals cargo maturation mechanisms associated with Golgi-like encystation vesicles in the early-diverged protozoan *Giardia lamblia*. *J Biol Chem* **281**, 7595-7604.
- Stein, R.C., and Waterfield, M.D. (2000). PI3-kinase inhibition: a target for drug development? *Mol Med Today* **6**, 347-357.
- Stephens, L.R., Eguinoa, A., Erdjument-Bromage, H., Lui, M., Cooke, F., Coadwell, J., Smrcka, A.S., Thelen, M., Cadwallader, K., Tempst, P., *et al.* (1997). The G beta gamma sensitivity of a PI3K is dependent upon a tightly associated adaptor, p101. *Cell* **89**, 105-114.
- Stirdivant, S.M., Ahern, J., Conroy, R.R., Barnett, S.F., Ledder, L.M., Oliff, A., and Heimbrock, D.C. (1997). Cloning and mutagenesis of the p110 alpha subunit of human phosphoinositide 3'-hydroxykinase. *Bioorg Med Chem* **5**, 65-74.
- Svard, S.G., Hagblom, P., and Palm, J.E. (2003). *Giardia lamblia* -- a model organism for eukaryotic cell differentiation. *FEMS Microbiol Lett* **218**, 3-7.
- Thompson, J.D., Higgins, D.G., and Gibson, T.J. (1994). CLUSTAL W: improving the sensitivity of progressive multiple sequence alignment through sequence weighting, position-specific gap penalties and weight matrix choice. *Nucleic Acids Res* **22**, 4673-4680.
- Thomson, A.B., Schoeller, C., Keelan, M., Smith, L., and Clandinin, M.T. (1993). Lipid absorption: passing through the unstirred layers, brush-border membrane, and

- beyond. *Can J Physiol Pharmacol* **71**, 531-555.
- Touz, M.C., Nores, M.J., Slavin, I., Carmona, C., Conrad, J.T., Mowatt, M.R., Nash, T.E., Coronel, C.E., and Lujan, H.D. (2002). The activity of a developmentally regulated cysteine proteinase is required for cyst wall formation in the primitive eukaryote *Giardia lamblia*. *J Biol Chem* **277**, 8474-8481.
- Tovar, J., Leon-Avila, G., Sanchez, L.B., Sutak, R., Tachezy, J., van der Giezen, M., Hernandez, M., Muller, M., and Lucocq, J.M. (2003). Mitochondrial remnant organelles of *Giardia* function in iron-sulphur protein maturation. *Nature* **426**, 172-176.
- Trubiani, O., Ciancarelli, M., Rapino, M., and Di Primio, R. (1996). Dimethyl sulfoxide induces programmed cell death and reversible G1 arrest in the cell cycle of human lymphoid pre-T cell line. *Immunol Lett* **50**, 51-57.
- Upcroft, J.A., and Upcroft, P. (2001). Drug susceptibility testing of anaerobic protozoa. *Antimicrob Agents Chemother* **45**, 1810-1814.
- Upcroft, P., and Upcroft, J.A. (2001). Drug targets and mechanisms of resistance in the anaerobic protozoa. *Clin Microbiol Rev* **14**, 150-164.
- Van de Weerd, B.C., and Medema, R.H. (2006). Polo-like kinases: a team in control of the division. *Cell Cycle* **5**, 853-864.
- Vanhaesebroeck, B., and Waterfield, M.D. (1999). Signaling by distinct classes of phosphoinositide 3-kinases. *Exp Cell Res* **253**, 239-254.
- Vesey, D.A., Cunningham, J.M., Selden, A.C., Woodman, A.C., and Hodgson, H.J. (1991). Dimethyl sulphoxide induces a reduced growth rate, altered cell morphology and increased epidermal-growth-factor binding in Hep G2 cells. *Biochem J* **277** (Pt 3), 773-777.
- Vieira, O.V., Botelho, R.J., Rameh, L., Brachmann, S.M., Matsuo, T., Davidson, H.W., Schreiber, A., Backer, J.M., Cantley, L.C., and Grinstein, S. (2001). Distinct roles of class I and class III phosphatidylinositol 3-kinases in phagosome formation and maturation. *J Cell Biol* **155**, 19-25.
- Vlahos, C.J., Matter, W.F., Hui, K.Y., and Brown, R.F. (1994). A specific inhibitor of phosphatidylinositol 3-kinase, 2-(4-morpholinyl)-8-phenyl-4H-1-benzopyran-4-one (LY294002). *J Biol Chem* **269**, 5241-5248.
- Wakefield, J.G., Stephens, D.J., and Tavaré, J.M. (2003). A role for glycogen synthase kinase-3 in mitotic spindle dynamics and chromosome alignment. *J Cell Sci* **116**, 637-646.
- Walker, E.H., Pacold, M.E., Perisic, O., Stephens, L., Hawkins, P.T., Wymann, M.P., and Williams, R.L. (2000). Structural determinants of phosphoinositide 3-kinase inhibition by wortmannin, LY294002, quercetin, myricetin, and staurosporine. *Mol Cell* **6**, 909-919.

- Walker, E.H., Perisic, O., Ried, C., Stephens, L., and Williams, R.L. (1999). Structural insights into phosphoinositide 3-kinase catalysis and signalling. *Nature* **402**, 313-320.
- Ward, S., Sotsios, Y., Dowden, J., Bruce, I., and Finan, P. (2003). Therapeutic potential of phosphoinositide 3-kinase inhibitors. *Chem Biol* **10**, 207-213.
- Welsh, G.I., Wilson, C., and Proud, C.G. (1996). GSK3: a SHAGGY frog story. *Trends Cell Biol* **6**, 274-279.
- Westhoff, M.A., Kandenwein, J.A., Karl, S., Vellanki, S.H., Braun, V., Eramo, A., Antoniadis, G., Debatin, K.M., and Fulda, S. (2009). The pyridinylfuranopyrimidine inhibitor, PI-103, chemosensitizes glioblastoma cells for apoptosis by inhibiting DNA repair. *Oncogene* **28**, 3586-3596.
- Wood, V., Gwilliam, R., Rajandream, M.A., Lyne, M., Lyne, R., Stewart, A., Sgouros, J., Peat, N., Hayles, J., Baker, S., *et al.* (2002). The genome sequence of *Schizosaccharomyces pombe*. *Nature* **415**, 871-880.
- Woodgett, J.R. (1990). Molecular cloning and expression of glycogen synthase kinase-3/factor A. *EMBO J* **9**, 2431-2438.
- Workman, P., Clarke, P.A., Guillard, S., and Raynaud, F.I. (2006). Drugging the PI3 kinome. *Nat Biotechnol* **24**, 794-796.
- Woscholski, R., Kodaki, T., McKinnon, M., Waterfield, M.D., and Parker, P.J. (1994). A comparison of demethoxyviridin and wortmannin as inhibitors of phosphatidylinositol 3-kinase. *FEBS Lett* **342**, 109-114.
- Wu, D., and Pan, W. (2010). GSK3: a multifaceted kinase in Wnt signaling. *Trends Biochem Sci* **35**, 161-168.
- Wymann, M.P., Zvelebil, M., and Laffargue, M. (2003). Phosphoinositide 3-kinase signalling--which way to target? *Trends Pharmacol Sci* **24**, 366-376.
- Yan, Y., and Backer, J.M. (2007). Regulation of class III (Vps34) PI3Ks. *Biochem Soc Trans* **35**, 239-241.
- Yang, H., Rudge, D.G., Koos, J.D., Vaidialingam, B., Yang, H.J., and Pavletich, N.P. (2013). mTOR kinase structure, mechanism and regulation. *Nature* **497**, 217-223.
- Yang, P., and Sale, W.S. (2000). Casein kinase I is anchored on axonemal doublet microtubules and regulates flagellar dynein phosphorylation and activity. *J Biol Chem* **275**, 18905-18912.
- Yichoy, M., Duarte, T.T., De Chatterjee, A., Mendez, T.L., Aguilera, K.Y., Roy, D., Roychowdhury, S., Aley, S.B., and Das, S. (2011). Lipid metabolism in *Giardia*: a

- post-genomic perspective. *Parasitology* **138**, 267-278.
- Yu, L.Z., Birky, C.W., Jr., and Adam, R.D. (2002). The two nuclei of *Giardia* each have complete copies of the genome and are partitioned equationally at cytokinesis. *Eukaryot Cell* **1**, 191-199.
- Zandomeni, R., Zandomeni, M.C., Shugar, D., and Weinmann, R. (1986). Casein kinase type II is involved in the inhibition by 5,6-dichloro-1-beta-D-ribofuranosylbenzimidazole of specific RNA polymerase II transcription. *J Biol Chem* **261**, 3414-3419.
- Zhang, C., Zhao, H., Liu, Y., Li, Q., Liu, X., Tan, H., Yuan, C., and Dong, Y. (2010). Isolation and characterization of a novel glycogen synthase kinase-3 gene, GmGSK, in *Glycine max* L. that enhances abiotic stress tolerance in *Saccharomyces cerevisiae*. *Biotechnol Lett* **32**, 861-866.
- Zhao, Y., Zhang, X., Chen, Y., Lu, S., Peng, Y., Wang, X., Guo, C., Zhou, A., Zhang, J., Luo, Y., *et al.* (2014). Crystal Structures of PI3K α Complexed with PI103 and Its Derivatives: New Directions for Inhibitors Design. *ACS Med Chem Lett* **5**, 138-142.
- Zhou, K., Pandol, S., Bokoch, G., and Traynor-Kaplan, A.E. (1998). Disruption of *Dictyostelium* PI3K genes reduces [32P]phosphatidylinositol 3,4 bisphosphate and [32P]phosphatidylinositol trisphosphate levels, alters F-actin distribution and impairs pinocytosis. *J Cell Sci* **111** (Pt 2), 283-294.
- Zhou, K., Takegawa, K., Emr, S.D., and Firtel, R.A. (1995). A phosphatidylinositol (PI) kinase gene family in *Dictyostelium discoideum*: biological roles of putative mammalian p110 and yeast Vps34p PI 3-kinase homologs during growth and development. *Mol Cell Biol* **15**, 5645-5656.
- Zhou, X.P., Marsh, D.J., Morrison, C.D., Chaudhury, A.R., Maxwell, M., Reifenberger, G., and Eng, C. (2003). Germline inactivation of PTEN and dysregulation of the phosphoinositol-3-kinase/Akt pathway cause human Lhermitte-Duclos disease in adults. *Am J Hum Genet* **73**, 1191-1198.